SINTERING OF 6061 ALUMINIUM ALLOY BASED PARTICULATE COMPOSITES AND THEIR SLIDING WEAR BEHAVIOUR

by

A. K. JHA

DEPARTMENT OF METALLURGICAL ENGINEERING

INDIAN INSTITUTE OF TECHNOLOGY KANPUR

APRIL, 1988

SINTERING OF 6061 ALUMINIUM ALLOY BASED PARTICULATE COMPOSITES AND THEIR SLIDING WEAR BEHAVIOUR

A Thesis Submitted
in Partial Fulfilment of the Requirements
for the Degree of

DOCTOR OF PHILOSOPHY

by

A. K. JHA

to the

DEPARTMENT OF METALLURGICAL ENGINEERING

INDIAN INSTITUTE OF TECHNOLOGY KANPUR

APRIL, 1988

Dedicated

to

My Parents

CERTIFICATE

This is to certify that this work "Sintering of 6061 Aluminium Alloy Based Particulate Composites and Their Sliding Wear Behaviour" has been carried out under our supervision by Shri A.K. Jha during July 1985 - March 1988, and it has not been submitted elsewhere for a degre

S.V. Prasad
Scientist
Regional Research Laboratory
C.S.I.R.
BHOPAL

G.S. Upadhyaya 28/4/88
Professor
Dept. of Metallurgical E
Indian Institute of Tech
KANPUR

ACKNOWLEDGEMENTS

The author is deeply indebted to his thesis supervisors, Prof. G.S. Upadhyaya and Dr. S.V. Prasad for their invaluable guidance and constant inspiration at every stage throughout the course of this work.

The author owes his gratefulness to the Director, Regional Research Laboratory (CSIR) Bhopal for kind permission and for extending all sorts of facilities and support for this course.

Special thanks are due to all my colleagues and friends for their co-operation and moral support during the course of this work.

The immence patience, sacrifice and moral support of my wife are highly appreciated.

Amol Kumar Jha

List of Papers Accepted/Communicated for Publication

1. Effect of Sintering Atmosphere and Alumina Addition on Properties of 6061 Aluminium P/M Alloy, Powder Metallurgy International (In Press).

2. Preparation and Properties of 6061 Aluminium Alloy-Graphite Particulate Composites by Powder Metallurgy Route, Powder Metallurgy (In Press).

3. Sintered 6061 Aluminium Alloy-Talc Particulate Composites, Transaction, Powder Metallurgy Association of India (In Press).

4. Dry Sliding Wear of Sintered 6061 Aluminium Alloy Based Particulate Composites Containing Solid Lubricant, Wear (Communicated).

TABLE OF CONTENTS

S Y N O P S I S

Sintered aluminium alloys have enough potential to replace conventional structural parts due to a wide range of properties attained by them. Introduction of second phase (dispersoid) practically may make the properties of such alloys even still more flexible. In the present investigation one of the common aluminium alloy of 6061 grade, which is amenable to compaction, sintering and secondary operations was selected as the matrix. In order to develop material for antifriction use solid lubricants (graphite and talc) were selected as dispersoids, whereas, hard particles (alumina and TiC) were used so as to impart high strength and wear resistance to the base alloy. Copper coating over graphite particles was also tried so as to improve its wettability with the matrix.

Aluminium alloy alongwith 4, 7, 10 and 14 vol. % of dispersoid were mixed in a mixer. Green cylindrical pellets of 12.7 mm diameter and approximately 6 mm height, and Metal Powder Industries Federation (MPIF) tensile test bars of approximately 6 mm height were compacted on a hydraulic press, at a pressure of 310 MPa. The green compacts were then sintered in a tubular furnace at a temperature of 615 $\pm$ 1^{o}C for 1/2 hrs. Three atmospheres namely argon (dew point: -40^{o}C), vacuum (1.33 x 10^{-8} MPa Hg pressure) and nitrogen (dew point: -38^{o}C) were used for sintering purpose. A set of sintered cylindrical compacts was also repressed in a tungsten carbide lined die at a pressure of 450 MPa. These were resintered at 510 $\pm$ 1^{o}C for 1/2 hrs in air. Both sintered and

resintered composites were heat treated to T6 condition as per schedule: solution treatment at 520°C for 1/2 hrs,/ quenching in water at room temperature, and ageing at 160°C for 18 hrs. Sintered composites were also subjected to thermo-mechanical treatment (TMT) as per the schedule: solution treatment (520°C, 1 hr) → deformation (open die, 310 MPa, approx. 25% reduction in height → ageing (160°C, 3 hrs).

Densification behaviour of the composites was monitored by evaluating dimensional changes, density, densification parameter (ΔD) and porosities. Brinell hardness of sintered, repressed-resintered and heat-treated compacts was measured using a load of 153 N. Microhardness of sintered and thermo-mechanically treated composites was measured using a load of 2.9 N. Tensile testing of argon sintered, and aged (T6 treated) MPIF test bars were carried out on an Instron testing machine at a cross head speed of 0.5 mm/min. Electrical resistivity of the compacts was measured on conductivity meter which works on eddy current principle. Surface roughness parameter R_a of the cylindrical wall of as sintered compacts was measured using the stylus instrument 'Talysurf 6'. Dry sliding wear behaviour of the composites was evaluated against rotating EN25 steel disc on a pin on disc apparatus, Effect of materials variables, such as type and amount of dispersoid test parameters viz. sliding speed, distance and applied pressure on the wear behaviour of composites was evaluated. Metallographic study on polished sample was carried out using both optical and scanning electron microscopes (SEM). Worn out surfaces, fractured surfaces and debris were examined under SEM using Wave Length Dispersive X-ray Spectroscope (WDXS) attachment.

Densification parameter of the sintered composites increased with addition of hard particles, but decreased with addition of soft particles with an exception of composites containing 4 vol.% talc. The sequence of densification parameter in decreasing order was as follows: TiC → alumina →

talc → copper coated graphite → uncoated graphite. In most of the cases ΔD value decreased to 4 vol. % dispersoid and remained constant with further dispersoid additions.

Brinell hardness variation of composites followed the sequence in decreasing order with the incorporation of dispersoid as: TiC → alumina/talc → graphite. Although the hardness of the composites improved after repressing-resintering and T6 treatment, but the effects of dispersoid were qualitatively similar. Although microhardness of the sintered composites increased after TMT, but the treatment was more effective for composites containing soft dispersoids than those containing hard dispersoids.

A marginal decrease in UTS and Y.S. of sintered composites was observed with addition of dispersoids as compared to the straight 6061 alloy. Percent elongation value of sintered composites decreased with addition of soft particles. An improvement in UTS value of sintered composites after T6 treatment was noticed. UTS of T6 treated composites decreased in following order with addition of: TiC/talc alumina → graphite, whereas percent elongation decreased in order for composites containing alumina → talc → TiC/graphite.

Electrical resistivity of the sintered composites increased with the additional dispersoids. Maximum increase in resistivity value was observed for composites containing graphite. Addition of alumina had least effect on the resistivity value of the composites. Nitrogen sintering imparted maximum increase in electrical resistivity as compared to other sintering atmospheres. Repressing-resintering resulted in a decrease in the electrical resistivity of the composites, whereas, T6 treatment increased the resistivity irrespective of the dispersoid addition.

Roughness parameter (R_a) of the composites were noticed to decrease in the order: graphite → 6061/TiC/alumina → talc.

Introduction of dispersoid resulted in an increased wear rate of the composites. Amongst the four dispersoids used, addition of graphite resulted in maximum wear rate of composite whereas, TiC addition showed a minimum. Wear loss of the composites increased with increasing sliding distance. With increase in applied pressure, wear rate increased substantially. Graphite containing composites showed improved wear behaviour at lowest applied pressure (i.e. 4×10^{-2} MPa). The wear rate also decreased with the increasing sliding speed. SEM micrograph of the worn out surface showed two distinct features: one was long and continuous grooves, while the other was patches of highly deformed region. Deformed regions were more pronounced in graphite containing composites. Four types of debris (needle shape, flaky, rounded agglomerate and fine equiaxed particles) were observed. Iron pick up by few debris were also identified.

6061 aluminium alloy like other sintered aluminium alloys undergoes liquid phase sintering. The presence of dispersoid affects the sintering behaviour of the composites depending on the nature of dispersoid. Due to its flaky shape graphite particles cover a large fraction of area within the matrix. During sintering, graphite layers restrict the diffusion path along the matrix, thus resulting in inadequate sintering of composites. Improved densification behaviour of the composites with addition of copper coated graphite is due to enhanced sintering in the presence of copper in the matrix. Composites containing talc showed better sinterability as compared to graphite containing composites. The positive effect of talc addition on densification of composites at lower volume fraction appeared to be attributed to the optimized matching of the magnesium silicate in talc with the matrix.

The particle size of alumina dispersoid was smallest (0.3 μm) among all the selected dispersoid as well as the matrix alloy. Such small particles may enter the octahedral

and tetrahedral sites in the packing of the matrix and thus makes the sinterability of the compact least effected. The best sinterability of TiC containing composites may be attributed to the extremely high hardness of TiC which induces stress field around the 6061 alloy matrix. Such a stress field would enhance diffusivity during sintering along the matrix/particle interface, thus promoting densification.

Mechanical properties variation of presently investigated composites has been explained on the basis of factors such as: porosity, dispersoid, work hardening, precipitation hardening and residual stresses etc. Porosity decreases mechanical properties of the composites in different ways. Indirect weakening of the matrix is caused by poor sintering of composites in the presence of porosity. Porosity decreases the effective cross sectional area resulting in lower applied nominal stress at which yield starts. Poor properties of composites containing graphite may be attributed to high porosity level present in them. Although in the present case the particle size and volume fraction of dispersoid is not favourable for strengthening through macro- or micromechanisms, the presence of substructure in composites with hard particles is not altogether ruled out. The crystal structure, particle morphology and intrinsic hardness of dispersoid in the composites do reflect the above correlation adequately.

It is quite obvious that any positive role played by dispersoid in improving the properties of the composites is mitigated due to presence of porosity in it. 6061 alloy system responds to age hardening because of fine Mg_2Si, coherent precipitate. Additional hardening effect of TiC may be envisaged by increased Y.S. value of composites after such addition. Another fact emerges that the work hardening response of heat treated 6061 alloy is better than any of the composites processed similarly, although preponderant contribution of precipitation hardening in all the composites is obvious. The overall predominating effect of strength loss

due to porosity would be much more higher than the strengthening imparted by the thermal residual stress.

Increase in hardness value of composites after TMT is a natural consequence of effective age-hardening due to presence of tangled dislocation substructure induced by deformation of composites. Comparatively higher degree of deformation for composites containing soft particles attribute to higher microhardness of such TMT composites. Over-ageing of hard particle containing composites during TMT may also be one of the causes of less increase in microhardness of such composites.

Variation in electrical resistivity of the composites in present case was attributed to the factors like high dew oint of sintering atmosphere, porosity, dispersoid and precipitates in the matrix . The higher electrical resistivity of omposites containing graphite is due to higher porosity level n such composites. Repressing-resintering of the sintered omposites results in decreased porosity thus imparting low esistivity. T6 treatment increases the electrical resistivity alues due to the formation of GP zone in the matrix.

Decreased roughness of the sintered 6061 alloy - l vol. % talc composite as compared to straight 6061 alloy is tributed to softness of the talc and its compatibility with e matrix. Although the porosities in the composites containing hard particles were low, but the associated high hardss value of dispersoid results in high R_a value.

Increase in wear rate with increasing amount of dispersoid has been correlated with properties of the sintered mpacts. High porosity level and low hardness of the compotes containing graphite results in increased wear rate. w wear rate for composites containing talc is attributed the compatibility of talc with the matrix and to low rosity level in composites. Introduction of hard particles so increases the wear rate of composites, the reason being

poor interfacial interaction between the particles and the matrix. Hard particles entrapped at the mating surface would moreover contribute to plowing and increased wear rate.

As the tests were carried out, after the initial run in period, a linear increase in wear rate of the composites with the sliding distance was obvious. At high applied pressure, increased friction at mating surfaces would give rise to high wear rates of composites. The positive effect of graphite in composites at lowest applied pressure could be due to its presence at mating surface, which prevented metal to metal contact

Ineffectiveness of solid lubricants because of its lower volume fraction in preventing the metal to metal contact during the test was found to be one of the major cause of the increased wear of the composites. Moreover soft lubricant particles get pulled off from the surface during preparation of sample. As the delamination type of wear was found operative, there was a possibility of engulfment of small solid lubricant particles in the large flake shape debris. Few model experiments were carried out, wherein exposure of solid lubricant (graphite or talc) particles was provided on the mating surface in the very beginning of the sliding wear test. Wear loss was considerably reduced in such experiments. However graphite was found to be far superior as compared to talc for such tests. Talc particles being softer than the graphite were not firmly attached to the surface and hence promoted metal-to-metal contact.

CHAPTER I

LITERATURE REVIEW

I.1. Introduction:

Although aluminium possesses suitable engineering properties, it could not occupy the adequate attention of powder metallurgy (P/M) manufacturer due to the lack of precision technical informations about fabrication techniques. Technical problems viz. galling of die walls i.e. cold welding of aluminium to tool, inferior flow characteristics of aluminium powder and high sensitivities for attainment of certain properties with processing parameters have been the major bottle necks.

Recent market trend and the combination of properties required these days indicate that aluminium P/M parts would pick up within no time as soon as the production know-how is made available. Enormous efforts are being made throughout the world to generate useful data on various aluminium alloys with best suitable processing techniques. Researcher at ALCOA have conducted studies by conventional P/M route on aluminium parts production.[1-6] Reports dealing with the production of wrought products by P/M route are also available,[6-8] where the alloy systems included the conventional aluminium alloy of 2XXX, 6XXX[1-5] and 7XXX[9] series and composites like SAP[7-8] and DISPAL.[10]

I.2. Powder Preparation and Cold Compaction:

Aluminium is well known for its severe seizing and galling characteristics against steel. Green compacts if allowed for a greater time of contact movement across the die wall, cause scoring, galling and seizure.[11] Higher the compaction pressure, the worse is the condition. Lubricating die walls during pressing appeared as the only method of producing compacts, but this also created practical problem. The effect of admixed lubricant to aluminium powder is discussed by Kehl et al.[12]

Other problem associated with aluminium compaction is its high affinity for oxygen. When exposed to air, oxide layer of approximately 100 Å coats the aluminium particles. Higher oxide content would have negative effect during pressing[13] through increased die wear and higher interparticle friction. Hard metal dies are desirable, as aluminium powder tends to weld on the steel die wall during pressing.

Aluminium alloys are compacted at comparatively low pressure 400-480 MPa (25-30 tsi). Commercially available 601 AB and 201 AB aluminium alloy premixes developed at ALCOA are compressible powders.[4] Table I.1 shows the composition of these alloys.

Pressure density curves of the alloys are shown in Figure 1.1. The alloy can be compacted to 90% of theoretical density at 192 MPa (12 tsi) and to 95% of theoretical density at 400 MPa (25 tsi). Due to the low compaction pressure

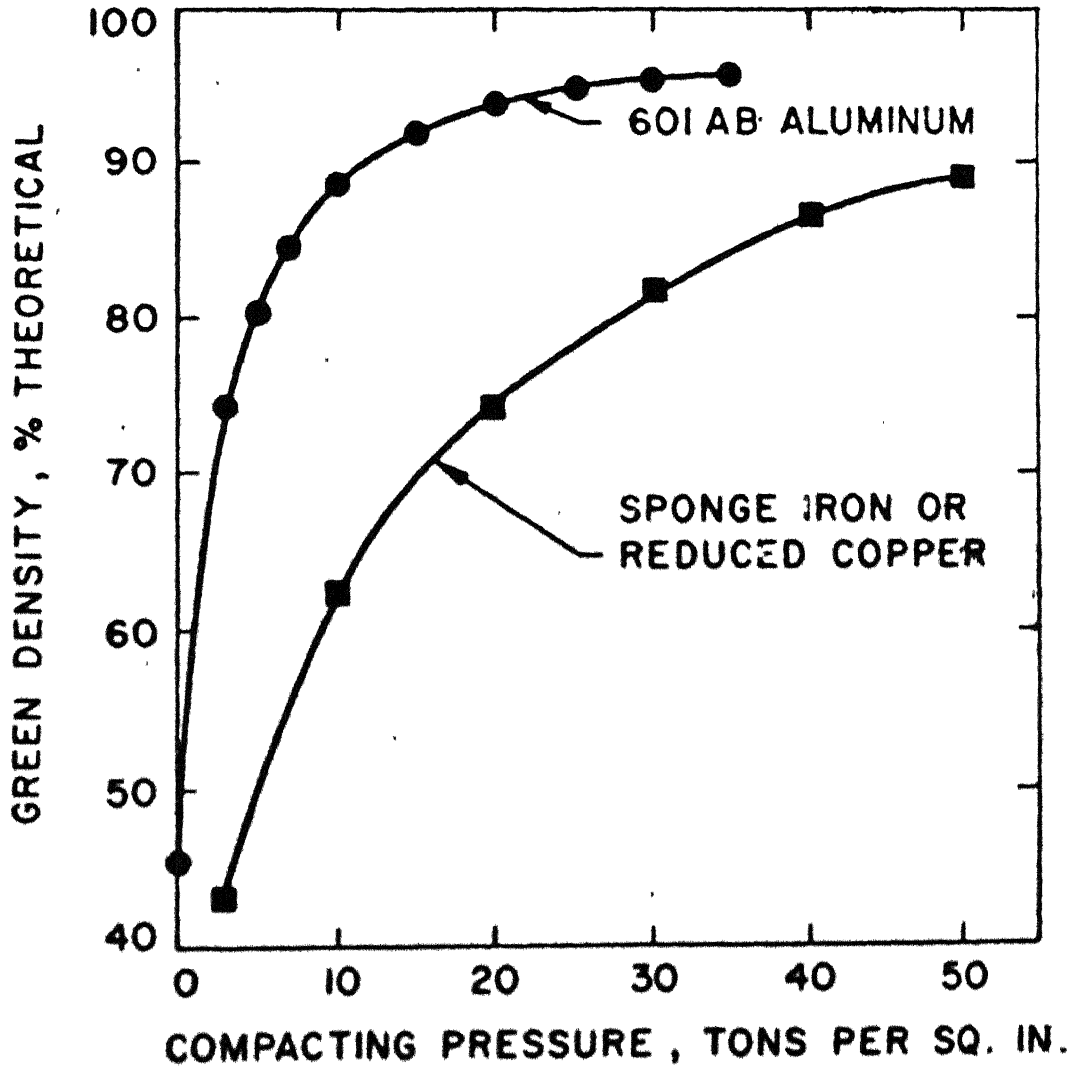

Fig-1.1 COMPRESSIBILITY OF ALUMINUM, IRON AND COPPER POWDERS[1]

Table I.1

Compositions of aluminium P/M premixes[4]

Element	601 AB Mass percent	201 AB Mass percent
Copper	0.25	4.4
Silicon	0.6	0.8
Magnesium	1.0	0.5
Lubricant	1.5	1.5
Aluminium	Rest	Rest

required large cross sectional area can be compacted on existing P/M equipment.

I.3. Sintering of Aluminium Alloy and Its Based Composites:

I.3.1. Aluminium and Its Composites:

Pure aluminium P/M parts are seldom being used. Sintering of aluminium powder presents a special problem. Besides the usual diffusion inhibitor i.e. nonreducible oxide film on the powder particles, lubricants also cause poor properties to the sintered compacts. During compaction the layers crack and metal to metal contact forms and thus the green compact undergoes solid state sintering. Pure aluminium powders compacted at different pressures and sintered for 30 minutes at 620°C have been reported by Goetzel.[14] Tables I.2 and I.3 show the physical and mechanical properties of sintered aluminium compacts. It was found that

Table I.2

Physical and mechanical properties of sintered aluminium compacts[14]

Compacting pressure tsi	Density gm/cc	Yield strength psi	Tensile strength psi	Elongation for 1" length, %	Reduction in area %
10	2.44	6160	8900	4.7	3.1
20	2.60	6460	11810	46.8	63.7
30	2.69	6660	11850	48.4	59.4
40	2.69	7600	11780	37.5	47.7

Table I.3

Mechanical properties of hot pressed aluminium compacts[14]

Hot pressing temperature ^{o}C	Brinell hardness	Ultimate tensile strength psi	Elongation %
300	33.7	12600	1.0
400	30.6	12400	2.0
500	28.4	12200	4.5
600	26.4	15400	34.0

tensile strength of compacts was comparable to that of wrought aluminium, whereas, elongation value fell somewhat short of the normal. Sintering of aluminium compact in dissociated ammonia for 1 hr at 615°C imparts elongation and reduction in area comparable to those obtained in wrought aluminium, while yield and tensile strength values are nearer to the lower limits of the wrought metals.

Sinterability and properties of aluminium with addition of a series of carbides viz. TiC, ZrC, NbC, Cr_3C_2, Mo_2C, WC, have been reported by Upadhyaya and Misra.[15] Composites were prepared by compaction, degassing and sintering in vacuum. It was reported that densification parameter decreased to zero value in case of ZrC, NbC, Mo_2C and WC dispersoid systems. The values were positive in case of TiC, while in case of Cr_3C_2, they were negative. Variation of hardness values as a function of carbide content is shown in Figure 1.2. Hardness values of composites containing Cr_3C_2 increased remarkably, whereas, Al-TiC showed moderate increment with increasing amount of carbide. In case of ZrC, NbC, Mo_2C and WC, hardness values remained more or less same. Among all the properties, hardness data presented better picture of the effect of refractory carbide on sintered aluminium. Two factors were considered responsible for their behaviour: (a) the mechanical properties of the individual carbide and (b) the interaction of the carbide at the aluminium particles interface. In order to achieve high mechanical properties for the composites, it was desirable that both the factors be

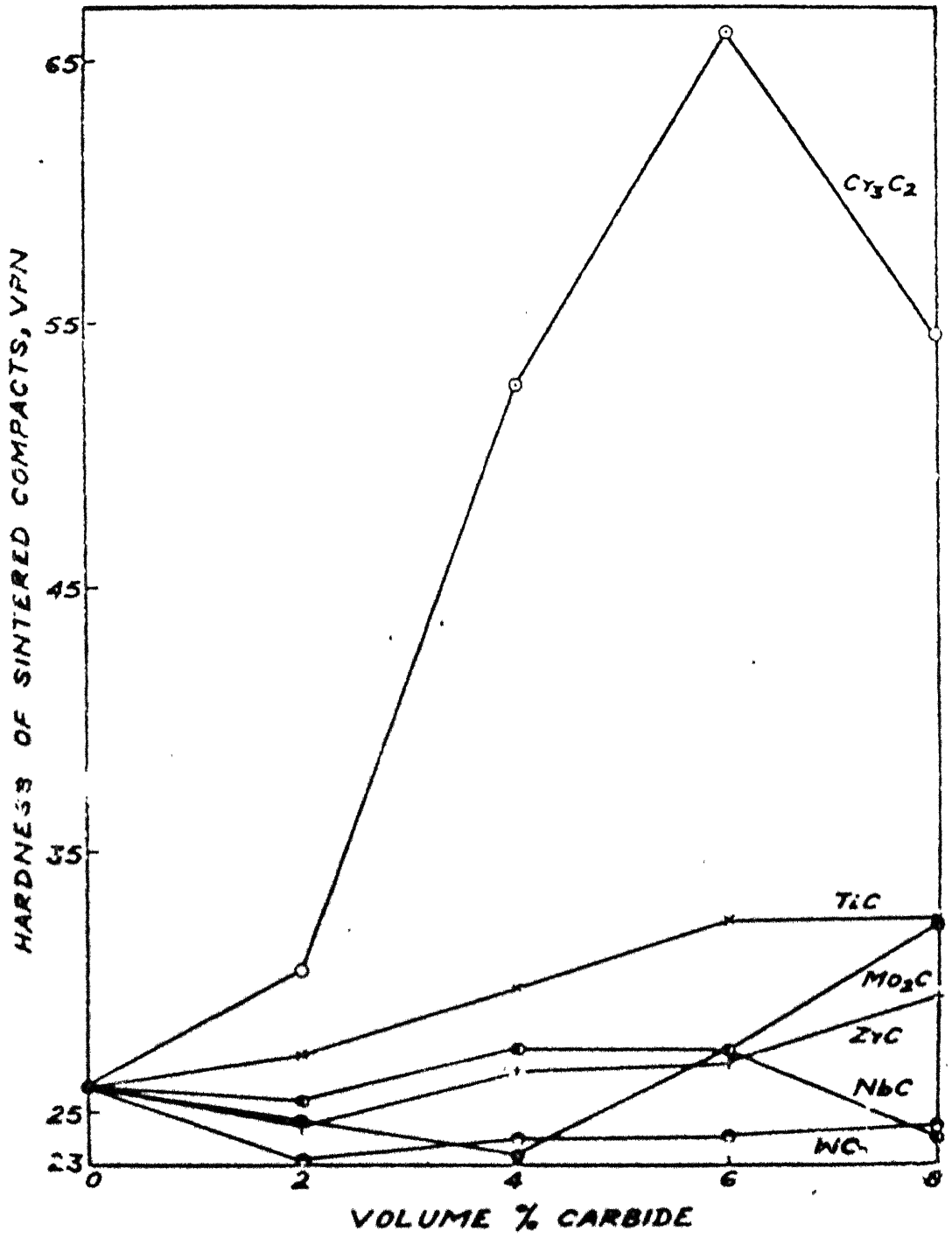

Fig. 1.2 Hardness variation of Al-carbide sintered compacts with respect to carbide contents.[15]

optimized. The justification of the above fact has been explained on the basis of electronic structure of the individual components and their stability under environment of different chemical species.

I.3.2. Sintering of Aluminium-Copper Alloys and Their Based Composites:

Among various aluminium alloys, aluminium-copper system has been studied more extensively. A wide range of work viz. effect of processing parameters, amount of copper, addition of solid lubricants on the sintered properties are reported.[16-19] Mathews[16] reported those parameters, which affected the sintered properties more effectively than other. For Al-2% Cu premix the sintering atmosphere, of hydrogen or dissociated ammonia did not make much difference, if dew point of both were in the range of $-28^{\circ}C$ to $-40^{\circ}C$. Sintering temperature of these systems were between the solidus and liquidus temperature but exact sintering temperature depended on the characteristics of the constituent powders. An elaborate report on this has been presented by Esper and Leuze.[17] Effect of powder particle size on the properties of Al-4 wt. % Cu alloy were reported after sintering the green compacts at $590^{\circ}C$ in dry nitrogen. With decreasing particle size of alloying additive, pore size of the sintered parts got reduced. The dilation effects started above $548^{\circ}C$ and subsequently tensile strength decreased. This phenomenon has been explained on the basis of quick liquefaction of small alloying particles, disappearance of liquid by

diffusion and the homogeneous structure of the compacts. Authors[17] on the basis of dilatometric measurement reported swelling of Al-Cu compacts, which was due to the penetration of aluminium grain boundaries by the melt. Densification parameter peak has been reported to be shifted towards lesser time with increasing amount of copper in aluminium.[18] The results were interpreted on the basis of liquid phase amount in Al-Cu alloy. More is the amount, better is sintering due to the liquid flow activated mass transport mechanism. Activator, such as boron appeared to decrease liquidus temperature of alloying, thus enhancing the liquid phase sintering. Experimental results on the sintering behaviour of Al-Cu system indicated[19] that effective sintering was possible, when the volume of liquid phase was >20%. The complete solution of copper is required during the sintering of Al-Cu premix compacts. Sintered aluminium alloy with 4 to 6 wt.% of copper has been reported to possess mechanical strengths near to those for the sintered bronzes.[11,20] Addition of solid lubricant (commercial amid wax) contributed to dimensional changes of compacts by the volume effect due to the decomposition of wax.[12] Effects are related to the spreading of liquified wax and co-existing enclosure of gas in the compact.

Copper coated alumina particles were also introduced in aluminium compact for preparation of Al-Cu-Al_2O_3 particulate composite.[21] Sintering was carried out in vacuum at 525°C for 24 hours. Dimensional growth of compact was

observed, which was attributed to the formation of $CuAl_2$ during sintering. Mechanical properties of composites got improved by age-hardening and subsequent deformation.

I.3.3. Sintering of Al-Cu-Si Alloy:

Sintering of Al-Cu-Si system is not studied in much detail. There is no evidence of significant solution of silicon during the sintering of Al-Cu-Si powder premix. The presence of free silicon has a deleterious influence on the mechanical properties of sintered alloys.[19] Addition of silicon to Al-Cu alloy reduces the eutectic temperature to 524°C. So the sintering temperature is reduced in comparison to Al-Cu alloy. Sintering thus results into retardation of the diffusion of copper. Silicon particles in general segregate at grain boundaries.

I.3.4. Sintering of Al-Cu-Si-Mg Alloy and Its Composites:

Al-Cu-Si-Mg system is studied in great detail by research group at ALCOA.[1-4] Effect of processing parameters on sintered properties is reported by Dudas and Dean.[1] 201 AB and 601 AB aluminium alloys were compacted to 85, 90 and 95% of theoretical density, sintered at 621°C in dry nitrogen and heat treated to different thermal cycles. Table I.4 shows the sintered properties of 601 AB and 201 AB aluminium alloys. Tensile strength varied from 110 to 310 MPa and hardness from 55 to 90 Rockwell for compact sintered and heat treated to T6 condition. Machinability, electrical conductivity and corrosion properties have also been reported.

Table I.4 Mechanical Properties of Sintered (a) 201AB (b) 601AB Aluminium Alloy[1]

(a)

Green Density		Thermal Condition[b]	Tensile Strength psi	Yield Strength psi	Elongation Percent in 1 in.	Apparent Rockwell Hardness
Percent	g/cm^3					
85	2.36	T1	24,500	21,000	2.0	60/65 R_e
		T4	30,500	26,000	3.0	70/75 R_e
		T6	36,000	-	-	75/80 R_e^c
90	2.50	T1	29,200	24,600	3.0	70/75 R_e
		T4	35,600	29,800	3.5	75/80 R_e
		T6	46,800	-	-	85/90 R_e
95	2.64	T1	30,300	26,200	3.0	70/75 R_e
		T4	38,000	31,000	5.0	80/85 R_e
		T6	48,100	47,500	2.0	85/90 R_e

(b)

85	2.29	T1	16,000	7,000	6.0	55/60 R_h
		T4	20,500	14,000	5.0	80/85 R_h
		T6	26,500	-	1.0	70/75 R_e
90	2.42	T1	17,500	8,000	7.0	60/65 R_h
		T4	-	-	-	80/85 R_h
		T6	32,500	31,000	2.0	75/80 R_e
95	2.55	T1	18,000	8,500	8.0	65/70 R_h
		T4	22,000	15,000	5.0	85/90 R_h
		T6	36,500	35,000	2.0	80/85 R_e

Alloy 601 AB exhibited electrical and thermal conductivity characteristics approximately 95% of wrought 6061 alloy under similar conditions. The effect of sintering atmosphere, dew point, temperature on the mechanical properties and dimensions of compacts have been extensively reported for 201 AB and 601 AB alloys.[2] Dimensional changes as a function of green density of compact are shown in Figure 1.3. Dimensions increased with increasing sintered density in all the atmospheres. There was either shrinkage or no change in dimension of green compacts compacted to 85% theoretical density, whereas, higher density compacts exhibited growth after sintering in dissociated ammonia and vacuum. Specimens sintered in nitrogen experienced shrinkage over the full density range. Alloy 201 AB provided combination of strength, ductility, impact and fatigue properties. Cold coining of sintered compacts raised strength but lowered the ductility, whereas, hot coining was proved suitable in improving the end properties.[3]

Amato et al.[22] also carried out the study of the sintering behaviour of 201 AB and 601 AB alloys. Alloy powders were compacted to 95% of theoretical density and sintered at 600°C in dry nitrogen and air followed by sizing and heat treatment. Air sintering was inferior to nitrogen sintering, but the differences in the properties could be minimized by optimizing the sintering cycle. Microstructure of the nitrogen sintered compacts were homogeneous and good bonding were obtained, whereas, air

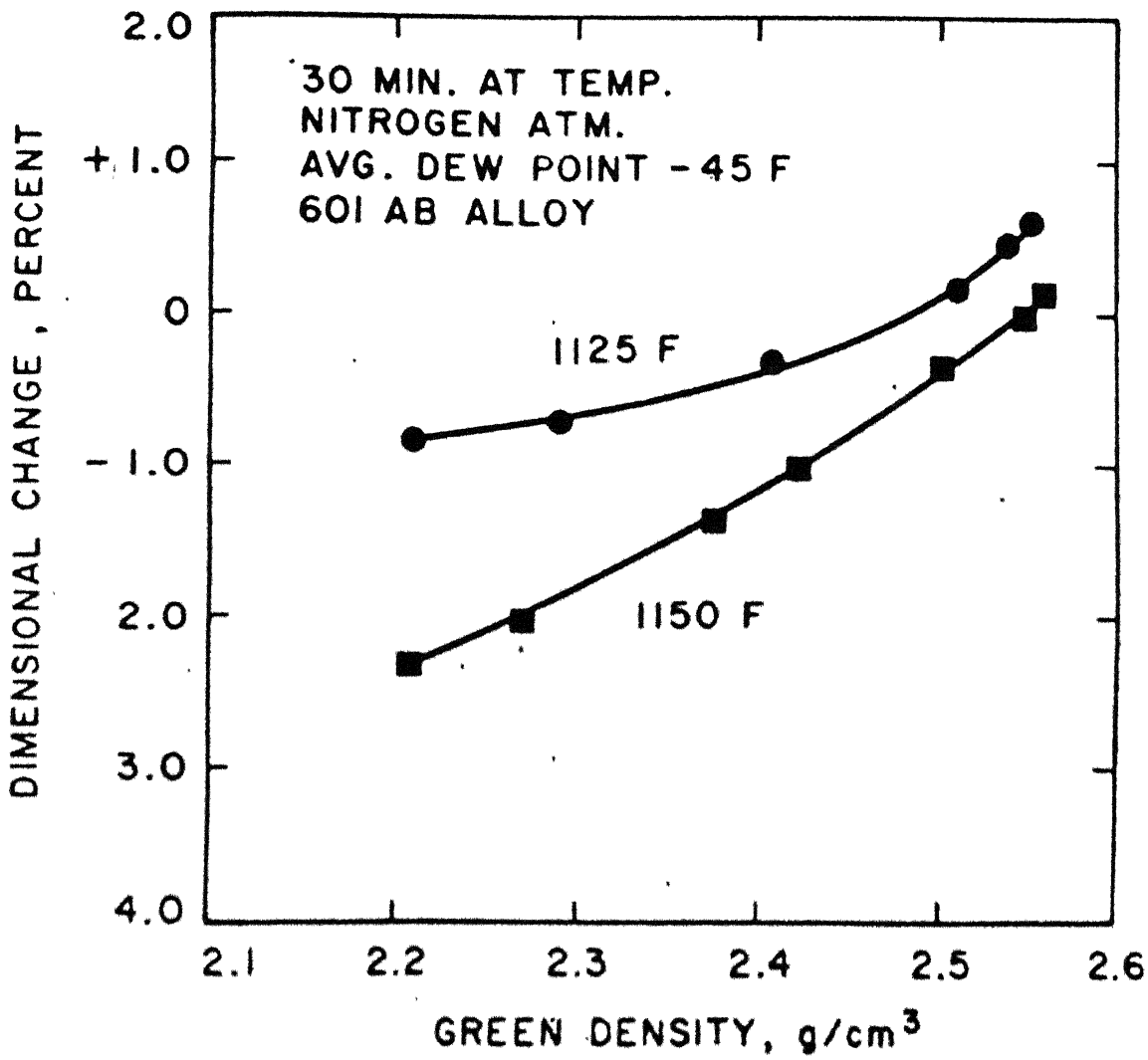

Fig.1-3 EFFECT OF DENSITY AND TEMPERATURE ON DIMENSIONS[1].

sintering induced eutectic segregation and inhomogeneity in the microstructure. 201AB attained better mechanical properties than the 601 AB alloy.

Further work is also reported on 201 AB alloy with addition of Co-Mo base intermetallic 'Tribaloy'[23]. Aluminium alloy with 5 to 20 vol.% of tribaloy were compacted and sintered in dry nitrogen. The composite had very high sliding wear properties. Best properties were obtained when a thin diffusion layer was created around the intermetallics in the structure.

Sintering behaviour of 201 AB alloy composites containing Tribaloy, WC, TiC-Mo_2C and alumina have been reported by Jha.[24] Variables like, volume fraction of dispersoid, sintering atmosphere (argon, nitrogen and vacuum) were used and effect on composites was studied. Sintering of such composites resulted in dimensional growth. More than 8 vol. % dispersoid addition imparted poor properties to the composites. Figure 1.4 shows the UTS values of various 2014 alloy base composites sintered in different atmospheres. Tribaloy imparted best properties to the composites due to the better compatibility of matrix/dispersoid resulting from improved wettability. Dryness of sintering atmosphere was reported[24] to effect the properties of the composites.

I.3.5. Sintering of Al-Zn Alloy:

A limited information is available on sintering of Al-Zn alloys.[25-26] In Al-Zn system, liquid phase sintering increases[26] the volume of the compacts, in case the Zn

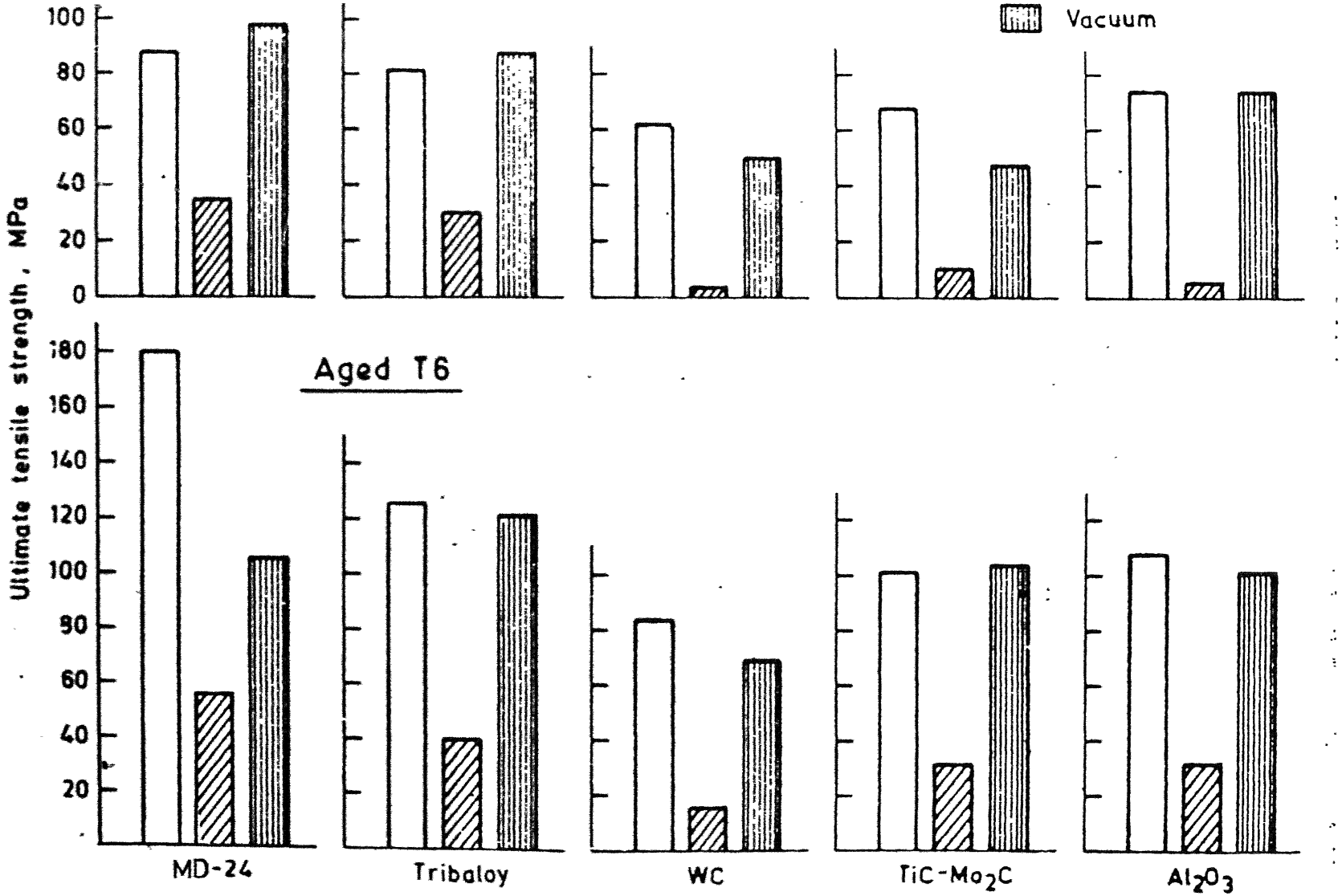

Fig. 1.4 Variation in the ultimate tensile strength of composites containing 4 vol. % dispersoids in as sintered and aged conditions[24].

concentration does not exceed its solid solubility limit at the sintering temperature. Such a volume growth appeared to be more, in case the particle size of the aluminium was large.

I.3.6. Sintering of Al-Zn-Mg Alloy:

Zinc imparts better corrosion resistance, higher mechanical and welding properties to Al-Mg alloy than Al-Mg-Si alloy. Esper and Leuze[9] studied the physical and mechanical properties of sintered Al-Zn-Mg alloys. Total amount of Mg and Zn was varied from 6 to 9 wt. % in the alloy. Maximum mechanical properties were attained for the compacts after sintering at 610°C. Dilation behaviour of Al-Zn-Mg is shown in Figure 1.5. It is evident that dimensions of the compact changes marginally up to 400°C beyond which dilation depended upon the alloying element. Dimensions remained unchanged for any alloy compositions between 510 to 600°C. Such variations were coinciding at melting point of Zn (420°C) and the eutectic temperature of Al-Mg (440°C).

I.3.7. Sintering of Al-Zn-Mg-Cu Alloys:

Addition of Cu to Al-Zn-Mg alloy system changes the sintering temperature for achieving the optimum properties. Sintering temperature of 590°C was found suitable for Al-Zn-Mg-Cu alloy, whereas in case of Al-Mg-Zn alloy sintering temperature of 610°C was required to achieve optimum property. Similar to wrought alloys, copper addition increased mechanical properties of Al-Zn-Mg alloy. In contrary to other

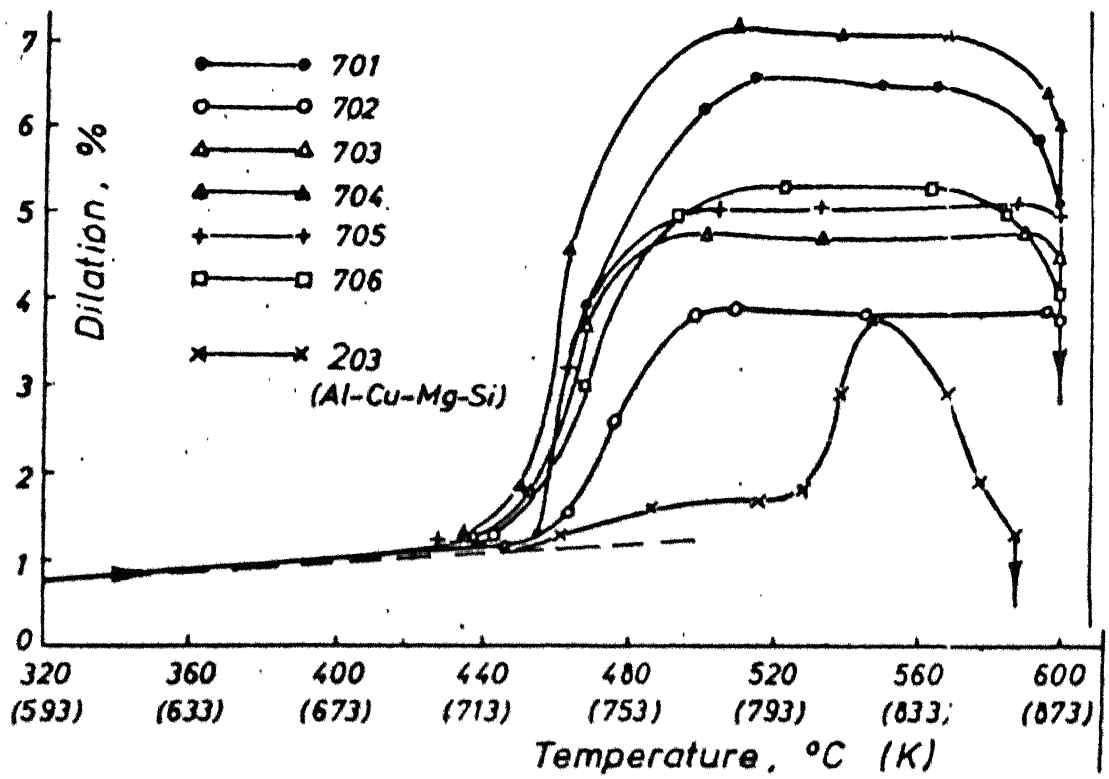

Fig-15 Dilatometer curves of the alloys 701 to 706[9]

mechanical properties, fatigue strength of the compacts were identical for sintered as well as heat-treated compacts.

I.4. Sintering Mechanism for P/M Aluminium Alloys:

Sintering of pure aluminium powder compacts is associated with unavoidable problems due to the thermodynamically very stable thin aluminium oxide film which coats the aluminium particle. The oxide film present thus prevents diffusion processes necessary for the formation of necks during sintering. Furthermore, it is impossible to reduce the aluminium oxide using normal sintering atmosphere.

Liquid phase sintering is the undisputed method for powder metallurgy processing of aluminium alloys. The advantages of such a production process are: low sintering temperature, fast densification, homogenization, high final densities and microstructures that often provide mechanical and physical properties superior to those of solid state sintered materials.[27]

Sintering of aluminium alloy containing copper, magnesium and silicon as alloying elements which form low melting eutectics with aluminium is example of transient liquid phase sintering.

There are three stages which are involved during liquid phase sintering.[28-30]

1. The liquid flow or particle rearrangement: While heating to sintering temperatures, areas which have built up low melting point compositions by diffusion during heating form a

a liquid phase. In conditions of good wetting (wetting angle $\theta < 90^{\circ}$) liquid phase is pulled by the capillary force into the particle necks and small pores. The liquid flow may also result in residual pores at the sites of the low melting point particles. If the network of solid particle is less rigid, capillary force may lead to a co-operative movement of melt and particles. Particle rearrangement results in shrinkage with an almost linear time dependence.

2. Dissolution and reprecipitation: The change in size shape and continuity of particles during sintering are associated with the dissolution of solid materials in the liquid phase and reprecipitation on other sites. Material dissolves at solid/liquid interfaces with higher chemical potential and reprecipitates at sites of lower chemical potential. This stage produces shrinkage at a less linear rate and produces the shape adjustment of adjacent grains which is characteristic of liquid phase sintered structure.

3. The solid state sintering: In case of imperfect wetting or if liquid phase is eventually dissolved into the solid solution, rigid skelton is formed and sintering proceeds by the established mechanism for solid state sintering i.e. diffusion transport from grain boundaries to the neck area. The shrinkage rate during this stage is lower than during the preceeding one.

A large number of literature[17,31,32] are available, which elucidate the mechanism of sintering of aluminium alloys.

Tenacious oxide, film over the aluminium particle is ruptured during compaction, thus resulting into metal to metal contact. During sintering the metal, i.e. aluminium expands more than its oxide layer over the particles and the hair line cracks are also developed on the oxide layer. A dry and non-oxidizing atmosphere is required to prevent oxidation, thus allowing diffusion and alloying. During heating when temperature exceeds the aluminium-alloying element solidus, a liquid alloy phase forms at the contact points, which ruptures the oxide layer. This results in a rapid alloying. In case of Al-Cu, at a temperature greater than the eutectic temperature, the eutectic alloy becomes liquid phase, which increases rapidly in amount till all the copper particles disappear. Alumina scale along the particle boundaries scatters into liquid phase resulting in a marked increase in the compact strength. If sintering is continued for a longer period, copper atoms diffuse into the aluminium matrix to become aluminium copper alloy.

To understand the spreading behaviour of liquid phase during sintering of Al-Cu alloy model experiments were carried out by Kehl and Fischmeister.[31] Schematics of their experiments are shown in Figure 1.6. When Al-Cu alloy of eutectic composition and aluminium substrate were kept in plane surface contact, no reaction occurred other than the rounding off into a drop shape of the eutectic alloy (Figure 1.6b). However, when metal to metal contact was established after indenting the point of a conical piece of eutectic

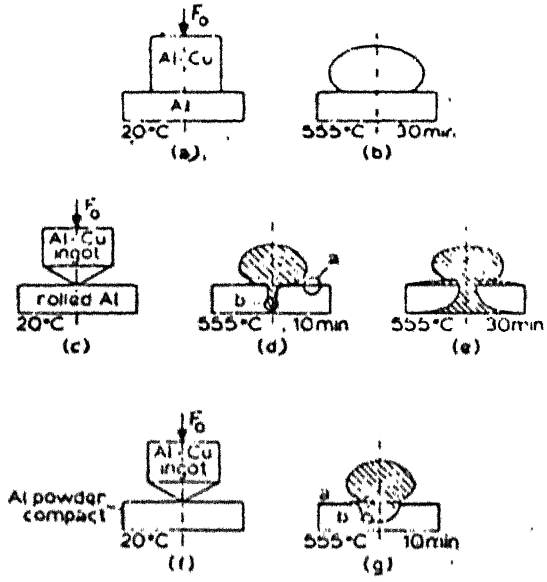

Fig 1.6 Schematics of spreading of Al-Cu melt on aluminium substrate[31]

alloy into the substrate, liquid spread fairly evenly over the substrate surface, undermining and lifting the oxide layer. After reaching the bottom surface of the aluminium disc the liquid again spreads between the surface and its oxide layer. When the substrate consisted of compacted aluminium particles the liquid penetrates uniformly in a hemispherical zone. The absence of wetting in case of plane contact and in the zone of tangency between alloy and substrate surrounding the point of indentation was explained by the fact that eutectic alloy was enclosed in a sac of oxide, so that only oxide to oxide contact was established. On the other hand, when the liquid alloy enters the enterior of the porous substrate through metal to metal contact formed by indentation, it finds an atmosphere in the void space on which oxygen has been largely consumed by reaction with the aluminium powder during heating. In this situation the advancing liquid was not oxidized but formed direct contact with the oxide on the particle which it could wet. The electron microscopic observation also showed that during sintering dendrite shaped copper particles melted earlier than the spherical ones. It was felt that the fine points of the dendrite copper particles penetrates the oxide skin of the aluminium more easily than the blunt contact made by the spherical copper powder.

Watanabe and Yamada[32] attempted to study the effect of copper adding method on the strength of sintered Al-Cu alloy compacts. Three methods for introducing copper in

the metal were used. For mixed powder, a blend of liquid atomized aluminium and electrolytic copper powders were selected, whereas for prealloyed powders, liquid atomized alloy powder was used. Composite powder was prepared by immersing the liquid atomized aluminium powder in aqueous solution of 3 wt. % copper sulphate. Sintering was carried out at 560^{o}C in hydrogen atmosphere. Maximum strength by each compact was attained after 60 minutes of sintering. It was reported that using only mixed powder, compacts of normal strength could be obtained. This was attributed to the adequate amount of liquid phase appearing over eutectic temperature in case of mixed powder. It was shown that the amount of liquid reached near the maximum value 33% until the beginning of the 560^{o}C after which it gradually decreased with time to near the minimum value(18%). According to phase diagram using prealloyed powder approximately 18% liquid phase would appear. And finally using composite powder, appearance of liquid phase could be similar to that of premix powders. Since not only do the aluminium and copper particle adhere together completely but also the contact area being extensive, the diffusion of copper atoms into the aluminium material should be comparatively more and, thus the amount of liquid phase in this case must be between the mixed and prealloyed ones. Schematic representation of structural changes of the Al-Cu compacts using mixed, prealloyed and composite powder is shown in Figure 1.7. It is evident from the figure that in the case of mixed

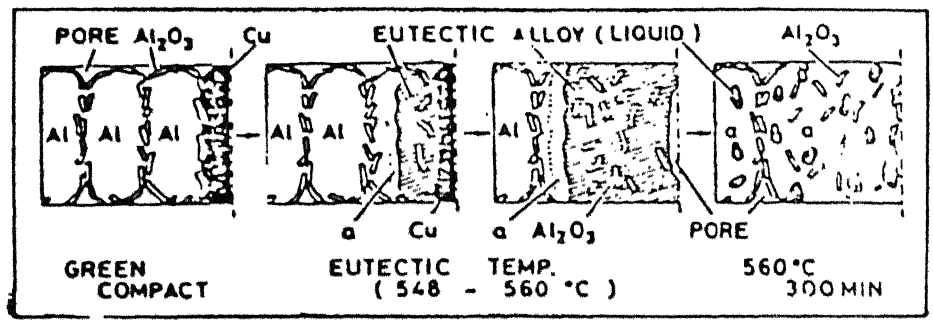

(a)

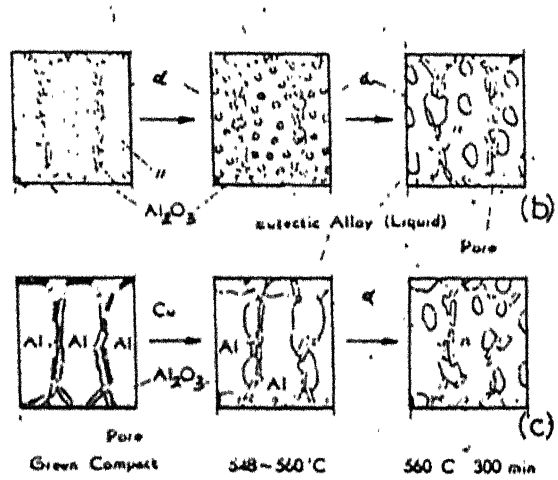

Fig. 17 Schematic representation of structural change of the aluminium-copper compact using (a) mixed (b) prealloyed (c) composite powder, during sintering[32]

powder the liquid phase appearing over the eutectic temperature during sintering was sufficient to remove the alumina scales from the particles boundary, unlike the prealloyed and composite powders.

1.5. Other Consolidation Methods for Aluminium Based Powders:

Among various methods of consolidation of metal powders, extrusion, hot-pressing and forging are noteworthy. Pickens[33] reviewed in depth various consolidation methods for high strength aluminium alloys. Schematics of the processes are given in Figure 1.8. Major impediment in the fabrication of aluminium-powder product is the oxide coating which reduces metal to metal contact and gives rise to poor end properties. Such a layer is undesirable as it creates safety hazard, when compacted at high temperature in the confined die due to rapid evolution of hydrogen. It is, therefore, advisable to degas and preheat the aluminium powder and/or green compacts at initial stages to impart excellent properties to the compacts. There are several ways by which steam after hydration may be removed from aluminium powders. Degassing is carried out in a suitable atmosphere at an ambient temperature for different periods. It has been reported[34] that powder should be degassed at a temperature equal to or greater than the temperature reached during processing or in operation, in order to get pore free and/or surface blister free components. Experiments have been carried out by authors[35] to explore the possibility of

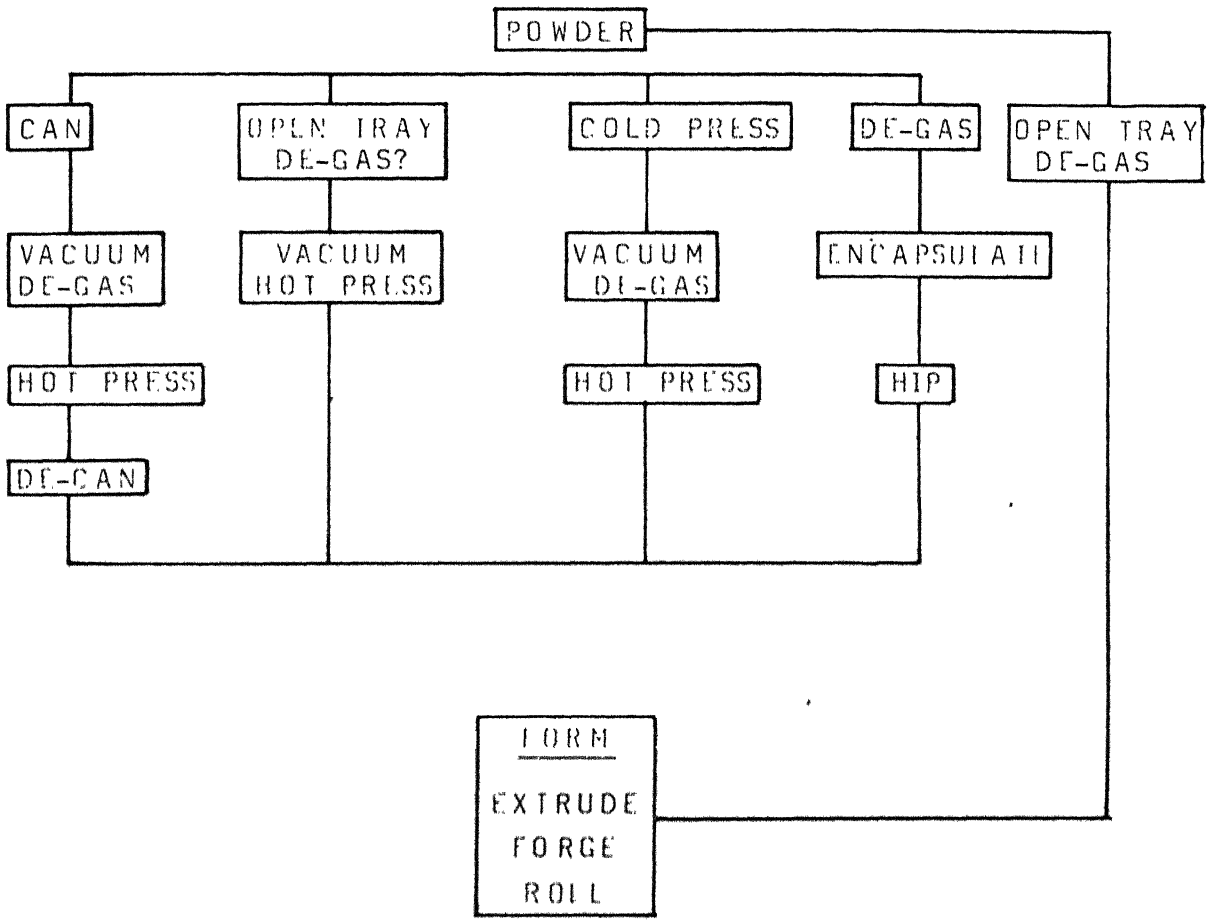

Fig.1.8 Schematics of processes for consolidation of aluminium alloy powders[33]

handling the aluminium powder for quite long time in open atmosphere without the risks of rehydration. It has been suggested that aluminium powder degassed at an elevated temperature in open tray in argon atmosphere would not rehydrate up to 120 hours. This process is quick and argon adsorbed can be removed easily during preheating. Time and temperature of degassing could be economized further by using vacuum heating of the powder. A temperature of 350°C and vacuum level of 3×10^{-4} torr has been found suitable for degassing the powder.[36] In general, after degassing powder is not exposed to air. In case of vacuum degassing powder is sealed in a can, degassed and formed directly viz. extruded, rolled or compacted. When the powder is directly compacted; preheating at 480°C for one hour in argon atmosphere gives rise to hydrogen free compacts. Recently it is becoming a common practice that once manufactured the powder must not be allowed to oxidize and P/M processing may be accomplished immediately. An alternative method is that powder be stored in helium atmosphere.

I.5.1. Hot Pressing:

Hot pressing method is now-a-days rarely used for any aluminium alloy development or part production. It produces net shape compacts having 100 percent density; annealing of the powder may be reduced, and large billets or preforms may be produced in one production cycle. In hot pressing amount of deformation is less as compared to

other forming techniques such as extrusion, forging etc. Major problem in this case is the selection of die material.

I.5.1.1. Aluminium:

Although oxide layers on the aluminium particles are undesirable a substantial improvement in properties due to the fine dispersion of ruptured oxide films in the matrix has been reported in literature.[14] Goetzel[14] has reviewed the properties of hot pressed aluminium compacts. Hot pressing temperature up to 500°C did not effect the UTS or elongation substantially, but compaction at 600°C imparted best combination of UTS and elongation.

I.5.1.2. Al-Si-Cu-Mg Alloy:

Aluminium alloy with up to 45% silicon by P/M route has been reported by Skelly and Dixon.[37] Processing steps involved cold isostatic pressing and hot pressing. Hot pressing temperatures were varied according to the eutectic temperature of alloys and suitable heat treatment were also carried out. In addition to dispersion of very fine primary silicon, eutectic phase was also refined. Copper and magnesium addition did not effect the size of primary silicon. Tensile strength, hardness and wear resistance of the Al-Si alloy increased by addition of copper and magnesium and by heat treatment. Increase in amount of silicon increased the UTS and decreased the elongation. Maximum mechanical properties were attained by Al-35% Si-2.5% Cu alloy, hot pressed at 550°C. Hot pressing

temperature higher than that of eutectic temperature of the alloy imparted better properties than the compacts pressed at a temperature lower than the eutectic.

I.5.2. Extrusion:

P/M aluminium-alloy is extruded in the same way as cast aluminium-alloy. Powder is first cold compacted and then hot extruded. P/M extrudates contain inherently a small amount of alumina due to the oxide layers on aluminium powder. Presence of oxide over aluminium powder alters the extrusion process properties of extrudates. Duszczyk and Jongenburger[38] reported the effect of oxide content on tensile properties of aluminium extrudates. Table I.5 shows the tensile properties of aluminium extrudates. Most of the high strength or stable P/M aluminium alloys are produced by extrusion method.[33] Table I.6 enlists the best properties obtained on high strength experimental P/M alloys. Comparison between the extrudates produced by powder metallurgy and ingot metallurgy route is reported by Duszczyk and Jongenburger[38] (Table I.7). Tensile strength of P/M extrusion product is superior to that of IM extrusion product but elongation value of IM extrudate is more than that for P/M extrudates. A series of technical reports are available describing the extrusion of aluminium alloy and its based composites.[3,39-42]

Table I.5
Tensile properties of aluminium extrudate[38]
(extrusion temperature - 573K)

Material	Reduction ratio	Proof stress 0.2% off set MN/m^2 R_{mo2}	Ultimate tensile strength UTS MN/m^2 R_m	Elongation %A
Al-0.3 Al_2O_3	1.32:1	incoherent product		
	1.6:1			
	2.1:1	80.0	114.0	8
	2.6:1	85.0	123.0	14
	3.2:1	91.0	132.0	17.5
Al-0.26 Al_2O_3	5:1	82.0		
	10:1	81.0		
	20:1	89.0		
	30:1	87.0	12.1	56
	40:1	90.0		
	50:1	90.0		
Al-1.1 Al_2O_3	5:1	105.9	115.1	4.0
	10:1	102.3	128.5	21.9
	20:1	101.7	126.7	24.0
	30:1	97.0	135.4	29.9
	40:1	103.8	136.4	28.8
	50:1	100.4	138.5	27.5
Al-1.9 Al_2O_3	5:1	121.0		
	10:1	118.0		
	20:1	123.0	160	25
	30:1	121.0		
	40:1	124.0		
	50:1	130.0		

Table I.6 Best Properties Obtained On High Strength PM Alloy[33]

Name of alloy	Process of powder manufacture	Basic composition (wt%)	Product form	Yield stress YS (MPa)	Ultimate tensile strength UTS(MPa)	Elongation (%)	Reduction a
	Atomized	10.36 Zn 3.08 Mg 2.03 Cu 1.74 Mn 0.2 Cr	Extrusion	810	820	4	
	Atomized	12,32 Zn 1.8 Mg 1.95 Cu 0.2 Cr	Extrusion	743	750	8	
7049	Splat-cooled	+ Fe + Ni + ODS	Extrusion	634	717	9	20
	Atomized	9.87 Zn 4.06 Mg 0.85 Cu 1.25 Mn 1.06 Fe 1.39 Ni		855	879	1.2	
MA67	Atomized	8 Zn 2.5 Mg 1.0 Cu 1.5 Co	Extrusion	641	669	11	
MA87	Atomized	6 Zn 2.5 Mg 1.5 Cu 0.4 Co	Extrusion	586	614	12	
Modified 7xxx	Atomized			641	683	5	
2024		+25 vol% SiC	Extrusion		641	1	
	Splat-cooled	9.8 Zn 7 Zn 2.5 Mg 1 Cu 0.8 Co		665	720	8	

TABLE I.7

Tensile properties of P.M. and I.M. aluminium alloys extruded product[38]

Alloy -series-	Proof stress 0.2% off set MN/m^2 Rmo2	Ultimate tensile strength UTS MN/m^2 Rm	Elongation %A	Remarks -Powder (P -Atomised (A) -Conventional -Rapidly solidified (-Ingot (i)
Al-Mn-(Cu) -3003-	145	207	24	P-A-C = 10^3 K_s^{-1} (cooling rate)
Al-3.6 Mn -3xxx-	140	208	27	P-A-C = 10^3 K_s^{-1}
Al-4.5 Mg-Mn-Cr -5083-	262	400	14	P-A-C = 10^3 K_s^{-1}
Al-7Mg-Mn -5xxx-	400	490	25	P-A-RS = 10^5 K_s^{-}
Al-10Mg-Mn -5xxx-	402	495	18.5	P-A-RS = 10^5 K_s^{-}
Al-4Fe-4Ni-4Co	492	500	9	P-A-RS = 10^5 Ks-
Al-2Fe	225	276	17	P-A-RS = 10^5 Ks-
Al-Mn(Cu)- -3003-	83	131	32	1
Al-4, 5Mg-Mn-Cr -5083-	138	303	28	1

I.5.2.1. Al-Mg Alloy:

Al-10 Mg shows extensive segregation during the normal ingot solidification which makes this alloy undeformable even at high temperature. Rapidly solidified powders of Al-10 Mg were compacted and hot extruded by Tan et al.[39] It has been reported that the pressure requirement of extrusion were less than that for cast Al-7 Mg. Properties of extruded Al-10 Mg alloys were comparable to the peak aged 7050 alloy. But the extrudates were extremely unstable and showed loss of strength at room temperature. Alloy also softens during extrusion which was explained on the basis of dynamic recrystallization. Mechanical properties of alloy depend upon the extrusion process parameters.

I.5.2.2. Al-Si Alloy:

Silicon improves the wear and heat resistance properties of aluminium. However, in cast alloy increasing silicon content (>20%) leads to lower strength and poor machineability. Extrusions of Al-Si (up to 30%) alloy produced by P/M have high room temperature strength and about 10 times higher ductility than the conventional cast alloy.[40] The process steps were: cold isostatic pressing the alloy powder, canning and degassing at 470°C and extrusion of compact with a speed of 20 mm/sec at 6.5 extrusion ratio. Extrusion of such alloys showed refinement and homogenization of silicon particles, which improves the

to those of cast alloys at room temperature and at 400°C. At 400°C UTS of the extrudates was independent of silicon content. Wear resistance of Al-17%Si alloy was superior at high sliding speed to that of cast alloys.

I.5.2.3. Al-Zn-Mg-Cu Alloys:

7XXX series of aluminium alloy is used as high strength material. Extensive work has been carried out at ALCOA and other organisations to improve the properties of this alloy. P/M route provides an excellent combination of strength, stress corrosion cracking and fatigue strength properties to 7XXX series alloys. Lyle et al.[3] studied the effect of size and shape of powder, on the properties of Al-Zn-Mg-Cu P/M extrusion. Compacts were made by following steps: isostatic pressing of prealloyed powder, heating of the compact in argon atmosphere and hot extrusion at a ratio of 10:1. Density of extruded product increased with decreasing powder size. Notch tensile strength, yield strength and elongation decreased with increasing amount of second phase particles. Irregular shaped powders were superior to those of other types. Vacuum preheating and compaction of fine irregular shaped particles resulted in superior transverse ductility and toughness for P/M 7075 and 7050 alloy, as compared to ingot metallurgy products.

Rapidly solidified powder of 7050 composition have been processed through extrusion process by Parkinson and Sheppard.[41] The process involved, cold compaction, heating and extrusion in the rod form. Canning and vacuum degassing

step were eliminated. A metastable phase was reported in the structure which underwent localized melting and caused blistering during heat treatment, but proper heat treatment could prevent blistering. Mechanical properties were correlated with the process variables. Increase in extrusion temperature resulted in increased elongation, although UTS was least effected.

I.5.2.4. Al-Zn-Mg-Cu-Co-Fe-Ni System:

P/M technique has the special feature that alloying elements which cannot be introduced in alloy by ingot route due to inherent problems associated with the process, can be successfully introduced in alloy by using prealloyed powder. Processing by ingot route results in segregation of coarse intermetallic phase particles and ingot cracking. Lyle and Cebulak[42] after addition of Co, Fe and Ni in Al-Zn-Mg-Cu P/M alloy, reported resistance to coarsening. Fabrication steps for these alloys were: cold compaction preheating, hot compaction, hot extrusion and heat treatment.

I.5.2.5. Al-Fe-Ni-Co Alloy:

McShane and Sheppard[43] have made use of extended solid solubility of Fe-Ni-Co in aluminium for stable structure at high temperature. Rapidly solidified aluminium powder containing 3.8% Fe, 3.6% Ni and 3.8% Co were selected for preparing the extrusions. The powders were compacted and extruded to the extrusion ratio 20:1 at elevated temperature. Extrudates were quenched immediately after extrusion.

The structure of extrudates were modified and were much coarser than the individual powder. Yield stress was affected by the extrusion parameters. Figure 1.9 shows the variation of proof stress and elongation of the extrudates with extrusion temperature. High temperature imparted lower tensile values. As the strengthening mechanism operative was dispersion hardening, higher temperature resulted in coarse dispersoid and large subgrain size, which finally deteriorated the mechanical properties. Elevated temperature properties of these alloys were also reported[43] to be promising.

I.5.2.6. $Al-Al_2O_3$ System:

SAP is one of the oldest P/M material which is produced by extrusion. Irmann[44] reported the preparation and elevated temperature properties of sintered aluminium powder. Aluminium flake powders were ball milled in air intensively to produce oxide in powder depending upon the amount of dispersoid required in the product. Milled powders were compacted, hot pressed and hot extruded or forged. Extrudates exhibited high temperature strength, which remained maintained even after prolonged heating at 500°C. It was shown[45] that the room temperature mechanical properties of extrusion were a function of oxide content of the powder. Higher the oxide content higher was the tensile strength and hardness, and lower the ductility.

Lenel et al.[8] reported that the tensile strength and yield strength of aluminium powder extrusion were the

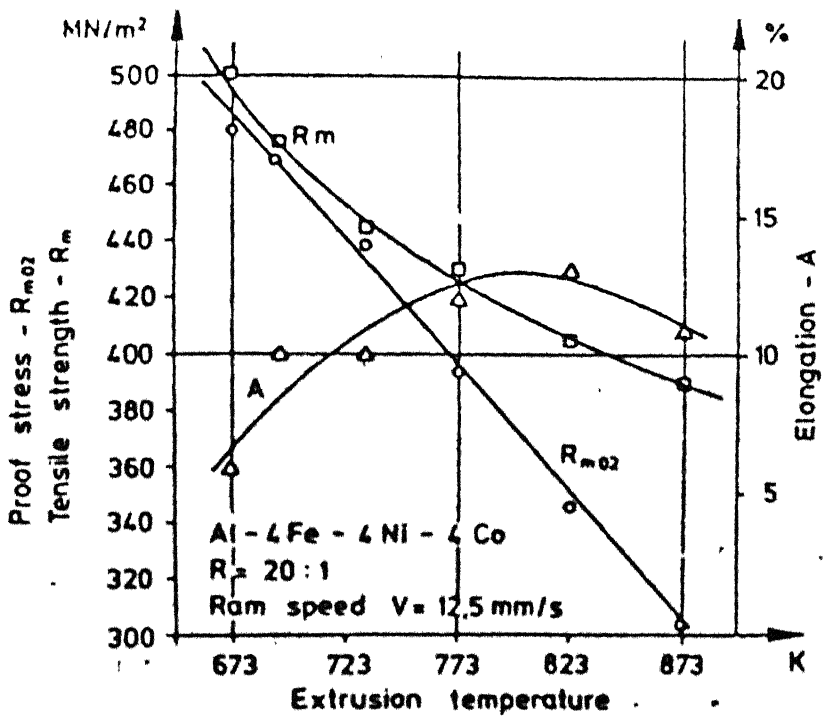

Fig. 19 Variations of stress and elongation with extrusion temperature[43]

function of the flake powder thickness. The production of extruded rods from aluminium powder involved the following steps: Compaction, hot pressing and hot extrusion at a reduction ratio of 16:1. Prior to processing the powders, these were treated to increase the oxide content by heating in air or steam. Oxide content varied from 1.1 to 16.5% whereas flake thickness ranged from 0.4 to 2.3 μm. Diameter of the flakes were from 5 to 147 μm. Tensile strength of the composite at room temperature and at 400°C increased linearly with logrithm of flake thickness.

Aluminium-alumina composite was also produced by conventional compaction followed by cold extrusion.[46] Aluminium with up to 30% oxide were mixed in planetary ball mill, compacted and extruded. Extrudate had good strength properties in combination with excellent wear resistance.

A comprehensive work on extrusion of aluminium-metal oxide system is reported by Hansen.[47] Effect of materials and process variables on the properties of extrusion was studied. Variables included size of aluminium and aluminium oxide powders, concentration of oxide, types of oxides, temperature of extrusion, reduction ratio, heat treatment and homogenization of products by double extrusion. Al_2O_3, SiO_2, and ZrO_2 were selected as dispersoid. Process steps involved were: blending, cold compaction, hot compaction, extrusion and heat treatment. Microstructure of the extrusions showed deformed cylindrical shaped aluminium particles alongwith oxide agglomerates. With decreasing size of

aluminium powder, size of the oxide agglomerates as well as distance between mixed boundaries (i.e. with oxide) decreased and tensile strength and rupture life of the compacts increased. Reduction in temperature of billet increased the tensile strength and decreased the elongation of the composites where at tensile properties at 400°C were uneffected. Sheppard and Chare[48] also reported that low extrusion temperature resulted in high proof stress and low elongation for Al-Al_2O_3 composites. Figure 1.10 shows the variation of proof stress and elongation as a function of extrusion temperature for aluminium-alumina composites.

High temperature stability of Al-Al_2O_3 is attributed to the dispersoids of alumina particle in the matrix. It is pointed out[49] that high temperature stability of Al-Al_2O_3 system made by mechanical alloying is retained to temperature only at 50°C below the melting point of aluminium. A systematic study on strengthening of Al-Al_2O_3 associated with such processing(i.e. mechanical alloying)is reported in literature.[50]

I.5.2.7. Al-Al_4C_3 System:

Al-Al_4C_3 composites produced by extrusion method is reported by Jangg et al.[51] A suitable additive (carbon black) was added to aluminium powder which after mechanical milling turned to be Al_4C_3. Carbon up to 5% could thus be admixed to aluminium powder; correspondingly 20% Al_4C_3 could be introduced in the composite. Powder mixtures were compacted and extruded at 550°C with a reduction ratio of

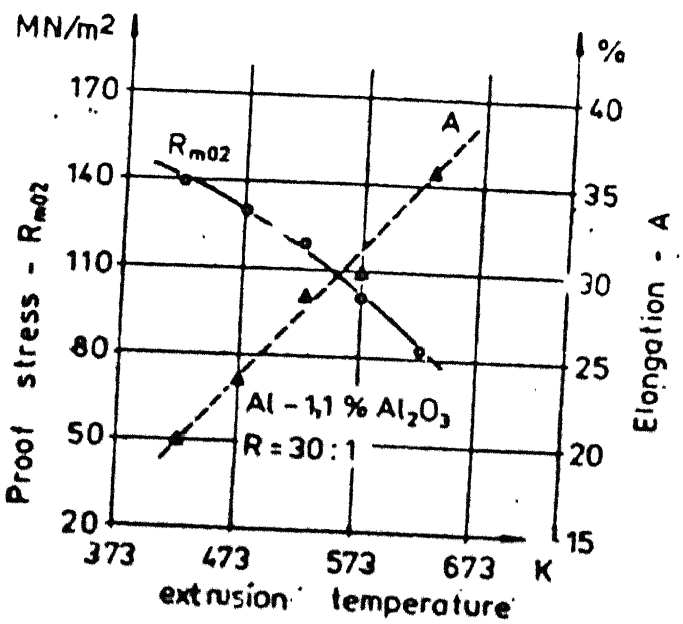

Fig 10. **Proof stress and elongation as a function of extrusion temperature**

1:9. A size range from 100 to 300 μm of carbide dispersoid imparted best properties to extrudates. The products had excellent room and elevated temperature properties. Tensile strength of composites increased with increase in carbide addition and decreased at high temperature. Al_4C_3 dispersoids were stable at high temperature, and did not tend to agglomerate.

I.5.2.8. Al-Al_2O_3-Al_4C_3 System:

A new class of material named as 'DISPAL' is synthesised by Arnhold and Baumgarten[10] and reported to be stable at high temperature. Aluminium powders were ball milled with carbon (graphite) in air. By varying carbon additions and milling condition, a suitable combination of carbide and oxide could be generated, preferably in the range of 0 to 3 wt. % carbon and 0.4 to 2.5 wt. % oxygen. Oxide and carbide were reported to be interchangeable as dispersoid and total maximum amount of dispersoid was 18 vol. %. Fabrication steps included: powder cold isostatic pressing, heating and extrusion. A temperature of 500°C and extrusion ratio 35:1 were selected to disperse the oxide effectively in matrix. The composite showed stability even at a temperature of 500°C.

I.5.2.9. Al-Glass System:

Glass (borate and silicate) has been incorporated in aluminium by a route of compaction and hot extrusion and forging.[52] Powder mix was first compacted to 80%

theoretical density and then was extruded at 540°C with deformation ratio of 98%. Both the constituents in the composite could be deformed and an atomic bond was formed between the new surfaces generated due to deformation. Such a phenomenon imparted superior mechanical and tribological properties to the composites. Al-20% glass showed 50% wear as compared to normal age hardened Al-2Cu-Mg alloys. Wear resistance of Al-12Si also increased in extruded form after glass addition.

Table I.8 lists tensile properties of extrudates of aluminium and its composites.

I.5.3. Forging:

Powders which have high tap density (i.e. round shaped powders) may directly be forged to final product with near to theoretical density. P/M forgings have superior properties than the conventional I/M forging and the overall cost of products also reduced.

I.5.3.1. Al-Zn-Mg-Cu Alloy:

Forging of 7075 aluminium alloy involved the steps of: cold isostatically pressing, sintering the compact at 570°C and hot forging at 400°C.[3] Forged product had superior properties than the conventional cast forge.

I.5.3.2. Al-Zn-Mg-Cu-Fe-Ni-Co System:

Lyle and Cebulak[42] reported the forging techniques applied to high strength 7XXX series P/M aluminium

Table 1.8 Tensile properties of aluminium and its based composite extrudates

Alloy composition	Extrusion Ratio	UTS (MPa)	YS (MPa)	% Elongation	Reference
Al-10Mg	30:1	495	450	18	39 Tan et.al.
Al-6.5Zn-2.3Mg-1.5Cu	10:1	648	599	9	42 Lyle & Cabulak
Al-8Zn-2.5Mg-1Cu-1.6Co	10:1	710	675	9	-do-
Al-8Zn-2.5Mg-1Cu-0.8Fe-0.8Ni	10:1	696	668	8	-do-
Al-6.18Zn-2.39Mg-2.38 Cu	20:1	550	525	15	41 Parkinson and Sheppard
Al-3.8Fe-3.6Ni-3.8Co	20:1	500	490	8	43 Mcshane and Sheppard
Al-10Al_2O_3	16:1	393	-	8	8 Lenel et.al.
Al-6Al_2O_3	15:1	206	133	18	47 Hansen
Al-18(Al_2O_3 + Al_4C_3)	35:1	370	340	10	52 Kainer et.al.

alloys. Co, and Fe and Ni were added to Al-Zn-Mg-Cu alloy. Processing involved; cold compaction, preheating, hot compaction, extrusion to forging stock, forging and heat treatment. 7XXX alloy which contained Co showed presence of Co_2Al_9 particles on grain boundaries which induced stress corrosion cracking attack.

I.5.3.3. $Al-Al_4C_3$ System:

In order to develop low cost composites with Al-C, Al-1Cu-1.5C and Al-2Mg-1.5C, forging techniques were tried by Jangg and Huppmann.[53] P/M forgings had properties equivalent to these of extrudates of same compositions. Processes involved were reaction milling of lamp carbon black in an attritor mill, compaction of granules in preform shape and forging of elevated temperature in a closed die. Effect of forging temperature, and design of forging die on properties of forgings were also studied. Metallographic studies showed that at a forging temperature of 400°C, fracture started at boundaries of granules revealing very poor bonding amongst the particles. However at 600°C forging temperature excellent bonding and homogeneous structures were obtained. Superiority of this process as compared to extrusion process was the economic fabrication of product. Such a consideration may lead to further applications for such dispersion strengthened P/M products.

I.5.3.4. Al-Glass System:

Aluminium and glass (borate and silicate) have been fabricated by Kainer et al.[52] All the steps involved were similar to the extrusion method, with the final step of forging in a temperature range of 550-600°C with deformation of 10-20%. Metallographic study revealed the effect of forging temperature on dispersoids of glass in the forgings. At low temperature, the glass was present as individual fragments, whereas at high temperature glass was present as a continuous phase. The composite produced by forging route showed improved wear resistance.

I.5.4. High Energy Rate Forming:

High energy rate forming is employed to impart high strength and uniform density to the compact. The properties of compacts attained by this method are attributed to the generation of high pressure waves transferred to powder mass confined in a die. Two methods are practiced to generate high rate compaction wave. One by use of impeller actuated by compressed gas and the other by explosive isostatic compaction. A unique set of alloy compositions have been produced by dynamic compaction. Pure aluminium and Al-1.6Cu-2.5Mg-0.2Cr and 5.6Zn were selected as base alloy and steel (up to 20%) and lead (up to 40%) were added as dispersoid.[54] Powders were mixed and compacted by compressed air. Degassing was not required for aluminium powder. This technique facilitated high volume of additives to be mixed with the

aluminium powder. Undesirable chemical reactions, which are inherent with sintering, were also avoided. Steel additive attributed high abrasion resistance, whereas lead increased the seizure resistance of the compacts.

I.6. Interfacial Studies on Aluminium-Alloy Based Composites:

Properties of two phase material depend mainly on two factors. First is the intrinsic properties of each constituent and second is the bonding between the matrix and second phase. Bonding is evaluated by the study of interaction zone, which in turn depends on the wetting behaviour i.e. contact angle and reaction between the two phases. Decrease in wetting angle, increases work of adhesion, and reaction at interfaces results in better bonding between the matrix and dispersoid.

In solid/liquid/gas phases at equilibrium condition, as shown in Figure 1.11, the vectors could be equated according to Youngs[55] as

$$\gamma_{sv} = \gamma_{sl} + \gamma_{lv} \cos\theta \qquad (1)$$

$$\theta = \cos^{-1} \frac{\gamma_{sv} - \gamma_{sl}}{\gamma_{lv}}$$

where γ_{sv} = surface energy of the solid

γ_{lv} = surface tension of the liquid

γ_{sl} = solid liquid interfacial energy

Wetting is promoted if θ is less than 90°. For θ to be less than 90°, $(\gamma_{sv} - \gamma_{sl})$ must be positive. The work of

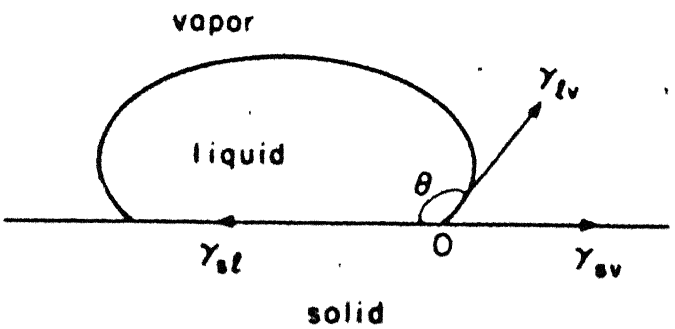

Fig.11 Contact angle θ of a liquid drop resting on a solid substrate.

adhesion W_a i.e. the bonding force between the liquid and solid phase is defined as

$$W_a = \gamma_{lv} + \gamma_{sv} + \gamma_{sl} \quad (2)$$

Combining equations (1) and (2) gives

$$W_a = \gamma_{lv}(1 - \cos\theta)$$

The bonding force between the liquid and solid phase may thus be expressed in terms of the contact angle and the surface tension of liquid.

Rohatgi et al.[56] reported various techniques to improve wettability of molten aluminium-alloy over different ceramics. The main techniques are:

(i) Use of metal coating such as Ni and Cu on refractory particles

(ii) addition of reactive elements such as Mg, Cu, Ti, Zr and P to melt

(iii) heat treatment of particles, and

(iv) ultrasonic treatment of the melt.

Table I.9 lists the different techniques applied to aluminium-ceramic systems.

Wetting of second phase (particles, fibres and whiskers) by aluminium alloy may be described under three categories:

Aluminium-Carbide system

Aluminium-Oxide system

Aluminium-Nonoxide - dispersoid

Table I.9

Techniques to improve aluminium- ceramic particle wettability[56]

Technique	Particle	Matrix
Metal coating on ceramic particles	Ni or Cu coated graphite, shellcher mica, Al_2O_3	Al and Al-alloy
Addition of reactive elements to melt	Graphite	Al-alloy (P)
	Graphite, shellchar, zircon, silica, mica, rice husk ash	Al or Al-alloy (Mg)
Heat treatment of particle before dispersion	Al_2O_3, graphite	Al or Al-alloy
Ultrasonic treatment	Al_2O_3, graphite WC (15-21 kHz) Al_2O_3 (20 kHz)	Al

In the present section, in order to fully appreciate the interfacial phenomena, both cast and P/M composites have been considered.

I.6.1. Aluminium-Carbide-System:

A wide range of carbides were dispersed in various aluminium alloys by casting as well as powder metallurgy route. The wetting between carbides and Al-alloys depends on variables such as, heat of formation, stoichiometry of carbides, valence electron concentration, interfacial reactions etc. Relationship between wetting behaviour or work of adhesion and heat of formation of carbides was established by Ramqvist.[57] It was found that work of adhesion decreased with increase in the

heat of formation of carbides. High heat of formation gives rise to strong interatomic bonds and poor interaction with other phases i.e. poor wetting. Wetting of refractory carbides by aluminium melt at various temperature is also reported.[58-60] Heat of formation of carbides was found to increase the contact angle between the carbide and matrix resulting in poor wettability.

Wettability between the refractory carbides of metal has also been correlated on the basis of stable electronic configuration of metals.[61-62] Atoms of the metal which do not wet refractory carbides have completely filled or completely vacant d shell, whereas, transition metals which wet carbides have partially filled d shells. Thus sharing of partially filled d shells between the atoms of two phases facilitate the interaction between the two phases. Elements of groups IIIb-Vb have completely filled or empty d shell thus do not wet the carbide. Wetting angle between the metal and transition metal carbide has been reported[62] to decrease with increasing valence electron concentration. Figure 1.12 shows the wetting angle of liquid metals in contact with transition metal carbides of different valence electron concentration. It is evident that increase in valence electron results in decrease in stability of these carbides. Table I.10 shows the contact angle and work of adhesion of group IV-VI transition metals.

Interfacial reaction increases the work of adhesion thus facilitating wetting between the two phases. Contact

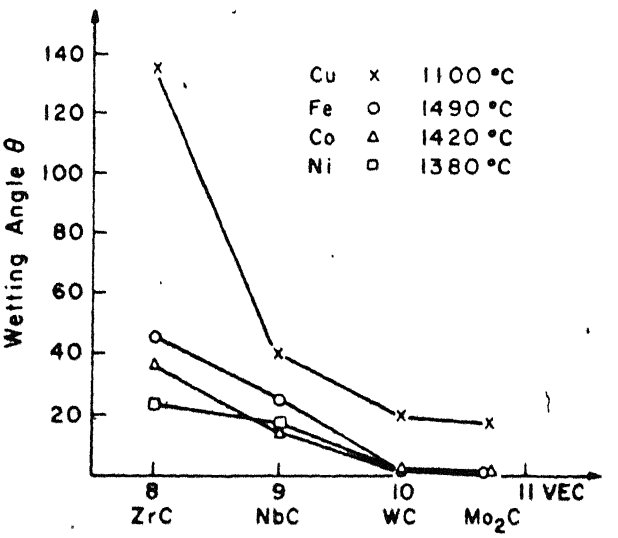

Fig. 1.1.2 Wetting angle of liquid metals in contact with transition metal carbides of different valence electron concentration[62].

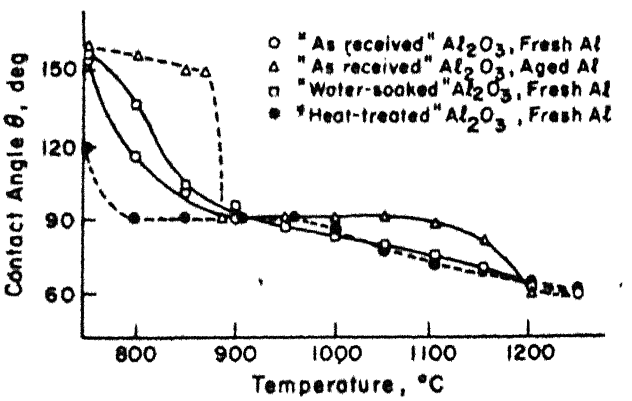

Fig. 1.1.3 Change in contact angle with temperature for the system Al-Al_2O_3[75].

Table I.10 Contact angle and work of adhesion of group IV-VI transition metals on carbides[62]

Group	Carbide	Al, 900°		Ga, 800°		In, 250°		Tl, 400°		Si, 1500°	
		θ	W_A	θ	W_A	θ	W_A	θ	W_A	θ	W_A
IV	TiC	148	139	147	113	145	700	127	196	32	1590
	ZrC	150	123	134	216	143	111	128	191	22	1660
	HfC	148	139	-	-	-	-	-	-	-	-
V	VC	130	326	120	354	119	280	111	314	Adsorbed	
	NbC	136	256	108	790	151	70	121	237	"	
	TaC	145	164	130	253	154	60	138	125	"	
VI	Cr_3C_2	120	457	120	354	143	111	133	156	"	
	Mo_2C	131	314	118	375	150	75	130	175	"	
	WC	135	274	122	333	148	85	135	147	"	

angle between metal and carbide in metal carbide system has been reported to decrease with time.[57] In most of the cases it decreases up to some equilibrium value which remains constant thereafter.

Interfaces between aluminium-alloy and SiC fibres/whiskers have been studied by a number of investigators.[63-68] After isothermal exposure of 6061 alloy - SiC composite at 500°C in air for 161 hours accicular and cubic structure phase appeared at the interface which were identical to $\beta'Mg_2Si$ and βMg_2Si phases. Interfaces between matrix alloy (2014 and 6061) and whisker in wrought PM composite were examined extensively using high resolution and conventional TEM by Nutt.[68] Presence of MgO particles signly or in clusters were observed around the SiC whiskers in the composite. Intermetallic dispersoid $Cu_2Mn_3Al_2O$ was also identified as one of the phases present at the interface.[69] $CuMgAl_2$ phase was also observed along the whisker at a number of places. Interface structure in artificially aged 2124 aluminium alloy-SiC composite showed magnesium enriched precipitate free zone.[70] A continuous layer of polycrystalline oxide (MgO) layer of approximately 3 nm thick along SiC particle has been reported in 6061 alloy-SiC composite.[68]

I.6.2. Aluminium-Oxide System:

A number of oxides viz. Al_2O_3, SiO_2, TiO_2, ZrO_2 have been introduced into aluminium alloy and the interfaces between the matrix and second phase materials have been characterised. Simple exposure of alumina particles or fibre

to unalloyed aluminium melt does not facilitate bonding between the two at a temperature below 900°C. However elements like magnesium which can react with fibre and decrease the surface tension of the melt can improve the wetting of alumina. Alumina reacts with many divalent metal oxides and form aluminates, structure of which is similar to the structure of spinel formation which promotes strong bonding between the matrix and second phase material.

Mechanical stirring of the semi-solid mixture of aluminium alloy with alumina has been reported[71] to result in wetting or bonding of alumina with the melt. Magnesium rich compound such as MgO and nonequilibrium phase β-Al_8Mg_5 along the alumina particles were observed in Al-Mg-Al_2O_3 composites.[72] In Al-Cu alloys small amount of $CuAl_2$, iron rich Cu_2FeAl_7 and cupric aluminate phase were formed[71] depending on the alloy composition. Copper accumulation was observed along the alumina fibre in as cast condition, which reduced to the copper level present in the matrix after heat treatment. Enrichment of Mg and Cu was detected around the alumina fibre in Al-Cu-Mg alloy. Heat treatment of such composites resulted in dissolution of $CuAl_2$ and $CuMgAl_2$ in the matrix, but a thin Cu-rich ring was noticed around the fibre.[71] Coating with Nichrome and Ti-Ni (duplex) have been found to promote wetting between the aluminium and alumina.[73-74] At 900°C aluminium wets alumina and contact angle has been reported to decrease with time.[75] Figure 1.13 shows the change in contact angle with temperature for

$Al-Al_2O_3$ systems. Aluminium alloy composites containing SiO_2[76] TiO_2 and ZrO_2[77] have been prepared by liquid metallurgy technique. A reaction zone rich in magnesium at outer periphery of SiO_2 particles was observed.[76] Addition of magnesium was found necessary for adequate dispersion of TiO_2 or ZrO_2 particles into Al-Si melt.[77] Preferential segregation of magnesium at particle/matrix interface was confirmed by microprobe X-ray elemental analysis. Polycrystalline continuous alumina fibre when added to Al-Li matrix by vacuum infiltration process,[78] resulted in reaction zone identified as lithium-aluminate $LiAl_5O_8$. Reaction zone formed, grows in the fibre with increasing exposure time or higher lithium content.

I.6.3. Aluminium - Nonoxide Dispersoids:

Contact angle between aluminium melt at 700°C and graphite or mica is approximately 150°C, thus aluminium does not wet these particle below 700°C. However nickel[79] or copper[80] coating on graphite and mica particles facilitate wetting of the particles due to low contact angle of nickel or copper in the order of 60°C with aluminium melt. Eustathopoulos et al.[81] has reported the formation of Al_4C_3 phase around the carbon fibre in aluminium melt at 800°C, when carbon was chemically cleaned with NaOH and HNO_3 at 860°C. Untreated carbon reacted with aluminium melt at 860°C compactness of oxide layer on carbon was considered to be suppressed at 860°C. At 1200°C graphite particles could be

introduced in aluminium alloy melt.[82] Interfaces showed a visible layer of reaction product Al_4C_3 indicating reaction induced wettability.

A long exposure (~100 hrs) at 530°C of aluminium/graphite fibre composite resulted in Al_4C_3 formation at the interface.[83] Oxidation model of Al_4C_3 formation at Al/ interface has been proposed by Muruyana and Rabenberg.[84] According to this model carbon-oxygen bonds are formed; carbon-carbon bonds are broken and the products are transported away. Phosphorus and boron compounds were considered to be effective reaction inhibitor for graphite fibres in an aluminium alloy thus resulting in improved wettability through bond strengthening. Erturk[85] has reported Al_4C_3 platelet growing perpendicular to the fibre surface in aluminium composite prepared by pressure casting. Uncoated pitch 55 graphite fibres of 10 μm in diameter were used for the study. Addition of 7% Si and 0.5% Mg to aluminium suppressed the occurrence of interface reaction products. This alloy exhibited second phase particles (pure Si) at the interface and throughout the matrix, with little interfacial reaction. In case of Al-4.5 Cu and Al-7.8 Mg alloy as matrix Al_4C_3 precipitate were not as pronounced as in case of pure aluminium. In Al-Cu alloy, Al_2Cu phase was observed, whereas other (non-carbide) particles could not be identified in Al-Mg alloy.

In aluminium-pitch fibre composite two phases Al_2Mo_3C and $Mo_{12}Cu_3Al_{11}C_6$ were found to be present at the

interfaces, whereas $Al_3B_{48}C_2$ and $AgAlO_2$ were also present in the matrix.[86]

Cobalt-molybdenum based intermetallic "Tribaloy" particles were introduced in aluminium-alloy matrix.[23] Microstructure of aluminium-Co-Mo base P/M composites revealed a thin diffusion layer around the particles in the matrix. Best tribological properties were reported for the composites with presence of such diffusion layers. A strong bonding between 6061 aluminium alloy matrix and boron fibres were observed on the fracture surface of the composites.[64-65] Isothermal exposure at $773^{\circ}K$ for 137 hrs of such composites gave rise to AlB_{12} and AlB_2 phases at the interface, thus resulting in poor interface strength.

Silicate glass particles have been incorporated in Al and Al-3% Mg melt by vortex method i.e. by stirring the melt.[87] Microscopic study revealed formation of a thin layer around the glass particles. The layers were considered to be a result of peripherical melting of dispersed glass particles or due to the reaction of glass particles with the melt. Deformation (extrusion) of P/M composite consisting of aluminium alloy as matrix and particles of borate and silicate glass as dispersoid resulted in the formation of an atomic bond between new surface imparting superior mechanical and tribological properties to the composites.[52]

Aluminium alloy composite containing stainless steel fibre were also prepared by wrought P/M route (hot pressing).[88] EPMA study revealed presence of Al, Fe, Ni elements at

metal/fibre interface. Microhardness measurement indicated formation of complex intermetallic of Fe and Al around the steel fibres.

I.7. Sliding Wear of P/M Aluminium-Alloys:

Due to their wide ranging properties, aluminium alloys and their based composites containing soft and hard particles have been studied in detail for tribological behaviour. Addition of hard particles improves the sliding wear properties due to the matrix strengthening. Soft particles, which are solid lubricants, induce antifriction properties to the base matrix. A good deal of literature[23,37,40,46,90,91] is available describing the wear (adhesive and abrasive) properties of aluminium alloy based composites. Effect of dispersoid addition and test parameters on the composites alongwith probable mechanism have also been reported in literature.[4,23,46,91] Most of the composites undertaken for evaluation of sliding wear properties were prepared by casting route. Rather limited information is available on sliding wear properties of composites prepared by P/M route.

Aluminium-silicon alloys have been widely studied for anti-seizing behaviour due to its good resistant to wear and low coefficient of thermal expansion.[89] Sintered aluminium compacts with 37% silicon have been reported to attain 20% higher wear resistance than that of the conventional AlSi12MgCuNi piston alloy, but this alloy has very low elongation. Aluminium AlCr10 and AlFe8SiC2 prepared by

P/M route showed identical and 20% higher value of wear resistance respectively as compared to AlSi12MgCuNi piston alloy. These alloys are attractive material for piston manufacturers, because they behave in the same way as the cast alloy but are superior in terms of heat resistance properties. Skelly and Dixon[37] reported on the wear behaviour of hypereutectic alloy powder Al-35% Si with small amount of Cu and Mg, when isostatically cold pressed followed by hot pressing. Addition of Cu and Mg were found to improve the wear resistance of the alloys. Al-Si powder metallurgy alloys were reported[40] to be more suitable than that of cast alloy as piston material due to comparatively better wear resistance, strength, creep resistance, thermal expansion and machinability of the former. Aluminium alloy with up to 30% Si prepared by cold compaction followed by extrusion is reported by Kuroishi et al.[40] Specific wear (mm^2/kg) decreased with increasing silicon content and effect of sliding speed was also found to be minimum for this alloy.

Wear properties of commercially developed 201 AB and 601 AB alloy have also been evaluated by various investigators.[4,23,90] Crossed cylinder wear tests of 201 AB and 601 AB in as sintered and heat treated were carried out by Dudas and Brondyke[4] in lubricated conditions. Anodizing treatment of such alloy has been suggested[4] to impart the abrasion resistance coating to the surface much the same way as carburizing or nitriding of sintered steel parts. Self lubricated bearing of 201 AB were also synthesised[90] by

conventional powder metallurgy route and tested against 9SMnPb23 carburised and hardened steel (R_c: 58). Oil content of the porous bearing (porosity <80%) was indicated to be important parameter to control the wear behaviour of the bearing. Heat treatment did not alter the wear characteristics of the bearing.

Daver and Ferriss[23] have developed MD69 wear resistance P/M aluminium alloy consisting of 90 vol. % of AlCu2Mg1-Si .3 alloy and 10 vol. % of Co-Mo base intermetallic called 'Tribaloy'. Improvement in sliding wear properties was attributed to the interaction i.e. thin diffusion layer around Tribaloy particles. Reduced coefficient of wear and reduction in surface damage were reported[23] for the composites.

Aluminium-10 wt. % Zn alloy containing maximum up to 45% of corundum produced by conventional P/M route was evaluated by Anand and Kishore[91] for dry sliding wear characteristics against rotating high chromium hardened steel disc. Optimum wear resistance was attained by composites containing 15% corundum. Asperities on the iron disc were reported to be sheared by hard corundum particles thus resulting into less wear of composites. Iron was detected to be embedded into pores of surface and its presence was confirmed in the debris. A large amount of corundum gave rise to high wear loss as more surface cracks were found on the surface due to more region of poor cohesion and stress concentration. A delamination wear mechanism was indicated to be operative under the experimental condition.

Grosch and Brockmann[46] reported the sliding wear of Al-Al_2O_3 composites prepared by compaction of powder premix followed by extrusion. Addition of alumina was found to increase the wear resistance of the composites as compared to the straight aluminium powder compact. Larger alumina particles imparted superior properties than the fine particles. SEM study showed the transfer and embedding of hard alumina particles into soft (450 Hv) steel disc and subsequently facilitating grooving effect on the pin leading to a high wear loss. However the above condition was not true for these cases, where hard disc (750 Hv) was used. In latter case, adhesion wear mechanism was found operative. Aluminium-steel-lead admixed alloy composite has been reported by Raybould.[54,92] The composites were prepared by dynamic compaction and pin on disc type of wear test was carried out in a stagnant oil bath Al-Pb alloy had a very poor adhesion wear. Addition of steel to Al-Pb alloy improved the wear resistance. Tests at low load showed oxidative type of wear which changed to metallic wear at higher loads. Annealing of compacts at 350 and 450°C did not alter the adhesive wear.[92]

I.8. Scope of the Present Work:

In addition to its inherent properties such as light weight, corrosion resistance, sintered aluminium products offer many advantages, like energy saving due to low compaction pressure and low sintering temperature. The use of sintered aluminium components has of late emerged as a valid alternative

for structural parts manufacturer. It has replaced a number of ferrous based components in automobile industries. The economic advantage in replacing copper base P/M bearings, which are consumed in large quantity is still more attractive.

While the literature abounds in data on mechanical properties, very little has been reported on wear behaviour of sintered aluminium alloys. Being governed by a large number of factors, which are interdependent, the wear behaviour prediction of sintered product is rather difficult. From design point of view, it is important to have information regarding wear behaviour of material in order to ensure the integrity of parts for use in machinery.

6061 aluminium alloy has a moderate strength and high ductility. It is suitable for compaction and sintering as well as subsequent working and heat treatment operations. Like other aluminium alloys, the sintering of 6061 alloy is also critical due to its sensitivity to sintering temperature, atmosphere etc. in attainment of final properties. By using different sintering atmospheres, densification and other related properties of such alloys may be varied to a great deal. Evaluation of properties of sintered materials in various atmospheres may lead to optimization of sintering process for the best end properties.

The introduction of solid lubricant in the aluminium alloy matrix has also been realised extensively. Graphite and talc, which are inexpensive solid lubricants may be dispersed in 6061 alloy matrix to develop antifriction materials.

Due to the requirement of high volume fraction and homogeneous dispersion of these particles in the matrix, conventional P/M route is suitable to develop such composites.

Development of aluminium alloy composite with hard dispersoid is also important in view of their potential for high strength and wear resistance. Refractory oxides and carbides are common hard materials and with this in view the introduction of alumina and TiC dispersoids in the 6061 alloy matrix was aimed at. Such refractory stable dispersoids would also be useful in maintaining the elevated temperature mechanical properties.

In the present investigation, composites consisting of 6061 aluminium alloy with soft (graphite, talc) or hard (alumina, TiC) dispersoids were prepared by the conventional P/M route. Various atmospheres viz. argon, vacuum and nitrogen were used during sintering. Such composites are amenable to secondary operations like heat treatment, repressing-resintering, thermomechanical treatment etc. The effect of material variables such as type and amount of dispersoid, and process variables like sintering atmosphere, on the physical and mechanical properties of composites were evaluated. Mechanism of sintering of straight 6061 alloy and its based composites is also discussed in the framework of liquid phase sintering. Alteration of sintering response due to presence of soft or hard dispersoids in the matrix is explained on the basis of physical as well as chemical factors.

Sliding wear studies on such composites are equally significant from tribological viewpoint. For this, experiments were planned using different test parameters, e.g. sliding speeds, sliding distance, applied pressure, and the wear was correlated with other properties of the composites. Some models experiments on the mechanism of lubrication of solid lubricants (graphite and talc) during dry sliding wear tests were also proposed.

CHAPTER II

EXPERIMENTAL PROCEDURE

Composites were prepared using the premix powder of 6061 aluminium alloy composition as base alloy and graphite, talc, alumina and titanium carbide as dispersoid particles. Different volume fractions of dispersoid particles were mixed with aluminium alloy premix, compacted into green cylindrical and MPIF tensile test piece shapes. The compacts were subsequently sintered at 615^{o}C in various atmospheres. Some selected specimens were subjected to secondary operations, viz. repressing-resintering, heat treatment and thermomechanical treatment. Physical, mechanical and dry sliding wear properties of the composites in different conditions were also evaluated.

II.1. Raw Materials and Their Characteristics:

Physical characteristics of all powders were evaluated using ASTM standards. Microphotographs of the powders were obtained using JEOL 35CF Scanning Electron Microscope. To achieve this, powder particles were mounted on the brass stud using double sided tape and were coated with a thin layer of gold before SEM study.

Chemical composition and physical characteristics of raw materials used in the present investigation are as follows:

1) 6061 Aluminium-Alloy Premix:

6061 Aluminium alloy premix of MD69 grade was obtained from M/s Alcan Ingot and Powders, New Jersey, U.S.A. TableII.1 enlists its powder characteristics.

Table II.1

Chemical composition and physical characteristics of 6061 alloy premix

Chemical composition (Mass %)						Apparent density Mg/m^3	Mesh	Mass %
Al	Mg	Si	Cu	Cr	Lubricants (parts)			
98.05	1.0	0.6	0.25	0.1	1.5	1.3	+200	45
							+250	21
							+325	19
							+400	25

Equiaxed and elongated shape particles with highly irregular/coarse surface are evident from the microphotograph (Figure 2.1a).

2) Graphite Powder:

Graphite powder received from Rajahmundri mines was beneficiated by the supplier. Further cleaning of beneficiated graphite was carried out by boiling the graphite particles in 10% NaOH solution for 30 minutes washed with distilled water followed by boiling in concentrated hydrochloric

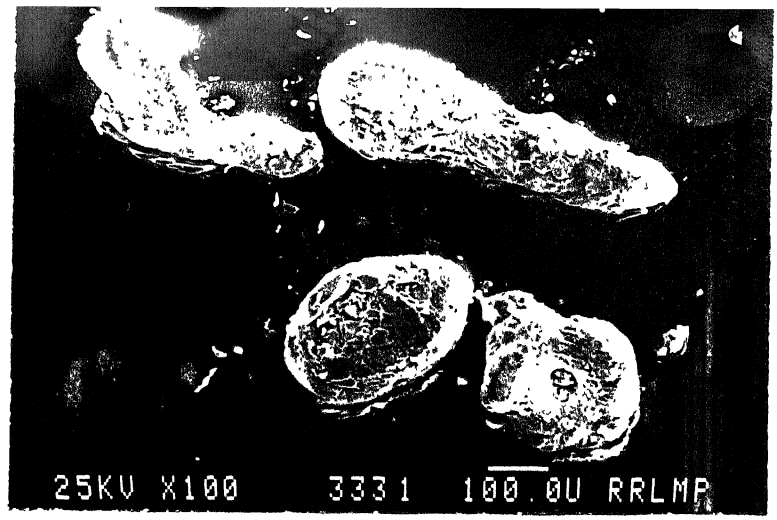

(a)

(b)

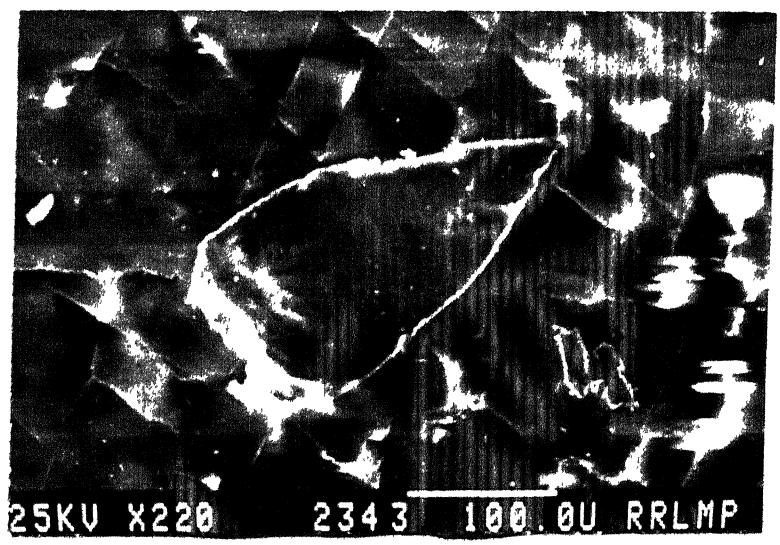

(c)

Fig. 2.1 contd.

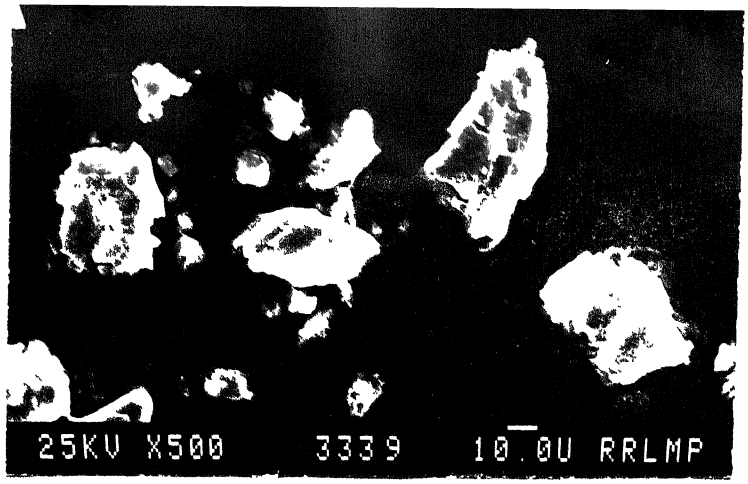

(d)

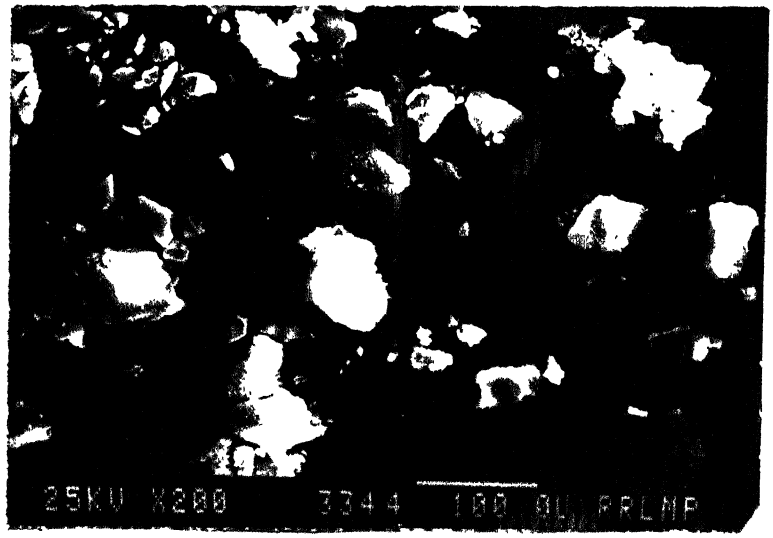

(e)

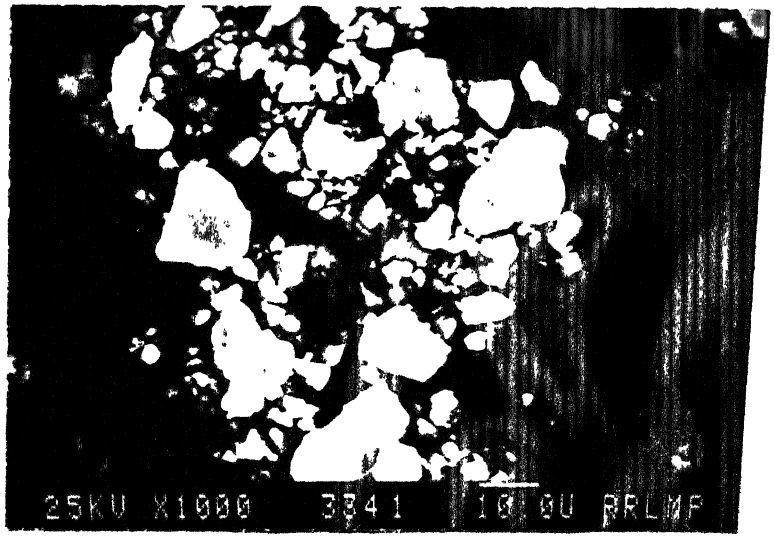

(f)

Fig. 2.1. SEM micrographs of various particles (a) 6061 alloy premix, (b) natural graphite, (c) copper coated graphite, (d) talc, (e) alumina, (f) TiC.

acid for 30 minutes. Finally the particles were washed with distilled water and dried at a temperature of 150°C. Table II. 2 shows the composition and characteristics of treated graphite particles used in the present investigation.

Table II. 2

Chemical composition and physical characteristics of natural graphite particles

Chemical composition (Mass %)				Apparent density Mg/m^3	Average particle size (μm), FSSS
Moisture	Ash	Volatile materials	Carbon		
0.15	0.6	0.86	98.39	0.52	6.2

SEM microphotograph (Figure 2.1b) of graphite particles shows the flaky and layered structure.

As the sintered composites revealed pores between matrix alloy and graphite particles (a full details are given in next chapter), a set of experiments were carried out with copper coated natural graphite powder in order to eliminate such porosities. Electroless method[93] was followed for this purpose. Particle surface was sensitized and activated using $SnCl_2$ and $PdCl_2$ solution respectively and electroless copper coating of the particle was carried out in Fehling formaldehyde solution. The schematics of the process is as shown in Figure 2.2.

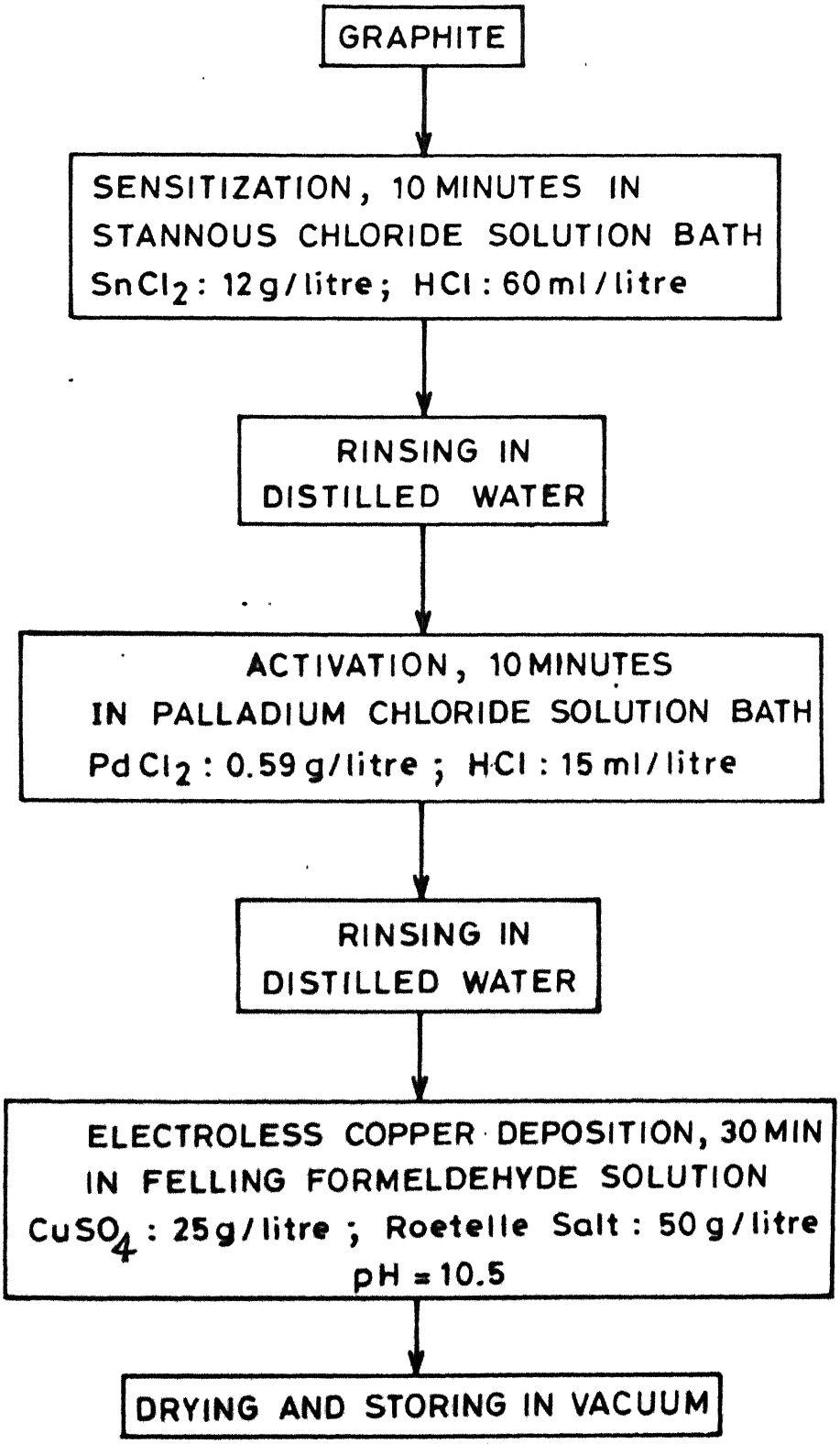

Fig. 2.2 Schematics of copper coating process on natural graphite particles [93].

Graphite particles were agitated by magnetic stirrer in respective solution baths during sensitization, activation and copper deposition. A thin coating of approximately few μm thickness was obtained over the graphite particles. Figure 2.1c shows the SEM microphotograph of copper coated graphite particle.

3) Talc Powder:

Talc lumps received from Rajasthan mines were ground to fine size using a mortar and pestle. Fine talc particles were cleaned by the method similar to that described for graphite particles. Talc particles after cleaning were analysed using X-ray diffractometer, infrared spectroscope (IR) and differential thermal analyser (DTA) techniques.

X-ray diffraction data of talc powder is shown in Table II.3. Peaks were identified by matching with the standard peaks of talc. It can be seen from the table that talc has the prominent X-ray diffraction peaks corresponding to d values of 0.465, 0.310 and 0.186 nm. The peak corresponding to d values of kaolinite, which is normally associated with talc was not present in the currently used talc.

Infrared spectrum (Figure 2.3) of cleaned talc indicates sharp absorption peak at 3675 cm^{-1} corresponding to hydroxyle (-OH) group. Presence of absorbed water can be seen at 3443 and 1574 cm^{-1} in the I.R. spectrum. Other peaks at 1018, 669, 466 cm^{-1} show the presence of Si-O, Al-OH, Mg-O and Fe-O bond in talc. DTA curve (Figure 2.4) of talc shows endothermic peak at approximately 950°C. It has been

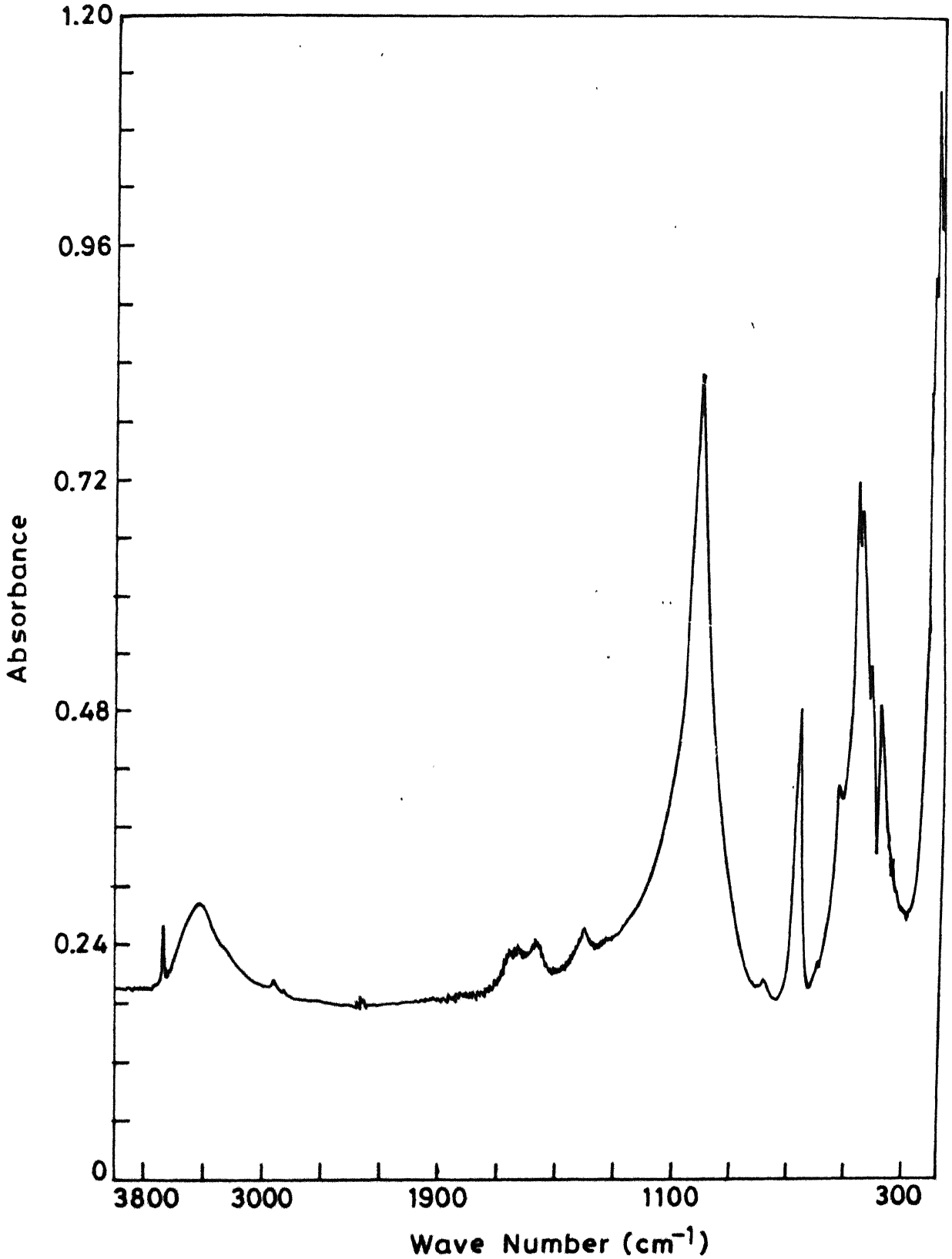

Fig. 2.3 Infra-Red spectra of talc powder.

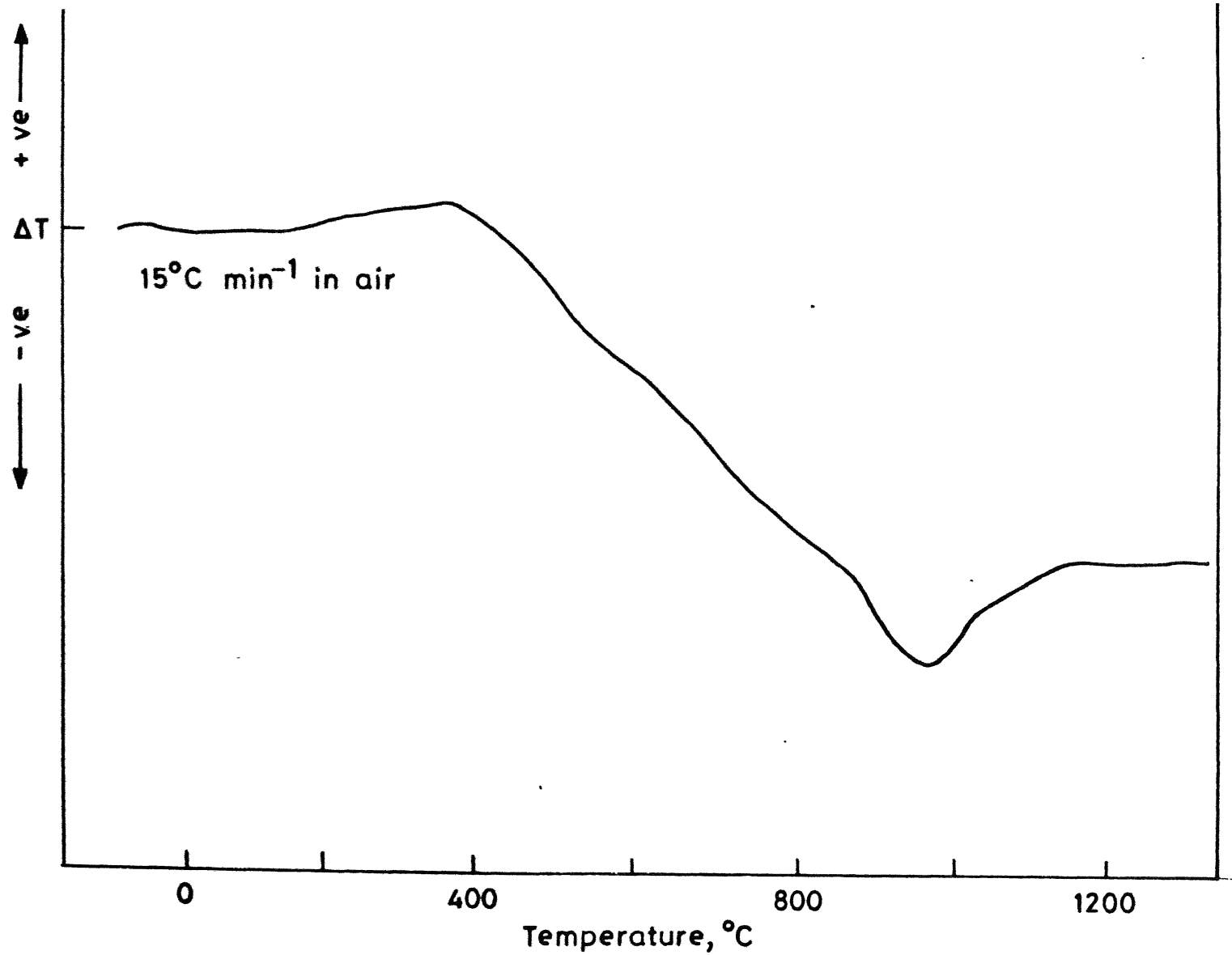

Fig. 2.4 DTA curve for talc powder.

Table II.3

X-ray diffraction data of talc particles

2 θ (deg.)	d value (nm)	I/I_o	Identification*		
			Compound	d value (nm)	Plane
19.073	0.46532	20	Talc	0.466	004
28.769	0.31031	100	Talc	0.312	006
48.887	0.18630	9	Talc	0.187	-

* From Powder diffraction File No. 6-0221 and 13-558.

reported in literature[94] that talc undergoes decomposition beyond 850°C losing its combined water. Endothermic peak in present study can be attributed to such a dissociation at 950°C. Chemical composition and physical characteristics of talc are given in Table II.4.

Table II.4

Chemical composition and physical characteristics of talc particles

Chemical composition, Mass %								Apparent density Mg/m^3	Average particle size (μm) FSSS
SiO_2	MgO	CaO	Al_2O_3	Fe_2O_3	Alkaline materials	Ignition loss	Moisture		
55.85	33.2	3.00	1.5	0.47	Rest	4.20	0.05	0.52	5.7

Irregular shape particles of talc are shown in Figure 2.1d.

4) Alumina Powder:

Alumina α-grade 'Linde A' was obtained from Union Carbide Corporation, U.S.A. Apparent density and average particle size of alumina particles were 0.29 Mg/m^3 and 0.3 microns respectively. Variation in particle size of alumina is shown in Figure 2.1e.

5) TiC Powder:

Titanium carbide powder of grade A: 3855 was obtained from Treibacher Chemische Werke, Austria. Table II.5 enlists the chemical composition and physical characteristics of TiC powders

Table II.5

Chemical composition and physical characteristics of TiC powder

Chemical composition (Mass %)					Apparent density Mg/m^3	Average particle size (μm) FSSS
C (total)	C (free)	Fe	O	Ti		
19.4	0.08	0.05	0.06	Rest	1.51	3.45

Irregular shape particles of TiC are shown in Figure 2.1f.

II.2. Preparation of Composites:

Composites of 6061 alloy premix with different dispersoids were prepared by conventional powder metallurgy route involving the following steps: mixing, compaction and sintering. A set of sintered compact was repressed and resintered. Sintered and resintered compacts were heat treated to T6 condition.

II.2.1. Powder Preparation:

Aluminium alloy 6061 premix alongwith 4, 7, 10, and 14 vol. percent of dispersoids viz. graphite, talc, alumina and TiC were mixed in a double cone blender (Model 529 of Netzsch, West Germany make) for one hour. Volume fraction represents the proportions of the constituent powders in loose form. Calculation of volume fraction was done using the apparent density value of each powder.

II.2.2. Green Compaction:

Single acting hydraulic press (Masta, U.K. make) of 100 ton capacity was used to prepare the cylindrical pellets of 12.7 mm diameter and ~6 mm height. Double acting hydraulic press of 200 ton capacity (Busmann Damag make) available at M/s Mahindra Sintered Products, Pune was used to prepare the tensile test pieces of Metal Powder Industries Federation (MPIF) standard. Figure 2.5 shows the dimensions of the MPIF tensile test piece. Dies were lubricated with a thin layer of zinc stearate prior to each compaction. Green densities of the compacts were measured by displacement

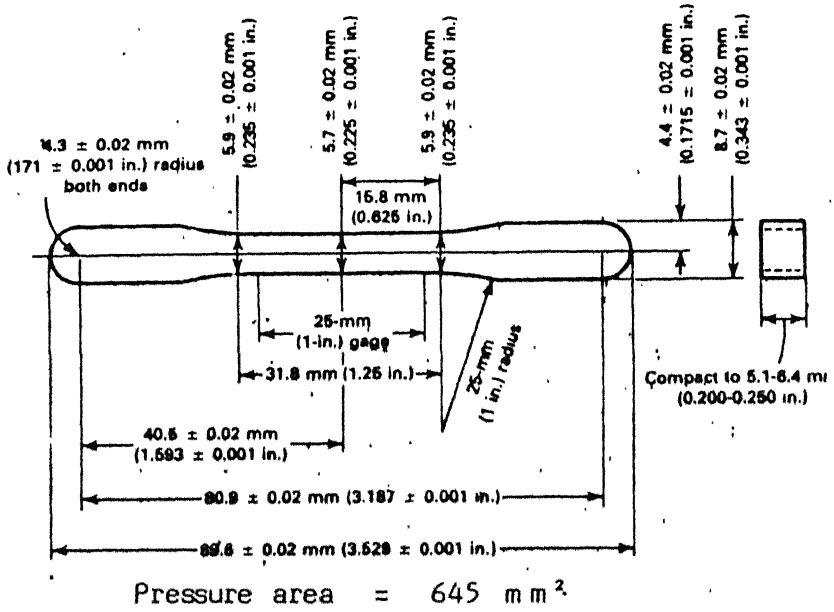

Fig. 2.5 MPIF Tensile test bar.

method using single pan balance (Mettler H51 AR) with least count of 0.01 mg. Pressure was selected by preparing green compacts of 6061 alloy using a range of pressures from 150 to 450 MPa. Increase in green density of compacts was not significant beyond the pressure 310 MPa (Figure 3.1). The optimised compaction pressure of 310 MPa was therefore selected to prepare the composites throughout this study.

II.2.3. Sintering:

Kanthal wound tubular furnace of 50 mm tube diameter was used for controlled atmosphere sintering of the green compacts. A constant heating zone of 10 cm was calibrated at the centre of the furnace tube and samples were kept on perforated rectangular graphite boats. Sintering was carried out at 615 $\pm$ 1^{o}C for 30 minutes in different atmospheresi.e. argon (dew point: -40^{o}C), nitrogen (dew point: -38^{o}C) and vacuum (1.33 x 10^{-8} MPa Hg pressure). As the sintering temperature range for the alloy in the present case is very narrow, accuracy is maintained to control the sintering temperature. Proportional temperature controller (401 D Indotherm make) with an accuracy of $\pm$1^{o}C control was therefore used to control the sintering temperature. Controlled heating and cooling rates of 10^{o}C and 3^{o}C per minute respectively were also maintained. Dew point measurement of the gases were carried out with dew point meter 6848A 102C of Casella make.

II.3. Repressing and Resintering:

A set of sintered cylindrical compacts was repressed in a tungsten carbide lined die at a pressure of 450 MPa. For this a die with 12.7 mm diameter and 3 percent taper at one end was used. Repressed compacts were resintered at 510 ± 1°C for 30 minutes.

II.4. Heat Treatment:

Both sintered and resintered composites were heat treated to T6 condition. Samples were solutionized at 520°C for 30 minutes, quenched in water at room temperature and aged at 160°C for 18 hours.

II.5. Thermomechanical Treatment (TMT) of Composites:

Following treatments were carried out for TMT of the composites.

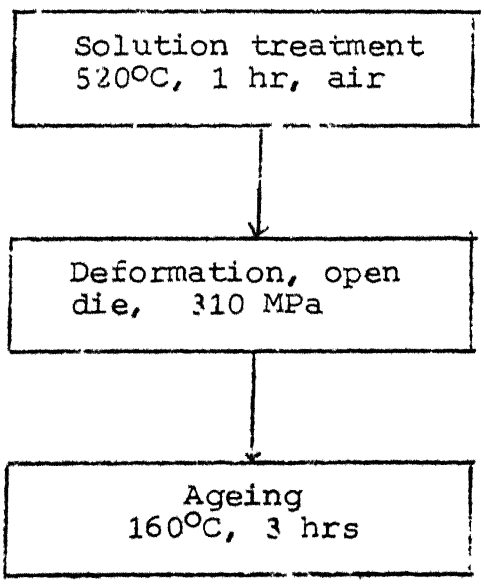

A pressure of 310 MPa on solution treated composites resulted in approximately 25 percent reduction in the height of the cylindrical compacts.

II.6. Properties Evaluation:

Physical, mechanical and sliding wear properties of composites were obtained after different processing stages (i.e. sintered, heat treated etc.) for their characterisation.

II.6.1. Densification Behaviour:

Densification behaviour of the composites were monitored by evaluating dimensional changes, density and densification parameter.

II.6.1.1. Linear and Radial Dimensional Changes:

Heights and diameters of pellets were measured with a vernier calliper with least count of 0.02 mm. Percentage linear and radial dimensional changes were calculated using the following formulae:

$$\% \text{ linear dimensional change} = \frac{l_1 - l_o}{l_o} \times 100$$

l_o = Initial height of compacts

l_1 = Height of compacts after sintering

$$\% \text{ radial dimensional changes} = \frac{d_1 - d_o}{d_o} \times 100$$

d_o = Initial diameter of compacts

d_1 = Diameter of compacts after sintering.

II.6.1.2. Density and Porosity:

Sintered densities of the composites were measured using the method described by Arthur[95]. For this the sintered compacts were impregnated with xylene in vacuum and weighed in air and water. Formulae used for the calculations of sintered density and porosity levels are as follows:

$$\text{Sintered density} = \frac{A}{B - C}$$

$$\text{Interconnected porosity, } \varepsilon_i = \frac{B - A}{(B - C).\rho_x}$$

$$\text{Total porosity, } \varepsilon_t = \frac{(B - C) - (A/\rho_m)}{(B - C)}$$

$$\text{Closed porosity, } \varepsilon_c = \varepsilon_t - \varepsilon_i$$

A = mass of sintered specimen in air

B = mass of sintered specimen in air after impregnation of xylene

C = mass of sintered specimen in water after impregnation with xylene

ρ_x = density of xylene

ρ_m = theoretical density of sintered material.

II.6.1.3. Densification Parameter:

Densification parameter (ΔD) values were calculated by using the formula

$$\Delta D = \frac{\text{Sintered density - Green density}}{\text{Theoretical density - Green density}}$$

Such a parameter takes care of even a slight variation in green density during preparation of the green compacts.

II.6.2. Mechanical Properties:

II.6.2.1 Hardness:

Brinell hardness of sintered, resintered and heat treated compacts were measured on Brinell-cum-Vickers hardness testing machine Model HPO 250 of 'Fritz Heckert', Leipzig make, using a load of 153 N. Hardness of compacts after TMT were measured on microhardness tester model 8613 of Leitz Wetzlar make. For comparative study microhardness of one set of sintered compacts was also measured. In both cases microhardness indentations were made on the aluminium alloy matrix using a load of 2.942 N.

II.6.2.2 Tensile Mechanical Properties:

Tensile testing of selected sintered and aged (T6 treated) MPIF specimens were carried out on Instron machine (model 1185) of 10 tons (10×10^4 N) capacity at a cross head speed of 0.5 mm/min. Yield strength for 0.2 percent off-set and percent elongation of the composites were calculated from the Instron recorded plots.

II.6.3. Electrical Resistivity:

Electrical resistivity of compacts was measured on a conductivity meter type 757 (Technofour make) which works on eddy current principle.

II.4.4. Surface Roughness Measurement:

Stylus instrument 'Talysurf 6' of Taylor-Hobson make (Figure 2.6) was used to measure the roughness value of cylindrical wall of the as sintered compacts. The instrument

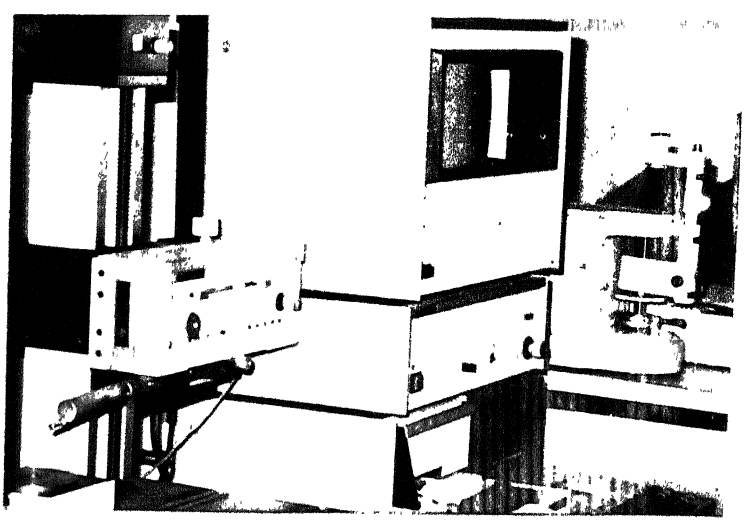

Fig. 2.6. Stylus instrument "Talysurf 6".

essentially consists of a sharply pointed stylus which rests lightly on the surface and traverses slowly across it. Up and down movement of the stylus relative to a suitable datum are magnified and recorded. Rotary attachment of the unit in R/ISO mode and 0.25 mm cut off length was used for roughness measurement R_a parameter of roughness, which is an arithmatic mean of the departure of the roughness profile from the mean line is reported in present study.

II.6.5. Sliding Wear Study:

Pin on disc system was used to study the dry sliding wear behaviour of sintered compacts. To achieve this a lapping machine (Kent Mark II) was modified. Figure 2.7 shows the pin-on-disc apparatus used in present study cylindrical compacts were used as pin, whereas, EN25 steel heat treated to a hardness value of R_c 32 was used as the disc. Steel disc was polished to a roughness of 1 μm (CLA) before each test. Sintered compacts were polished with 220 grade SiC paper and disc was run against the pin (sintered compact) with a pressure of 0.12 MPa (load 10 N) and sliding speed 0.5 m/s until the whole surface of pin was in full contact with disc i.e. run in period was over. Disc was then repolished to a roughness value of 1 μm. After each test specimen (pin) was rinsed with flowing water, cleaned with methanol followed by drying in hot air. Specimen before and after wear test was weighed and difference in weight was computed as mass loss during the test.

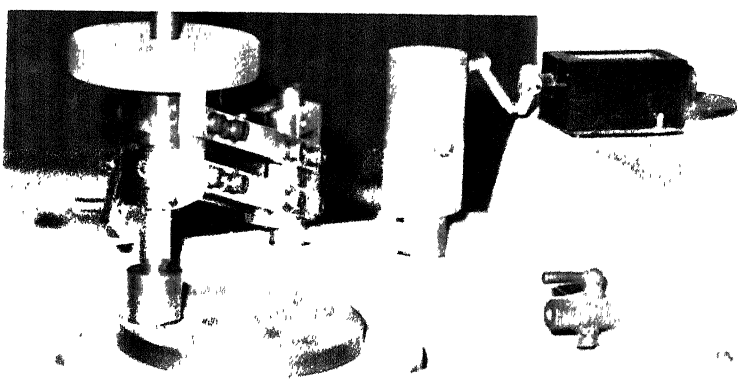

Fig. 2.7. Modified lapping machine used as pin-on-disc apparatus.

Effect of volume fraction of dispersoid on sliding wear was studied using the parameters:

Sliding speed : 0.5 m/s

Applied pressure : 12×10^{-2} MPa

Sliding distance : 250 meters

A total of eight readings for each composition was taken and an average value with mean standard deviation is reported. Effect of test parameters on dry sliding wear was studied on 6061 aluminium alloys and composites containing 7 vol. percent of dispersoid (i.e. graphite, talc, alumina or TiC). To study the effect of sliding speed on wear, pressure and sliding distance were maintained as 12×10^{-2} MPa and 250 meters respectively and speed was varied from 0.25 to 1.25 m/s. To study the effect of applied pressure on pin, pressure was varied from 4×10^{-2} MPa to 24×10^{-2} MPa. Sliding speed and distance were maintained at 0.5 m/s and 250 meters respectively. In one set of experiment, applied pressure and speed were maintained as 12×10^{-2} MPa and 0.5 m/s whereas as sliding distance ranged from 125 to 500 meters. For these tests an average of 4 reading are reported.

Model experiments were also carried out on some selected specimens. Graphite or talc particles were laid over the wear path during the test, maintaining simpler test parameters. Tests were also carried out on specimen with protruded dispersoids (graphite or talc on the surface). To achieve this, composites after run in condition were etched with 5% HF solution for approximately 30 minutes, and cleaned with water and methanol.

II.7. Metallography:

II.7.1. Optical Microscopy:

The sintered compacts were manually polished over Lunn major (Struers make) water rinsed polishing board which was provided with SiC papers of grit size 220, 320, 500 and 1000. Final polishing was done over MOL polishing cloth on struers polishing machine DAP3 using 0.3 μm alumina suspended in distilled water. HF solution of 0.5% concentration was used as the etchant. Microstructures were observed under Leitz Wetzlar make optical microscope at X200 magnification.

II.7.2. Scanning Electron Microscopy:

Scanning electron microscope (SEM) JEOL 35CF equipped with wave length (WDXS) and energy (EDXS) dispersive X-ray spectroscopes was used to study the fractured, worn out and metallographic polished surfaces of composites and base alloy.

II.7.2.1. Sintered Composites:

Samples polished for metallography were examined under SEM. Presence of dispersoid, types of porosities and compatibility of the dispersoid with 6061 alloy matrix were examined.

II.7.2.2. Fractography:

6061 alloy and composites containing 14 vol. percent of each dispersoid were selected for fractography

Micrographs of fractured surface of tensile test pieces were observed at different magnifications. Presence of dispersoid were confirmed using the EDXS study over the composite surface.

II.7.2.3. Wear Surface and Debris:

Worn out surface of the compacts were examined under SEM after cleaning with water and methanol. Debris collected during the test were mounted on brass stud using double sided tape and were examined after coating with a thin (100 Å) layer of gold. Elemental analysis of the debris was carried out using WDXS attachment of SEM.

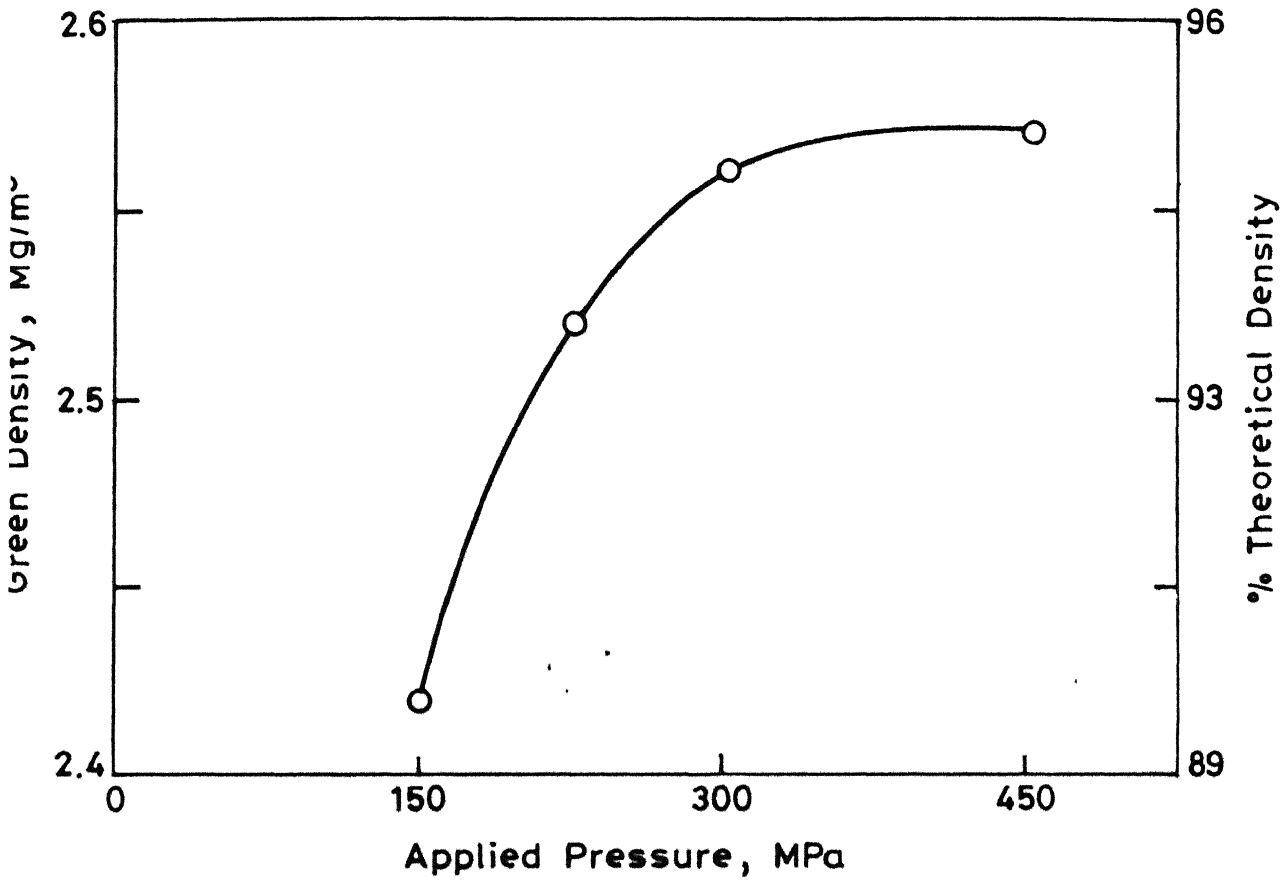

Fig. 3.1 Variation of green density / relative density of 6061 premix compact as a function of applied pressure.

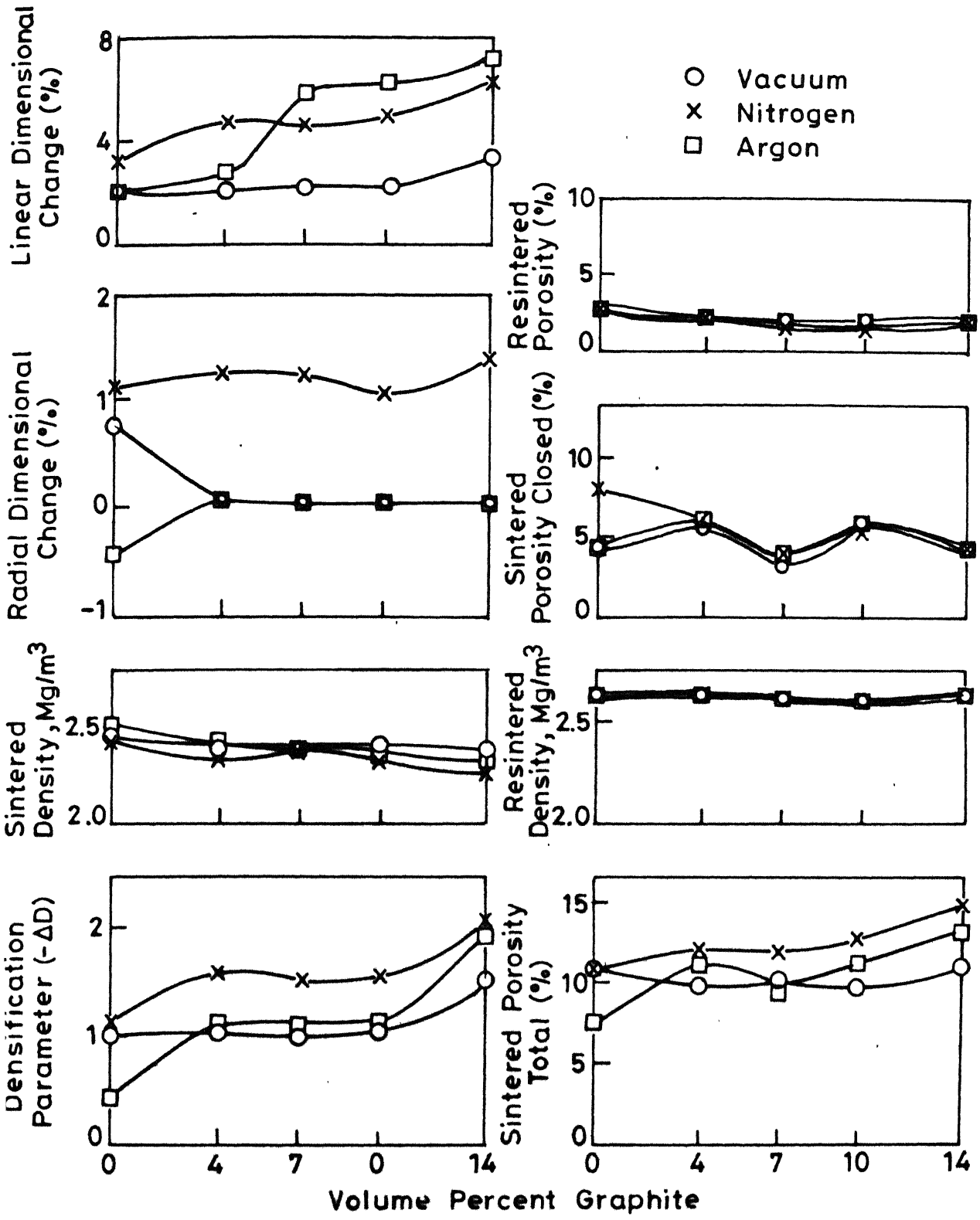

Fig. 3.2 Sintering behaviour of 6061 alloy-natural graphite composites as a function of dispersoid content.

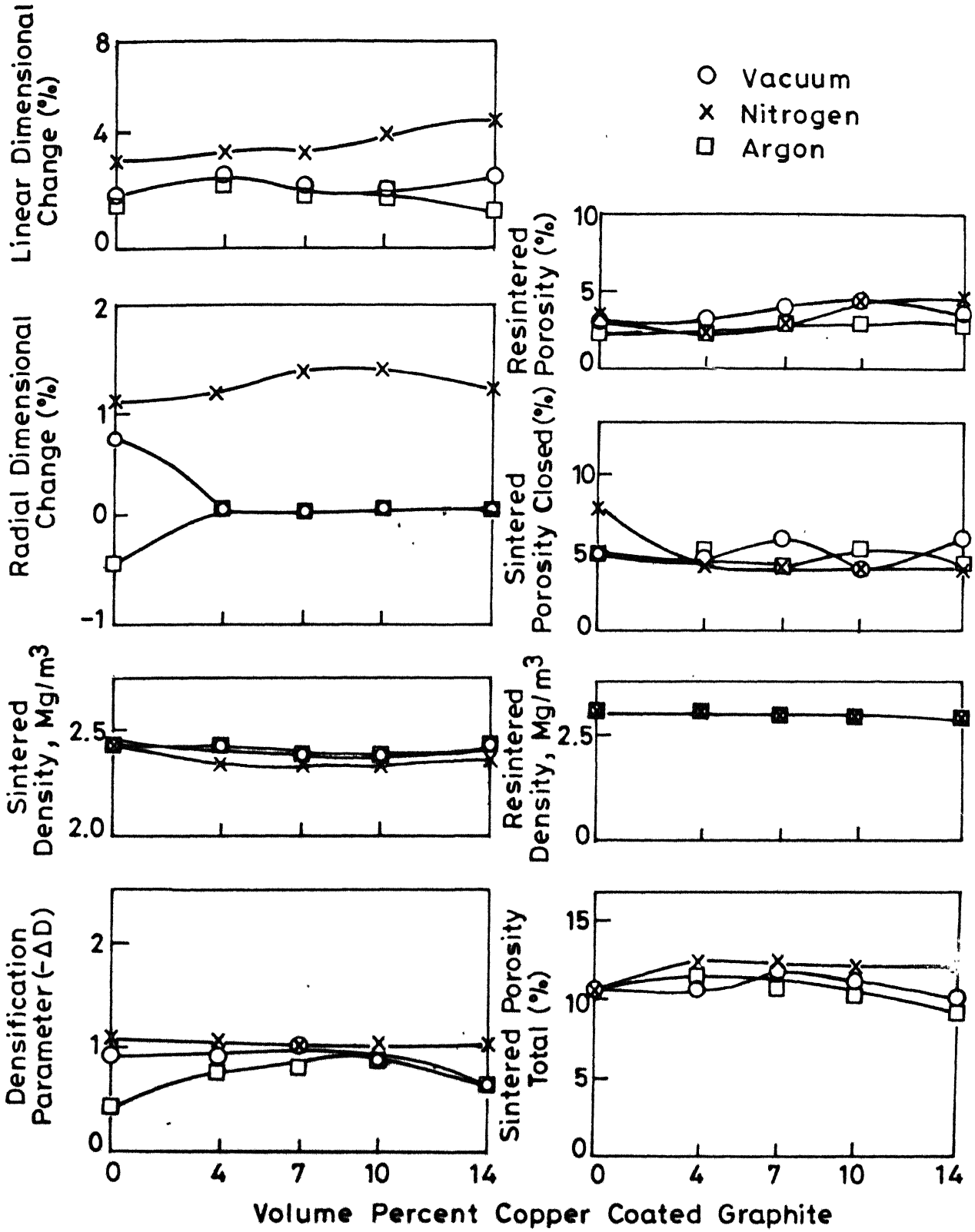

Fig. 3.3 Sintering behaviour of 6061 alloy-copper coated graphite composites as a function of dispersoid content.

change. However, nitrogen sintered compacts showed swelling in the radial direction. Density of argon sintered compacts decreased by 7% with addition of 14 vol. percent of uncoated graphite particles. Densification parameter (ΔD) varied corresponding to those of dimensional changes. ΔD of composites remained constant with volume fraction of copper coated graphite, after sintering in nitrogen.

Sintered total porosity of the composites showed an increase in its value with increasing amount of uncoated graphite. Sintered porosity of the composites practically remained constant with volume fraction of coated graphite. Approximately 25% of total porosity was of close type in all the cases.

III.2.2. Hardness:

Figures 3.4 and 3.5 show the Brinell hardness variation of composites containing uncoated and copper coated graphite particles in sintered condition as a function of volume fraction of dispersoid. Sintered hardness of the composites decreased with volume fraction of the uncoated graphite particles. A marginal increase in hardness values for the composites containing copper coated graphite and sintered either in argon or vacuum can be noticed (Figure 3.5). Hardness of the composites containing copper coated graphite and sintered in nitrogen remained constant with variation in the graphite content.

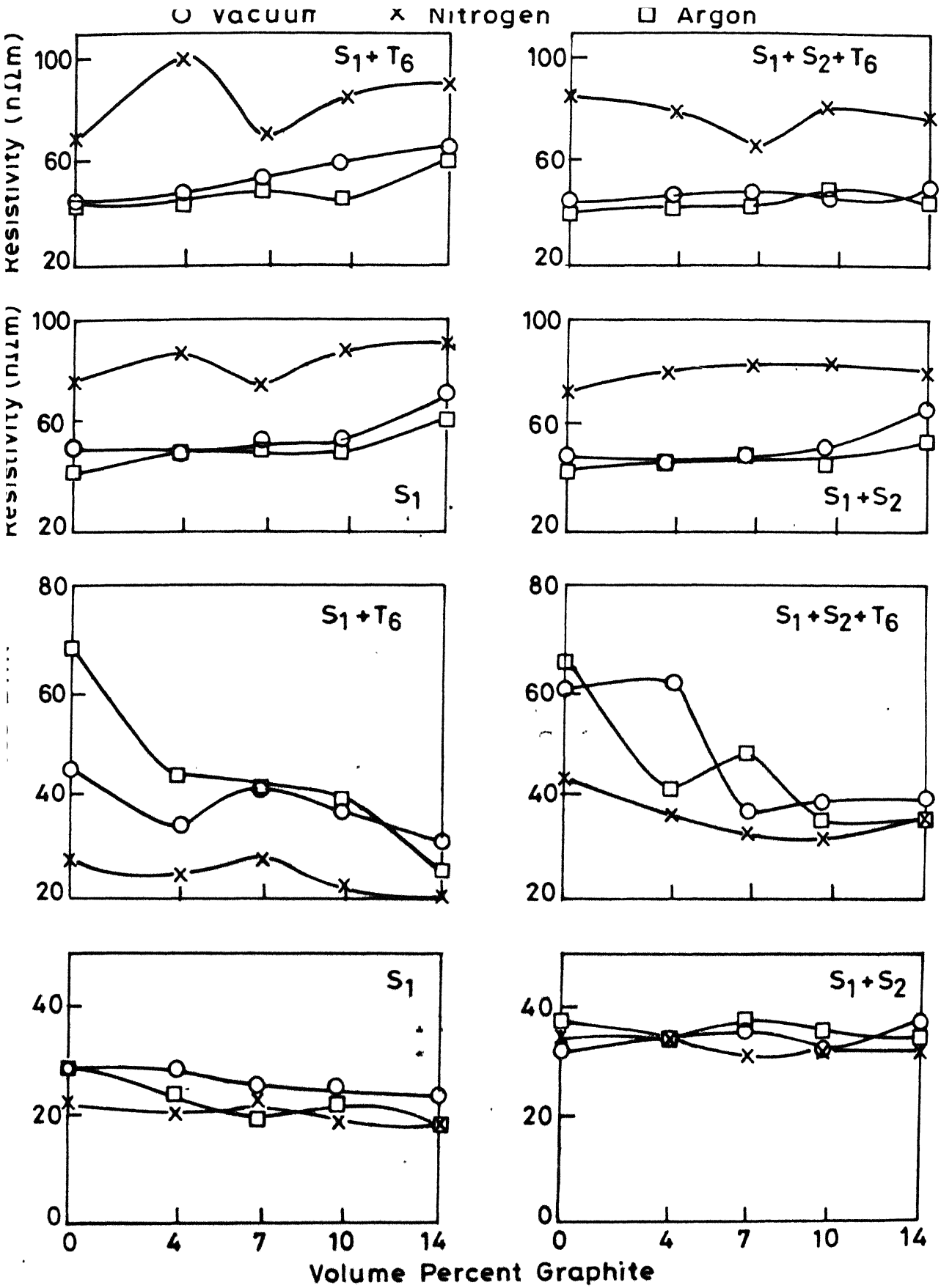

Fig. 3.4 Hardness and electrical resistivity variation of sintered and heat treated 6061 alloy - natural graphite composites as a function of dispersold content.

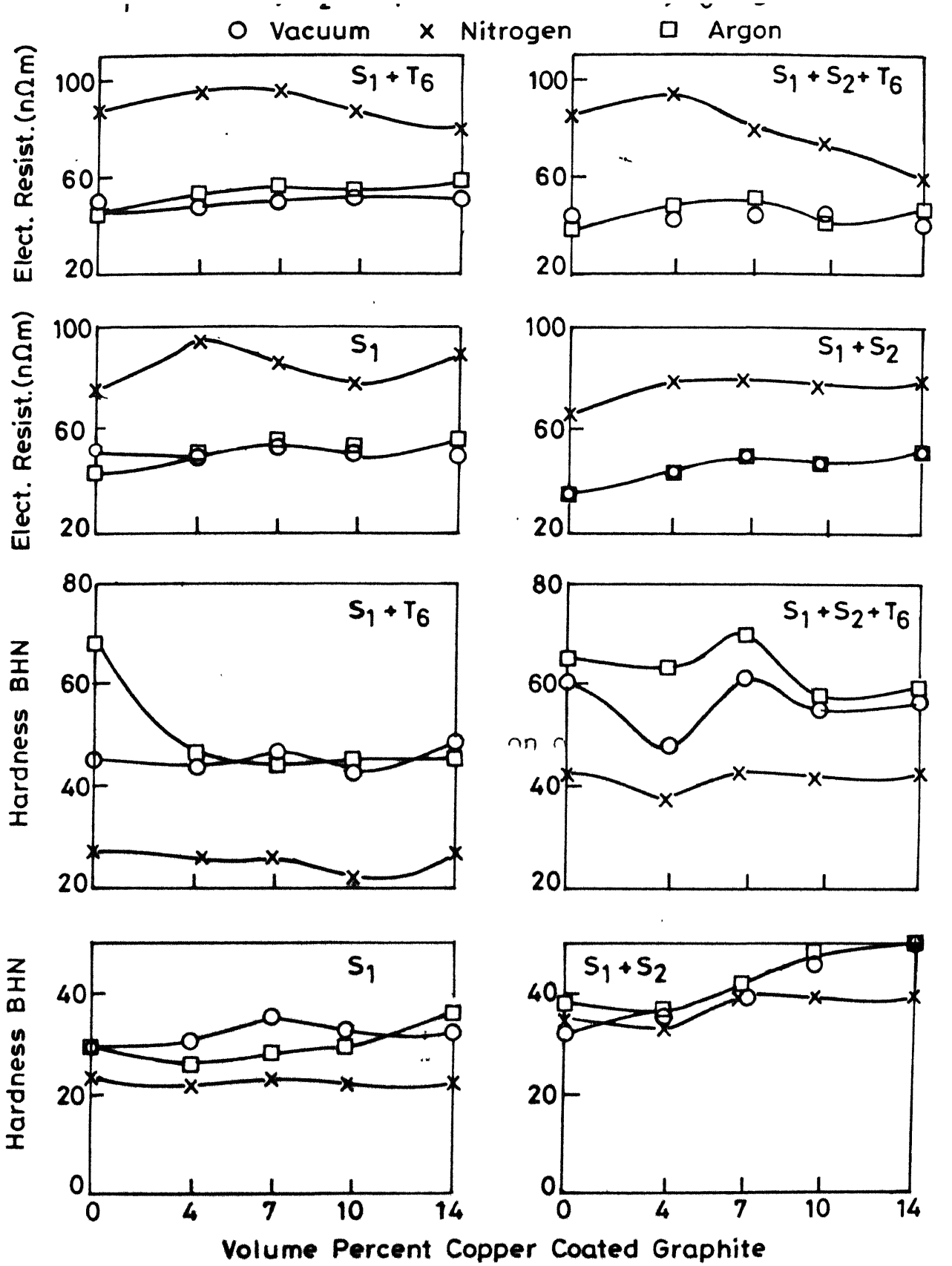

Fig. 3.5 Hardness and electrical resistivity variation of sintered and heat treated 6061 alloy-copper coated graphite composites as a function of dispersoid content.

III.2.3. Tensile Mechanical Properties:

Table III.1 shows the mechanical properties of 6061 alloy and composites containing 7 vol. % of uncoated graphite. There is a marginal decrease in UTS value of sintered composites with addition of 7 vol. % graphite. However, yield stress and percent elongation decreased by 20% with the same amount of graphite addition.

Table III.1

Tensile properties of sintered 6061 alloy and 6061 alloy-7 vol. % graphite composites

Compositions	UTS MPa	Y.S. MPa	Percent elongation
6061 alloy	90	65	15
6061 - 7 vol. % graphite	87	48	12

III.2.4. Electrical Resistivity:

Electrical resistivity variation (Figures 3.4 and 3.5) of the sintered composites show an increase in the values after uncoated graphite addition. Increase in the resistivity values were less in case of the composites with copper coated graphite as compared to uncoated ones. It is evident that nitrogen atmosphere sintering imparted maximum resistivity for any of the compositions.

III.2.5. Surface Roughness:

Surface roughness value (CLA) of 6061 alloy composites remained uneffected with addition of 14 vol. % of graphite. R_a values were 1.8 and 1.9 μm for straight 6061 alloy and its composites containing 14 vol. % of graphite particles.

III.2.6. Microstructure:

Optical micrographs of sintered 6061 alloy and composites containing 7 and 14 vol. % of uncoated and copper coated graphite are shown in Figure 3.6. The microstructures of the compacts containing copper coated graphite showed well revealed grains (Figures 3.6c and e). Finely dispersed constituents can also be observed in the centre of the grains. Composites containing uncoated graphite particles revealed relatively less number of matrix grain. Emergence of porosity with increasing volume fraction of graphite could not be observed from the micrographs.

SEM micrographs of the sintered compacts of 6061 aluminium alloy (Figure 3.8) show the presence of interconnected and closed porosity in the matrix. Interconnected as well as interfacial porosities are also evident in Figure 3.9a. Micrograph of composites containing 14 vol. % of copper coated graphite (Figure 3.9b) reveals absence of porosities at the matrix dispersoid interface. X-ray dot mapping obtained by WDXS analysis (Figure 3.10) for copper showed the presence of copper throughout the matrix.

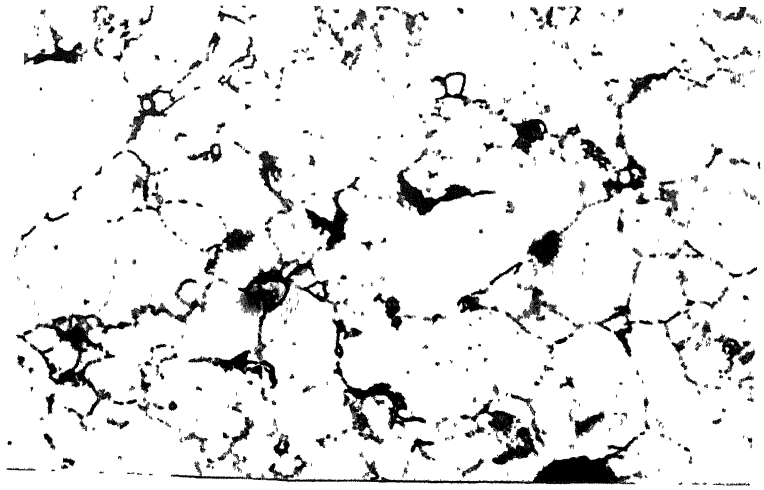

(a)

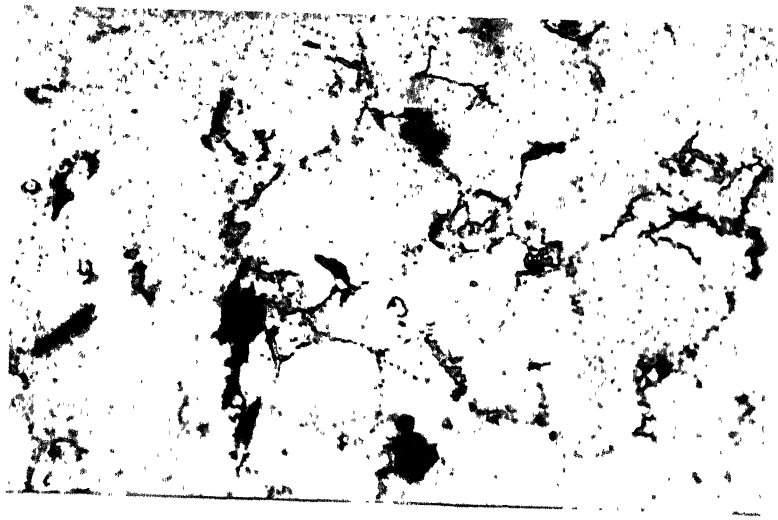

(b)

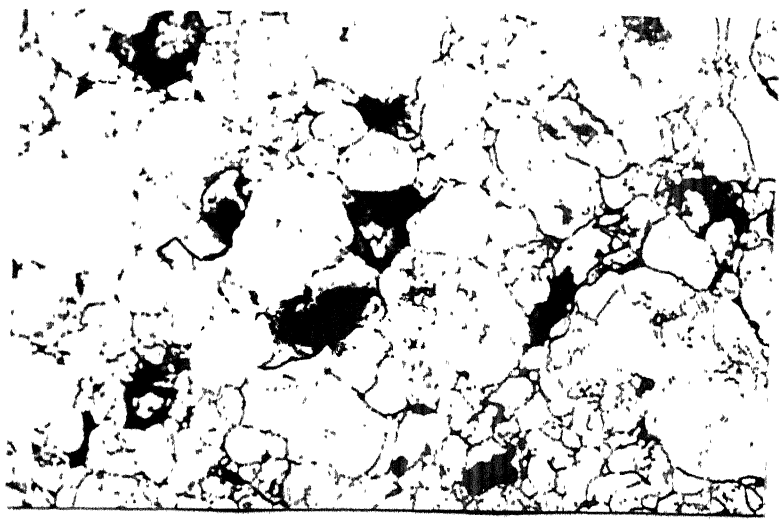

(c)

Fig. 3.6 contd.

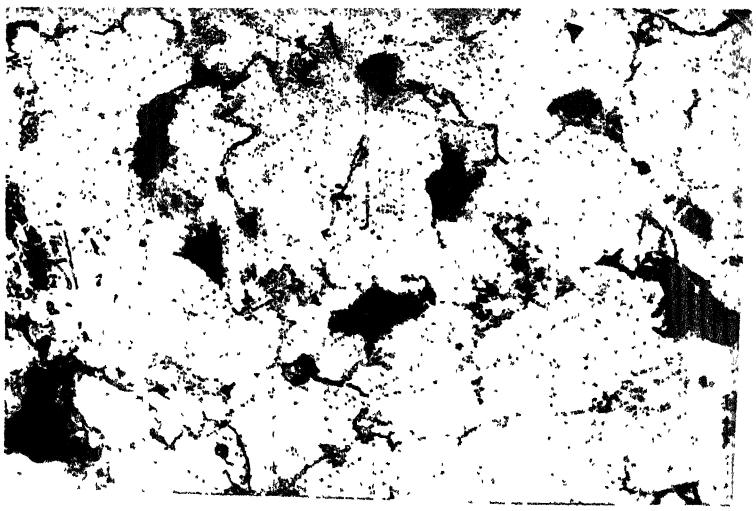

(d)

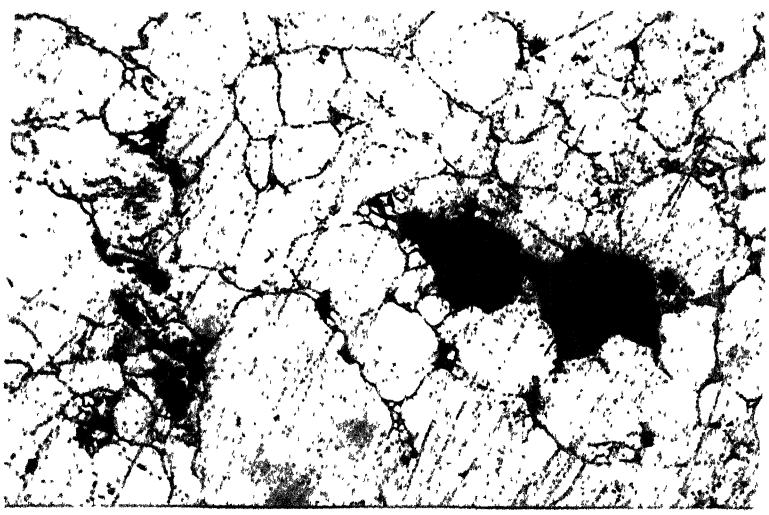

(e)

Fig. 3.6. Optical micrographs of sintered 6061 alloy and its composites containing (a) 0 percent graphite (b) 7 volume percent graphite (c) 7 volume percent copper coated graphite (d) 14 volume percent graphite (e) 14 volume percent copper coated graphite (all after argon sintering) (X200).

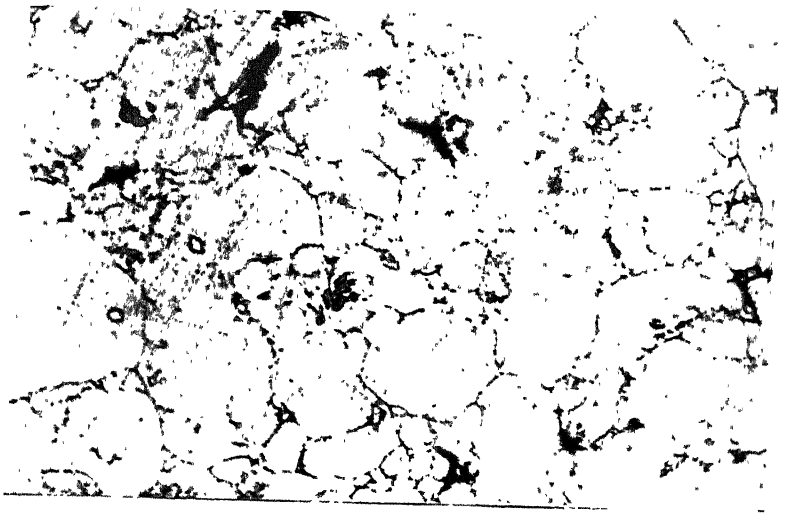

(a)

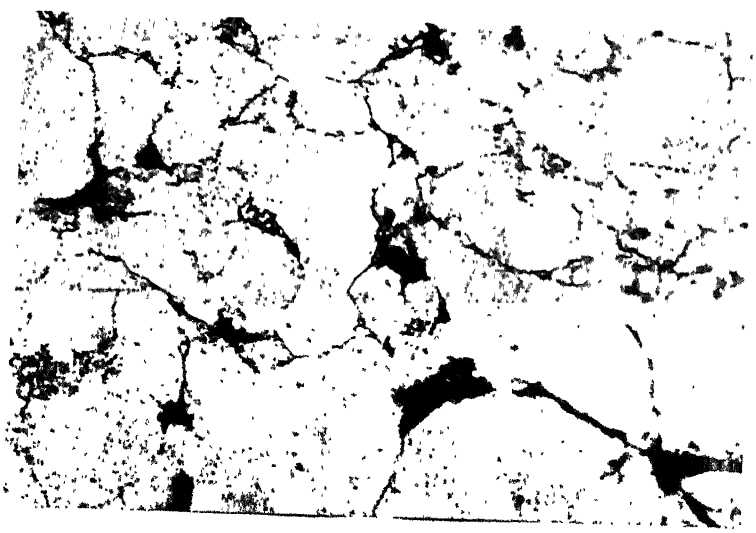

(b)

(c)

Fig. 3.7 contd.

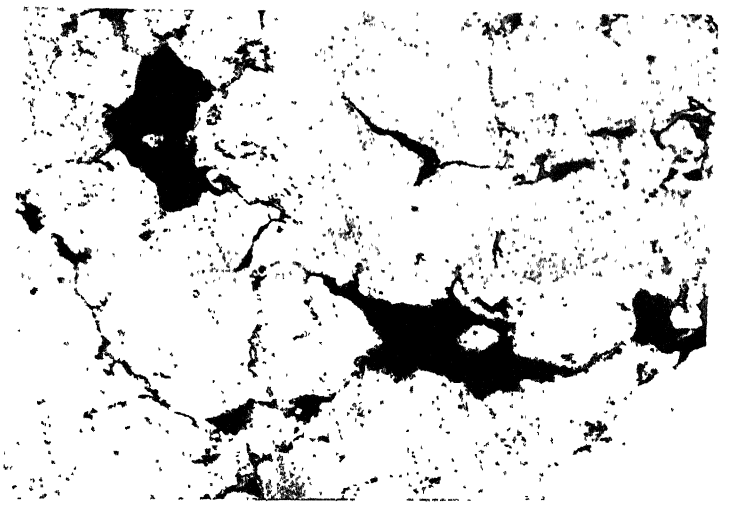

(d)

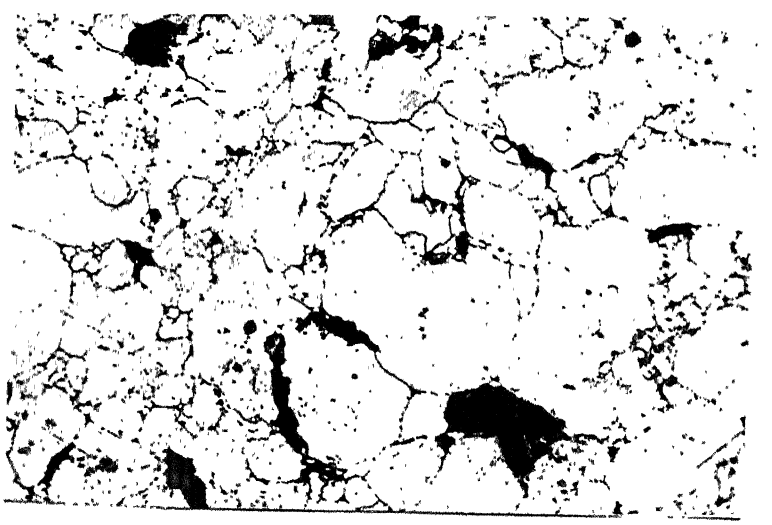

(e)

Fig. 3.7. Optical micrographs of repressed-resintered 6061 alloy and its composites containing (a) 0 percent graphite (b) 7 volume percent graphite (c) 7 volume percent Cu-coated graphite (d) 14 volume percent graphite (e) 14 volume percent copper coated graphite (all after argon sintering) (200X)

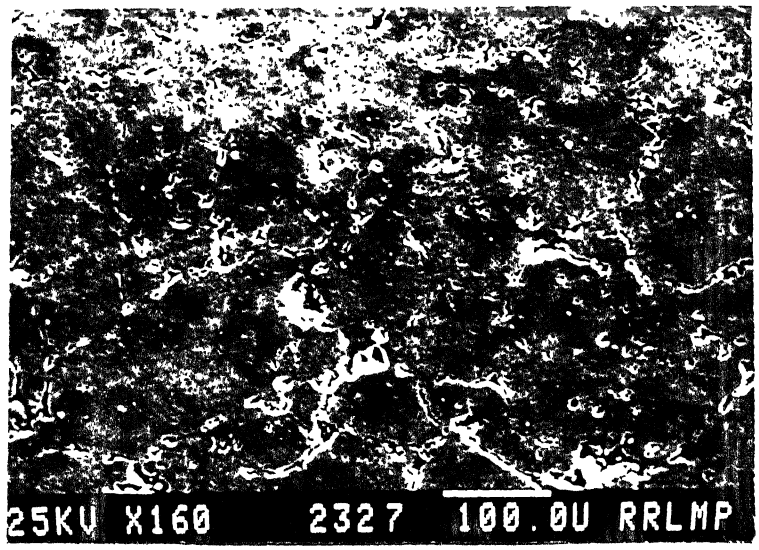

(a)

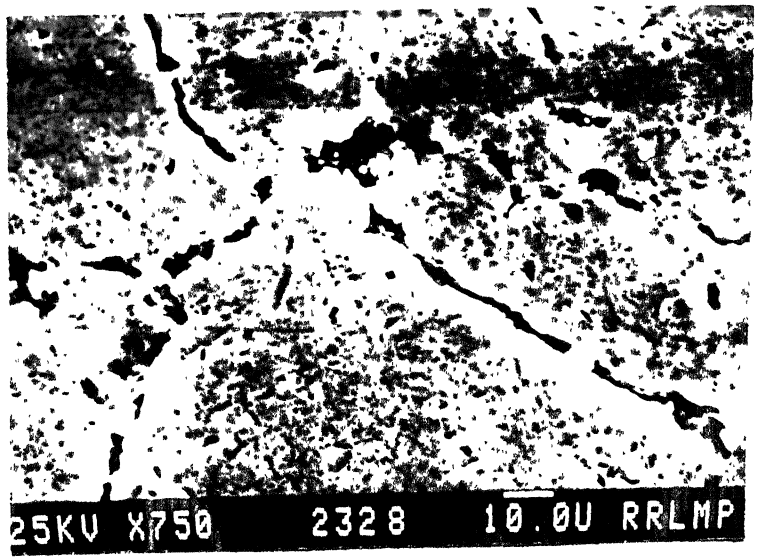

(b)

Fig. 3.8. SEM micrographs of 6061 alloy compact after argon sintering at different magnifications.

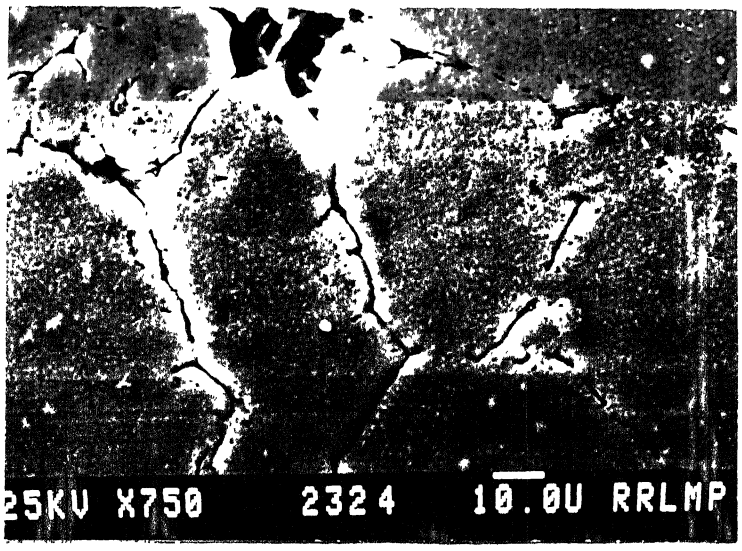

(a)

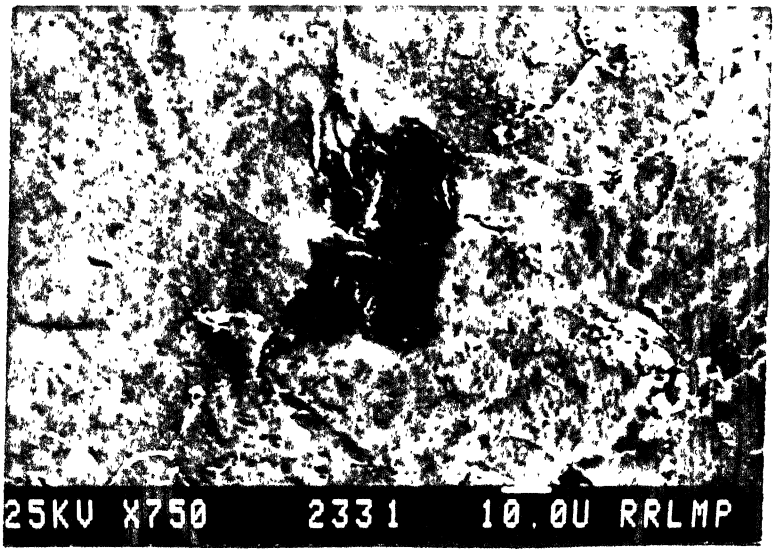

(b)

Fig. 3.9. SEM micrographs of composites containing (a) 7 volume percent graphite and (b) 14 volume percent copper coated graphite, after argon sintering.

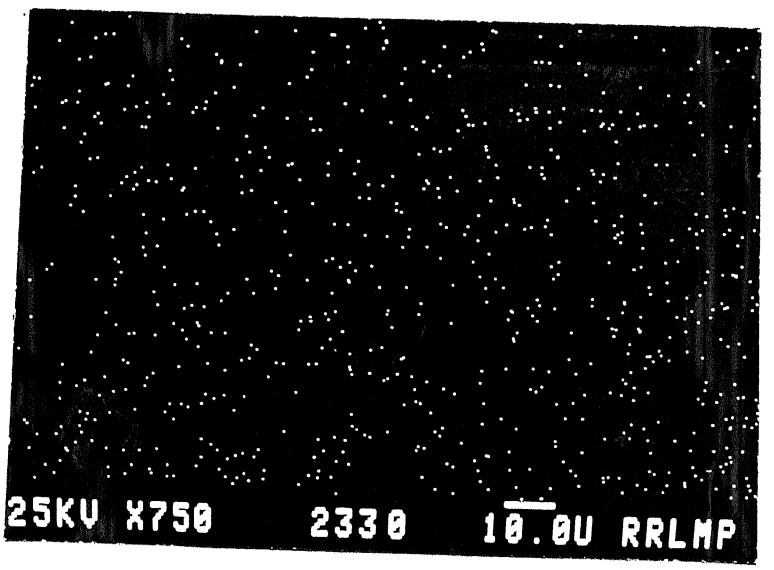

(a)

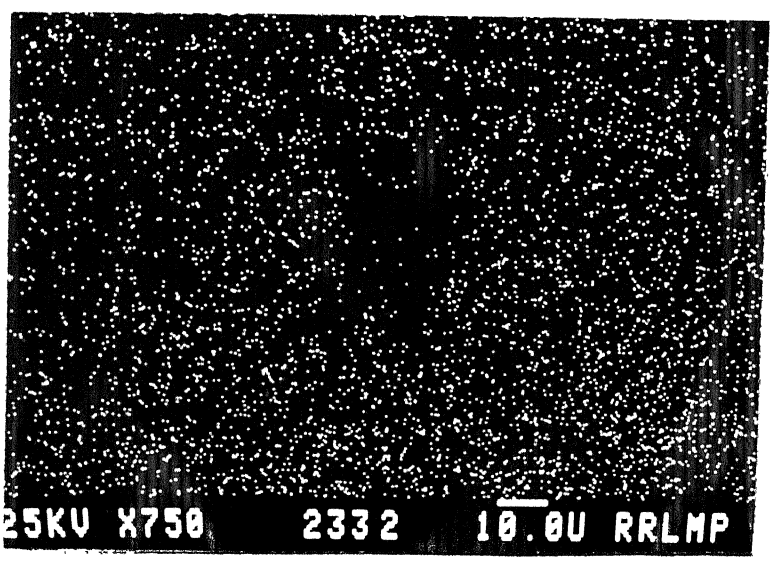

(b)

Fig. 3.10. WDXS mapping for CuK_{α} of 6061 alloy composites containing 14 volume percent graphite and (b) 14 volume percent copper coated graphite, after argon sintering.

III.3. Properties of Repressed-Resintered Composites:

III.3.1. Densification Behaviour:

Repressing and resintering of the sintered composites containing uncoated and copper coated graphite resulted in improved densification (Figures 3.2 and 3.3). Porosity level in the repressed-resintered compacts decreased to maximum of order of 60% in case of composites containing uncoated graphite.

III.3.2. Hardness:

Brinell hardness of sintered composites increased significantly after repressing and resintering (Figures 3.4 and 3.5). In case of composites containing uncoated graphite, volume fraction of dispersoid and sintering atmosphere did not influence the hardness, whereas hardness of the resintered composites containing coated graphite particles remained constant up to 4 vol. % of dispersoid. Further addition resulted in a linear increase in the hardness value. A maximum of 15% increase in hardness value can be observed for composites containing 14 vol. % of coated graphite when sintered in argon.

III.3.3. Electrical Resistivity:

Electrical resistivity value of composites decreased after resintering (Figures 3.4 and 3.5). Maximum values can be seen for the composites sintered in nitrogen atmosphere.

III.3.4. Microstructure:

Figure 3.7 shows the microstructures of repressed and resintered composites containing 7 and 14 vol. % of uncoated and copper coated graphite respectively. Micrographs of 6061 alloy compacts reveal a significant decrease in porosity after resintering. Emergence of well developed grain in composites containing copper coated graphite is also evident from the microstructures (Figures 3.7c and e).

III.4. Properties of Heat Treated Composites:

III.4.1. Hardness:

Effect of age hardening is maximum for compacts of 6061 alloy after argon sintering (Figures 3.4 and 3.5). Hardness value of aged composites decreased with volume fraction of uncoated graphite, whereas, amount of copper coated graphite did not effect the hardness of composite after age hardening.

III.4.2. Tensile Mechanical Properties:

Mechanical properties of heat treated composites as a function of volume fraction of graphite is shown in Figure 3.11. The plot reveals that UTS of the composites decreased with increasing volume fraction of graphite. Addition of 14 vol. % graphite resulted in 60% decrease in UTS value as compared to straight 6061 alloy. Yield stress of composites decreased linearly with volume fraction of graphite. A 50% reduction in Y.S. of composite after

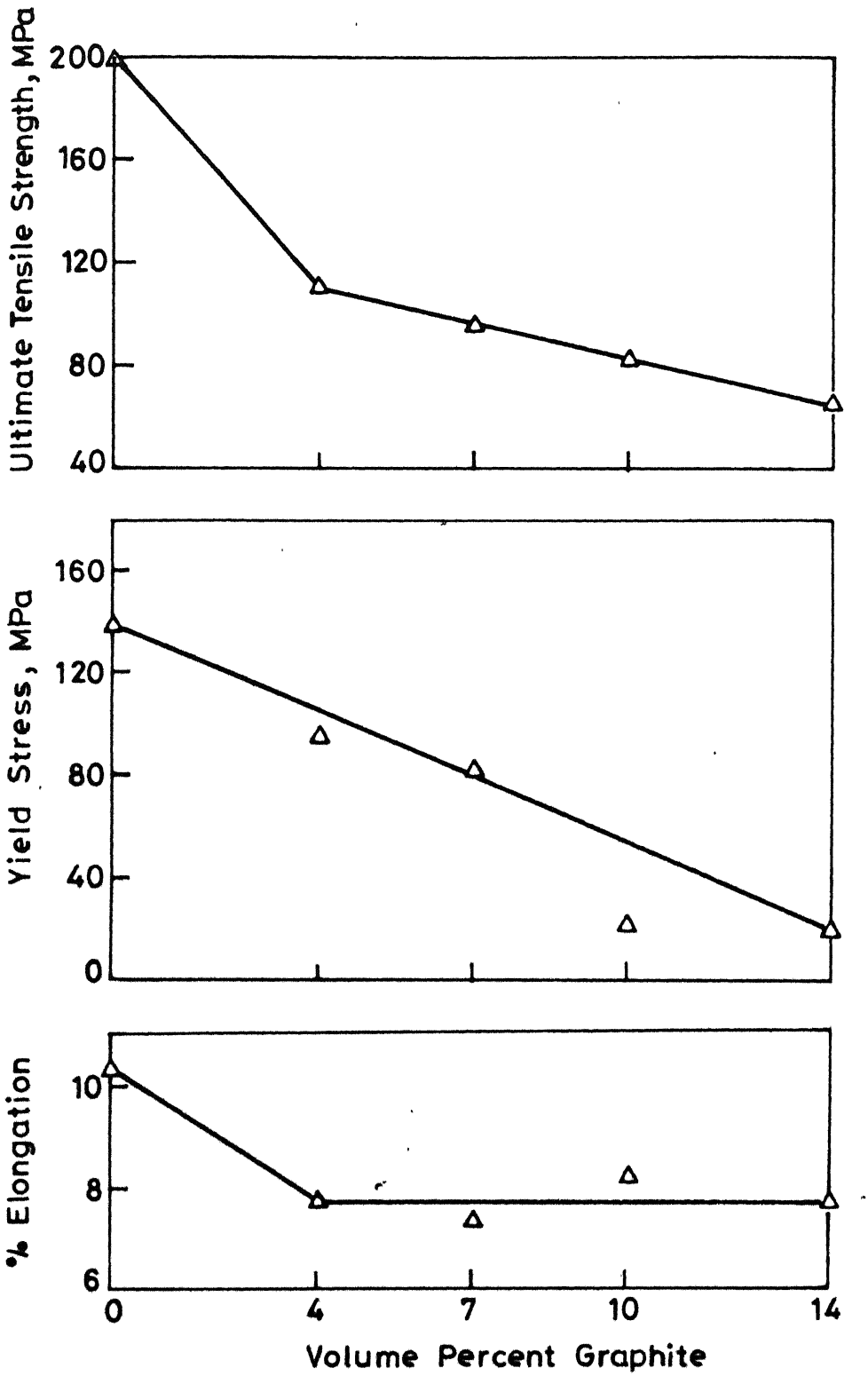

Fig. 3.11 UTS, Y.S. for 0.2% offset and % elongation variations of sintered and heat treated 6061 alloy-graphite composites as a function of dispersoid content.

14 vol. % graphite addition was observed (Figure 3.11). After the initial decrease with addition of 4 vol. % graphite, percent elongation value remained constant with further graphite additions.

III.4.3. Electrical Resistivity:

There was a marginal increase in resistivity value after age hardening of the composites (Figures 3.4 and 3.5). Resintered composites after T6 treatment had similar resistivity values to those of as sintered compacts after T6 treatment. It is evident that sintering in nitrogen imparted maximum resistivity even after the additional treatment of resintering and age hardening. Resistivity values of age hardened composites containing copper coated graphite decreased, when the dispersoid was beyond 7 vol.% .

III.4.4. Fractography:

SEM micrographs of fractured surfaces of age hardened 6061 alloy and composites containing 14 vol. % graphite are shown in Figures 3.12 and 3.13. Fractographs (Figure 3.12a) shows dimple formation of the size of 5 to 20 μm. Cracks can also be observed on the fractured surface (Figure 3.12c). Fractographs of composites containing 14 vol. % graphite (Figure 3.13) reveal significant tearing of the matrix at spots where graphite flakes are present. Deformed layer of the matrix is also noticeable (Figure 3.13b).

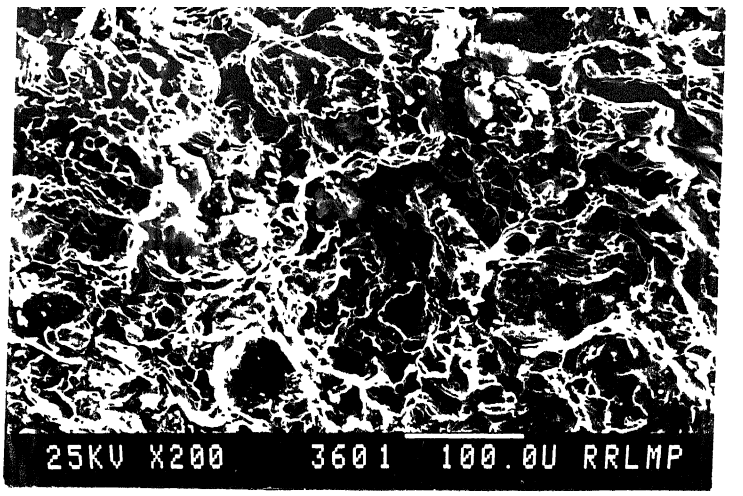

(a)

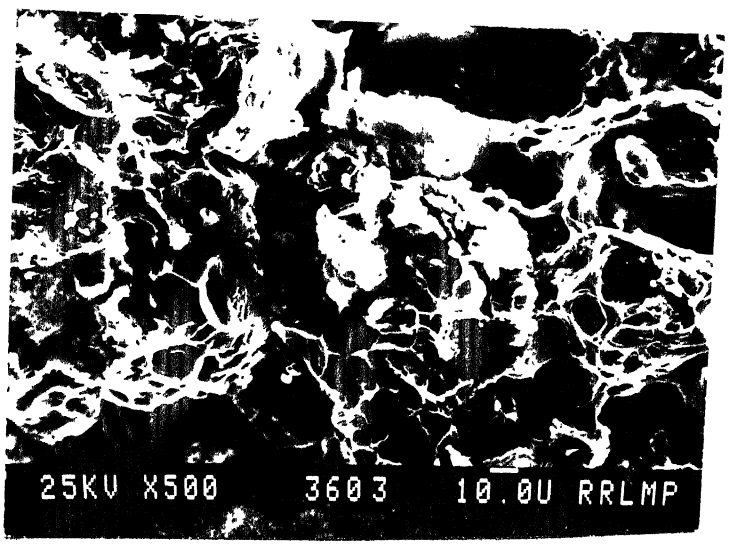

(b)

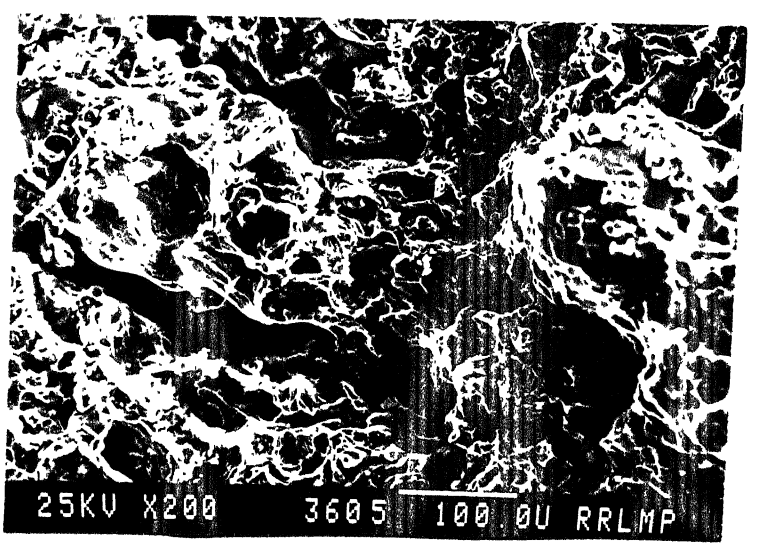

(c)

Fig. 3.12. SEM micrographs of fractured surface of sintered and heat treated 6061 alloy compact after tensile test (a and b at different magnifications).

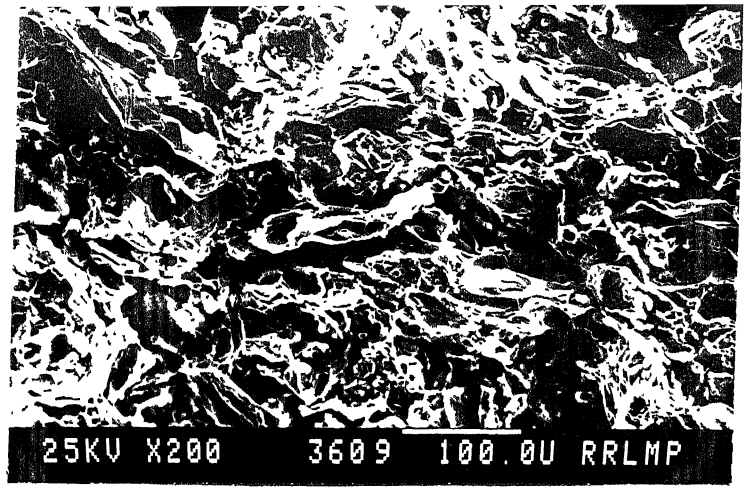

(a)

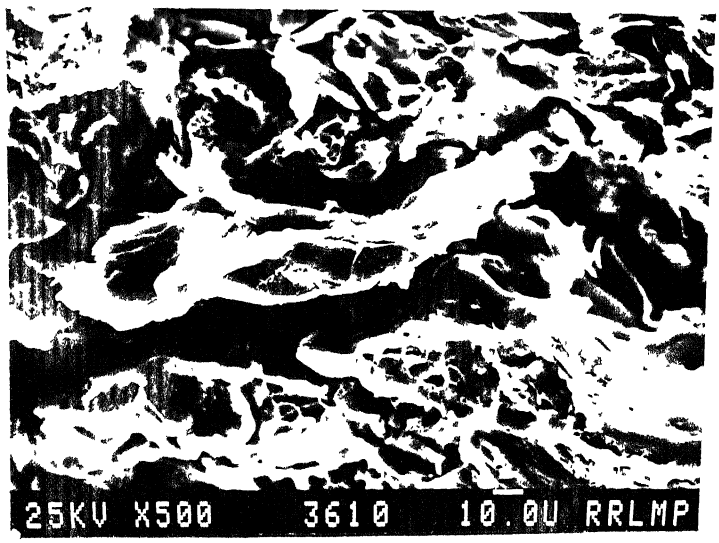

(b)

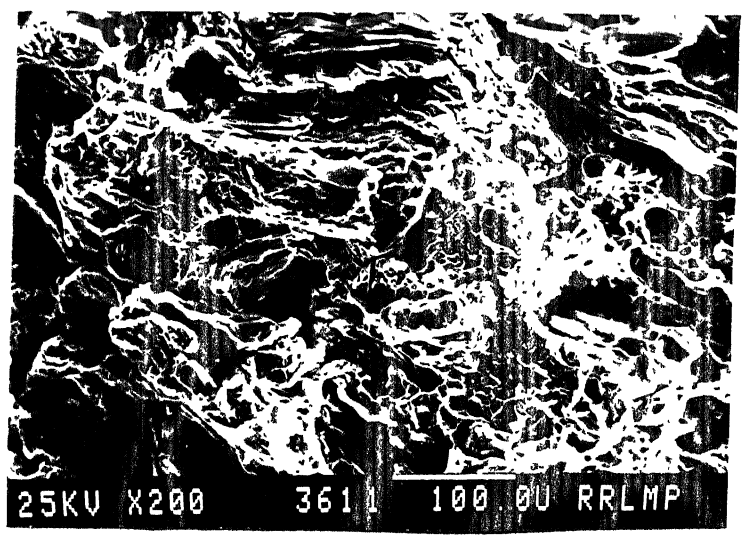

(c)

Fig. 3.13. SEM micrographs of fractured surface of sintered and heat treated 6061 alloy-14 volume percent graphite composites after tensile test (a and b at different magnifications)

III.5. Hardness Variation of Thermomechanically Treated Composites:

Figure 3.14 shows the microhardness variation of sintered and thermomechanically treated composites as a function of graphite volume fraction. Microhardness value of sintered composites remained uneffected with increasing amount of graphite, whereas, increase in its value can be observed for the composites after thermomechanical treatment up to 7 vol. % graphite. The hardness value decreased with further graphite addition.

III.6. Sliding Wear Study:

III.6.1. Wear Loss:

Figure 3.15 shows the effect of volume fraction of graphite on wear rate of the composites. It is evident that wear rate increased linearly with increase in the volume fraction of graphite. Wear rate increased by more than two times with addition of 14 vol. % of graphite.

Effect of sliding distance on the wear loss is shown in Figure 3.16. Wear loss was found to increase linearly with the sliding distance for 6061 matrix alloy as well as composites containing 7 vol. % graphite. It is also apparent that slope of the plot corresponding to composite containing 7 vol. % graphite is more as compared to the slope for straight 6061 alloy.

Figure 3.17 shows the effect of applied pressure on the wear rate of the matrix alloy and composites containing

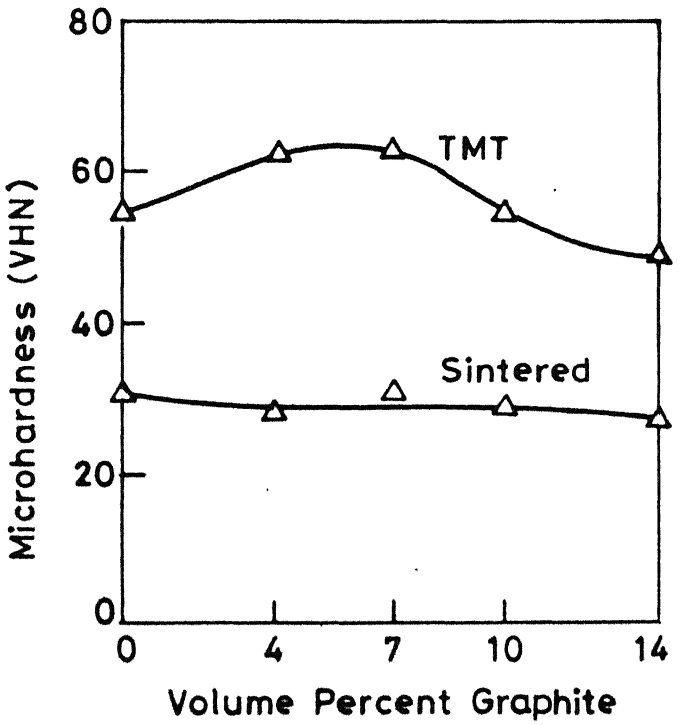

Fig. 3.14 Variation of Vickers hardness of sintered and thermomechanically treated (TMT) 6061 alloy and its graphite containig composites as a function of dispersoid content.

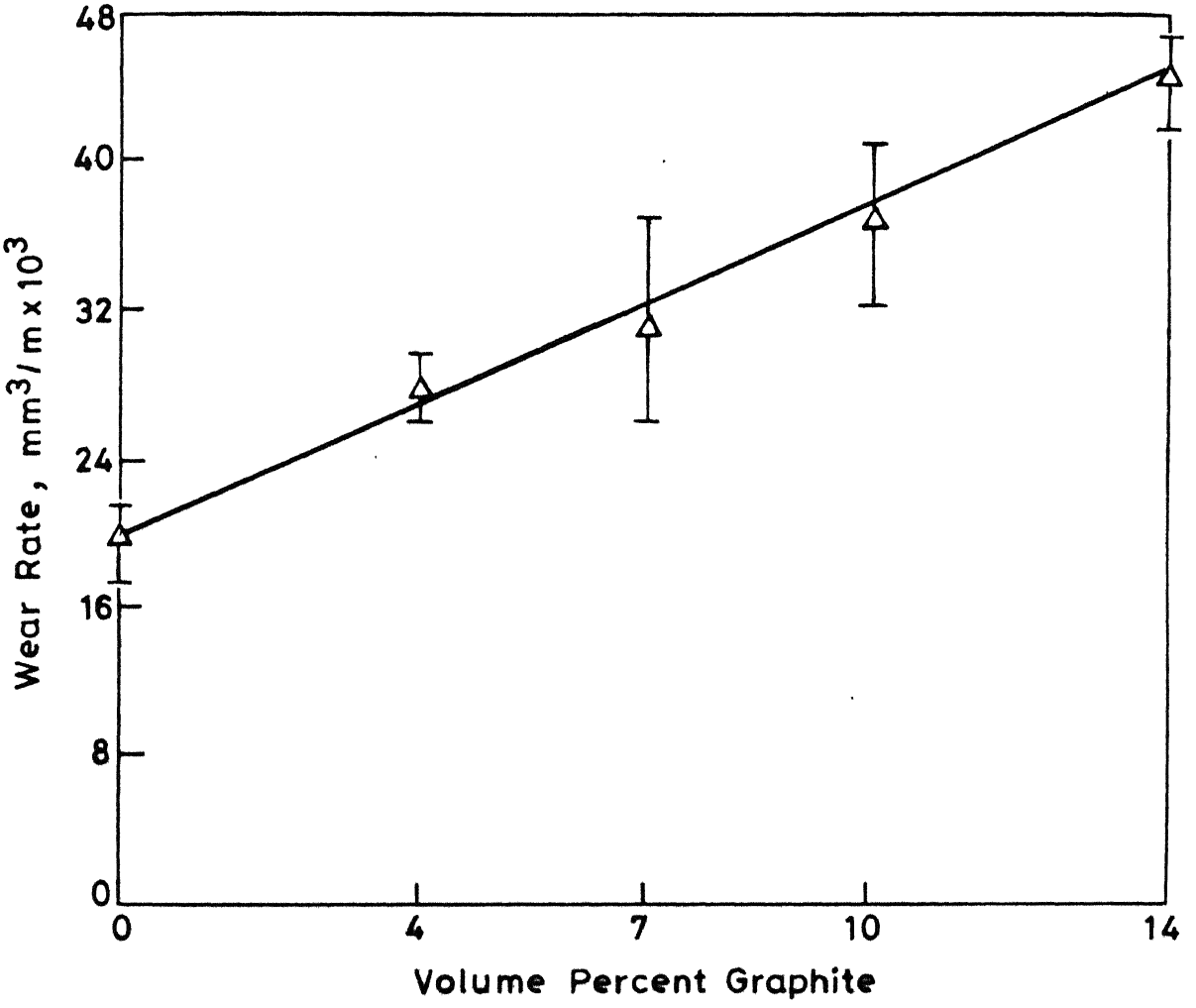

Fig. 3.15 Effect of volume percentage of graphite on the wear rates of sintered 6061 alloy composites (sliding speed: 0.5 m/s; Applied pressure: 12×10^{-2} MPa; Sliding distance: 250 meters)

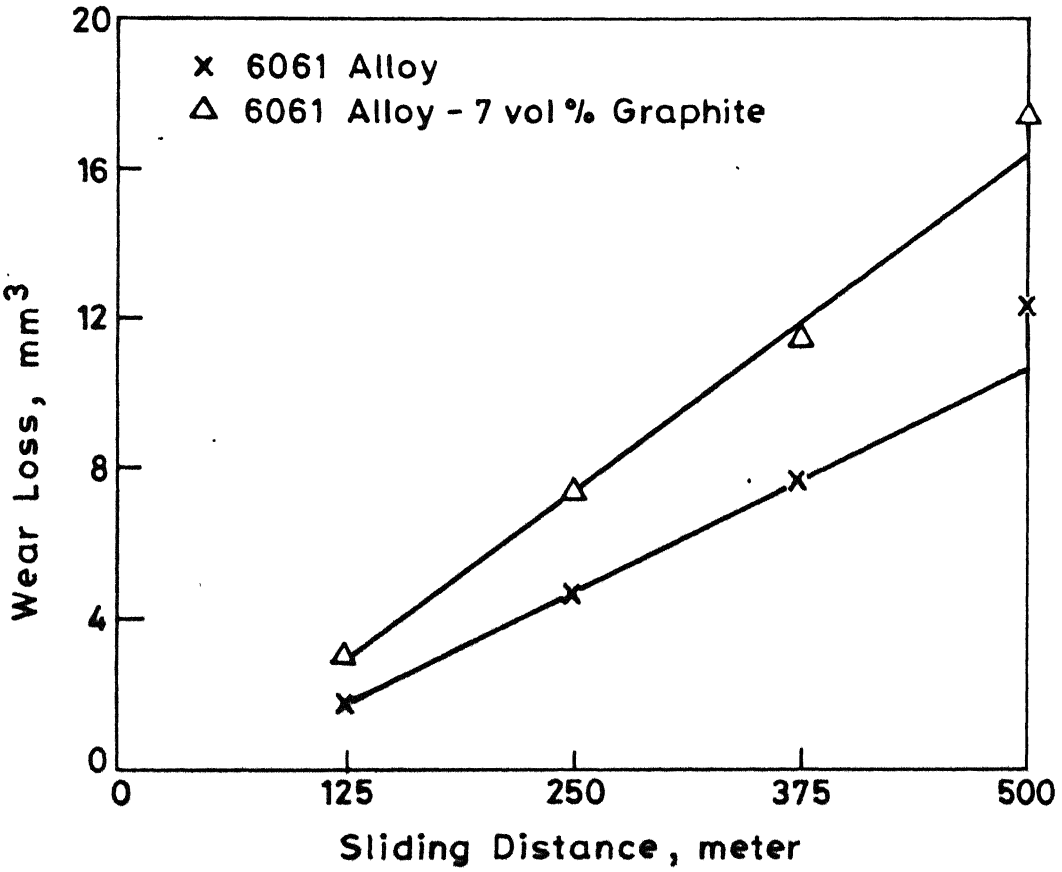

Fig. 3.16 Effect of sliding distance on wear loss of sintered 6061 alloy and its composites containing 7 vol % of graphite (Sliding speed: 0.5 m/s; Applied pressure: 12×10^{-2} MPa)

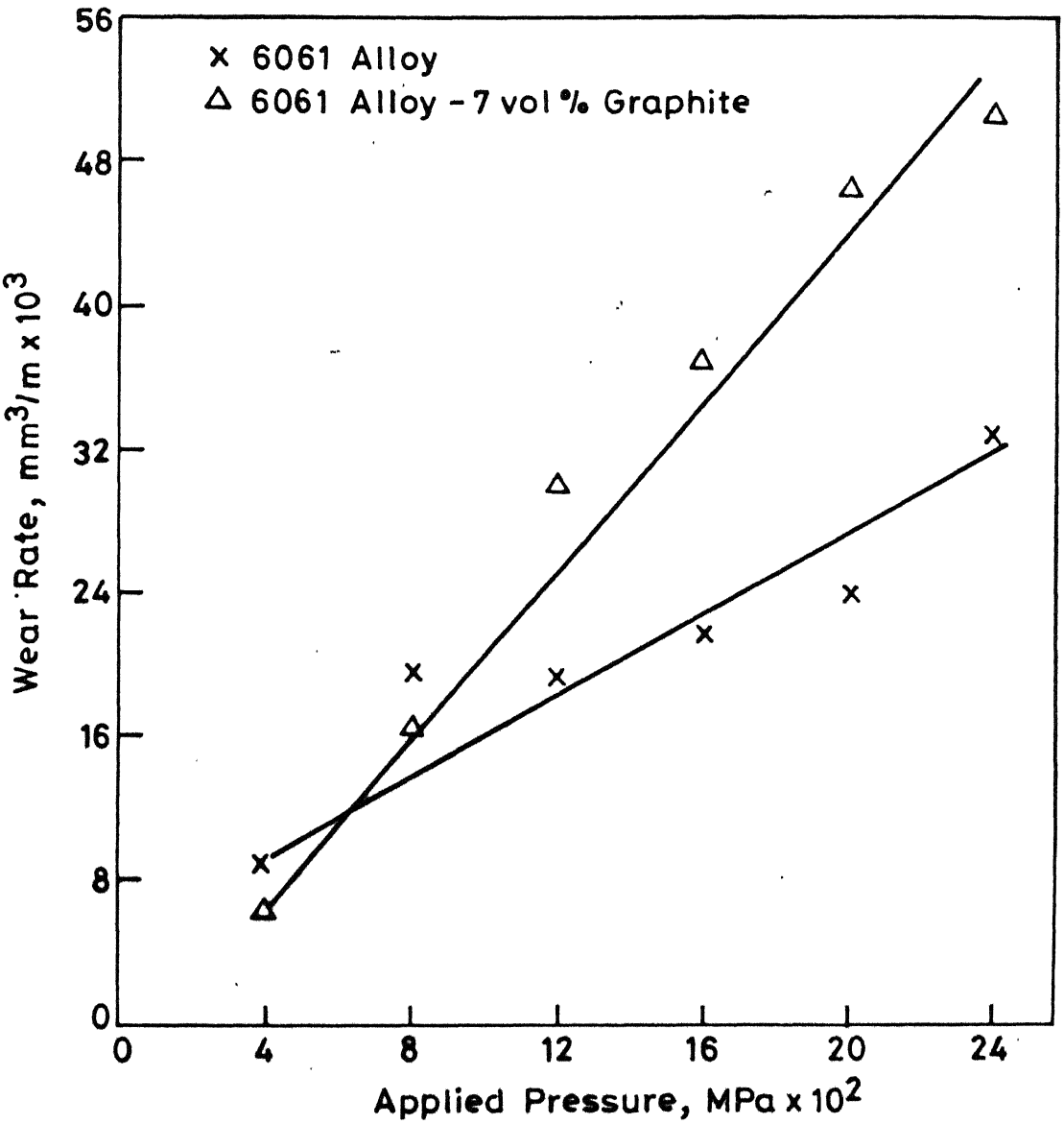

Fig. 3.17 Effect of applied pressure on the wear rate of sintered 6061 alloy and composites containing 7 vol % graphite (Sliding speed: 0.5 m/s; Sliding distance: 250 meters)

7 vol. % graphite. Although the wear rate was found to increase linearly with applied pressure for matrix alloy and composites with 7 vol. % graphite, at lower pressure i.e. 4×10^{-2} MPa wear rate of graphite containing composites was found to be less than that for straight 6061 alloy. At higher pressure, the trend was reverse.

Effect of sliding speed on the wear rate of 6061 alloy and its composites with 7 vol. % graphite is shown in Figure 3.18. Effect of sliding speed on the wear rate of composites containing graphite is only marginal, whereas, wear rate decreased subsequently with increasing sliding speed. Approximately 25% increase in wear rate of 6061 compact can be observed from the plot (Figure 3.18), when the sliding speed was reduced from 1.25 to 0.25 m/s.

III.6.2. SEM Study:

SEM micrographs of typical worn out surfaces of 6061 aluminium alloy and composites containing 7 vol. % graphite are shown in Figures 3.19 and 3.20. There appears to be no significant difference in the features of the worn out surfaces of matrix alloy and composites. There are two distinct features in the micrographs of worn out surfaces. One is the formation of long and continuous grooves and other the patches of severely damaged regions. Compared to the 6061 matrix alloy, worn out surface of composite containing graphite revealed more such patches. EDXS study (Figure 3.21) indicates a small amount of iron pick up by the worn out surface of 6061 alloy.

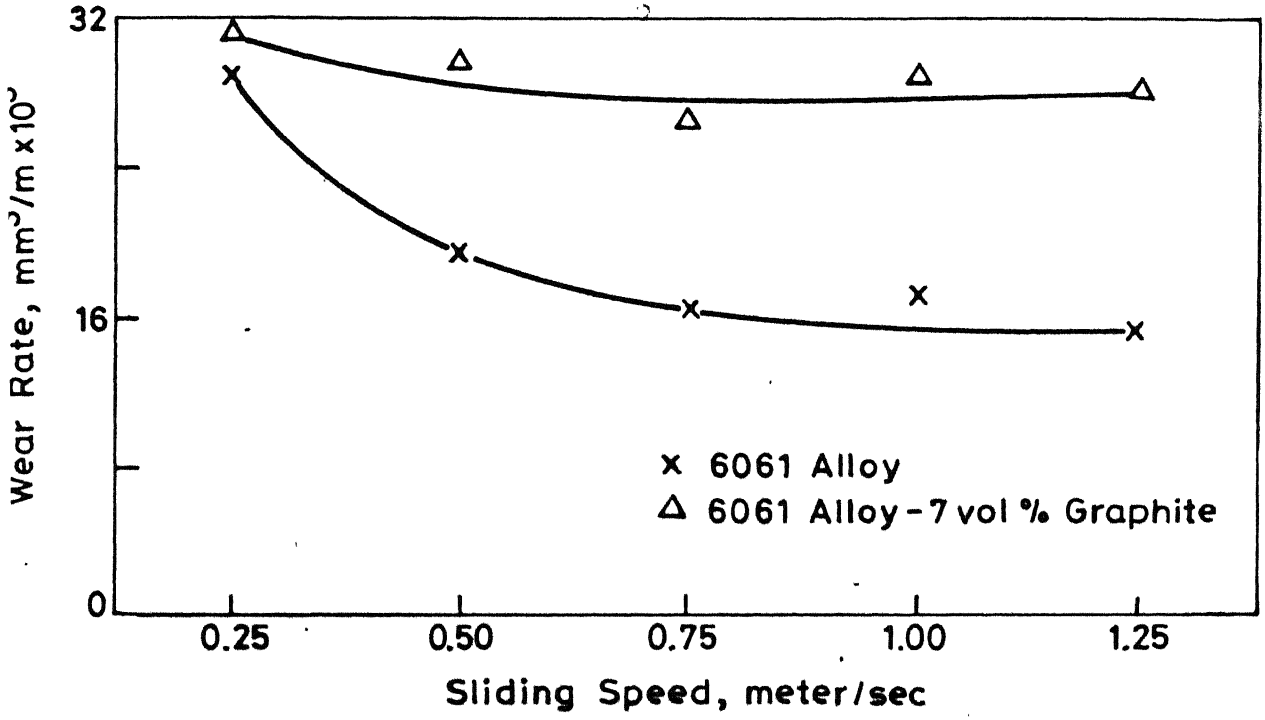

Fig. 3.18 Effect of sliding speed on wear rate of sintered 6061 alloy and composites containing 7 vol % graphite (Applied pressure: 12 $\times 10^{-2}$ MPa; Sliding distance: 250 meters)

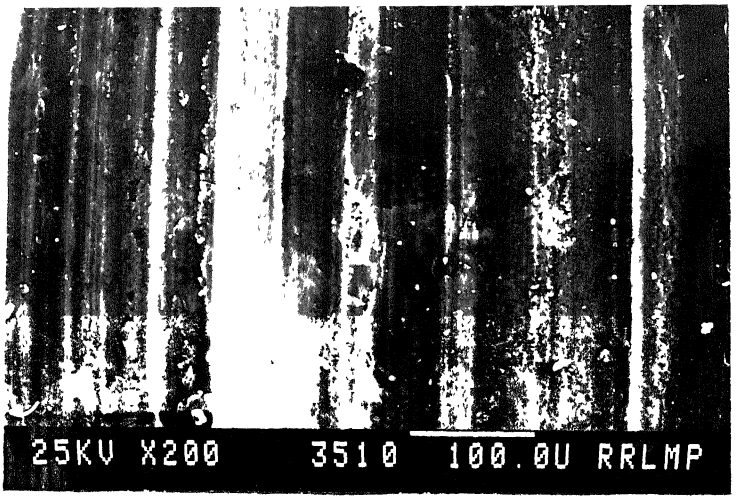

(a)

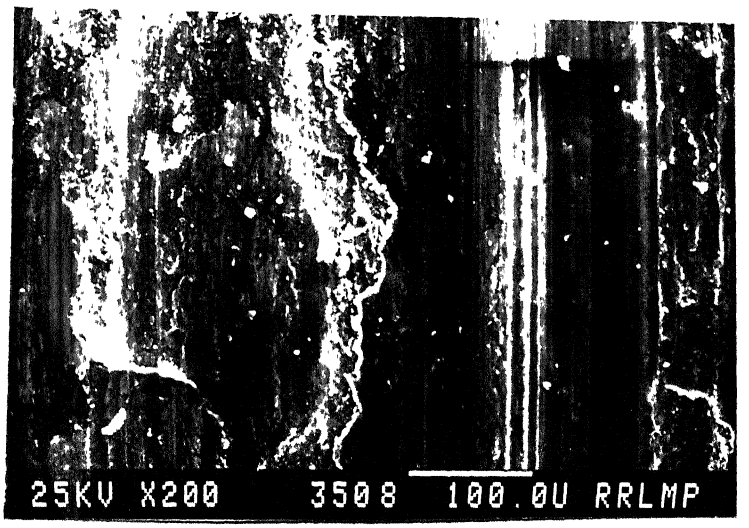

(b)

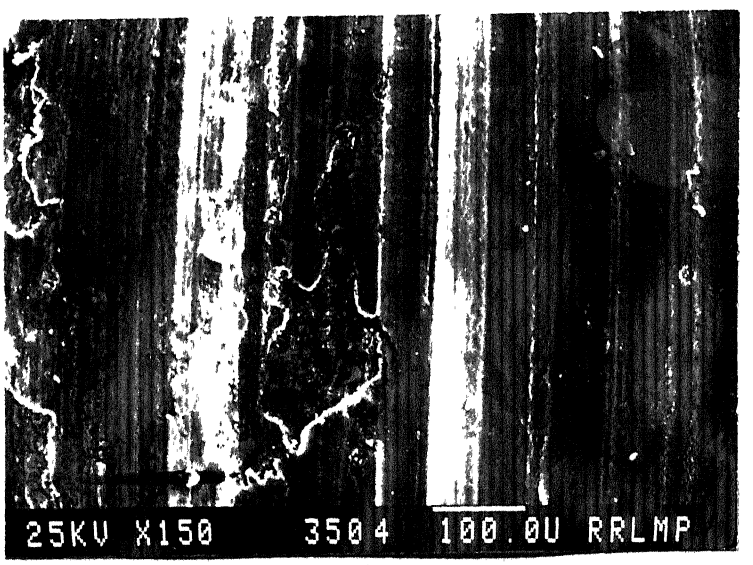

(c)

Fig. 3.19. Typical SEM micrographs of worn out surface of sintered 6061 alloy, showing presence of long and continuous grooves and patches of highly damage regions (Test parameters same as in Fig. 3.15).

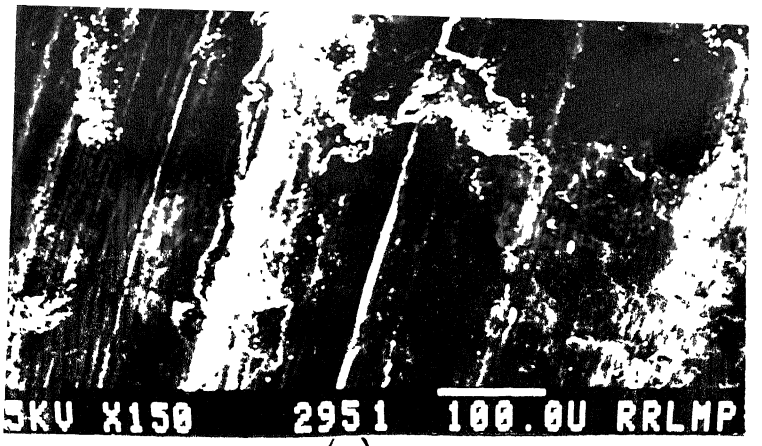

(a)

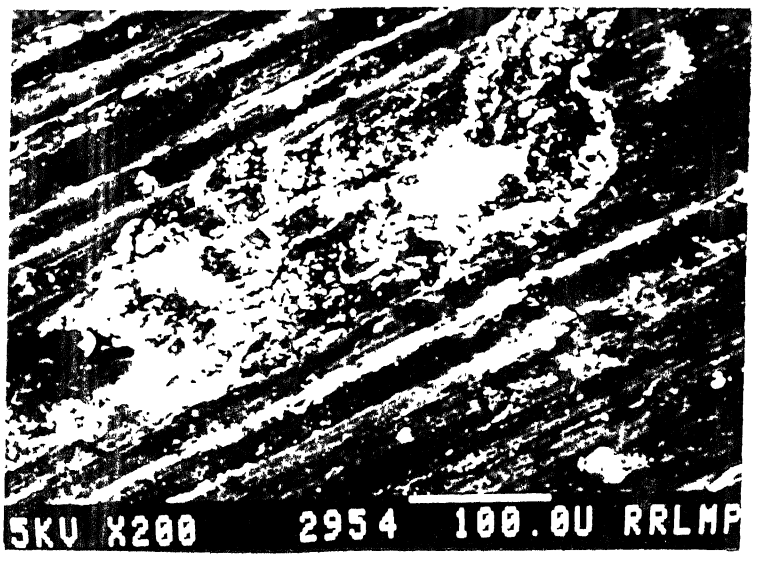

(b)

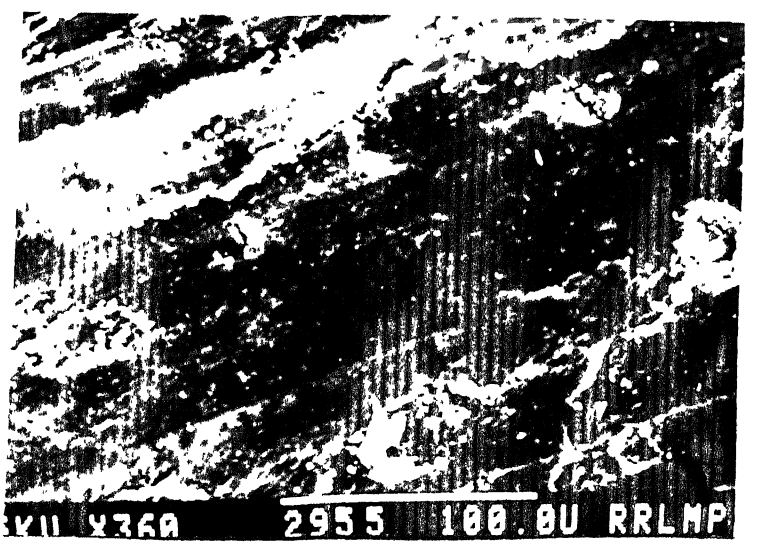

(c)

Fig. 3.20. Typical SEM micrographs of worn out surface of sintered 6061 alloy-7 volume percent graphite composites showing presence of long and continuous grooves and patches of highly damaged regions (Test parameter same as in Fig. 3.15).

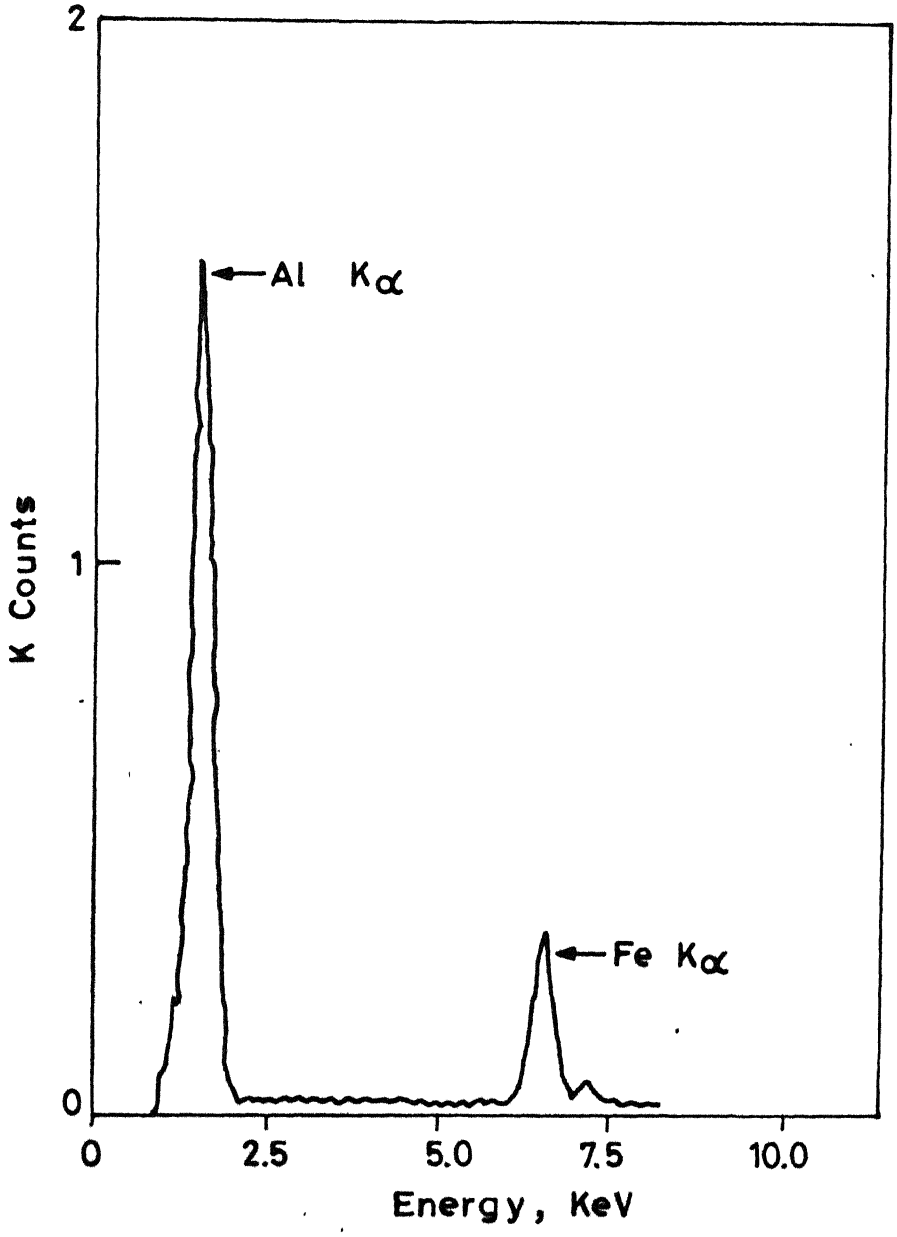

Fig. 3.21 Typical EDXS spectrum of worn out sintered 6061 alloy surface showing Al K_α and Fe K_α peak (test parameters same as in Fig. 3.15)

Debris collected from the wear test of 6061 alloy and composites containing graphite showed similar features (Figures 3.22 to 3.24). Four types of debris collected during the tests are as follows: long needle shape debris, of approximately 500 μm size were less in number and there was considerable amount of iron pick up by these debris as revealed by X-ray dot mapping (Figures 3.22b and e). Maximum number of debris were of flaky (size 100 to 200 μm) in nature. Presence of aluminium debris and iron pick up by few debris were found in this type of debris (Figures 3.22d and e). Figure 3.23 shows the rounded agglomerates (100 μm size) and fine particles (2 to 10 μm) debris. Both of these component in the debris were identified as aluminium based.

Typical SEM micrographs of worn out surfaces of 6061 alloy and its composites containing 7 vol. % graphite are shown in Figures 3.25 and 3.26. Microphotographs show that the worn out surface produced on 6061 alloy during higher speed wear tests (1.25 m/s) was found to be smoother as compared to those produced during low speed wear tests. On the other hand, sliding speed did not impart much difference in the worn out surface of 6061 alloy containing 7 vol. % graphite, when tested at extreme speeds.

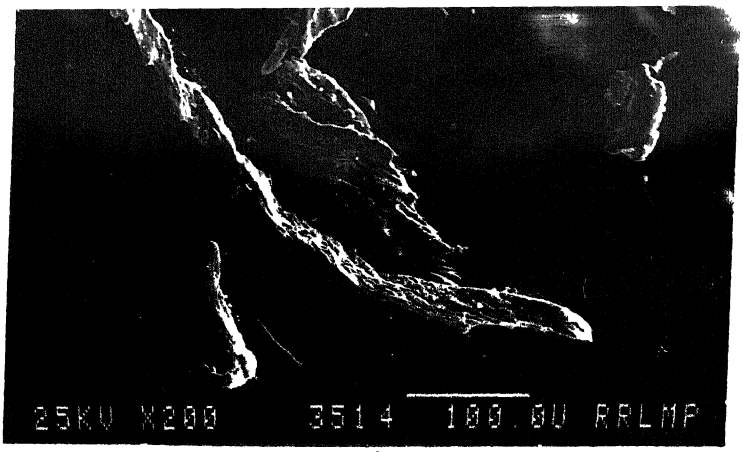

(a)

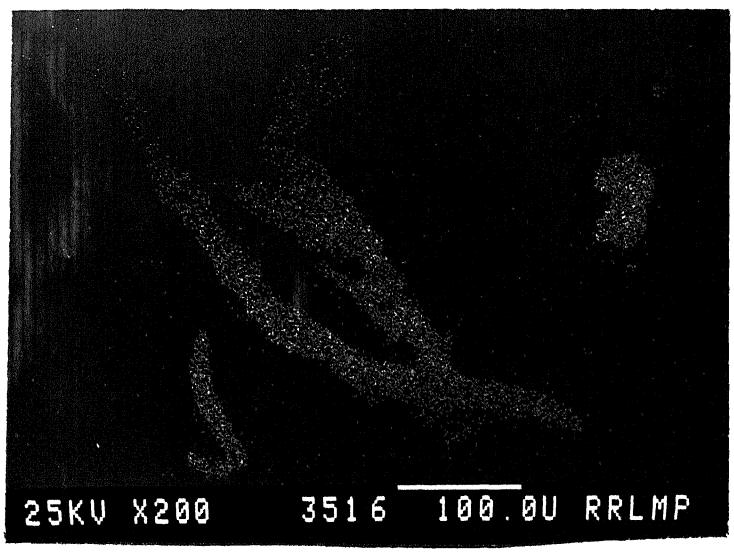

(b)

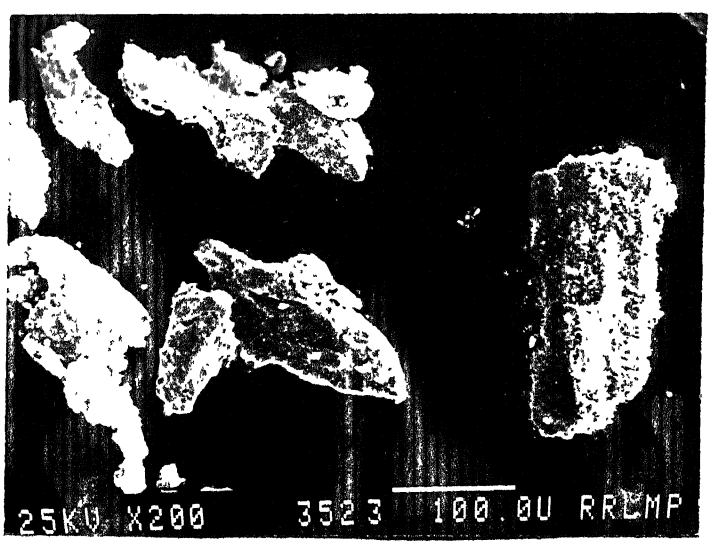

(c)

Fig. 3.22 contd.

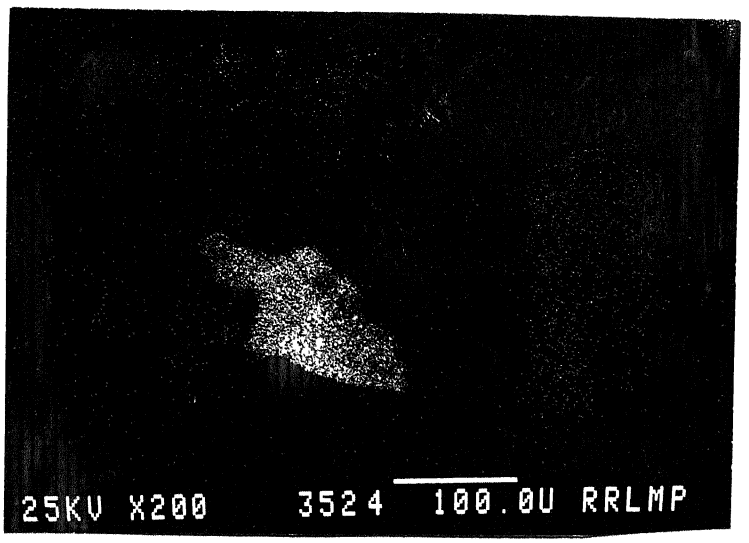

(d)

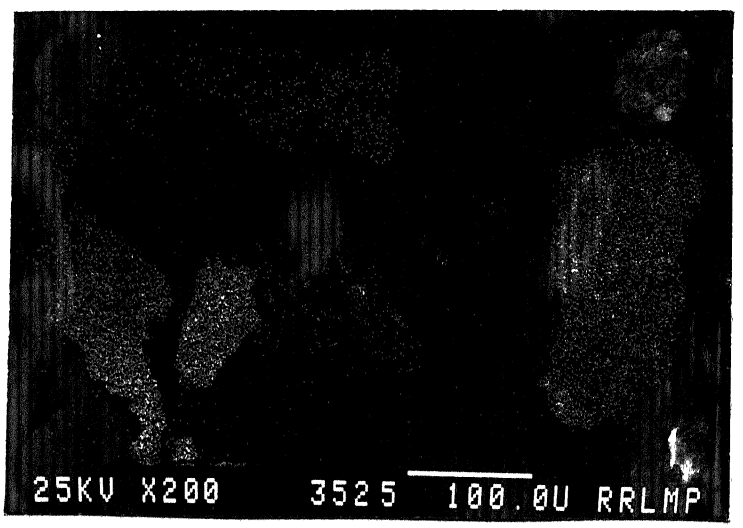

(e)

Fig. 3.22. SEM micrographs of wear debris of sintered 6061 alloy (a) long needle shape debris (b) X-ray dot mapping of (a) for FeK_α peak, (c) flake type debris, (d) X-ray dot mapping of (c) for AlK_α, (e) X-ray dot mapping of (c) for FeK_α (Test parameters same as in Fig. 3.15).

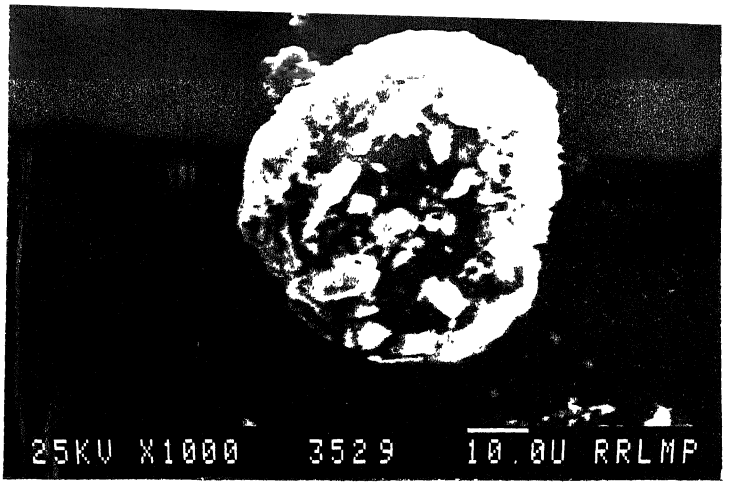

(a)

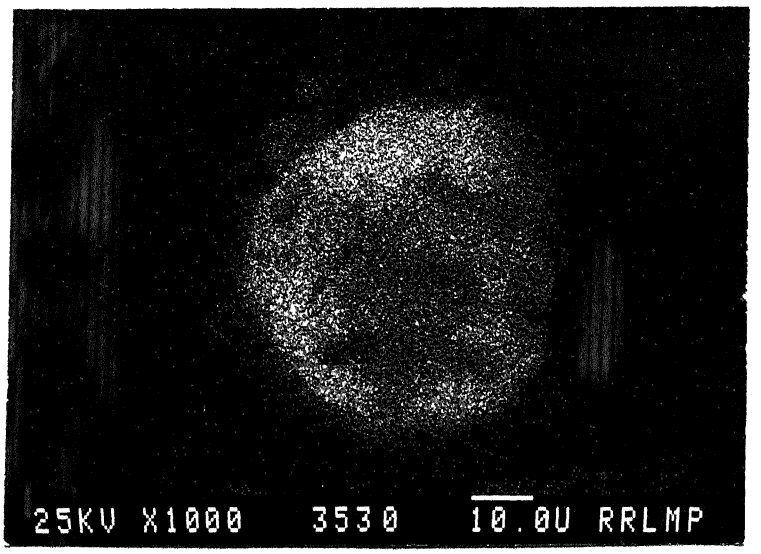

(b)

(c)

Fig. 3.23. SEM micrographs of debris of sintered 6061 alloy (a) rounded agglomerate debris particles (b) a corresponding X-ray dot mapping for AlK_{α} (c) extremely fine debris particles (Test parameter same as in Fig. 3.15).

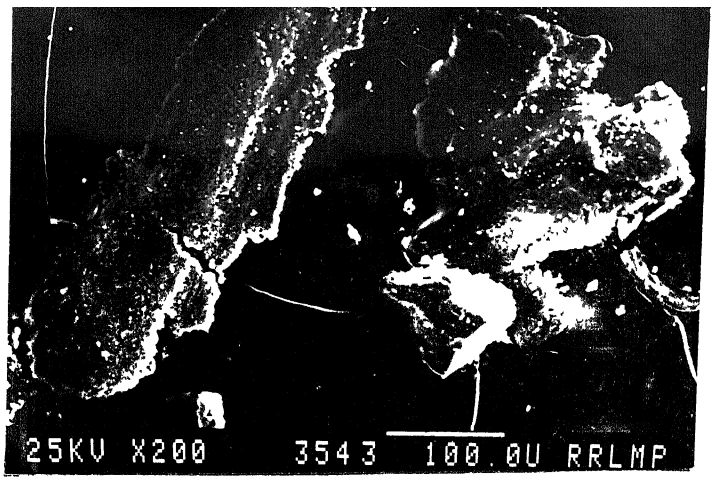

(a)

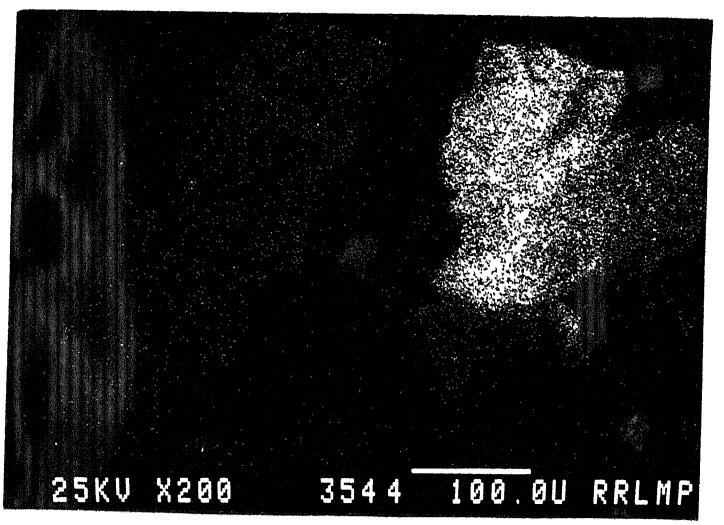

(b)

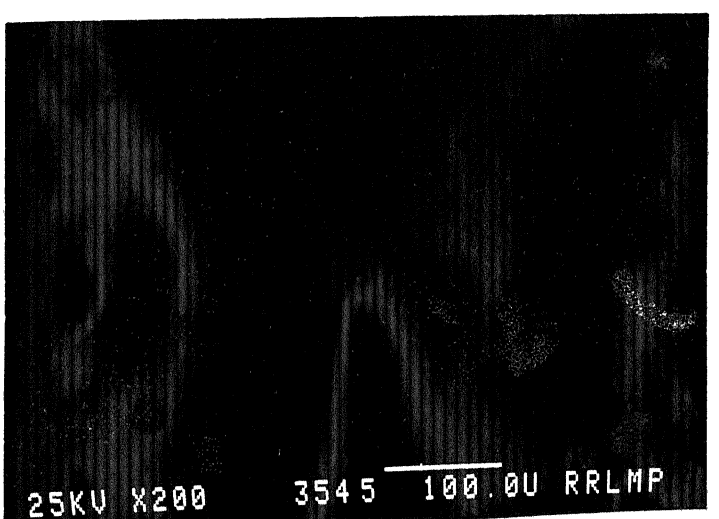

(c)

Fig. 3.24 contd.

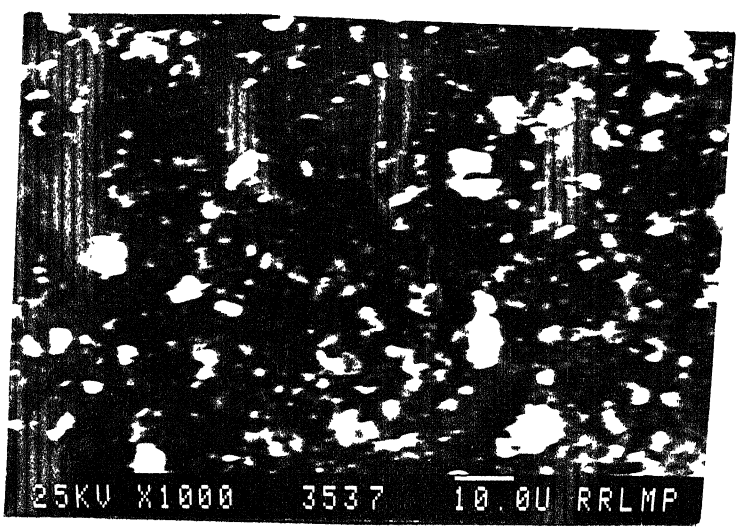

(d)

Fig. 3.24. SEM micrographs of wear debris of sintered 6061 alloy-7 volume percent graphite composite (a) flaky irregular shape debris (b) X-ray dot mapping of (a) for FeK_{α} peak (c) X-ray dot mapping for AlK_{α} peak of (a), (d) fine debris (Test parameter same as in Fig. 3.15).

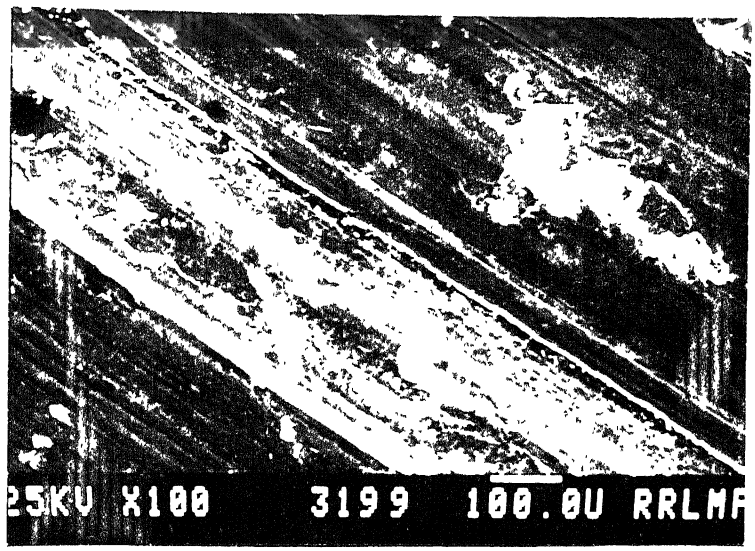

(a)

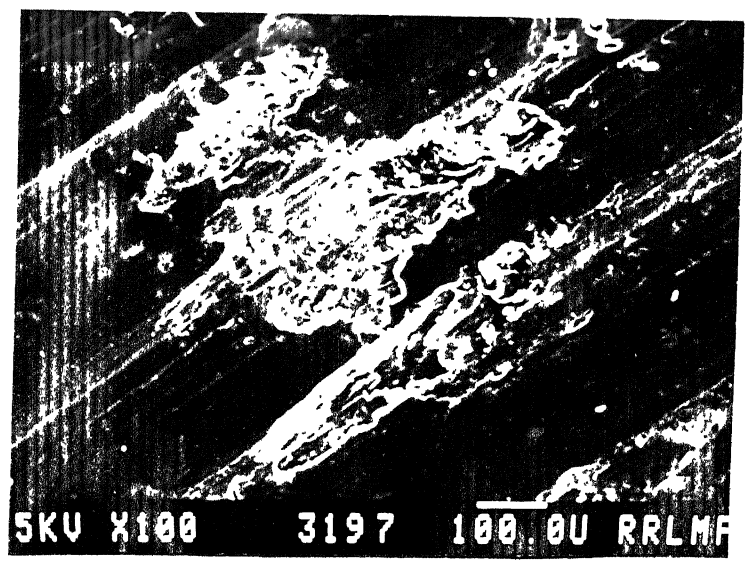

(b)

Fig. 3.26. SEM micrographs of worn out surface of sintered 6061 alloy-7 volume percent graphite composite at a sliding speed of (a) 0.25 m/s (b) 1.25 m/s (Applied pressure 12 x 10^{-2} MPa; sliding distance: 250 meters).

Part II

6061 Aluminium Alloy-Talc Particulate Composites

III.7. Properties of Sintered Composites:

III.7.1. Densification Behaviour:

Figure 3.27 shows the variation of dimensions of composites as a function of volume fraction of talc after sintering in various atmospheres. Percentage linear dimensional changes of the composites remained constant with volume fraction of talc, when sintered in nitrogen or vacuum. During argon sintering linear dimensions of the composites decreased up to 7 vol. % talc, followed by an increase with further talc addition. Radial dimensional change of nitrogen sintered composites remained constant up to 4 vol. % talc followed by an increase with further talc addition. In case of composites sintered in vacuum, radial dimensional change decreased for 4 vol. % talc composite and remained constant with further increase in the talc content. Radial shrinkage of the compacts after argon sintering was observed up to 7 vol. % talc addition.

Total sintered porosity of the composites remained constant after argon or vacuum sintering of the composites, irrespective of the amount of talc addition. Sintering in nitrogen imparted maximum porosity to the composites as compared to other sintering atmospheres. Closed porosities in sintered composites after vacuum or nitrogen sintering were found to be practically absent.

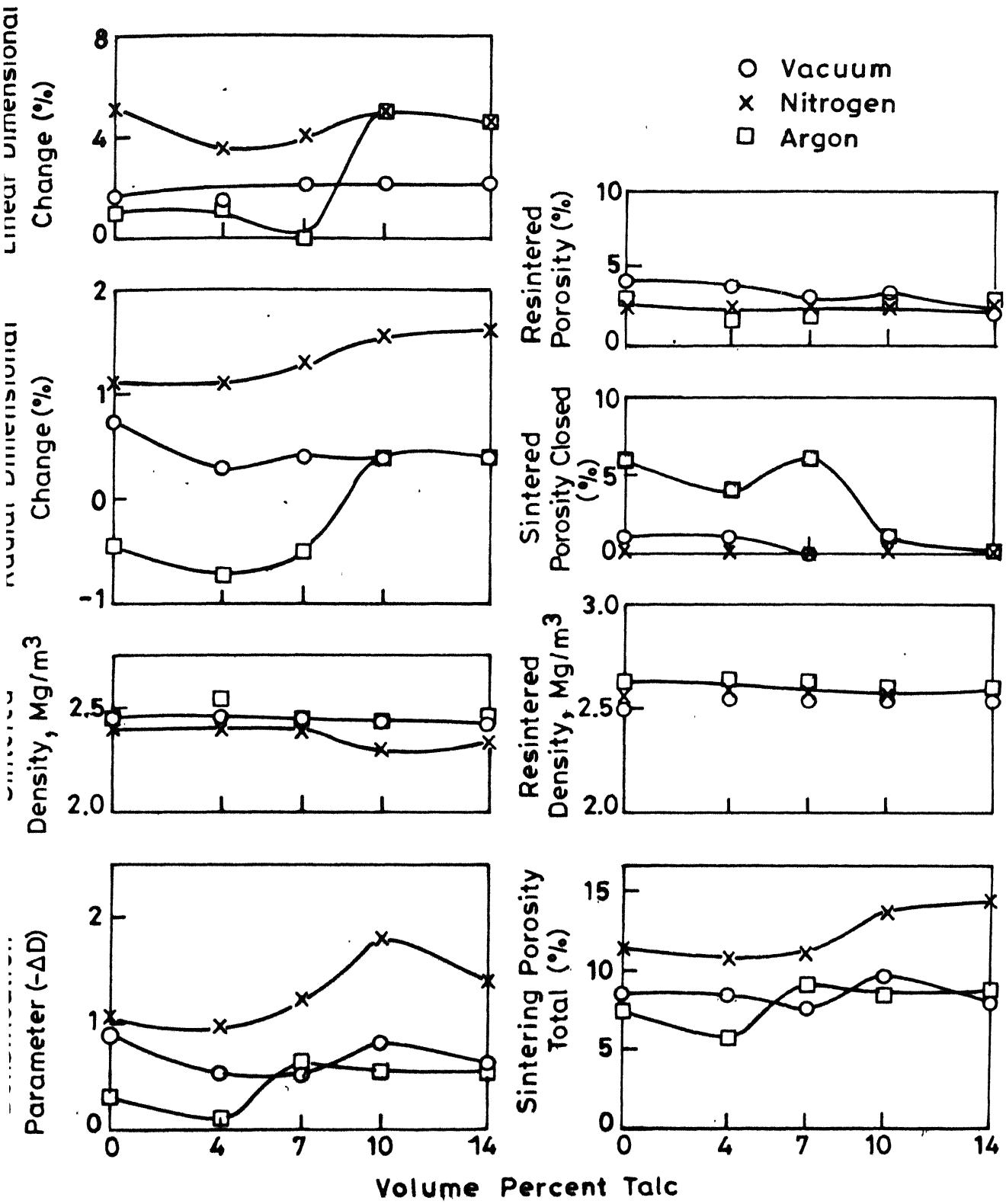

Fig. 3.27 Sintering behaviour of 6061 alloy - talc composites as a function of dispersoid content.

III.7.2. Hardness:

Figure 3.28 shows the hardness variation of 6061 composites as a function of volume fraction of talc. It is apparent that hardness remained constant with increasing talc content irrespective of the sintering atmosphere. Composites sintered in nitrogen atmosphere attained minimum hardness as compared to the composites sintered in other atmospheres.

III.7.3. Tensile Mechanical Properties:

Table III.2 enlists the mechanical properties of the sintered 6061 alloy and its composites containing 7 vol. % of talc.

Table III.2

Tensile properties of sintered 6061 alloy and 6061 alloy-7 vol. % talc composites

Composition	UTS MPa	Y.S. MPa	Percent elongation
6061 alloy	90	65	15
6061-7 vol. % talc composites	81	54	10

Tensile mechanical properties of 6061 alloy decreased significantly with addition of 7 vol. % talc. It is evident from Table III.2 that UTS of sintered composites decreased by 10% , whereas Y.S. decreased by 17% value after 7 vol. % talc. Percent elongation of the composites reduced to 60% of the value for straight 6061 alloy compact.

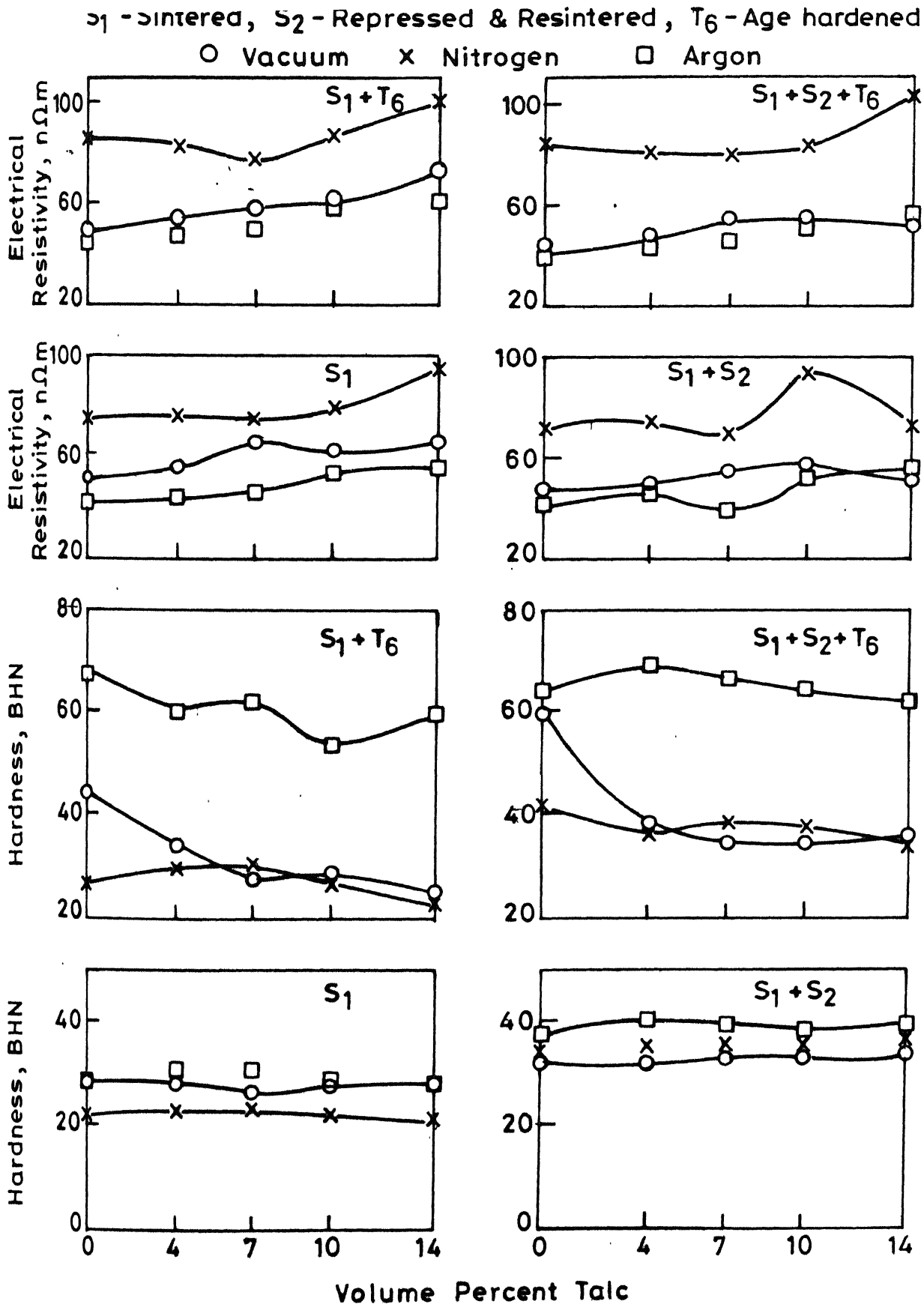

Fig. 3.28 Hardness and electrical resistivity variation of sintered and heat treated 6061 alloy - talc composites as a function of dispersoid content.

III.7.4. Electrical Resistivity:

Electrical resistivity of composites increased with increasing amount of talc in all the cases i.e. sintered in either vacuum, argon or nitrogen (Figure 3.28). Nitrogen atmosphere imparted maximum resistivity to composites as compared to those sintered in either vacuum or argon.

III.7.5. Surface Roughness:

Roughness (R_a) values of the cylindrical wall of sintered 6061 alloy and its composites containing 14 vol. % of talc were 1.8 and 1.42 μm respectively. A reduction by 38% of roughness is evident from the value, due to the addition of 14 vol. % talc in 6061 alloy.

III.7.6. Microstructure:

Optical micrographs of as sintered 6061 alloy composite containing 7 and 14 vol. % of talc are shown in Figures 3.29a and b.

Figure 3.31 shows the SEM micrographs of 6061 alloy containing 7 vol. % talc. Talc particles are clearly noticeable in the micrographs. X-ray dot mapping (Figures 3.31b and c) for magnesium and aluminium indicated the absence of aluminium and presence of magnesium over the talc particles.

III.8. Properties of Repressed-Resintered Composites:

III.8.1. Densification Behaviour:

After repressing and resintering porosity level of sintered composites decreased to approximately 50%

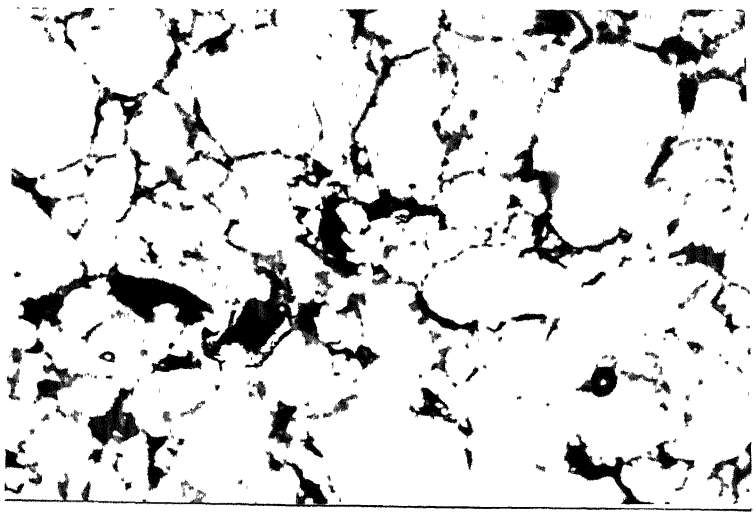

(a)

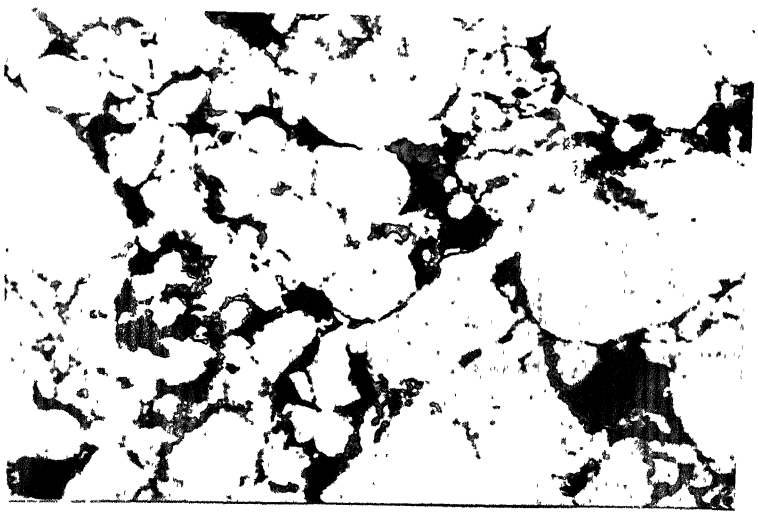

(b)

Fig. 3.29. Optical micrographs of sintered 6061 alloy composites containing (a) 7 volume percent talc (b) 14 volume percent talc (after argon sintering) (200X)

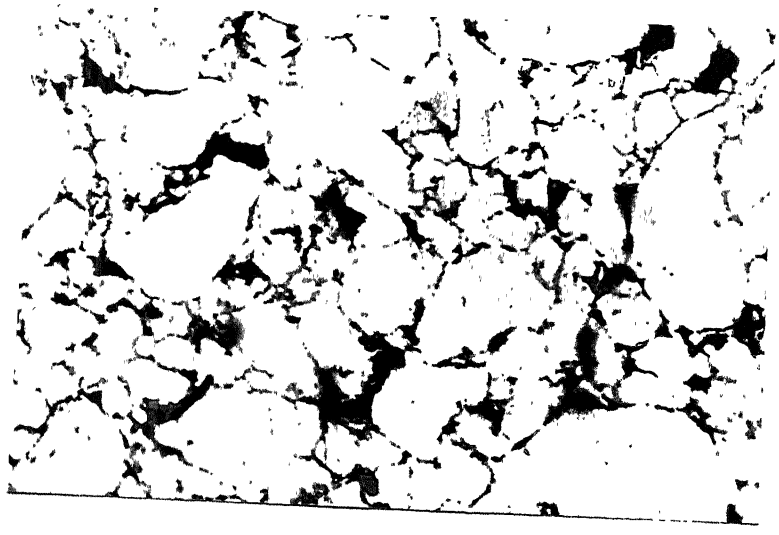

(a)

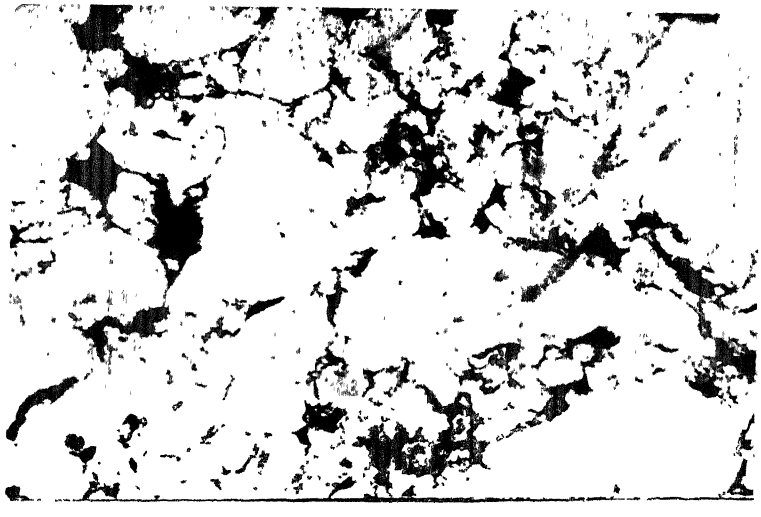

(b)

Fig. 3.30. Optical micrographs of repressed-resintered 6061 alloy composites containing (a) 7 volume percent talc (b) 14 volume percent talc (after argon sintering) (200X)

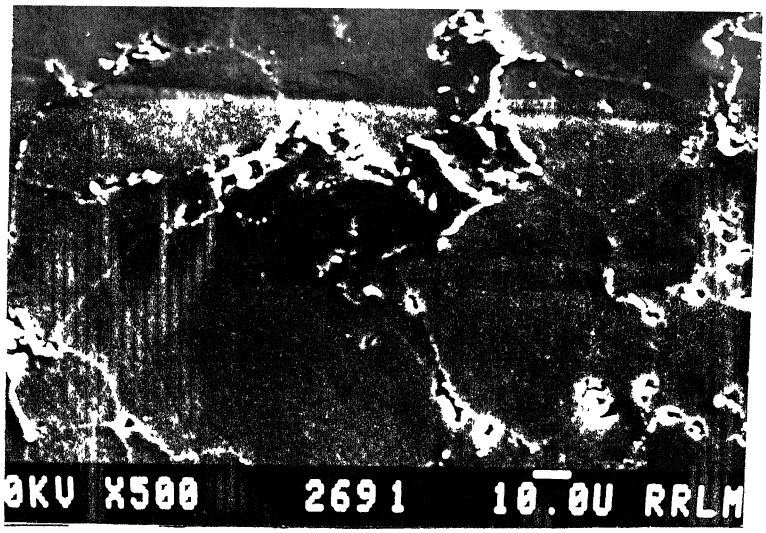

(a)

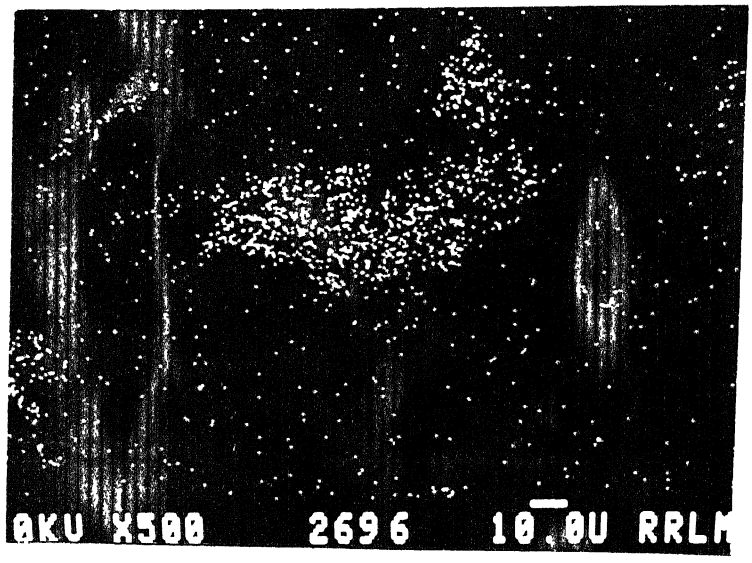

(b)

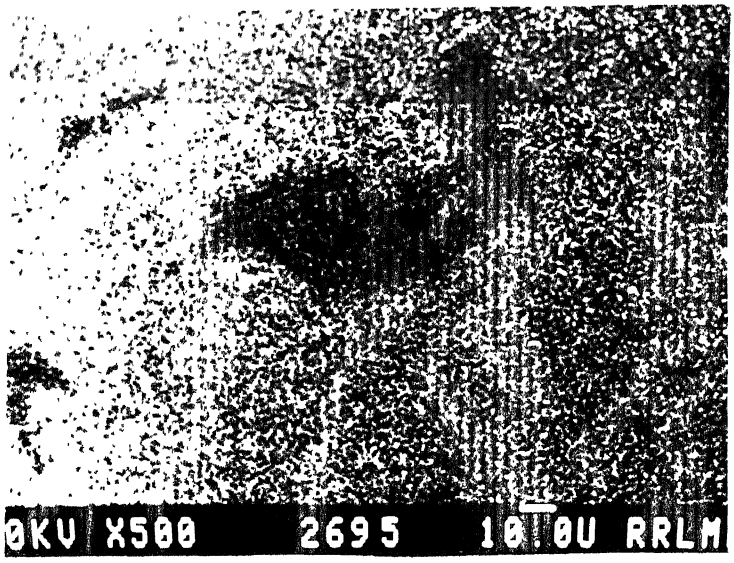

(c)

Fig. 3.31 contd.

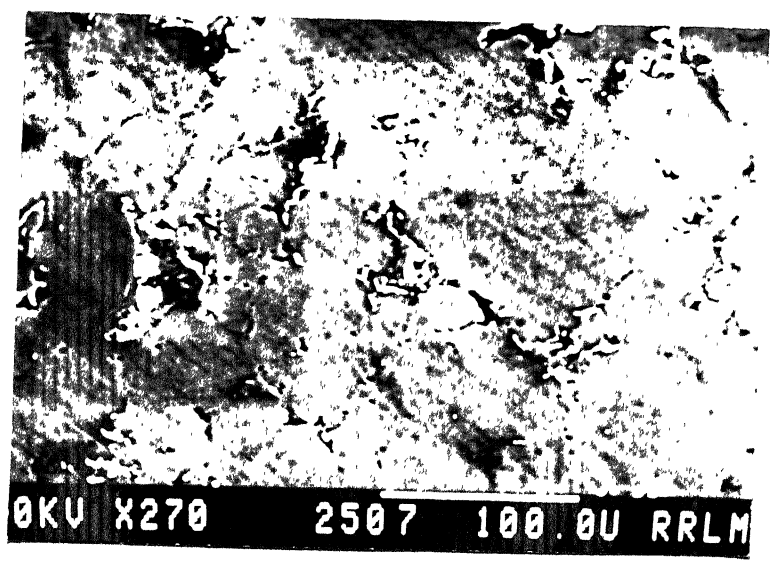

(d)

Fig. 3.31. (a) SEM micrographs of argon sintered 6061 alloy-7 volume percent talc composite (b) X-ray dot mapping of (b) for MgK_{α} peak (c) X-ray dot mapping of (b) for AlK_{α} peak (d) micrograph at low magnification.

(Figure 3.27). Corresponding increase in the resintered density were also observed. Effect of volume fraction of talc on the density of repressed-resintered composites was found to be insignificant.

III.8.2. Hardness:

Hardness of the sintered composites in general increased after repressing and resintering (Figure 3.28). Effect of talc content on the hardness value of the composite was not significant. Similar to hardness values of sintered composites, maximum hardness was attained after the repressing and resintering of composites sintered in argon atmosphere.

III.8.3. Electrical Resistivity:

Repressing-resintering had marginal effect on the electrical resistivity value of the composites (Figure 3.28).

III.8.4. Microstructure:

Optical micrographs of repressed-resintered composites containing 7 and 14 vol. % talc are shown in Figure 3.30.

III.9. Properties of Heat Treated Composites:

III.9.1. Hardness:

Hardness of the sintered and resintered composites increased after T6 treatment (Figure 3.28). Composites sintered in argon attained maximum hardness after T6 treatment.

Hardness value of heat treated composites sintered in argon or vacuum decreased with increasing amount of talc, whereas, the effect of talc content is least for composites sintered in nitrogen.

III.9.2. Tensile Mechanical Properties:

Figure 3.32 shows the mechanical properties variation of heat treated composites as a function of volume fraction of talc. There is a linear decrease in the UTS value of composites with increasing amount of talc. At 14 vol. % talc, the UTS of composites was reduced to 70% of the value for straight 6061 alloy.

Percent elongation of age hardened composites decreased with increasing volume fraction of talc. There was 30% reduction in the value of percent elongation due to addition of 14 vol. % talc.

III.9.3. Electrical Resistivity:

There was an invariable increase in the electrical resistivity of the composites after age-hardening (Figure 3.28). Effect of T6 treatment is pronounced in case of composites sintered in nitrogen.

III.9.4. Fractography:

Micrographs of fractured surface of composites containing 14 vol. % of talc are shown in Figure 3.33.

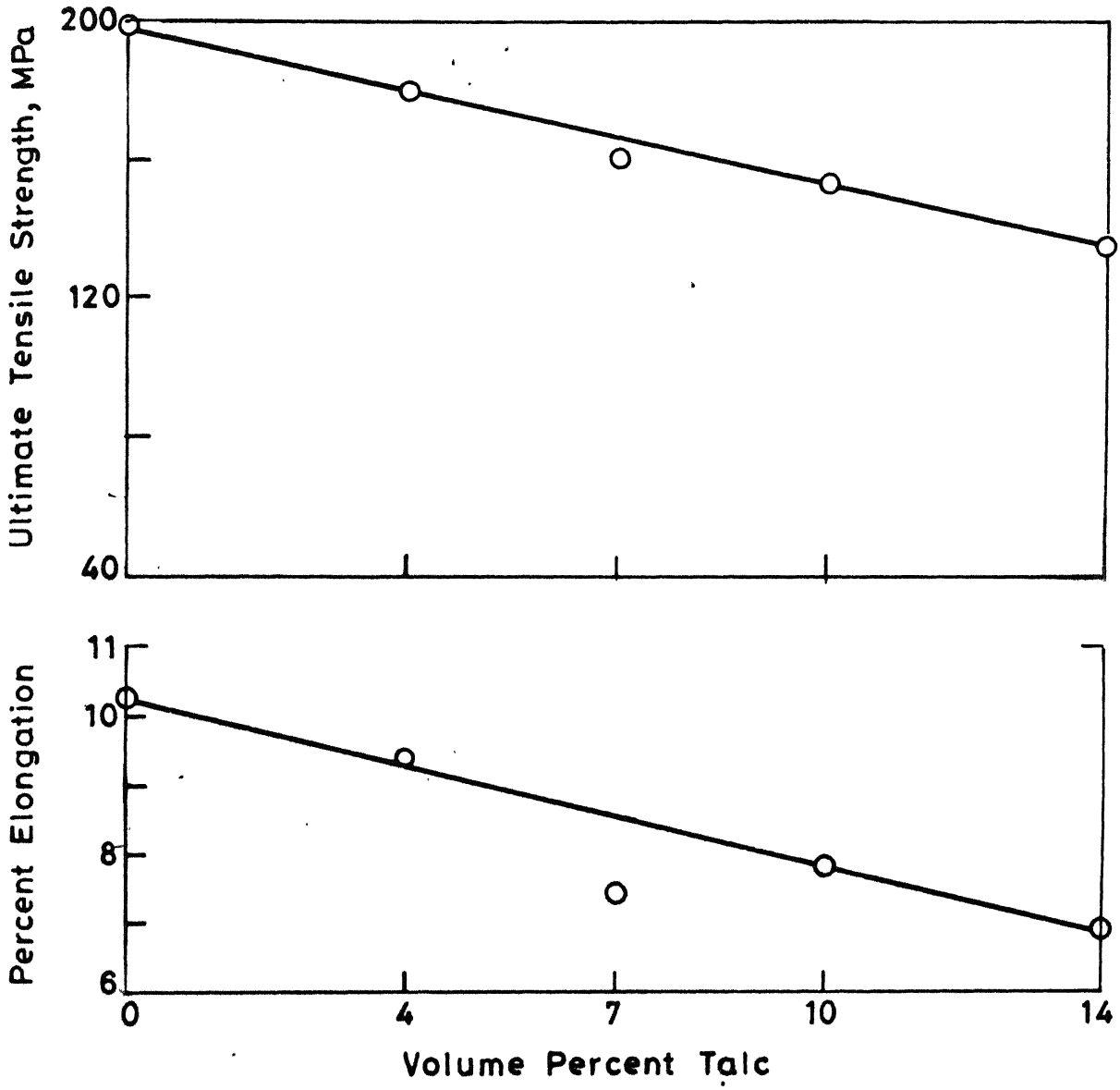

Fig. 3.32 UTS and percent elongation variation of heat treated 6061 alloy - talc composite as a function of dispersoid.

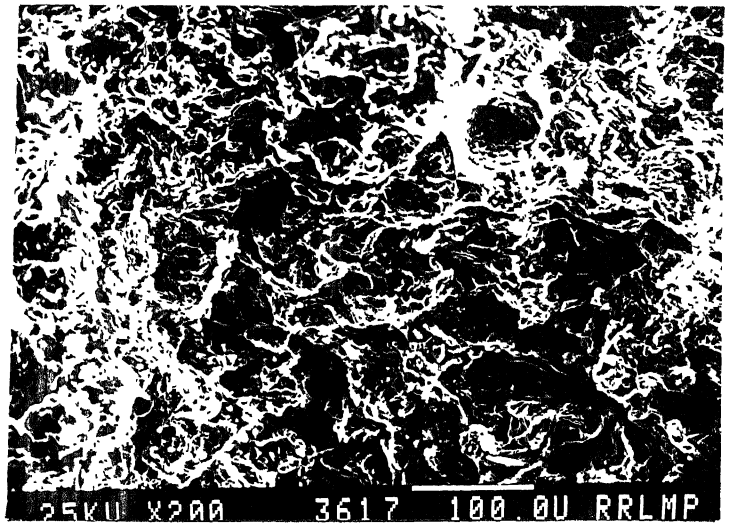

(a)

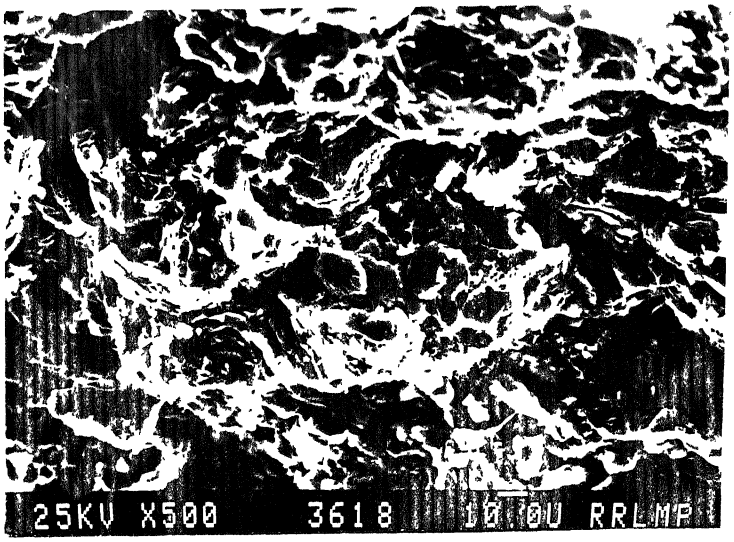

(b)

Fig. 3.33. SEM micrographs of fractured surface of sintered and heat treated 6061 alloy-14 volume percent talc composites after tensile test.

Fractographs do not show any dimple formation, inferring to brittle type of fracture. Talc particles could not be traced on the fractured surface.

III.10. Hardness Variation of Thermomechanical Treated Composites:

There is a marginal increase in microhardness value of the sintered composites due to talc addition (Figure 3.34). Thermomechanical treatment increased the microhardness value of the sintered 6061 alloy as well as composites containing talc. Microhardness of composites increased with up to 7 vol. % talc, which decreased with further talc addition.

III.11. Sliding Wear Study:

III.11.1. Wear Loss:

Wear rate of the composites remained constant up to 4 vol. % talc addition (Figure 3.35). A further addition of talc was found to increase the wear rate. A 20% increase in wear rate of composite due to additions of 14 vol. % talc is evident from Figure 3.35. Wear loss of composites containing 7 vol. % talc increased linearly with sliding distance (Figure 3.36). Slope of the plot of talc containing composites is similar to that of slope for straight 6061 alloy. Increased applied pressure resulted in an enhanced wear rate (Figure 3.37) of the composites containing 7 vol. % talc. An increase by three fold in wear rate due to increase in pressure from 4×10^{-2} to 24×10^{-2} MPa is also evident from Figure 3.37. Wear rate of the composites increased

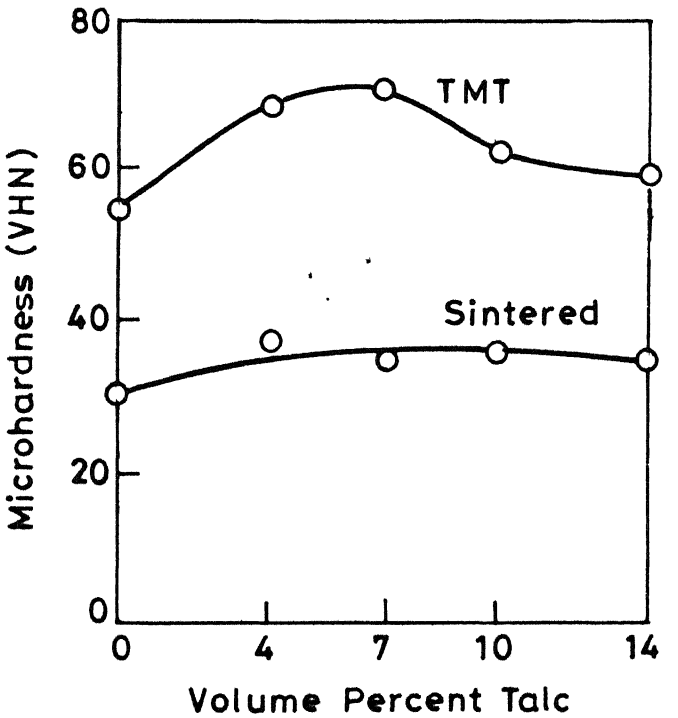

Fig. 3.34 Variation of Vickers microhardness of sintered and thermomechanically treated (TMT) 6061 alloy talc composites as a function of disper - soid content.

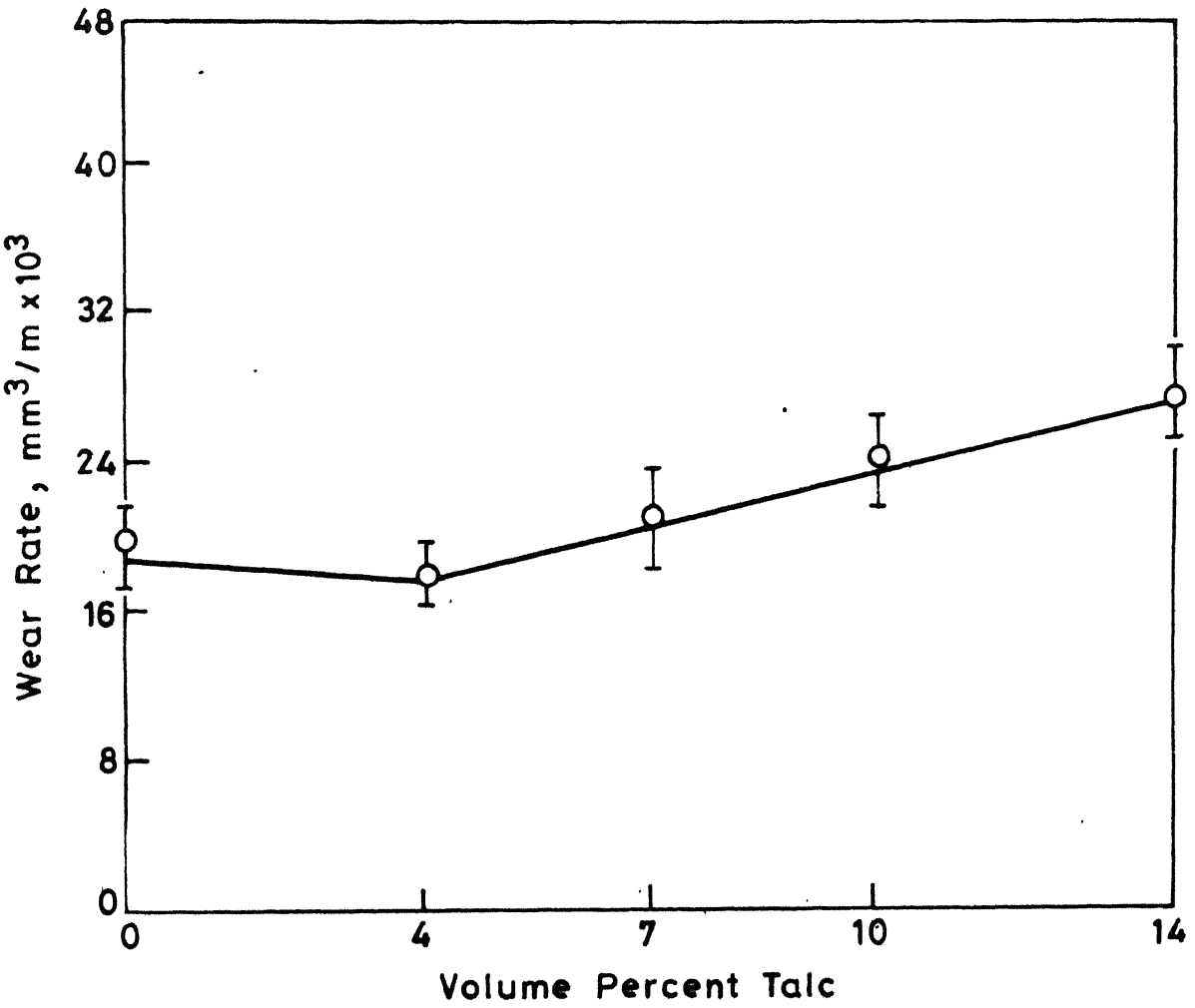

Fig. 3.35 Effect of talc content on the wear rates of sintered 6061 alloy composites (Sliding speed: 0.5 m/s ; Applied pressure : 12×10^{-2} MPa ; Sliding distance : 250 meters)

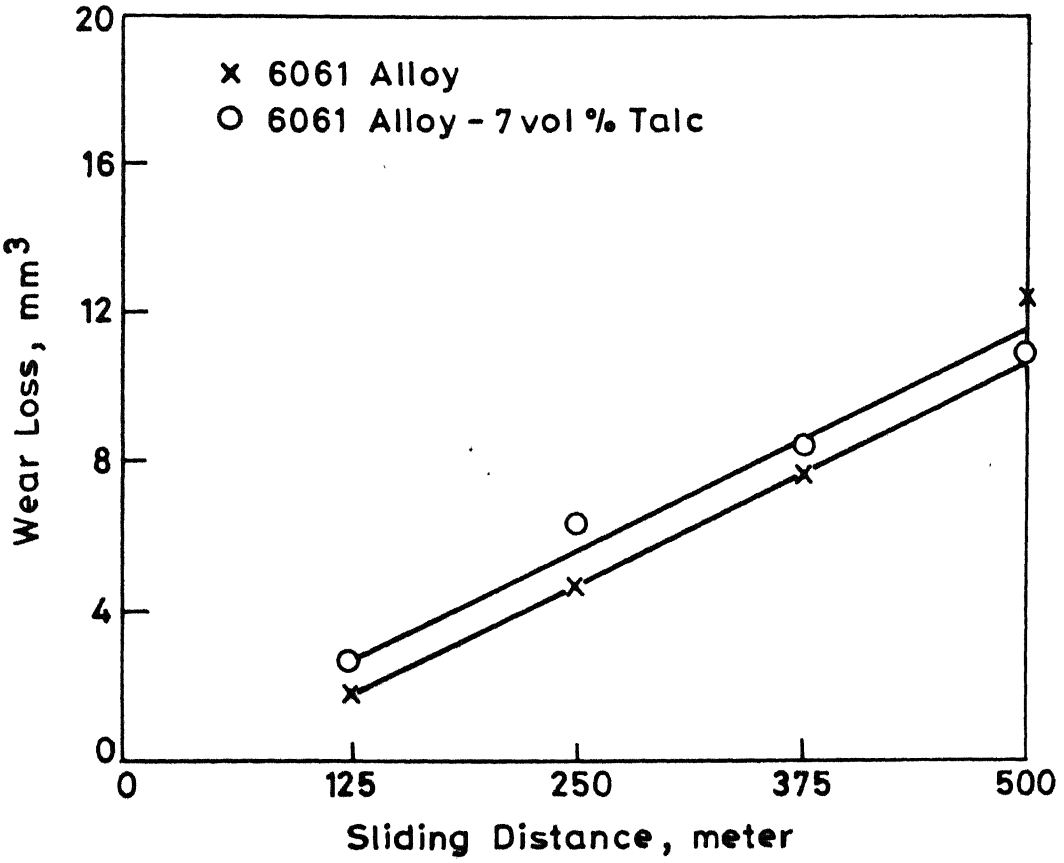

Fig. 3.36 Effect of sliding distance on wear loss of sintered alloy and its composits containing 7 vol % talc (Sliding speed 0.5 m/s ; Applied pressure: 12×10^{-2} MPa)

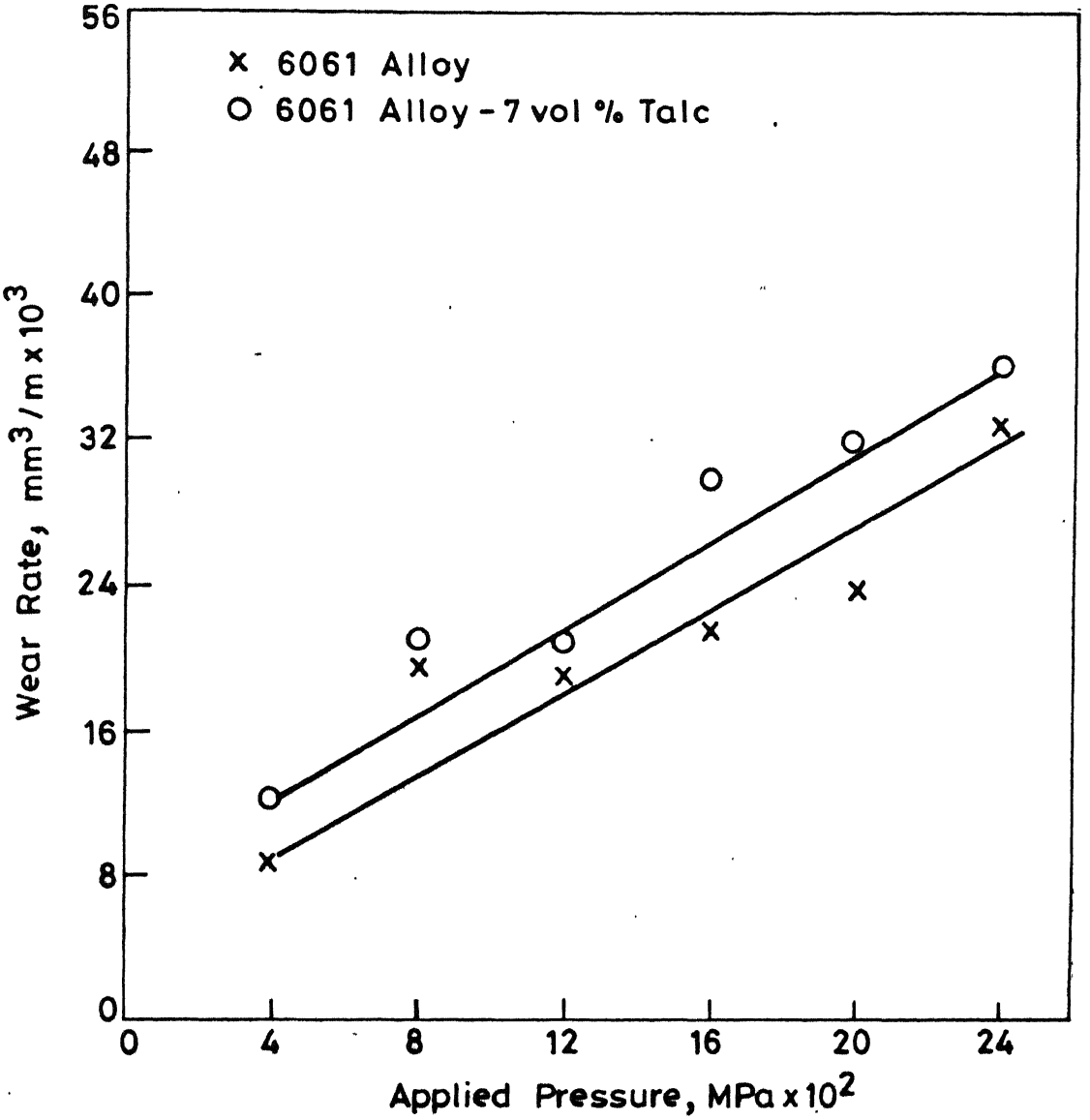

Fig. 3.37 Effect of applied pressure on the wear rate of 6061 alloy and its composites containing 7 vol % of talc (Sliding speed: 0.5 m/s ; Sliding distance: 250 meters)

substantially with a decrease in the sliding speed, particularly in the lower range of speed (Figure 3.38).

III.11.2. SEM Study:

SEM micrographs of worn out surfaces of 6061 alloy containing talc are shown in Figure 3.39. The two main features of worn out surfaces, as described in the previous section, are evident from the micrographs. Flake type debris prior to fragmentation from the surface is shown in Figure 3.39c. Debris collected during the test (Figure 3.40) of 6061 alloy-talc composites were very similar in shape, size and nature of that of debris collected from the test with 6061 alloy pin.

SEM micrographs of worn out surfaces of composites containing 7 vol. % talc after different sliding speeds are shown in Figure 3.41. A more severely damaged region can be observed (Figure 3.41a) for the worn out surface of composites when run at a lower speed i.e. 0.25 m/s.

Part III

6061 Aluminium Alloy-Alumina Particulate Composites

III.12. Properties of Sintered Composites:

III.12.1. Densification Behaviour:

Figure 3.42 shows the densification behaviour of 6061 aluminium alloy containing alumina particles after sintering in vacuum, nitrogen or argon. Linear dimensions of the

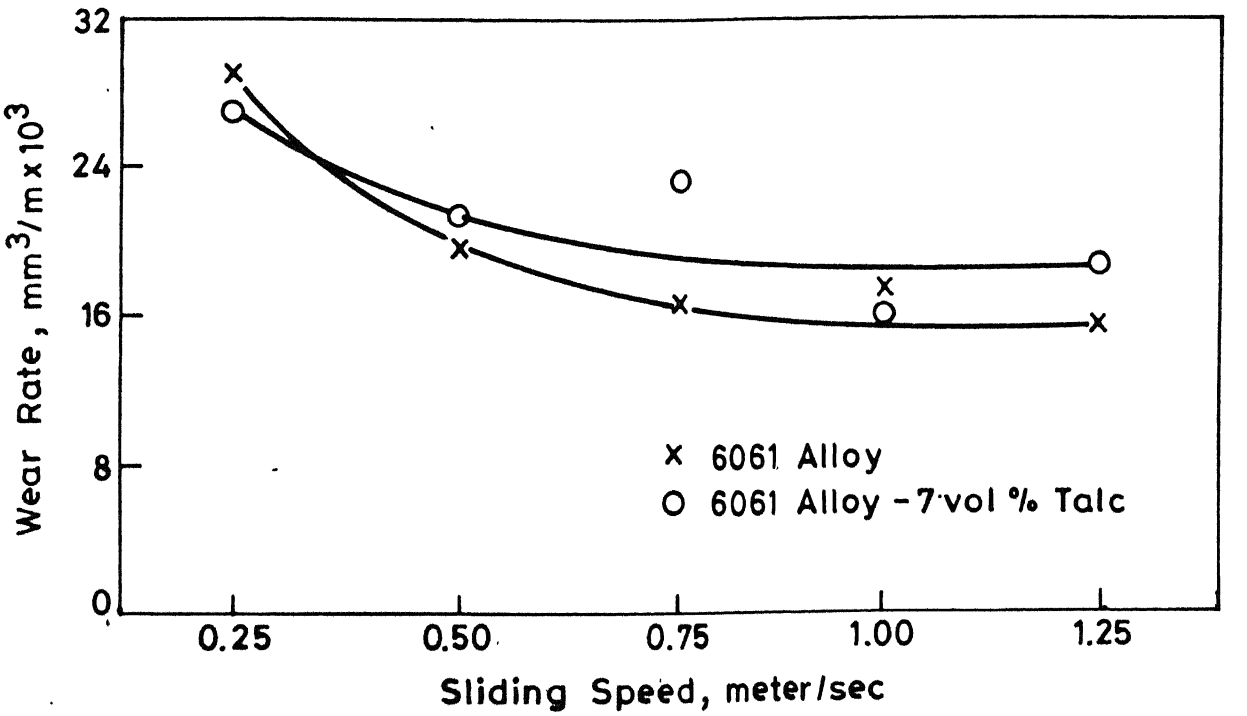

Fig. 3.38 Effect of sliding speed on wear rate of sintered 6061 alloy and its composites containing 7 vol % of talc (Applied pressure: 12×10^{-2} MPa; Sliding distance: 250 meters)

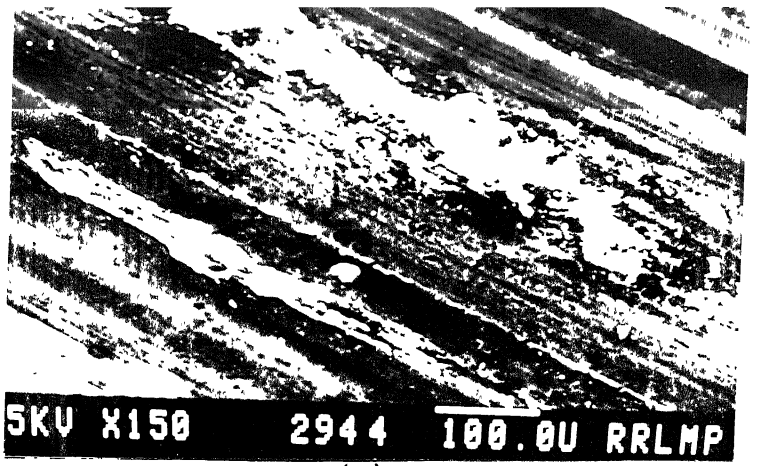

(a)

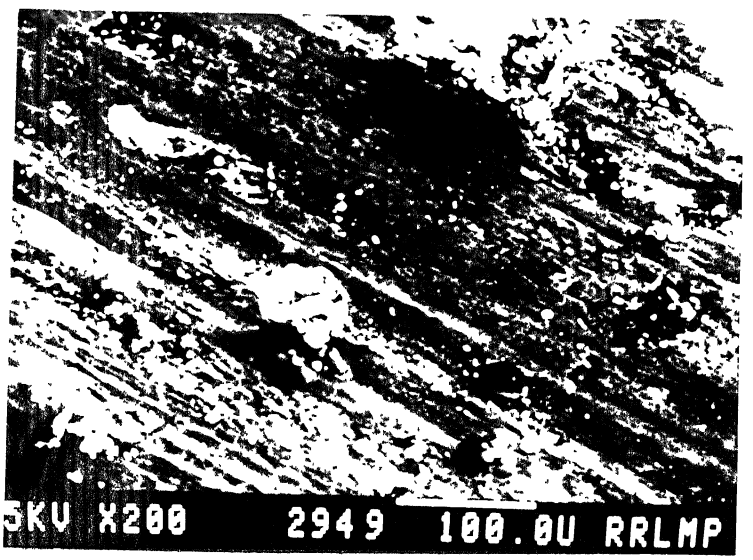

(b)

(c)

Fig. 3.39. Typical SEM micrographs of worn out surface of sintered 6061 alloy-7 volume percent talc showing the presence of long and continuous grooves and patches of highly damaged regions (Test parameter same as in Fig. 3.35).

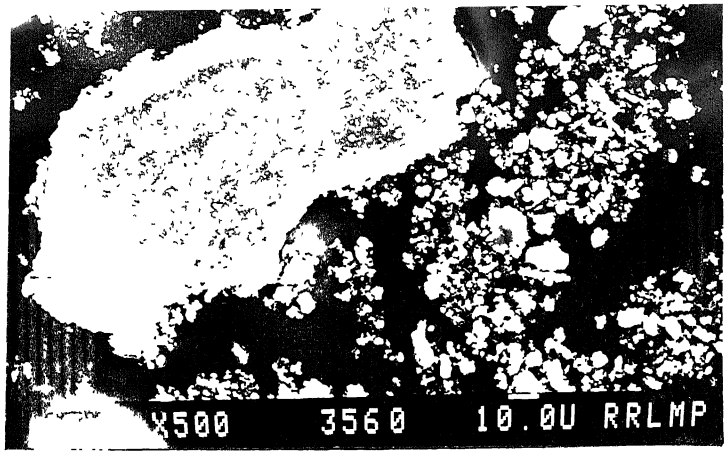

(a)

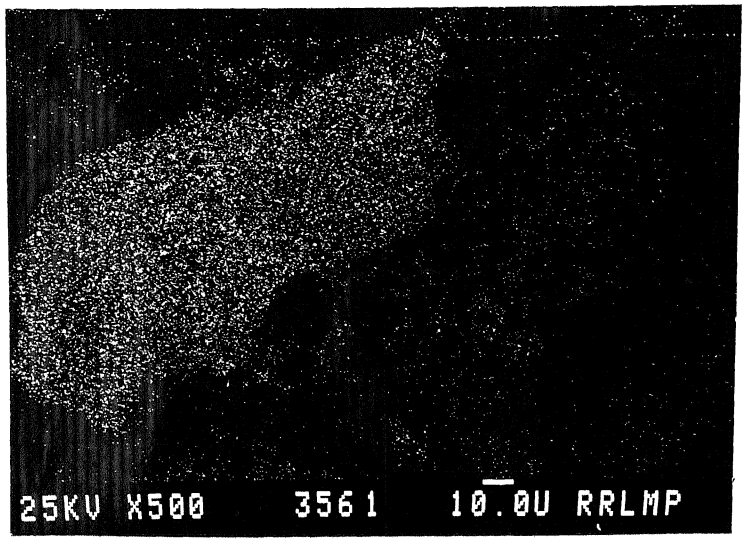

(b)

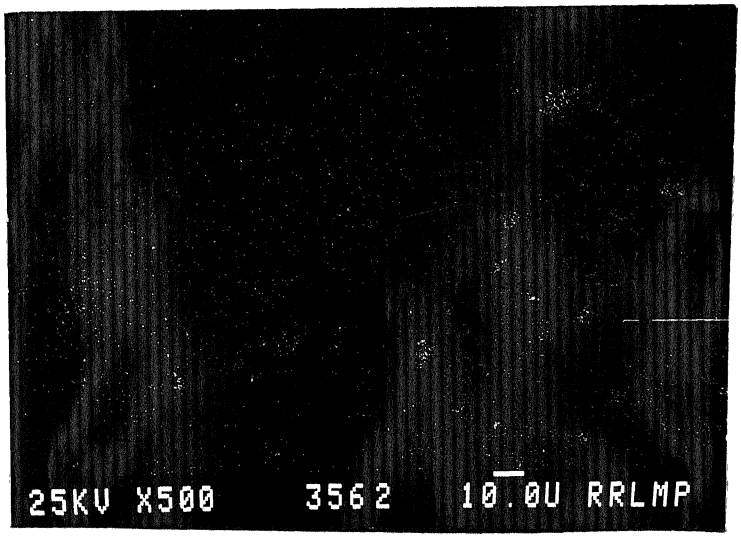

(c)

Fig. 3.40. (a) SEM micrograph of debris of 6061 alloy-7 volume percent talc composite showing flaky and fine debris particles (b) X-ray dot mapping for FeK_{α} peak (c) X-ray mapping for AlK_{α} peak (Test parameter same as in Fig. 3.35).

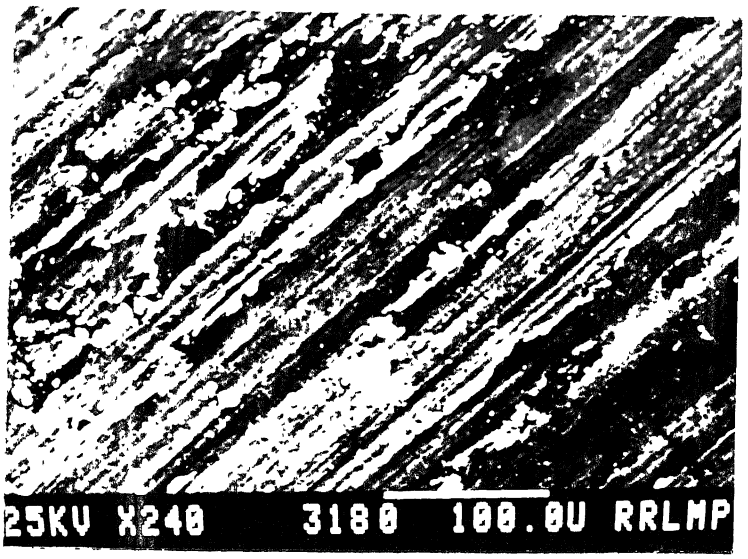

(a)

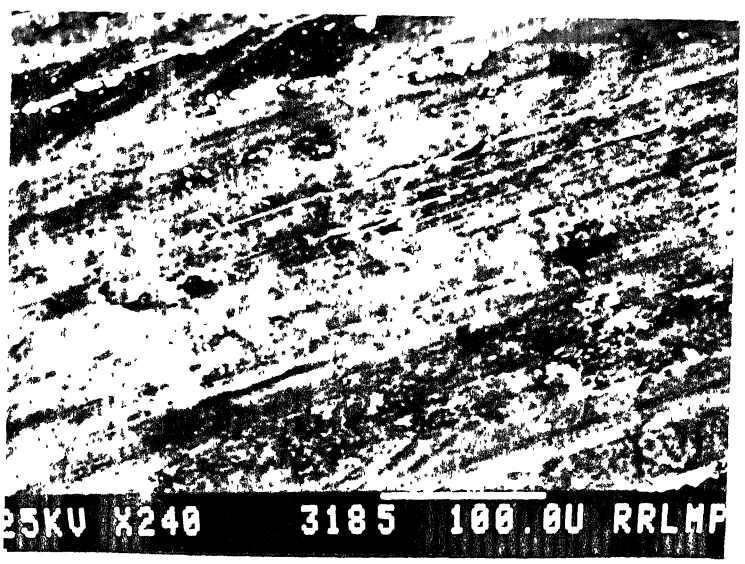

(b)

Fig. 3.41. SEM micrographs of worn out surface of sintered 6061 alloy-7 volume percent talc composites at a sliding speed of (a) 0.25 m/s (b) 1.25 m/s (Applied pressure: 12 x 10^{-2} MPa, sliding distance: 250 meters).

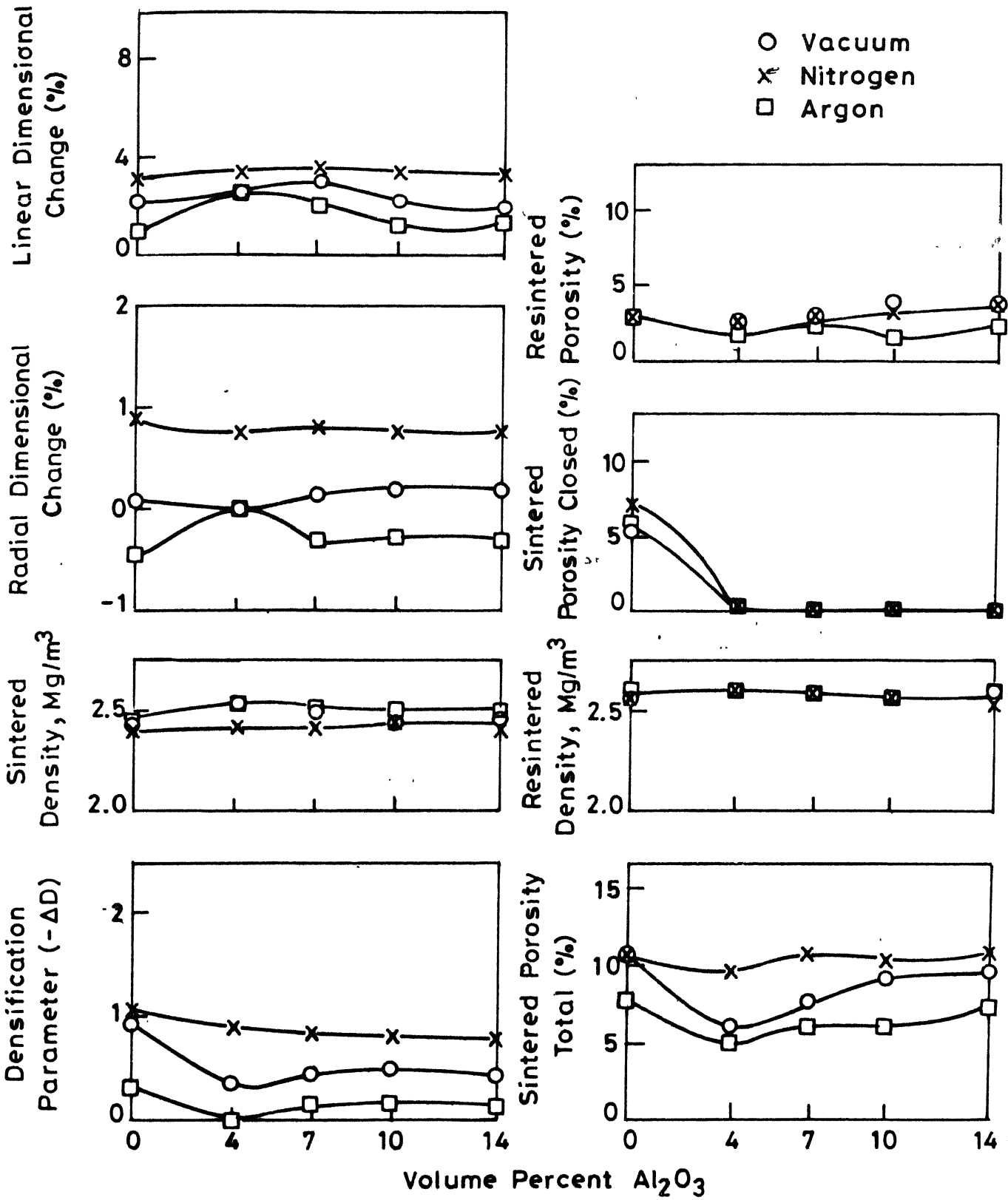

Fig. 3.42 Sintering behaviour of 6061 alloy - Al_2O_3 composites as a function of dispersoid content.

compacts increased marginally after sintering. The effect of the amount of dispersoid on the linear dimension of composites was practically insignificant. For linear dimensional stability argon appeared to be the best sintering atmosphere. In radial direction, the dimensions were only marginally affected after sintering in vacuum. Sintering in argon resulted in shrinkage of composites in the radial direction. Maximum dimensional changes were observed after nitrogen sintering. Densification parameter of the composites increased with volume fraction of alumina, when sintered in nitrogen. With addition of 4 vol. % alumina the ΔD value of the composites sintered in argon or vacuum, decreased subtantially as compared to those of 6061 alloy. ΔD remained constant with further addition of alumina for such composites.

Sintered porosity variation corresponds to that for densification parameter, such that, porosity remained constant irrespective of the alumina content when sintered in nitrogen. On the other hand, sintering in vacuum and argon resulted in a reduction in porosity level at 4 vol. % alumina. Sintered closed porosity of the composites reduced to zero with alumina addition (Figure 3.42).

III.12.2. Hardness:

Figure 3.43 shows the variation of hardness values as a function of volume percent of alumina particles. Sintered hardness remained uneffected with increasing volume of alumina addition. However, maximum hardness was attained by composites, after sintering in vacuum atmosphere.

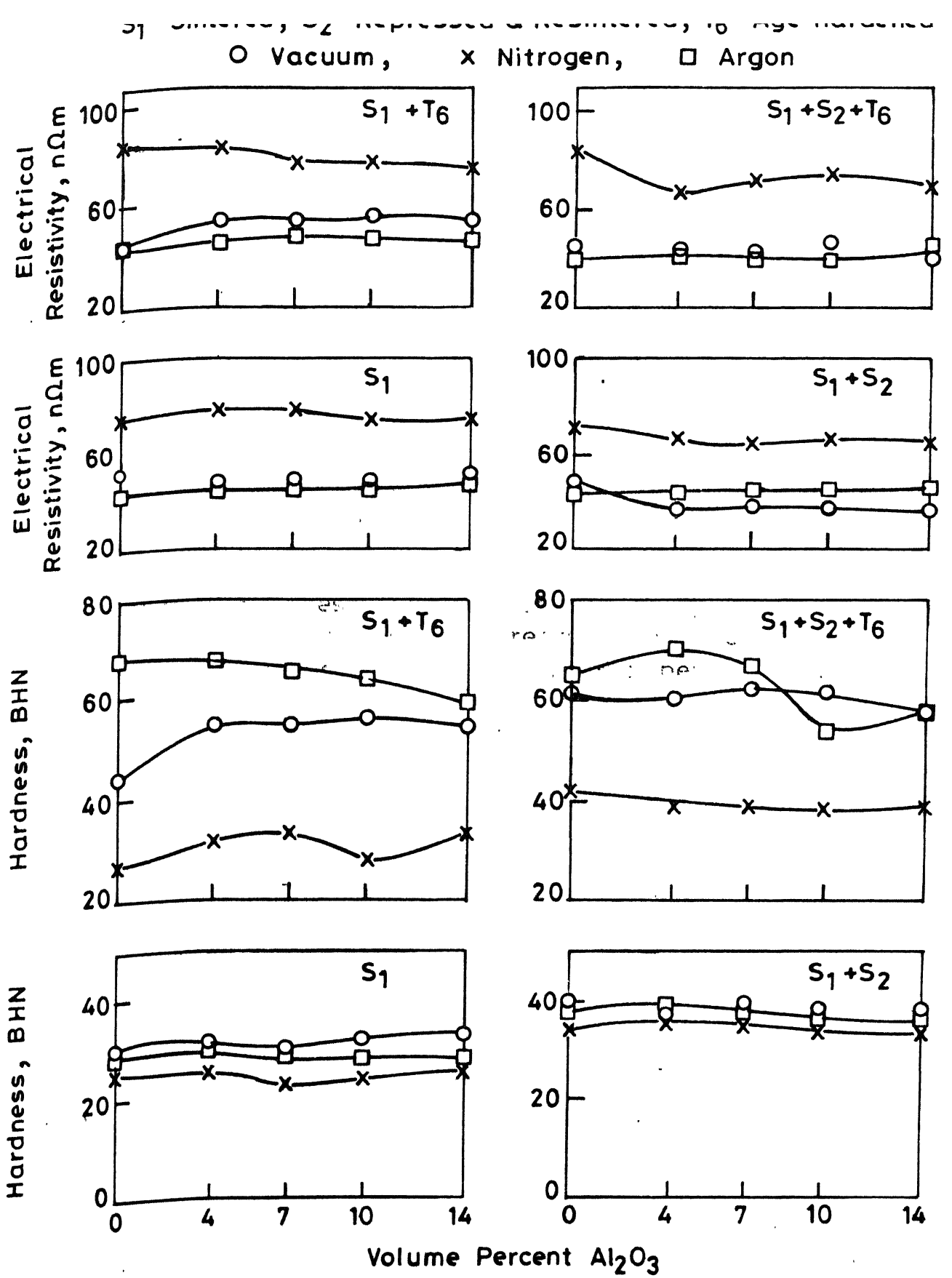

Fig. 3.43 Hardness and electrical resistivity variation of sintered and heat-treated 6061 alloy-alumina compositis as a function of dispersoid content.

III.12.3. Tensile Mechanical Properties:

Table III.3 shows the mechanical properties of sintered composites containing 7% of alumina.

Table III.3

Tensile properties of sintered 6061 alloy and 6061 alloy-7 vol. % Al_2O_3 composites (argon sintered)

Composition	UTS MPa	Y.S. MPa	Percent elongation
6061 alloy	90	65	15
6061-7 vol. % Al_2O_3	90	48	15

The values of UTS and percent elongation of sintered composites remained constant with addition of 7 vol. % of alumina, whereas, Y.S. decreased by 25%.

III.12.4. Electrical Resistivity:

Electrical resistivity values were unaffected with volume fraction of alumina in the 6061 alloy (Figure 3.43). However, the effect of sintering atmosphere was significant. Nitrogen atmosphere sintering imparted maximum value to the composites.

III.12.5. Surface Roughness:

R_a value of composites containing 14 vol. % alumina was 1.7 μm. Roughness value of sintered composites

remained constant with addition of 14 vol. % of alumina.

III.12.6. Microstructure:

Figure 3.44 shows the microstructures of sintered 6061 alloy composites containing 7 and 14 vol. % alumina. Increased amount of alumina in the matrix alloy powder promotes its predominance of the particle interfaces. Microstructure of composites shows agglomeration of alumina particles over the matrix. SEM micrographs (Figure 3.46) also confirms such agglomeration.

III.13. Properties of Repressed-Resintered Composites:

III.13.1. Densification Behaviour:

It is evident from Figure 3.42 that repressing and resintering of compacts resulted in a substantial reduction in the porosity. A reduction of approximately 50% in porosity level after repressing and resintering of the composites can be observed from the plot (Figure 3.42).

III.13.2. Hardness:

Brinell hardness of the composites increased after repressing and resintering, but the effect of sintering atmosphere was similar to that of the sintered ones (Figure 3.43).

III.13.3. Electrical Resistivity:

Repressing and resintering of the compacts resulted in reduction in resistivity values of composites

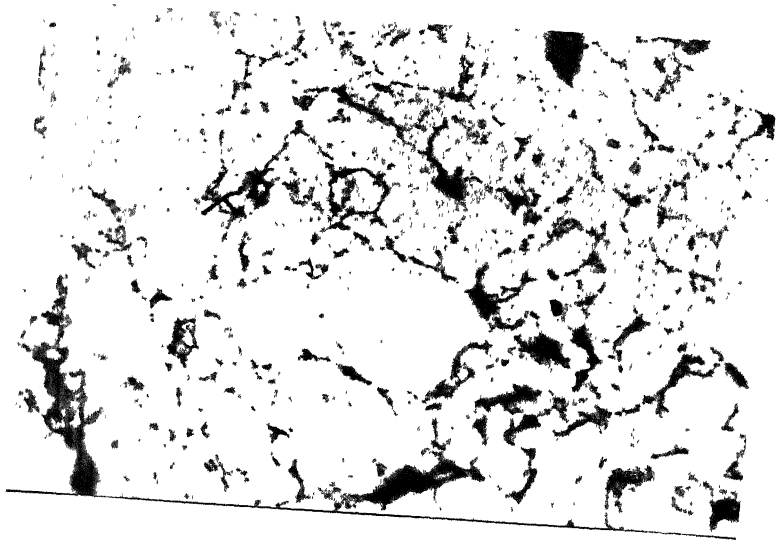

(a)

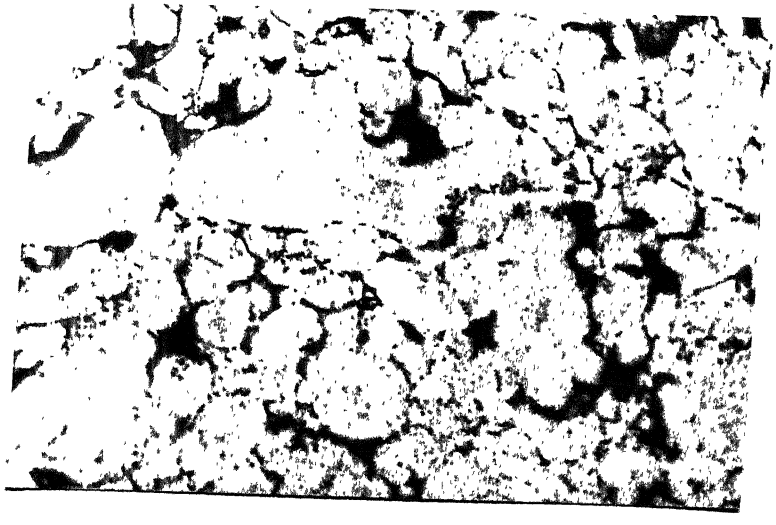

(b)

Fig. 3.44. Optical micrographs of sintered 6061 alloy composites containing (a) 7 volume percent alumina (b) 14 volume percent alumina (after argon sintering) (X200)

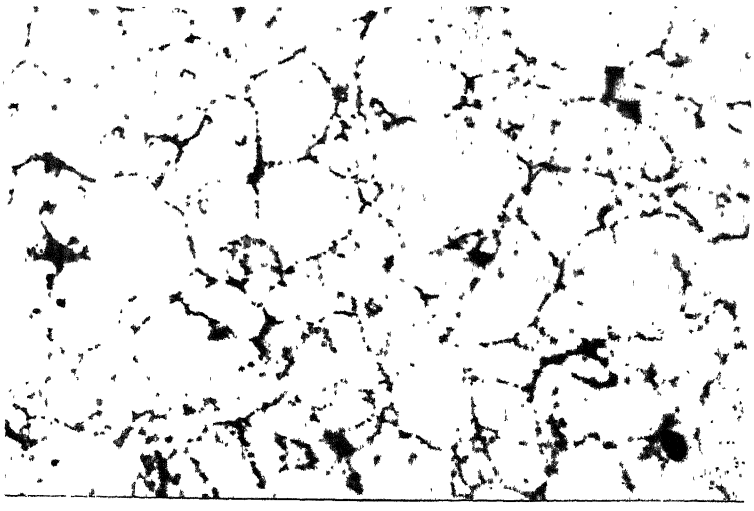

(a)

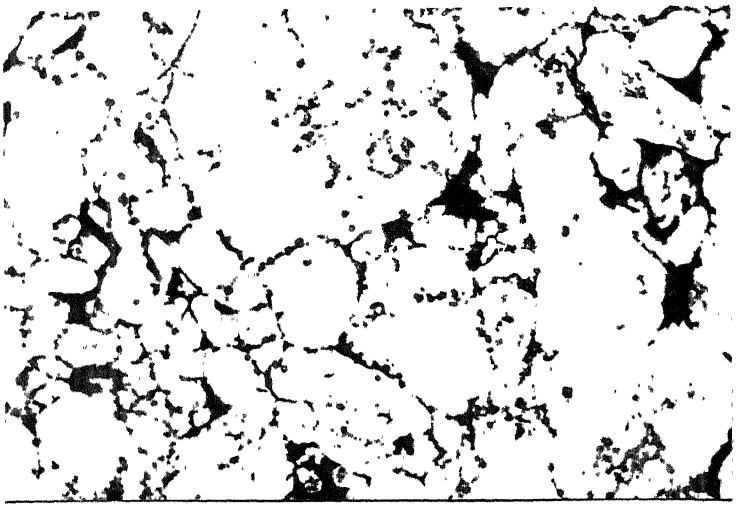

(b)

Fig. 3.45. Optical micrographs of repressed-resintered 6061 alloy composites containing (a) 7 volume percent alumina (b) 14 volume percent alumina (after argon sintering). (X200)

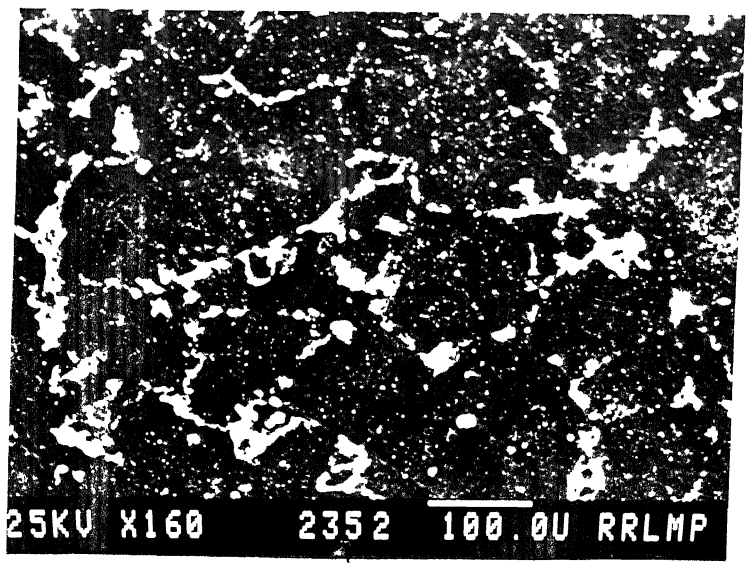

Fig. 3.46. SEM micrograph of argon sintered 6061 alloy-7 volume percent alumina composites.

sintered in any atmosphere i.e. vacuum, argon or nitrogen (Figure 3.43).

III.13.4. Microstructure:

Optical micrographs of repressed and resintered compacts (Figure 3.45) show the presence of fine alumina particles in the matrix. However, these micrographs do not reveal reduction in porosity level, when compared with the micrographs of as sintered composites (Figure 3.44).

III.14. Properties of Heat Treated Composites:

III.14.1. Hardness:

Hardness of the composites belonging to the present system improved after age-hardening (Figure 3.43). Effect of atmosphere on age hardening is similar to that for as-sintered compacts. The effect of dispersoid amount on age hardening is not substantial. T6 treatment of repressed and resintered composites sintered in argon exhibited the role of dispersoid content, such as, maximum hardness was attained at about 4 vol. % alumina. Hardness of the composites sintered in nitrogen remained constant with alumina content after age hardening.

III.14.2. Tensile Mechanical Properties:

Figure 3.47 shows the mechanical properties of the heat treated composites as a function of volume fraction of alumina. Initially with addition of 4 vol. % alumina UTS value of composites decreased by 25% as compared to UTS

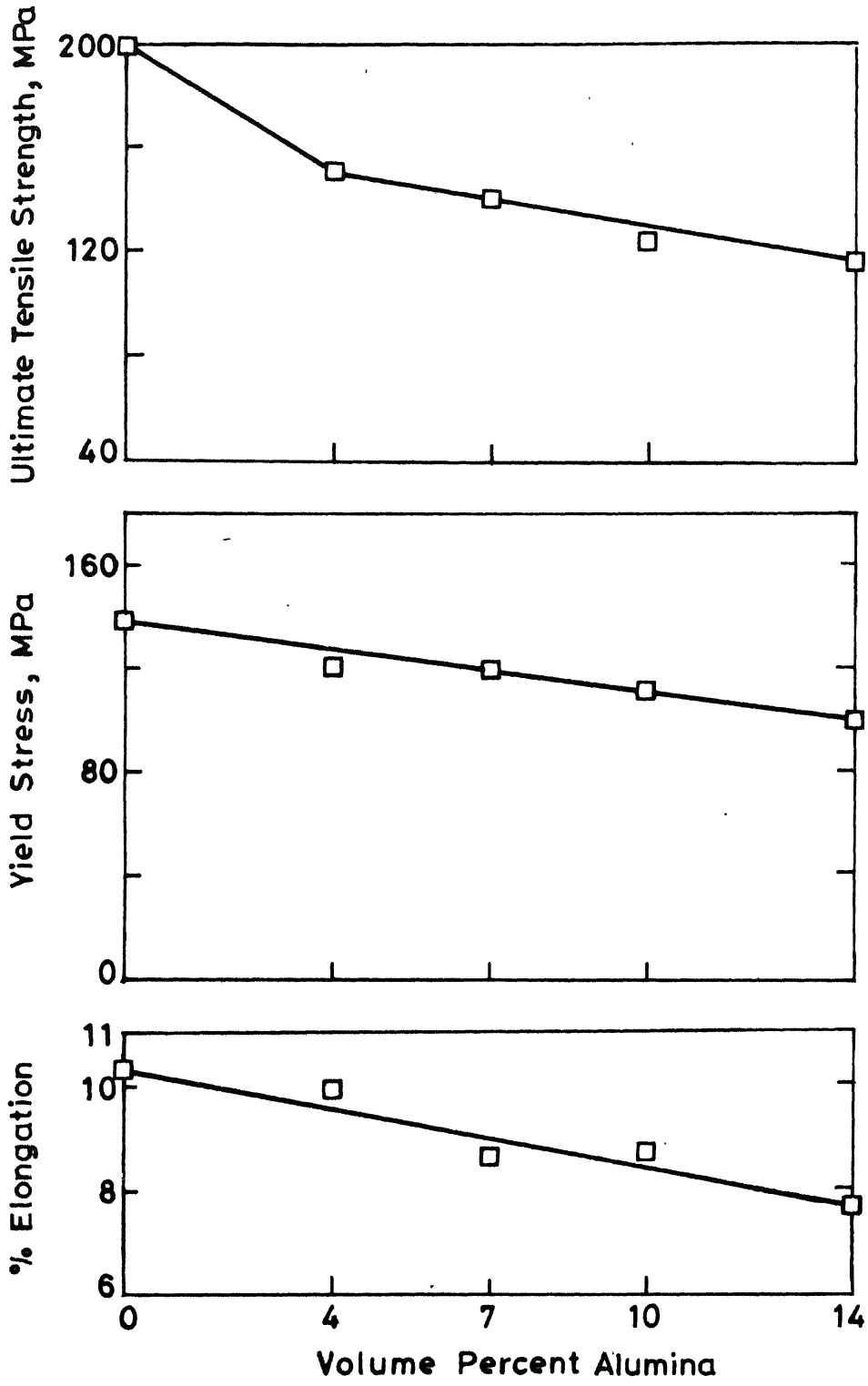

Fig. 3.47 UTS, YS for 0.2 % offset and % elongation variations of age hardened 6061 alloy-alumina composites as a function of dispersoid content.

of 6061 alloy. With further alumina addition less reduction in UTS value is evident. Y.S. of the heat treated composites decreased linearly with the amount of alumina in it. An addition of 14 vol. % alumina to 6061 alloy resulted in 25% reduction in Y.S. value of the composites. Percent elongation of composites decreased linearly with volume fraction of alumina.

III.14.3. Electrical Resistivity:

Resistivity of the composites increased after T6 treatment (Figure 3.43). Effect of age hardening on repressed-resintered composite is insignificant. Similar to the resistivity value of the sintered composites, maximum resistivity was attained after T6 treatment by the composites sintered in nitrogen.

III.14.4. Fractography:

Figure 3.48 shows fractographs of composites containing 14 vol. % alumina. Fractured surface showed brittle type of failure. Fine alumina particles are visible on the fractured surface (Figure 3.48c).

III.15. Hardness Variation of Thermomechanically Treated Composites:

Figure 3.49 shows the microhardness variation of sintered and thermo-mechanically treated composites as a function of volume percent of alumina. Microhardness value of sintered composites increased with volume fraction of alumina, whereas, the effect of alumina content is insignificant.

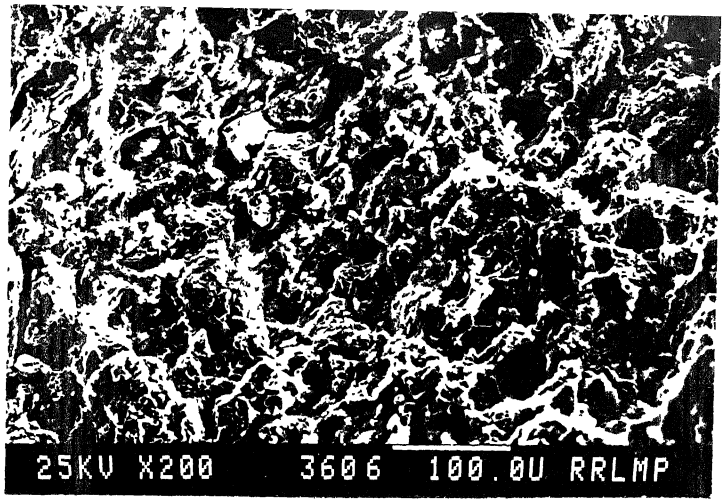

(a)

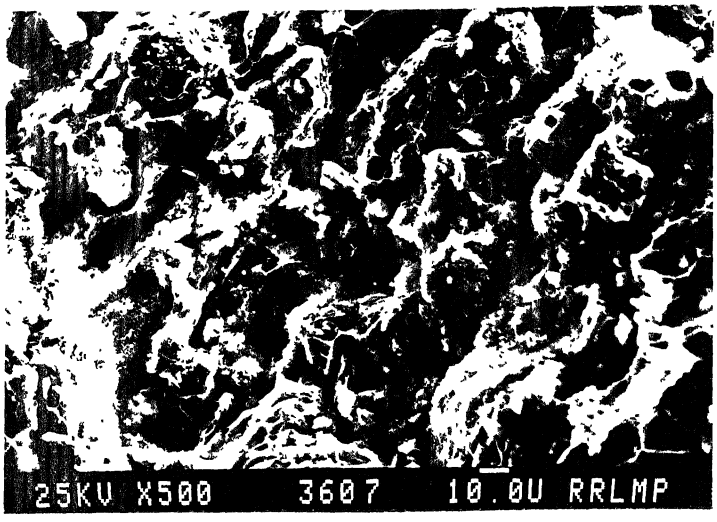

(b)

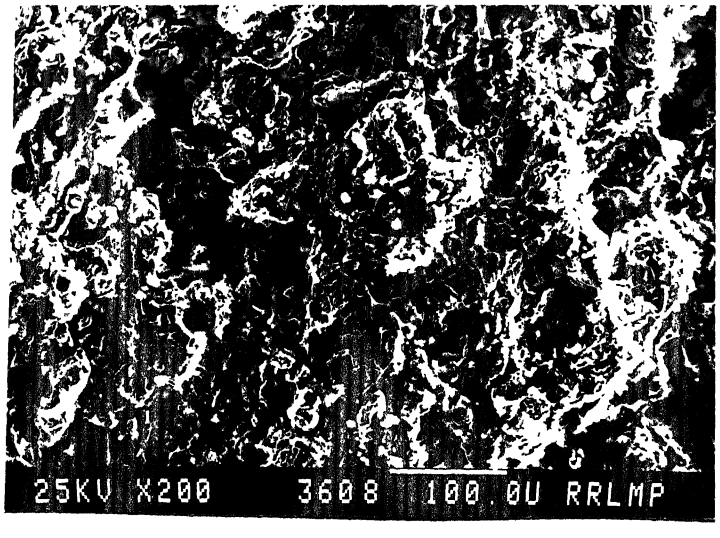

(c)

Fig. 3.48. SEM micrographs of fractured surface of sintered and heat treated 6061 alloy-14 volume percent alumina composite after tensile test (a and b at different magnifications).

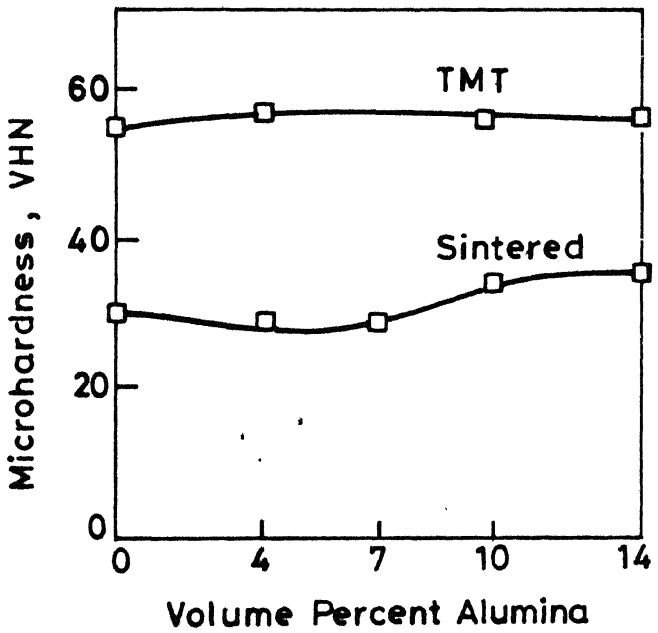

Fig. 3.49 Vickers microhardness variation of sintered and thermomechanically treated 6061 alloy-alumina composites as a function of dispersoid content.

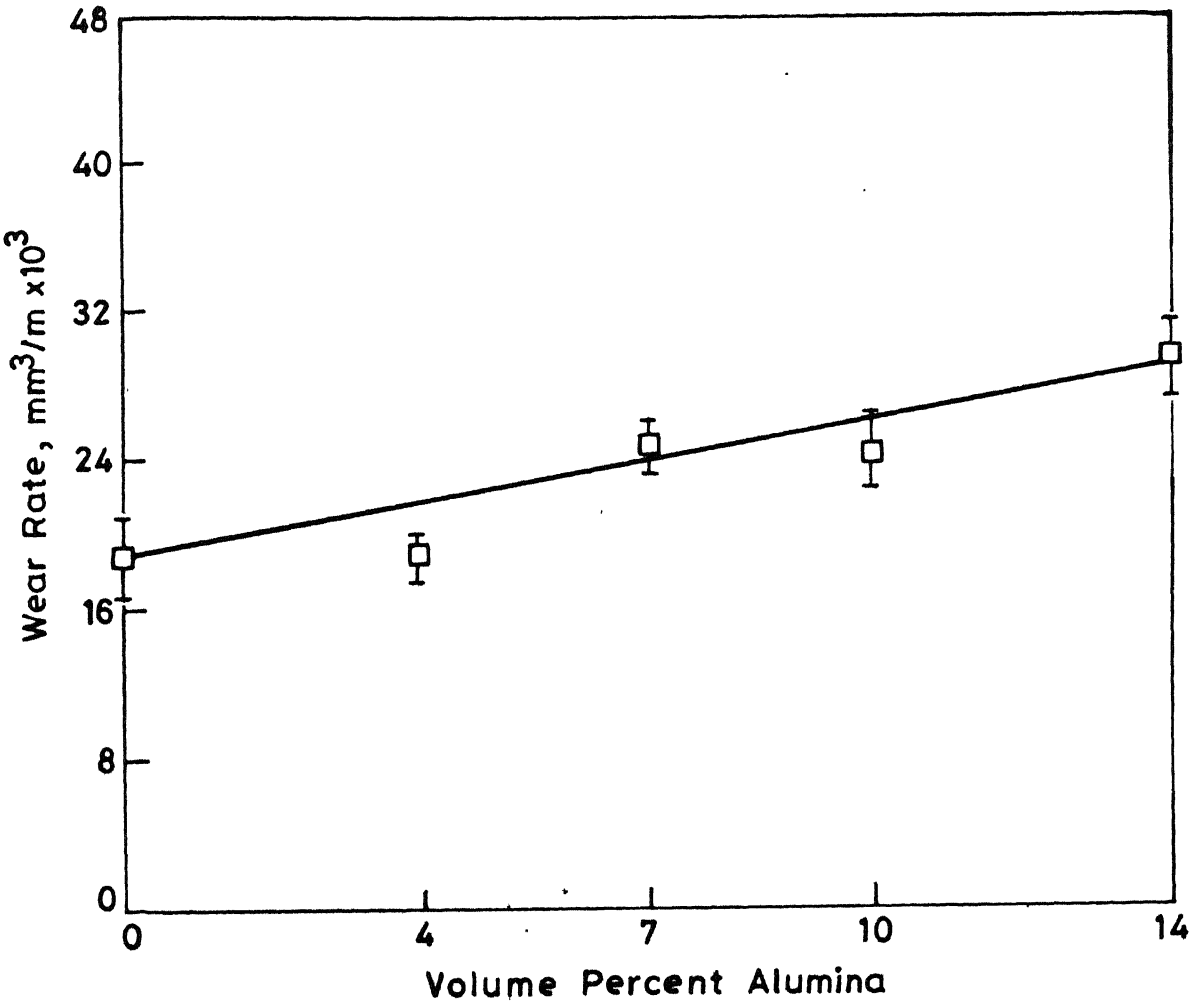

Fig. 3.50 Effect of alumina content on the wear rates of sintered 6061 alloy composites (Sliding speed: 0.5 m/s ; Applied pressure: 12×10^{-2} MPa ; Sliding distance : 250 meters)

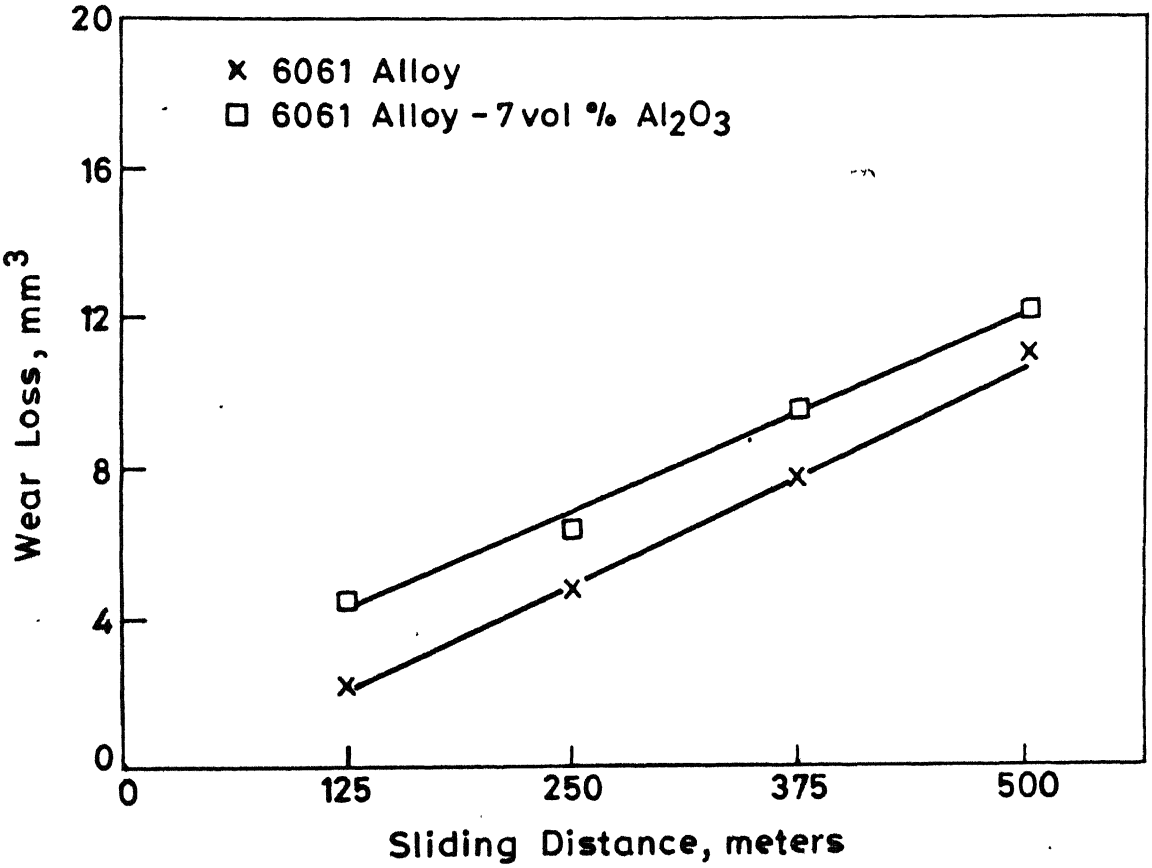

Fig. 3.51 Effect of sliding distance on the wear loss of sintered 6061 alloy and its 7 vol % alumina composites (Sliding speed: 0.5 m/s ; Applied pressure : 12×10^{-2} MPa)

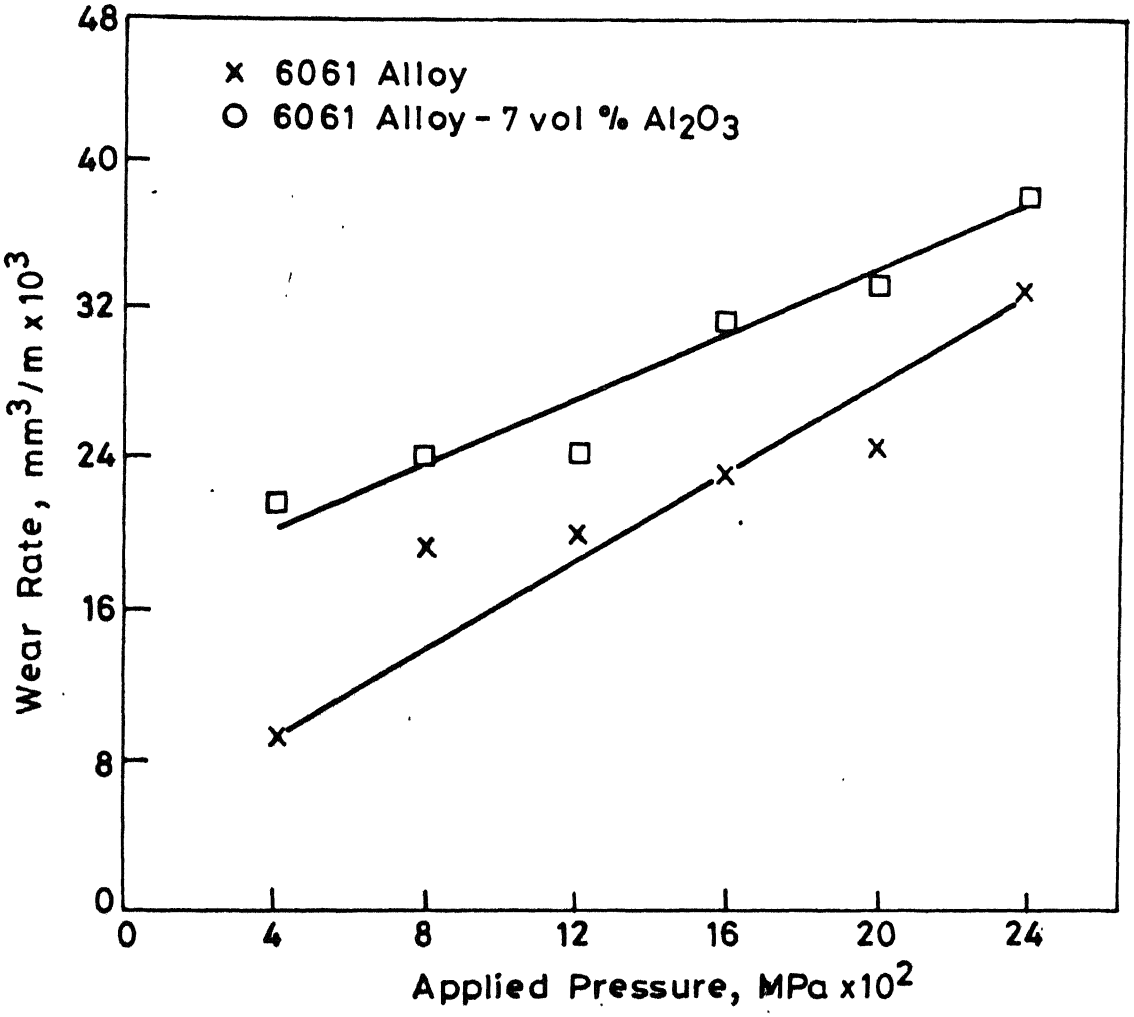

Fig. 3.52 Effect of applied pressure on the wear rates of sintered 6061 alloy and its 7 vol % alumina composites (sliding speed : 0.5 m/s ; Sliding distance : 250 meters .

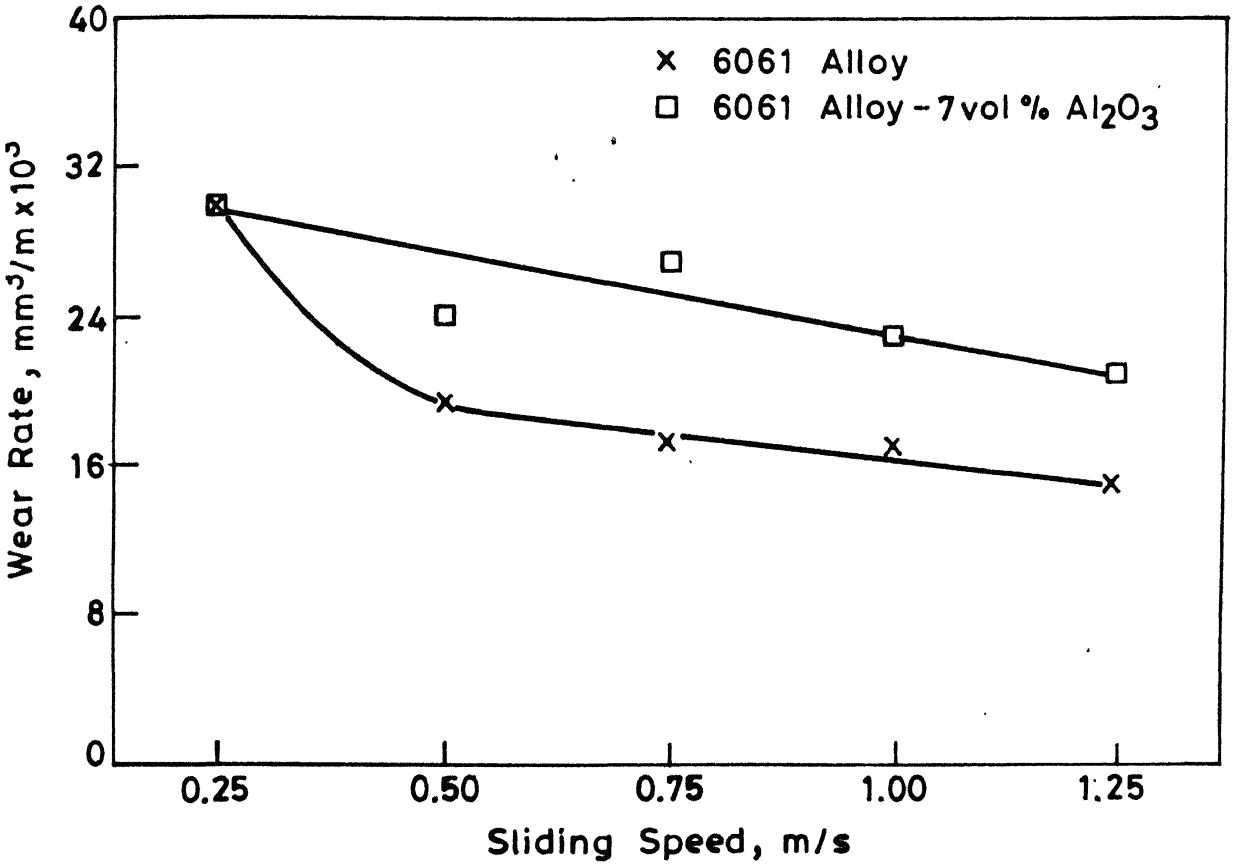

Fig. 3.53. Effect of sliding speed on the wear rates of sintered 6061 alloy and its 7 vol % alumina composites (Applied pressure: 12×10^{-2} MPa ; Sliding distance: 250 meters)

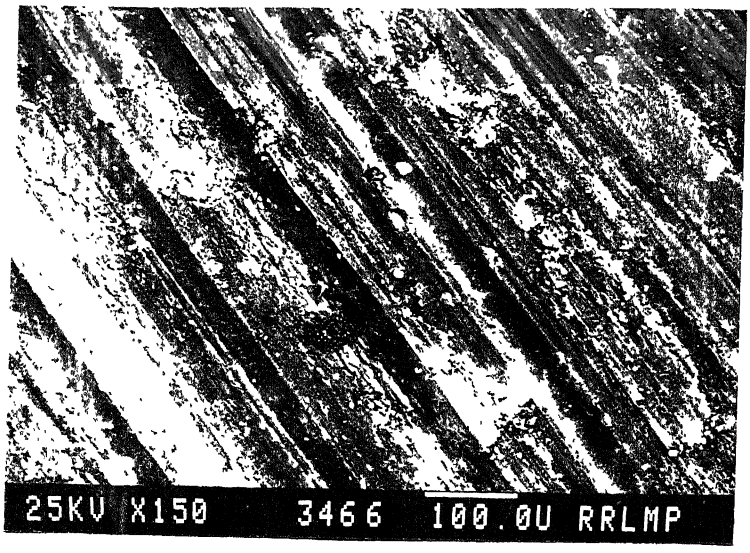

(a)

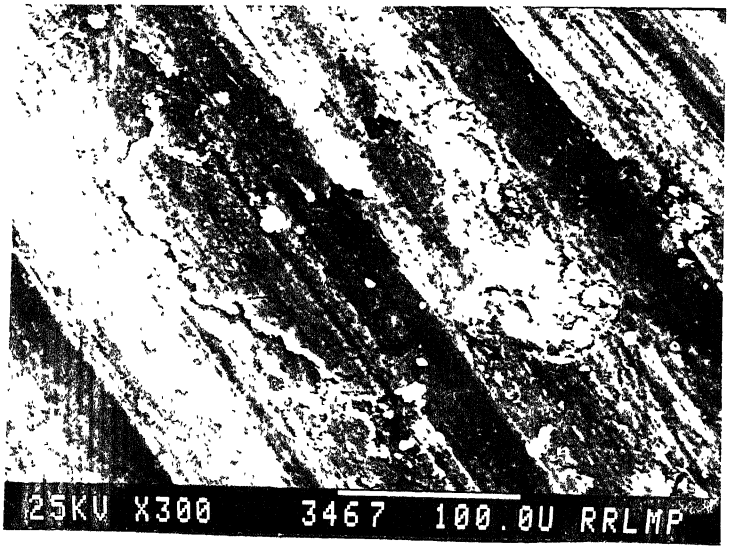

(b)

Fig. 3.54. Typical SEM micrographs of worn out surfaces of sintered 6061 alloy-7 volume percent alumina composites, showing long and continuous grooves and patches of highly damaged regions (Test parameters same as in Fig. 3.50).

debris in the process of fragmentation is evident from Figure 3.54b. Debris collected during the test of 6061 alloy - 7 vol. % alumina shows two types of particles (Figure 3.55). One is the fine particles of 1 to 10 μm (Figure 3.55d) and other is coarse flake type debris. Iron pick up by few such debris particles is also evident from the corresponding X-ray dot mapping of the debris (Figure 3.55b).

More damaged regions on the worn out surface of the composites tested at low sliding speed (i.e. 0.25 m/s) as compared to surface run at high speed are evident from Figures 3.56a and b.

Part IV

6061 Aluminium Alloy - TiC Particulate Composites

III.17. Properties of Sintered Particulate Composites:

III.17.1. Densification Behaviour:

Variation in dimensions of sintered composites as a function of volume fraction of TiC is shown in Figure 3.57. Linear dimensional changes remain constant with increasing volume fraction of TiC in any of the sintering atmospheres. Minimum linear growth was observed for composites after argon sintering. Radial dimensional changes of composites decreased with the addition of 4 vol. % TiC, which remained constant with further TiC addition,

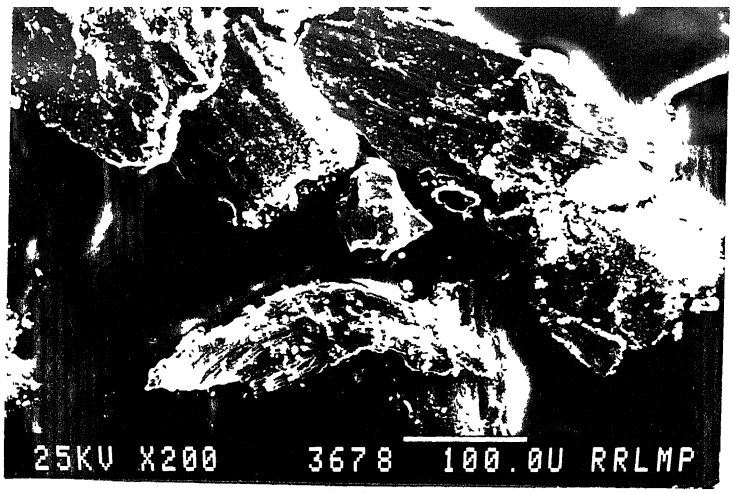

(a)

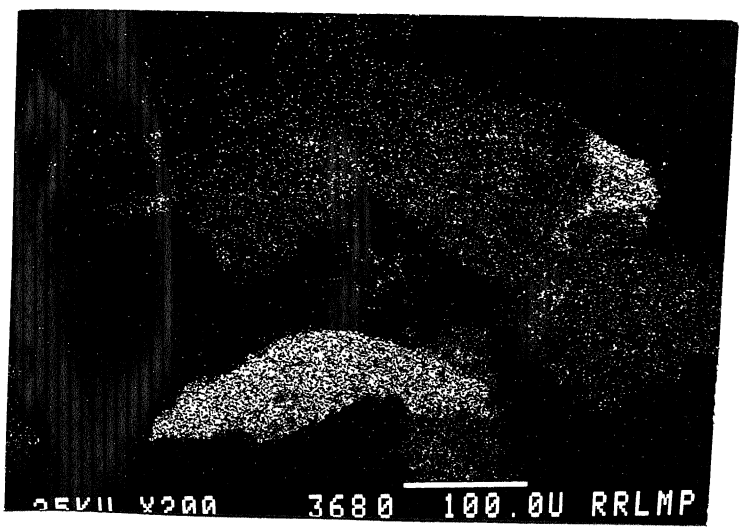

(b)

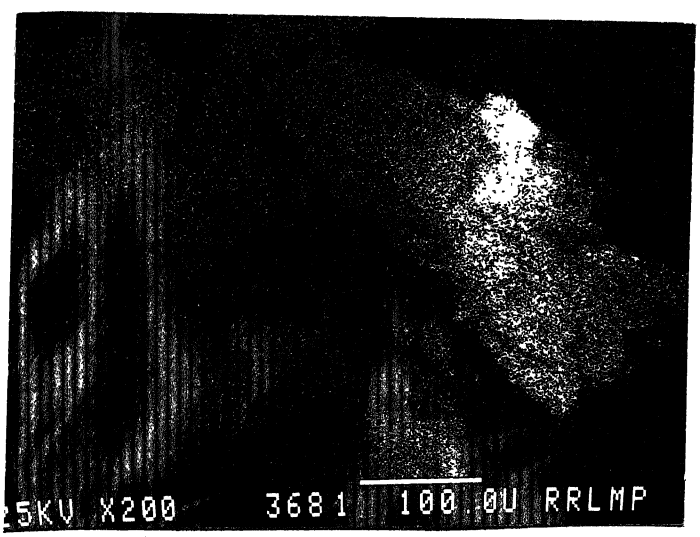

(c)

Fig. 3.55 contd.

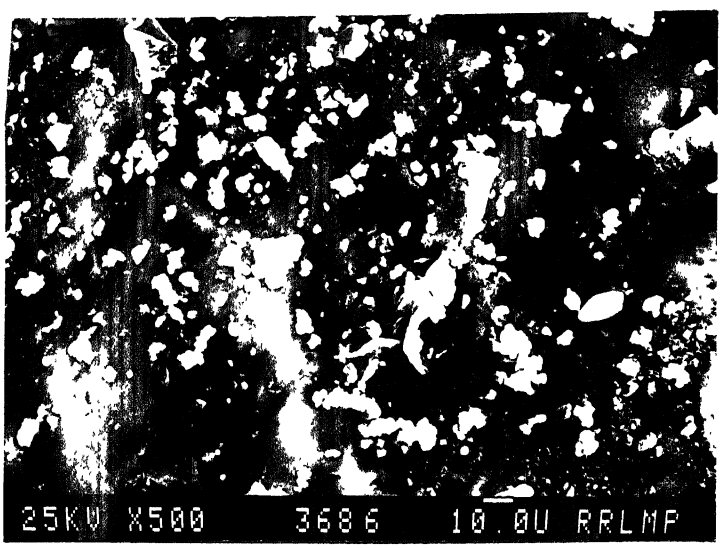

(d)

Fig. 3.55. SEM micrographs of debris of 6061 alloy-7 volume percent alumina composites (a) flaky debris (b) X-ray dot mapping of (a) for FeK_{α} peak (c) X-ray dot mapping of (a) for AlK_{α} peak (d) fine equiaxed debris particles (Test parameter same as in Fig. 3.50).

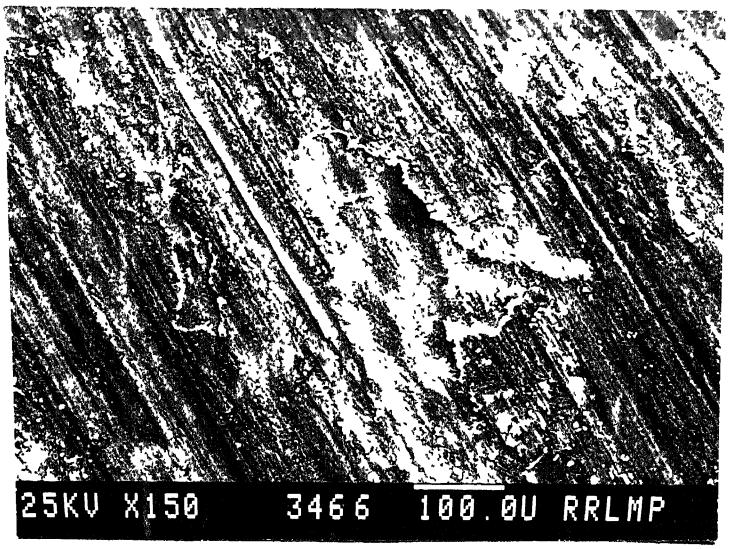

(a)

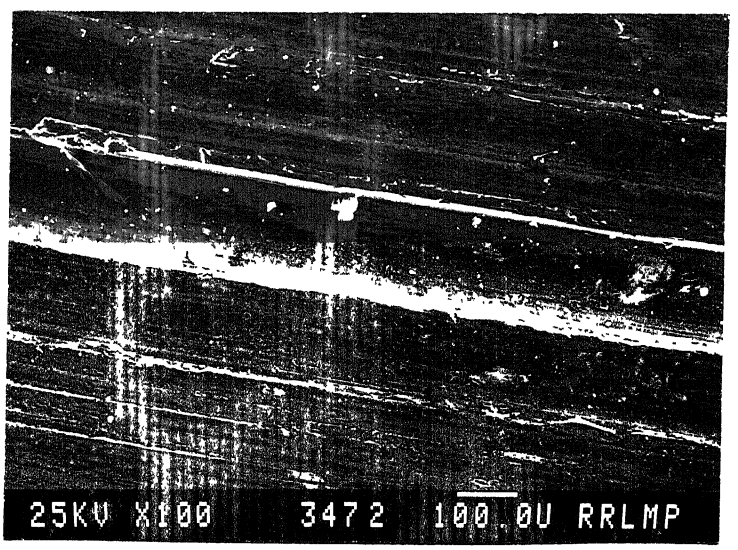

(b)

Fig. 3.56. SEM micrographs of worn out surfaces of sintered 6061 alloy-7 volume percent alumina composites at a sliding speed of (a) 0.25 m/s (b) 1.25 m/s (Applied pressure: 12 x 10^{-2} MPa, sliding distance: 250 meters).

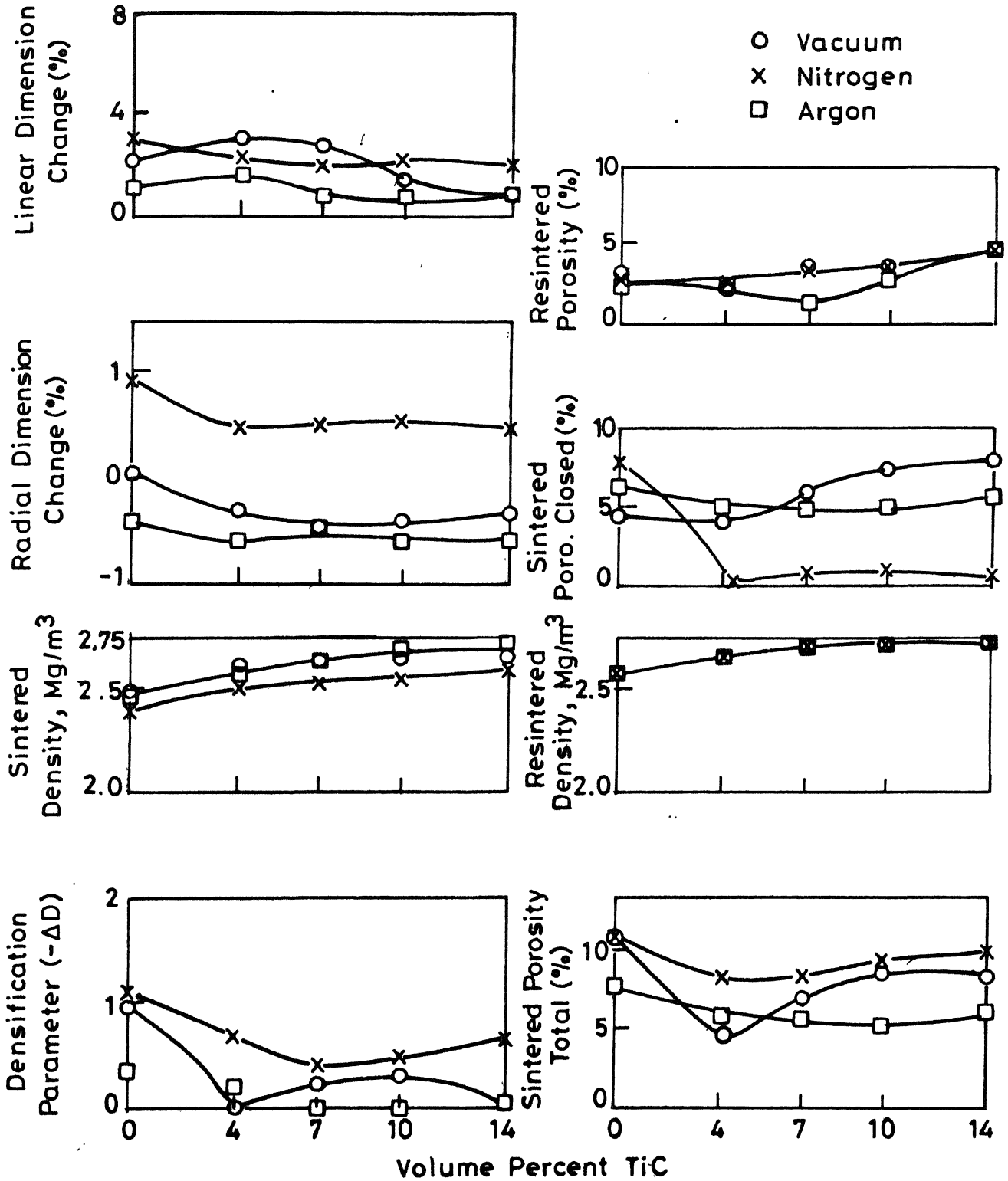

Fig. 3.57 Sintering behaviour of 6061 alloy-TiC composites as a function of dispersoid content.

irrespective of the sintering atmospheres. The composites exhibited radial shrinkage after argon or vacuum atmosphere sintering. Densification parameter increased with the addition of 4 vol. % TiC, which remained constant with further TiC addition. After nitrogen sintering, sintered closed porosity reduced to zero value with TiC addition. However, after vacuum or argon sintering, closed porosity approached to the value of the total sintered porosity indicating the absence of interconnected pores.

III.17.2. Hardness:

Brinell hardness of the sintered composites increased with the TiC addition (Figure 3.58) irrespective of sintering atmosphere. Maximum hardness was attained by the compacts sintered in vacuum followed by argon and nitrogen.

III.17.3. Tensile Mechanical Properties:

Table III.4 shows the mechanical properties of sintered 6061 alloy and its composite containing 7 vol. % of TiC.

Table III.4

Tensile properties of sintered 6061 alloy and 6061 alloy - 7 vol. % TiC composites (argon sintered)

Composition	UTS MPa	Y.S. MPa	Percent elongation
6061 alloy	90	65	15
6061 - 7 vol. % TiC	99	61	15

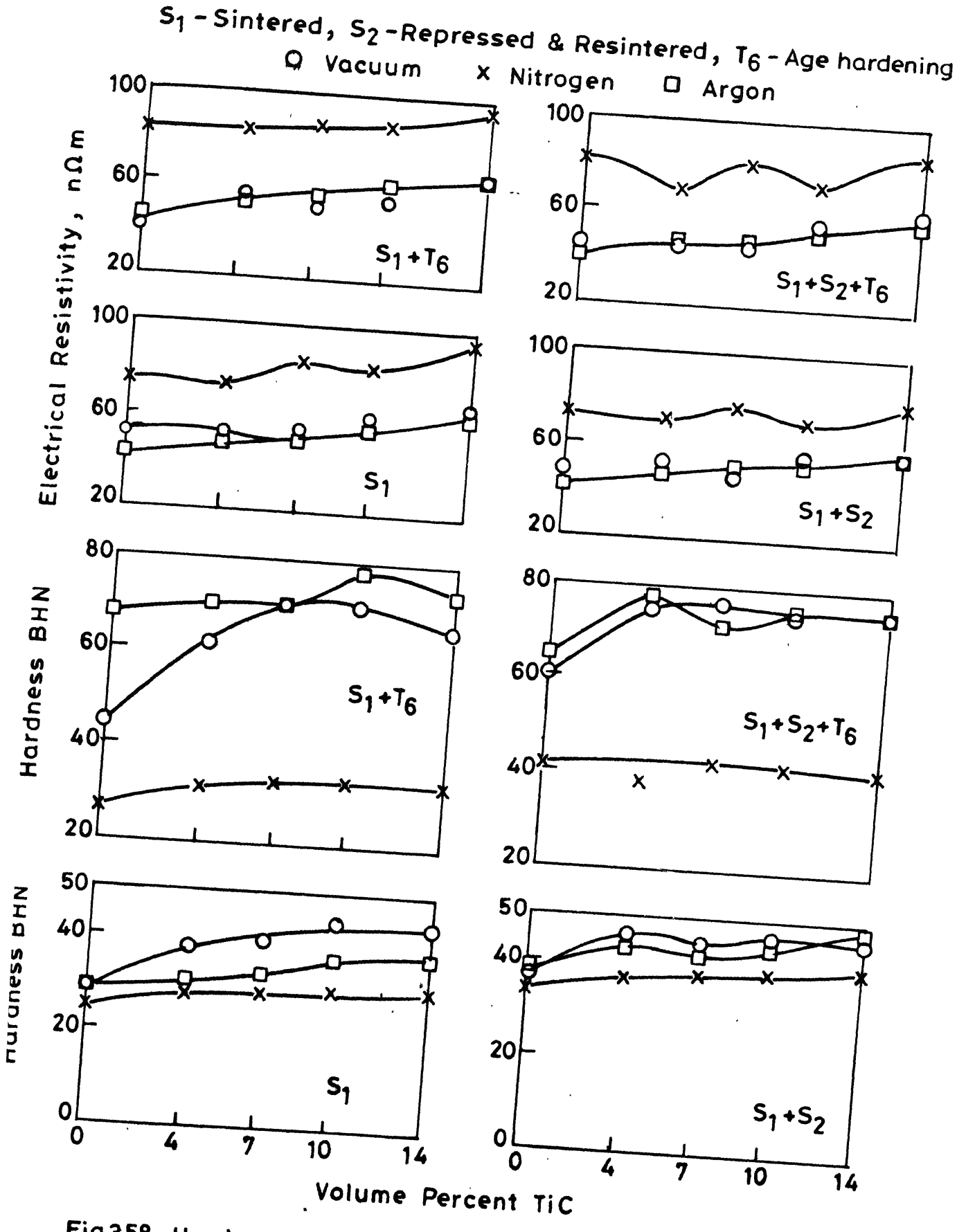

Fig.3.58 Hardness and electrical resistivity variations of sintered and heat treated 6061-TiC composites as a function of dispersoid content.

Increase in UTS of the sintered composites by 10% with addition of 7 vol. % TiC as compared to 6061 alloy was noticed. Percent elongation of composites remained constant, whereas Y.S. of composites decreased marginally with TiC addition.

III.17.4. Electrical Resistivity:

Electrical resistivity of the compacts increased with increasing amount of TiC, when sintered in any of the atmospheres (Figure 3.58). Sintering in nitrogen atmosphere resulted in maximum resistivity value.

III.17.5. Surface Roughness:

Surface roughness (R_a) value of the sintered 6061 - 7 vol. % TiC is 1.8 μm. This value is similar to that of the R_a value for sintered 6061 alloy composites.

III.17.6. Microstructure:

Due to the large difference in the mechanical properties of the matrix and TiC particles, metallographic preparation of the composite was difficult. Black patches representing TiC particles can be observed in the microstructure of sintered composites (Figure 3.59). More inhomogeneity in the composite containing higher volume of TiC is evident from the micrographs. SEM micrographs (Figure 3.61) of composites containing 7 vol. % TiC show TiC particle in the matrix. Interfaces are free from pores.

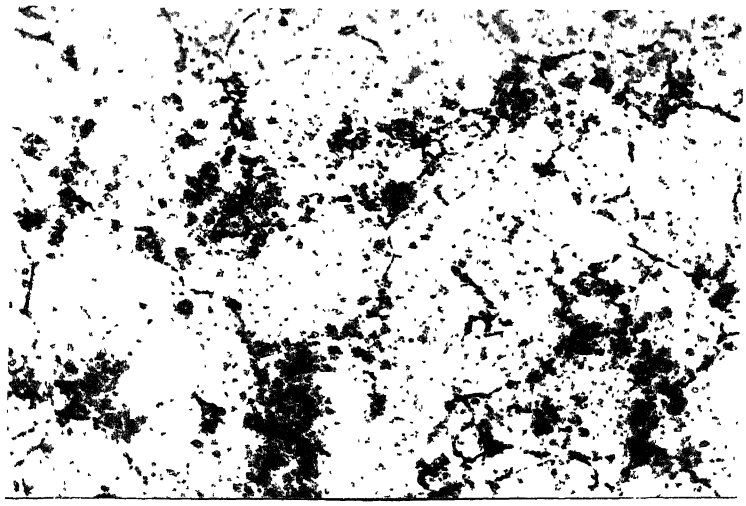

(a)

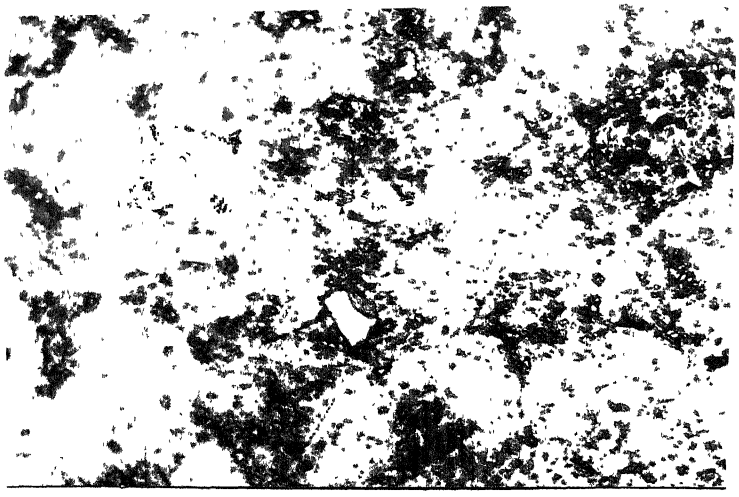

(b)

Fig. 3.59. Optical micrographs of sintered 6061 alloy composites containing (a) 7 volume percent TiC (b) 14 volume percent TiC (after argon sintering) (X200)

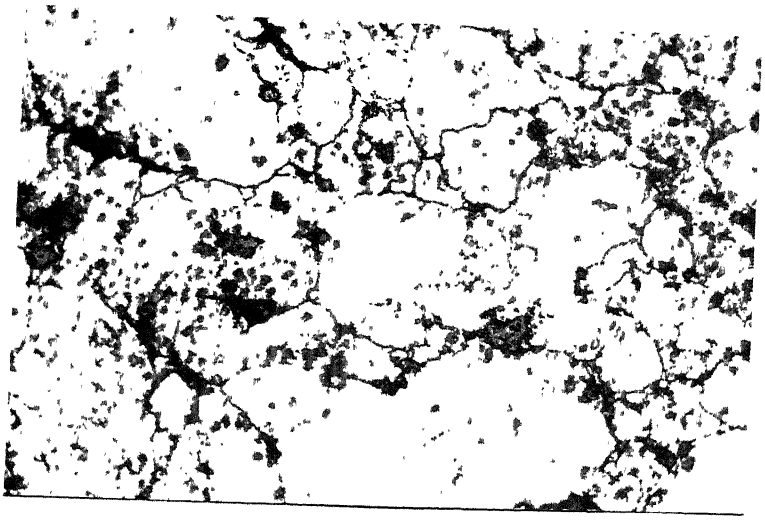

(a)

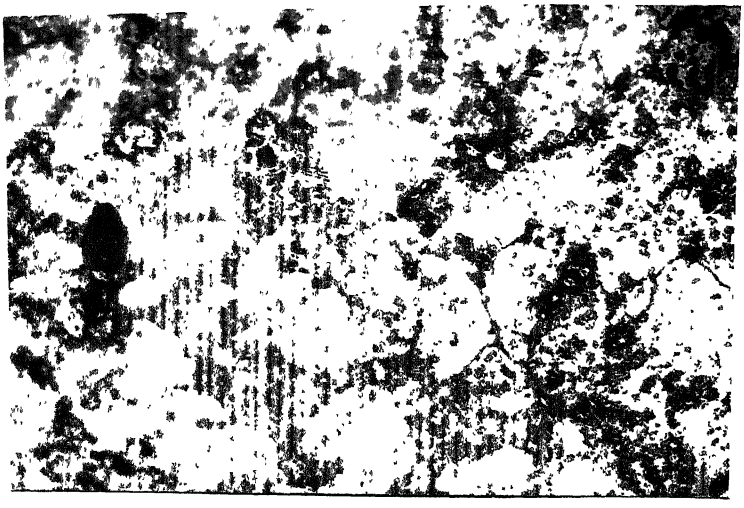

(b)

Fig. 3.60. Optical micrographs of repressed-resintered 6061 alloy composites containing (a) 7 volume percent TiC (b) 14 volume percent TiC (after argon sintering) (X200)

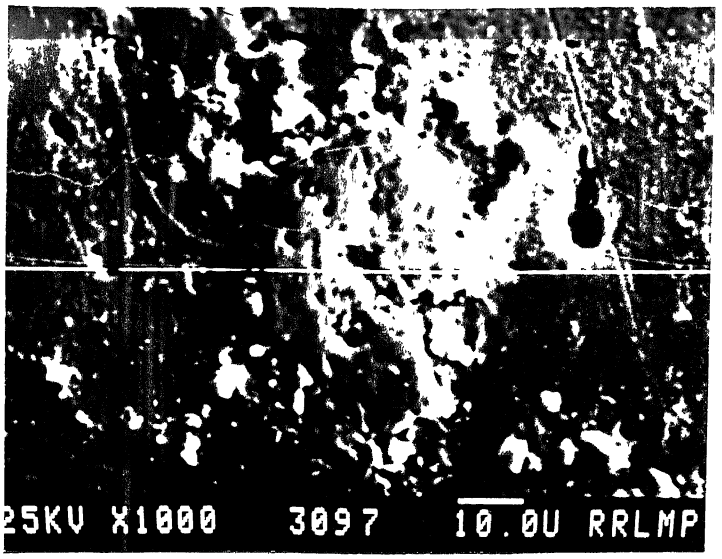

(a)

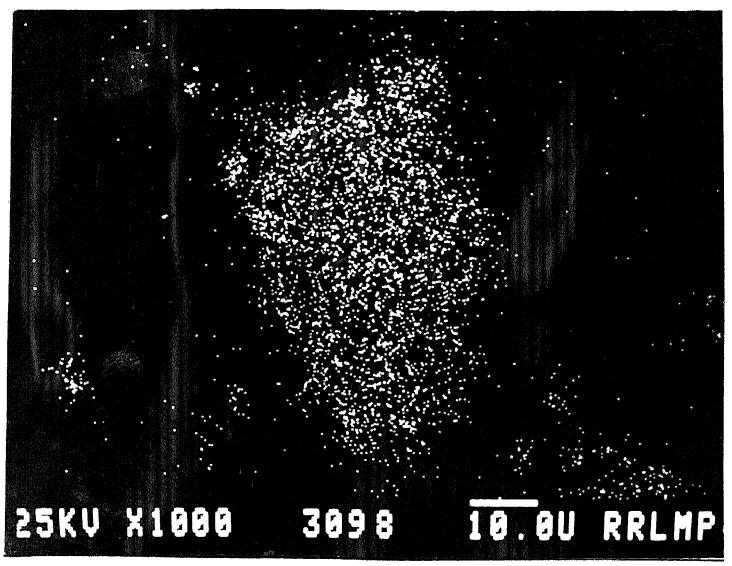

(b)

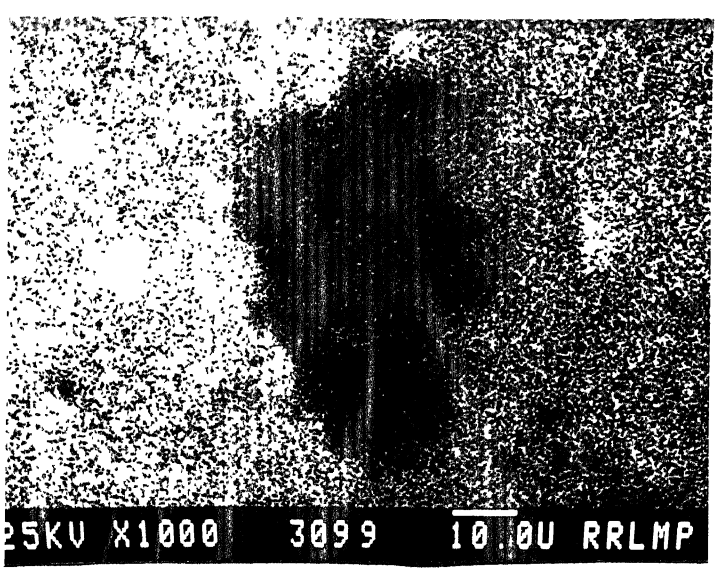

(c)

Fig. 3.61 contd.

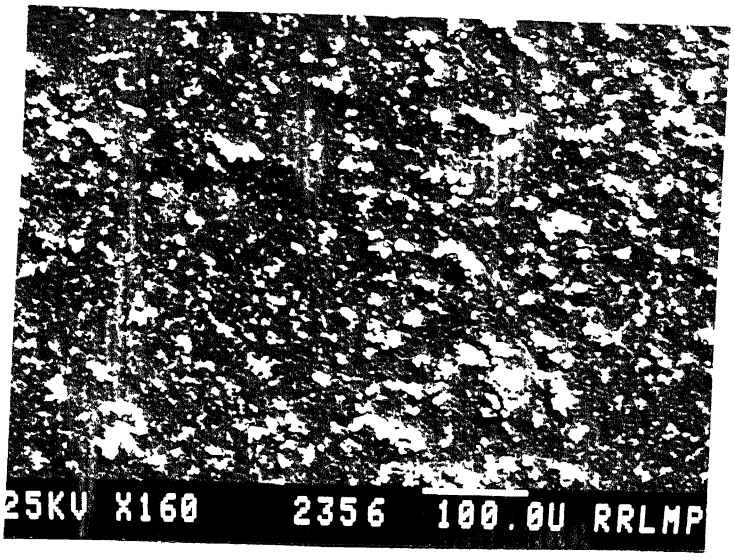

(d)

Fig. 3.61. (a) SEM micrographs of sintered 6061 alloy-7 volume percent TiC composites (b) corresponding X-ray dot mapping for TiK_α peak (c) X-ray dot mapping for AlK_α peak (d) micrograph at low magnification.

WDXS analysis confirmed the presence of TiC in the matrix (Figure 3.61b).

III.18. Properties of Repressed-Resintered Composites:

III.18.1. Densification Behaviour:

Repressing and resintering decreased the porosity level of the sintered composites to 50% (Figure 3.57) as compared to the value for sintered ones.

III.18.2. Hardness:

Hardness value of such category of sintered composites increased after repressing and resintering (Figure 3.58). A marginal increase in hardness value of the repressed and resintered composites with increasing amount of TiC is evident from the plot (Figure 3.58).

III.18.3. Electrical Resistivity:

Repressing-resintering decreased the overall electrical resistivity of compacts (Figure 3.58). Similar to that of as sintered case, resistivity values of the composites sintered in nitrogen was maximum in as repressed and resintered condition.

III.18.4. Microstructure:

Improved microstructure after repressing and resintering of the composites are shown in Figure 3.60. Emergence of grains can be observed in the microstructure of composites containing 7% TiC (Figure 3.60a).

III.19. Properties of Heat Treated Composites:

III.19.1. Hardness:

Effect of dispersoid addition is substantial after age-hardening of the composites, when sintered either in argon or vacuum (Figure 3.58). After age hardening of the repressed-resintered compacts, the effect of amount of TiC on the hardness is negligible. However hardness of the composites sintered in argon or vacuum increased with an addition of 4 vol. % TiC, which remained constant with further TiC addition.

III.19.2. Tensile Mechanical Properties:

Figure 3.62 shows the mechanical properties variation of heat treated composites as a function of volume percent of TiC. UTS decreased linearly with the volume fraction of TiC. Addition of 14 vol. % TiC in 6061 alloy resulted in 40% reduction in UTS value of the composites. Y.S. value of the composites containing 4 vol. % TiC was 20% more than that for straight heat treated 6061 alloy. After addition of TiC, Y.S. of the composites decreased linearly. Percent elongation of composites decreased with addition of TiC (Figure 3.62). Initially with addition of 4 vol. % of TiC percent elongation decreased significantly.

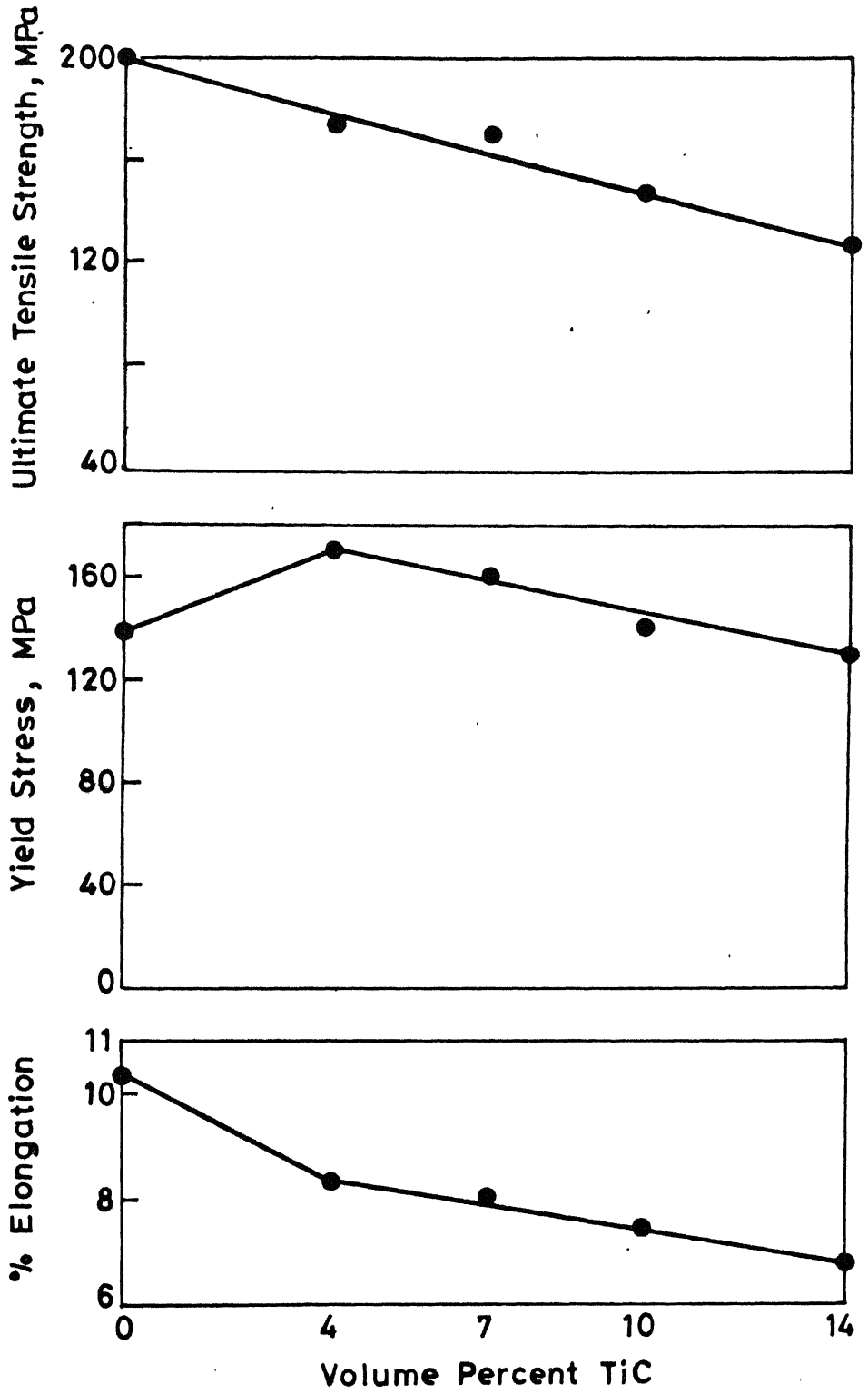

Fig. 3.62 UTS, YS for 0.2% offset and % elongation variation of sintered and age hardened 6061 alloy - TiC composites as a function of dispersoid content.

III.19.3. Electrical Resistivity:

Effect of age hardening on the resistivity values of the composites was marginal on sintered or repressed-resintered composites (Figure 3.58). Nitrogen atmosphere sintering imparted maximum resistivity to the compacts in age-hardened condition.

III.19.4. Fractography:

SEM fractographs of composites containing 14 vol. % TiC is shown in Figure 3.63. Presence of TiC particles are evident from the fractographs. High magnification micrograph (Figure 3.63c) shows brittle type of fracture.

III.20. Hardness Variation of Thermomechanically Treated Composites:

Figure 3.64 shows the variation of microhardness of the sintered and thermomechanically treated composites as a function of TiC content. TMT resulted in hardness improvement of the composites as compared to the sintered values. Microhardness of sintered composites increased with volume fraction of TiC. But after TMT, hardness of the composites, decreased with initial TiC addition, which remained constant with further addition.

III.21. Sliding Wear Study:

III.21.1. Wear Loss:

Composites containing TiC showed increased wear rate with increasing amount of TiC (Figure 3.65). But

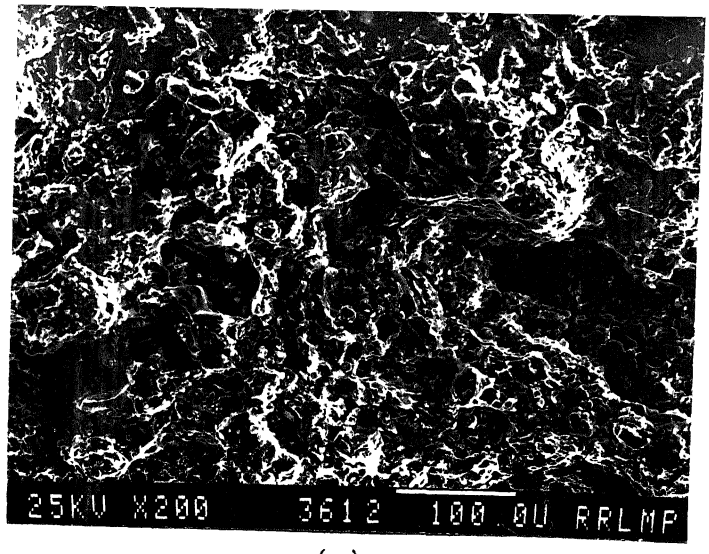

(a)

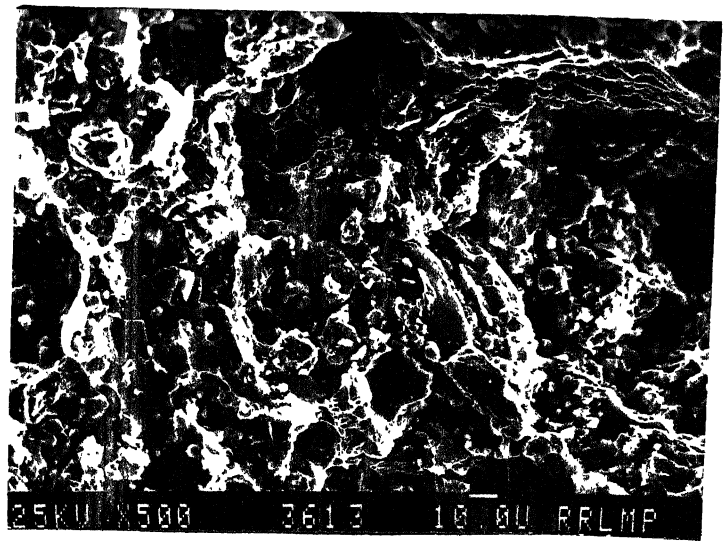

(b)

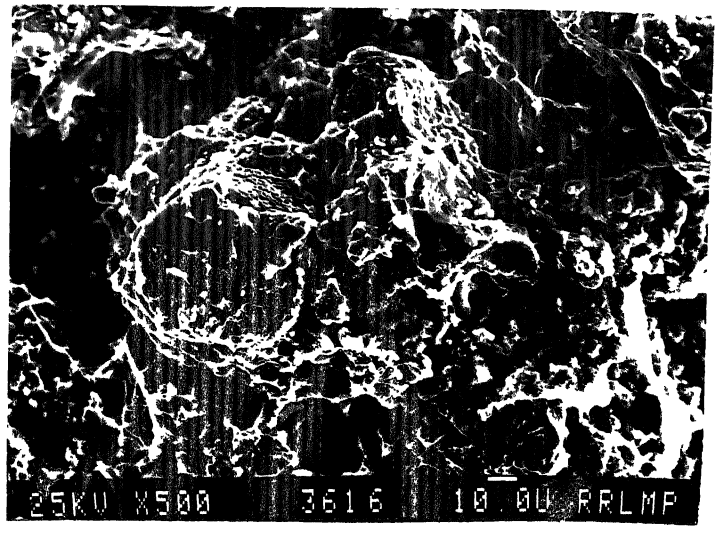

(c)

Fig. 3.63. SEM micrographs of fractured surface of sintered and heat treated 6061 alloy-14 volume percent TiC composites, after tensile test (a and b at different magnifications).

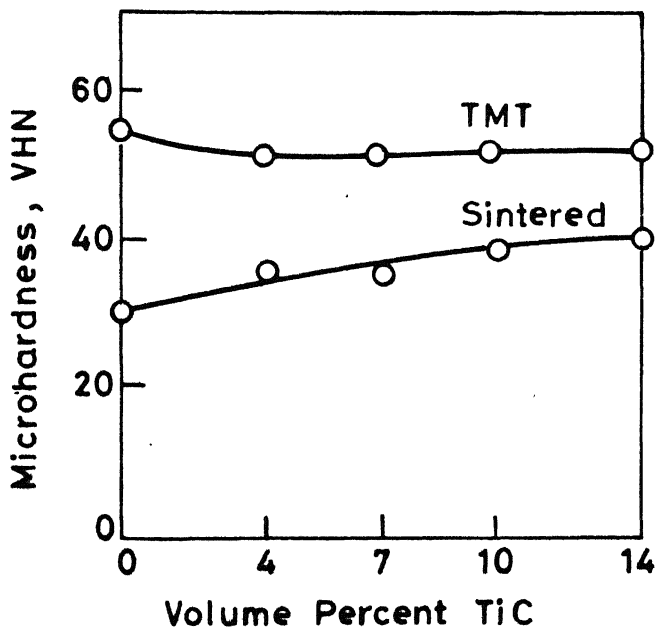

Fig. 3.64 Vickers microhardness variation of sintered and thermomechanically treated (TMT) 6061 alloy composites as a function of dispersoid content.

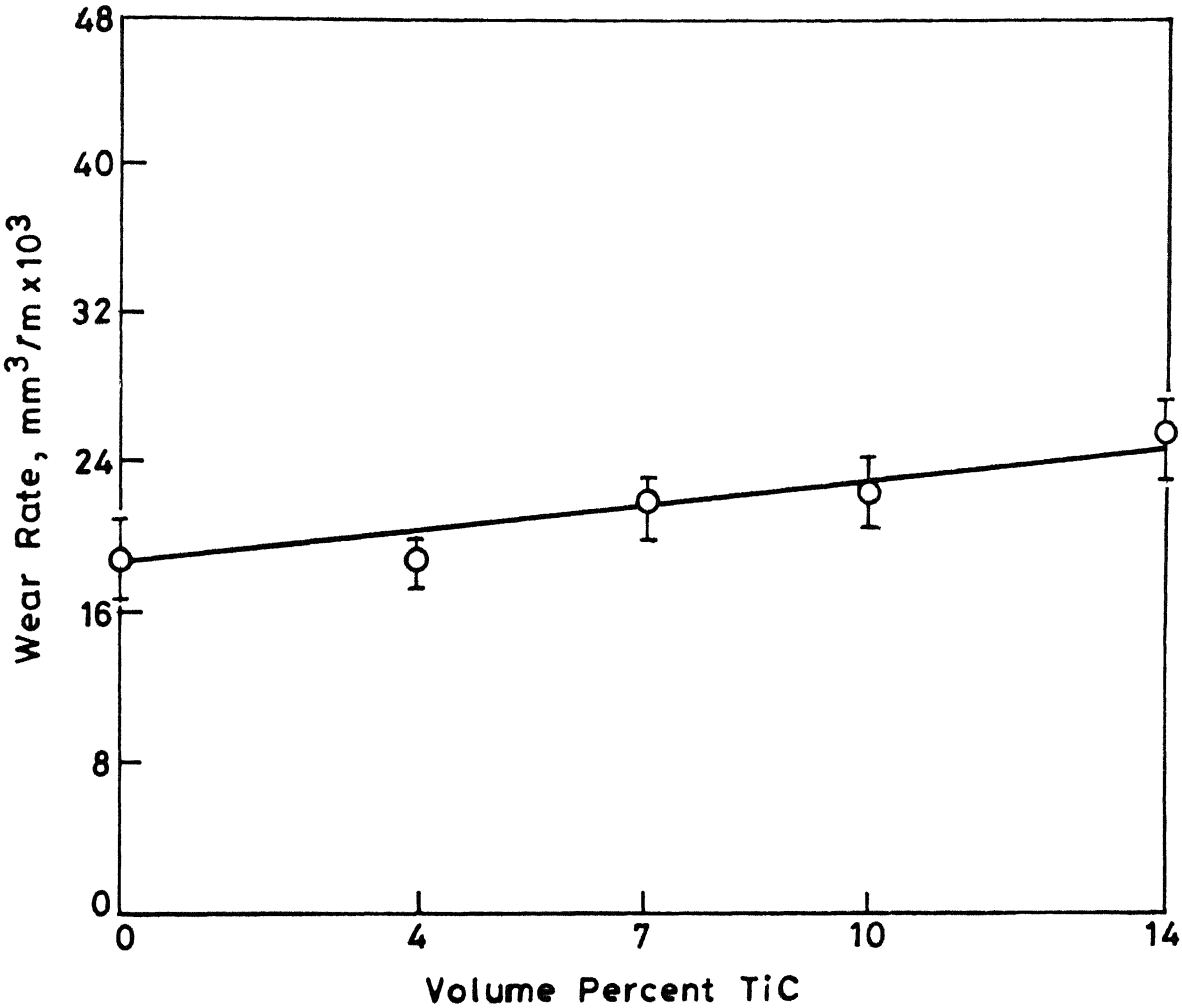

Fig. 3.65 Effect of volume percent of TiC on the wear rates of sintered 6061 alloy composites (Sliding speed 0.5 m/s ; Applied pressure: 12×10^{-2} MPa; Sliding distance : 250 meters .

increase in wear rate was marginal.

Wear loss of the composites containing 7 vol. % TiC increased linearly with the sliding distance (Figure 3.66). Slope of the plot for composite containing TiC is similar to that for straight 6061 alloy. With increase in the applied pressure wear rate of the composites increased linearly (Figure 3.67), but the slope of the plot is less as compared to 6061 alloy. Wear rate of the composites containing 7 vol. % TiC increased approximately three times when the sliding speed was reduced from 1.25 to 0.25 m/s (Figure 3.68).

III.21.2. SEM Study:

Figure 3.69 shows the micrographs of worn out surface of 6061 alloy - 7 vol. % TiC composites. Micrographs show sharp grooves and deformed regions similar to that observed in case of straight 6061 alloy.

Debris collected during the test of 6061 TiC composites (Figure 3.70) have same nature as the debris collected from alumina containing composites. Equi-axed fine particles of 1 to 10 μm (Figure 3.70d) as well as coarse flakes of approximately 100 μm size (Figure 3.70a) were present in the debris. Iron pick up by few flake shaped debris (Figure 3.70b) was also identified by WDXS analysis. Figure 3.71 shows the worn out surfaces of the composites tested at different sliding speeds. More severely damaged regions are evident from the micrograph of the composite tested at lower sliding speed i.e. 0.25 m/s, as compared to the composites tested at 1.25 m/s (Figure 3.71).

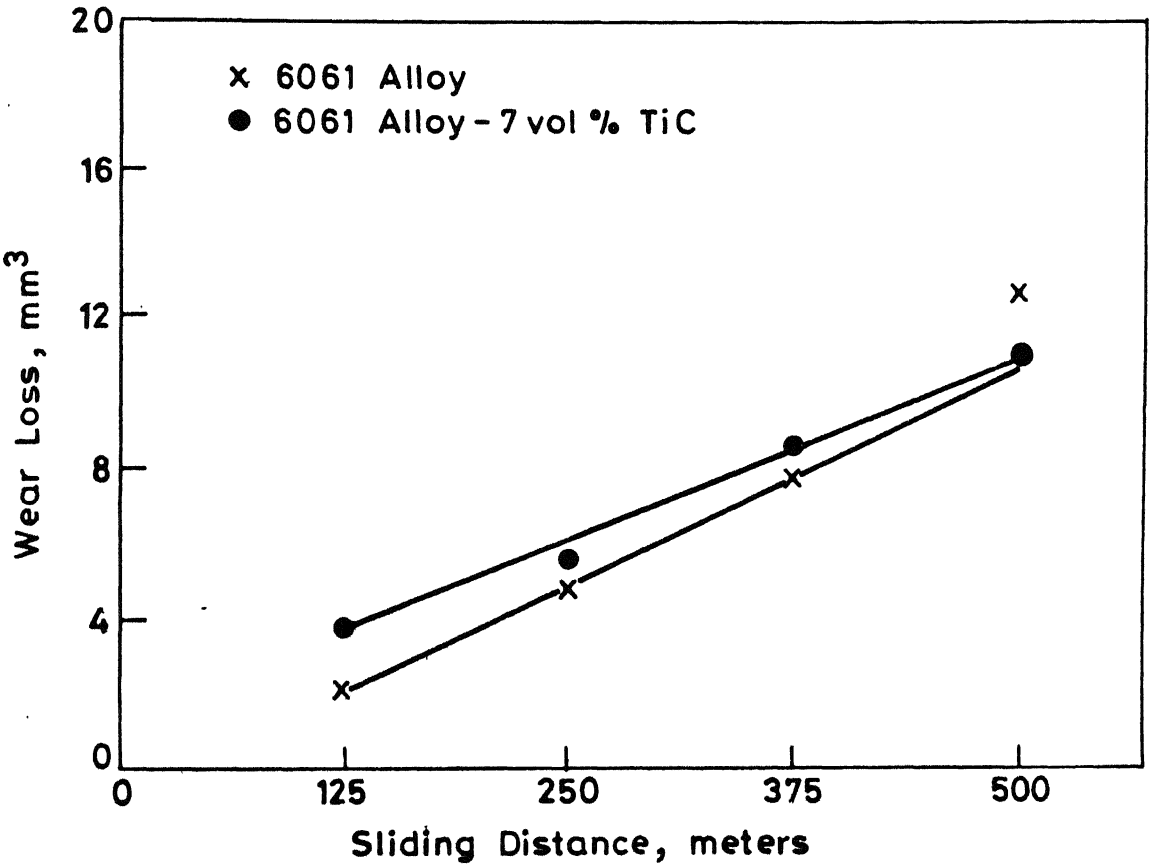

Fig. 3.66 Effect of sliding distance on wear loss of sintered 6061 alloy and its composits containing 7 vol % of TiC (Sliding speed 0.5 m/s; Applied pressure : 12×10^{-2} MPa)

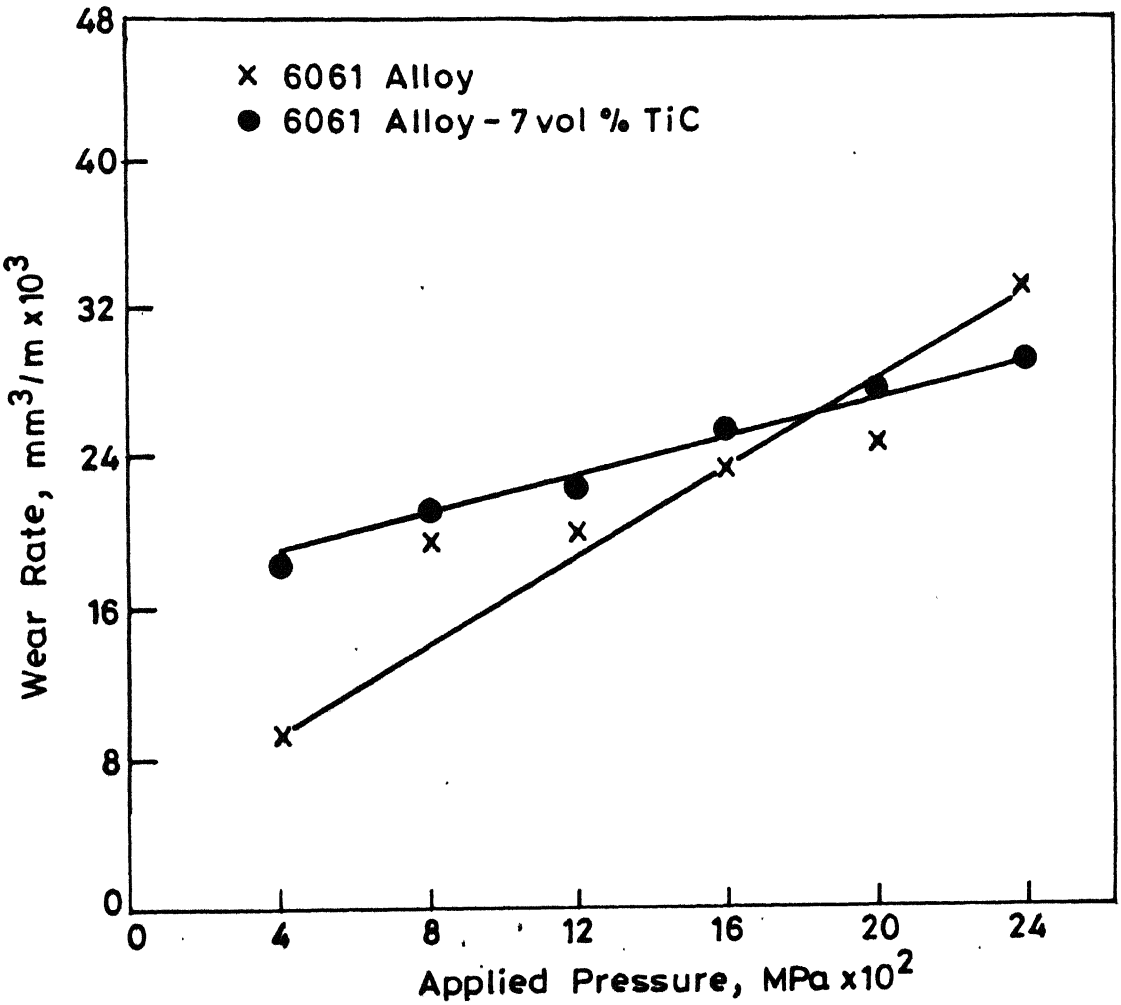

Fig. 3.67 Effect of applied pressure on the wear rates of sintered 6061 alloy and composites containing 7 vol % TiC (Sliding speed: 0.5 m/s ; Sliding distance : 250 meters)

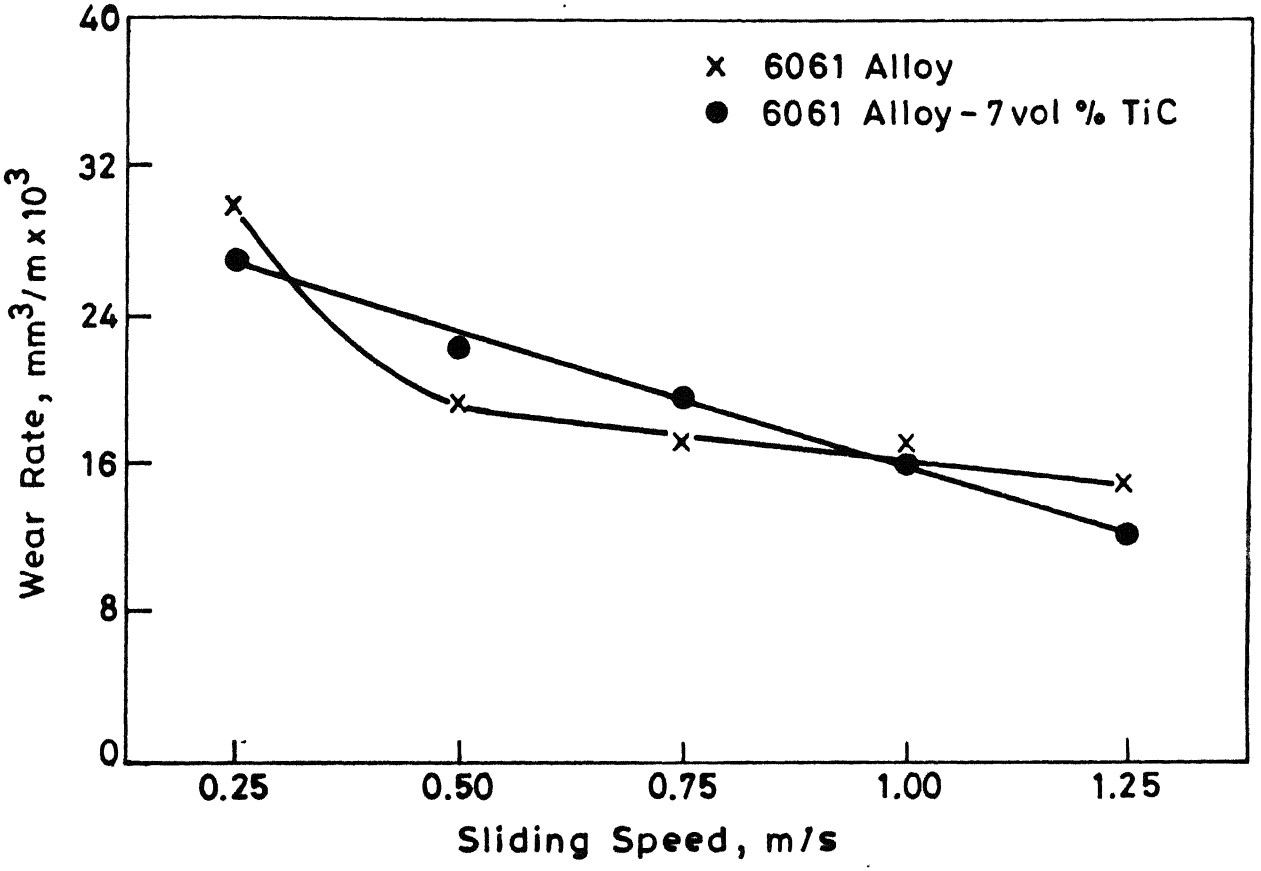

Fig. 3.68 Effect of sliding speed on wear rate of sintered 6061 alloy and composites containing 7 vol % TiC (Applied pressure : 12×10^{-2} MPa ; Sliding distance: 250 meters)

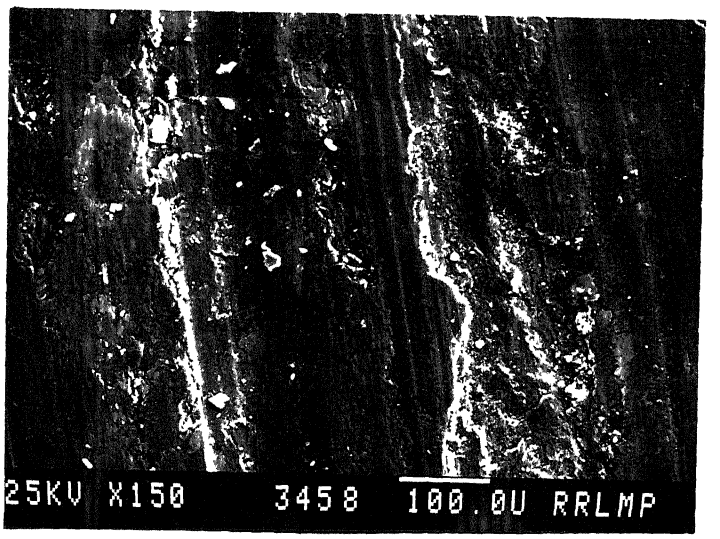

(a)

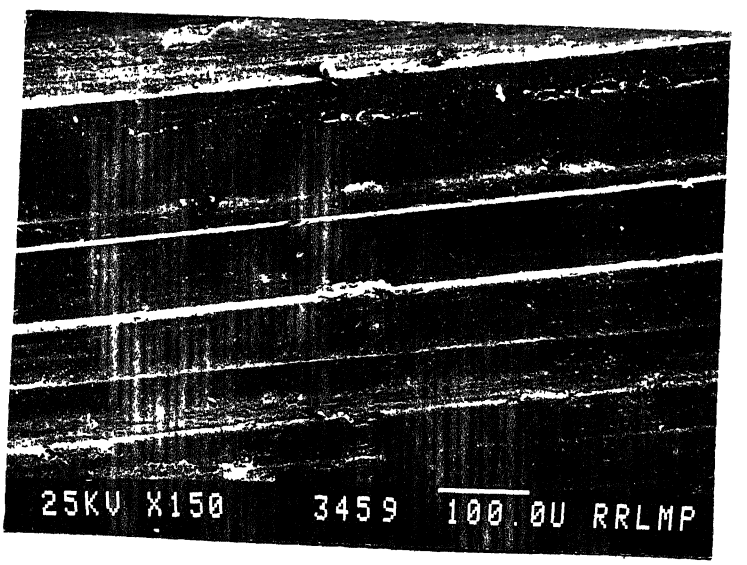

(b)

Fig. 3.69. Typical SEM micrographs of worn out surface of sintered 6061 alloy-7 volume percent TiC composites showing presence of (a) long and continuous grooves and (b) patches of damaged region (Test parameter same as in Fig. 3.65).

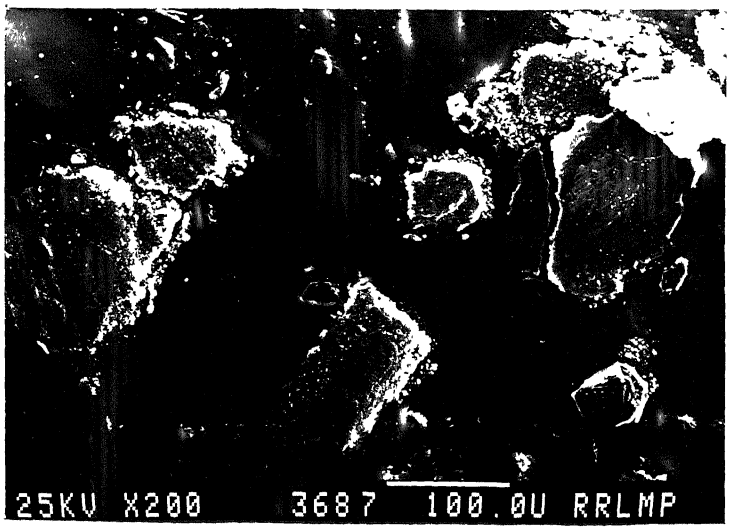

(a)

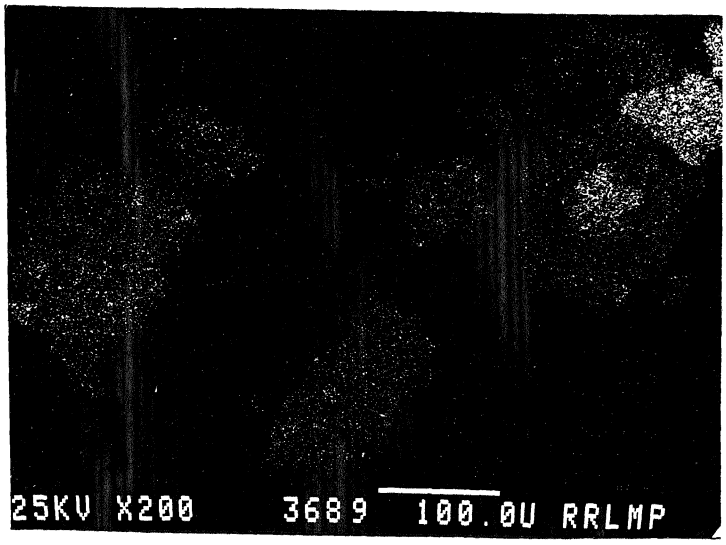

(b)

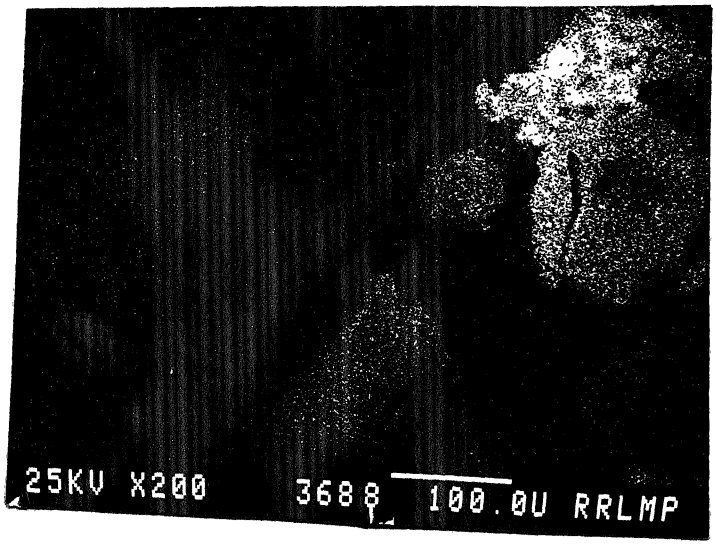

(c)

Fig. 3.70 contd.

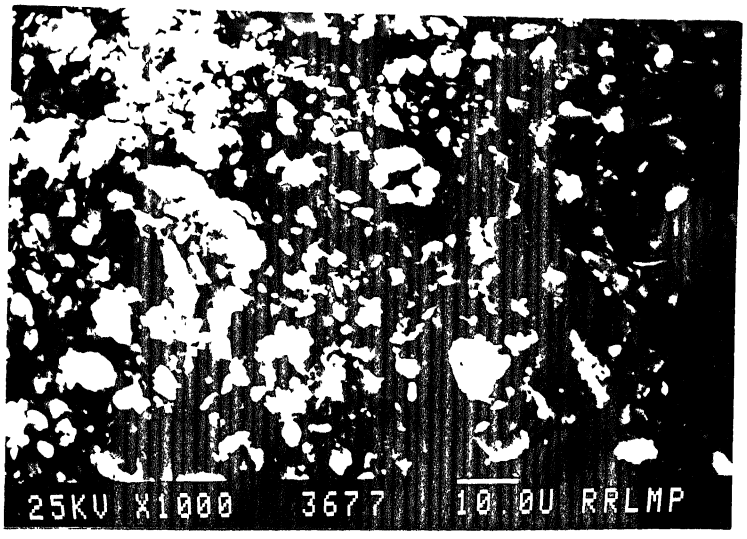

(d)

Fig. 3.70. SEM micrographs of debris of sintered 6061 alloy-7 volume percent TiC composites (a) flake shape debris (b) X-ray dot mapping of (a) for FeK_α peak (c) X-ray dot mapping of (a) for AlK_α peak (d) fine debris particles (Test parameters same as in Fig. 3.65).

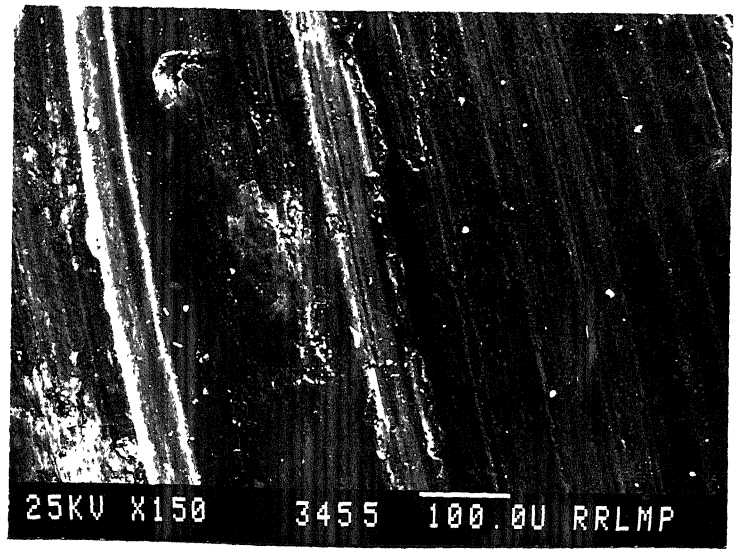

(a)

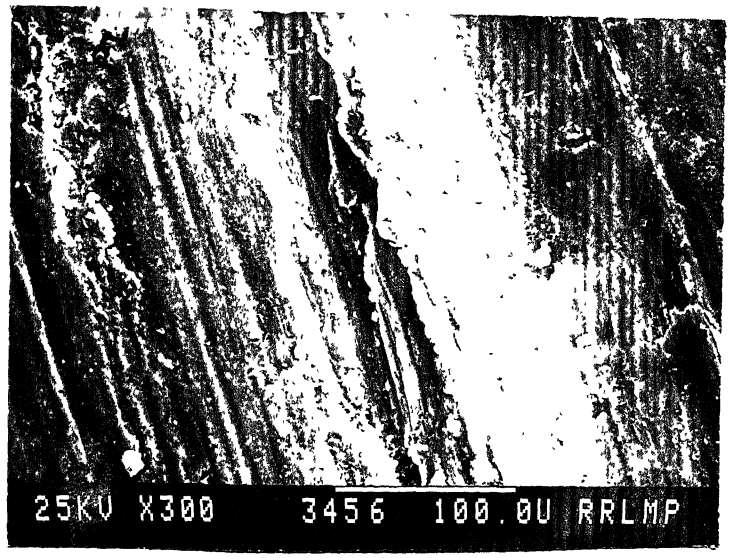

(b)

Fig. 3.71. Typical SEM micrographs of worn out surfaces of sintered 6061 alloy-7 volume percent TiC composites at a sliding speed of (a) 0.25 m/s (b) 1.25 m/s (Applied pressure 12 x 10^{-2} MPa; sliding distance: 250 meters).

CHAPTER IV

DISCUSSION

Aluminium P/M alloys are delicate systems when produced by conventional route i.e. mixing, compaction and sintering. Their susceptibility to react with impurities present in sintering atmosphere, apart from the stable oxide layer on aluminium particles and porosity in green compacts, gives rise to complexities during sintering. Incorporation of second phase particles (dispersoids) into aluminium alloy makes the sintering still more interesting due to the possible interaction of dispersoid with the matrix alloy.

6061 aluminium alloy system undergoes liquid phase sintering at the temperature of 615^{o}C selected in the present study. Eutectic melt formed at sintering temperature diffuses into the matrix:in the presence of porosity and various types of dispersoid will affect this. In the present study, sintering behaviour was monitored by dimensional changes and porosity variation of the composites. Properties like hardness, ultimate tensile and yield strengths, electrical resistivity and dry sliding wear are explained on the basis of sintering behaviour and also on the nature of individual dispersoid. Attempt is made to correlate the end properties of P/M composites containing different types of dispersoids.

IV.1. Sintering of 6061 Alloy:

6061 aluminium alloys contain silicon and magnesium to render them heat treatable. Liquidus and solidus temperatures reported[96] for this alloy are 652 and 582°C respectively. During P/M processing the alloy system (Al-Mg-Si) undergoes transient liquid phase sintering. When 6061 premix powder compact is heated, an eutectic liquid forms at relatively lower temperature (452°C) at the contact area of aluminium and magnesium. Magnesium (minor constituent) in conjunction with aluminium further diffuses into the melt and thus increases the amount of liquid phase. Eutectic liquid so formed spreads into the voids due to the capillary action. With further increase in temperature, an additional eutectic reaction between aluminium and silicon occurs at 577°C, thus increasing the melt volume. In case of quasibinary system Al-Mg_2Si, literature reports[97] an eutectic reaction at a temperature of 595°C. It is possible that during sintering such a reaction also contributes is liquid phase sintering, which on cooling gives rise to the emergence of Mg_2Si phase. Such a melt would naturally have a higher content of magnesium and silicon in it as compared to their individual solubilities in the adjacent solid aluminium particles.

The results of Savitskii and Martsunova[98] on liquid phase sintering of Al-Mg and Al-Si premix compacts showed growth in the former, but shrinkage in the latter. The authors suggested this to be related to the different extent of intersolubilities. It appears that the eutectic melt in

the former binary system is more wettable to the matrix, as compared to the Al-Si eutectic melt. The growth of the compacts may be viewed as disintegration of the particles along their grain boundaries because of melt penetration under favourable situations. However, any definite conclusion on the dimensional stability of the sintered aluminium-alloy compact is rather difficult, as it depends on other factors as well, like: sintering temperature and period, density of green compact, particle size of the powders, and the type of sintering atmospheres and their dew points.[99]

According to German[100] the enhanced sintering in the presence of liquid phase is due to three factors: i) solubility; ii) segregation; and iii) diffusion. In 6061 alloy system, if one looks at the relevant binary constitutional diagrams, it is apparent that difference in the melting point of base metal (i.e. aluminium) and the eutectic isotherm of aluminium-magnesium (211^{o}C) is greater than that for aluminium and the isotherm of aluminium-silicon (86^{o}C). Further, the solubility of magnesium in aluminium is 12 mass percent, whereas, the solubility of the other constituent, namely silicon, is practically nil. This clearly indicates that magnesium addition in aluminium has a pivotal role during sintering of aluminium alloys.

From the electronic structure point of view all the three elements in the 6061 alloy i.e. Mg, Al and Si belong to the same Group in the Periodic Table with similar outermost electron configuration. Magnesium being metallic in nature is

more compatible with aluminium matrix as compared to silicon, which has a covalent bonding. The higher solubility of magnesium in aluminium as compared to silicon in aluminium is a direct manifestation of this fact.

It is evident from results that 6061 alloy compacts in general swell after sintering. Dudas and Thompson[2] reported that sintering of aluminium premix compacts of 6061 system resulted in dimensional growth if the green density of compacts was high and/or dew point of the sintering atmosphere were high. In the present study, as the dew point of the gases selected were comparatively low (Ar: $-40^{o}C$ and N_2: $-38^{o}C$), it appears that the growth is governed by the higher level of the green densities (95 percent T.D.) of the compacts. Closed porosities which amount to 25 percent of total porosities in the compacts are expected to exert hydrostatic pressure at elevated temperature, thus promoting dimensional increase in the compacts. The formation of solid solution from the elemental powders also plays an important role in swelling during sintering.[101] An additional factor may be the penetration of eutectic liquid between adjacent particles, pushing them apart, when the dihedral angle is low. As highlighted by Kehl and Fischmeister[102] the melt may also rupture the oxide film over the aluminium particle surface, thus contributing to volune expansion.

It is clear from the present results (Figure 3.2) that the extent of linear and radial dimensional changes are different for 6061 alloy compacts. Hausner[103] reviewed the

anisotropy of shrinkage of metal powder compacts after sintering and found that orientation of particle surfaces, voids and grain boundaries during compaction contribute to the directional movement of material within the matrix. It has also been reported[104] that as the pore does not change uniformly during sintering, compacts do not grow equidistantly. Above type of phenomenon takes place due to the density distribution within the compacts. Such factors appear to affect the results of the present alloy systems as well.

Aluminium P/M alloy processing is very sensitive to the sintering atmosphere. Atmospheres containing low level of moisture and oxidizing gases are suitable to impart best properties to such materials. At dew point above $-40^{\circ}C$ mechanical properties such as strength and ductility decrease sharply and gross expansion of the compact may also result.

Among the presently used atmospheres nitrogen imparted maximum swelling and inferior mechanical properties to the composites (Figure 3.2). Dew point and oxygen content of nitrogen were $-38^{\circ}C$ and 149 ppm respectively as against $-40^{\circ}C$ and 119 ppm for argon. Comparatively higher dew point and oxygen level present in nitrogen might have resulted in the poor mechanical properties of the composites after sintering in this atmosphere. Properties (dimensional change and mechanical) of the composites sintered in vacuum were intermediate between those for nitrogen and argon. Better properties after argon sintering as compared to vacuum appears to be due to lack of any volatilization loss of the alloying

additions, which is generally associated with the latter. It is interesting to note that the effect of atmosphere is similar, whether the alloys are in sintered or aged conditions.

IV.2. Effect of Dispersoid and Its Volume Fraction on Densification Behaviour of Composites:

Presence of graphite in the 6061 alloy premix resulted in swelling of the composites (Figure 3.2). Due to its flaky shape, graphite particles cover a large fraction of the area within the matrix. The layers of graphite may shear during the compaction which may increase its area coverage in the matrix. During sintering graphite layers will restrict the diffusion path along the matrix, thus resulting in an increase in the interconnected porosity. On the other hand, in composites containing copper coated graphite (Figure 3.3), such porosities were reduced to a considerable extent. The benefits of using copper coated graphite in respect to the densification of composite are two fold. First: the addition of copper in the form of coating over graphite particles imparts enhanced sintering by alloying the matrix. As it is well known, aluminium-copper alloy system undergoes liquid phase sintering. When the compact, made of premix powders is heated, the alloy formation begins at a comparatively low temperature along the contacts of aluminium and copper particles. The liquid phase, thus formed by eutectic reaction, acts as nucleus and its amount increases rapidly till copper around the liquid is consumed in forming the eutectic melt. The liquid then spreads into the surrounding voids of

the compacts by capillary force. The tenacious alumina film over the aluminium particles are partially broken during the green powder compaction. Because of the presence of eutectic melt, the alumina film is drawn into the liquid phase. Having given sufficient time, copper diffuses into the aluminium matrix causing eutectic melt to decrease in amount. Increased amount of copper throughout the matrix after sintering is apparent from Figure 3.10b. This phenomena facilitates material transport and results in good particle to particle bonding.

Graphite is prone to moisture absorption resulting in incompatibility with aluminium. This fact was confirmed by the presence of interfacial porosity (Figure 3.9a) in the composites containing uncoated graphite particles. However, this may not be a problem in case of copper coated graphite particles.

Coming to the next dispersoid, talc has a chemical formula of $3MgO.4SiO_2.H_2O$ with a very low hardness (1 in Mohs scale) even softer than graphite. Composites containing talc showed better sinterability as compared to the graphite containing composite; particularly ΔD values of the composite sintered in all atmospheres were higher for the former (Figure 3.27). The positive effect of talc addition on densification below 4 volume percent appears due to the optimized matching of the magnesium silicate in talc with the matrix. It is interesting to mention here that any magnesium bearing compound is more compatible with aluminium

as compared to other refractory materials like graphite and alumina. However, addition of talc over 4 volume percent showed a decrease in densification, which may be attributed to constriction of the diffusion cross section for the lattice and grain boundary diffusion of matrix atoms.[105]

Coming to hard dispersoids, alumina addition favours densification of composites, although insignificantly (Figure 3.42). Levi et al.[71] have reported better wettability of aluminium melt containing magnesium with alumina. The reason given by the authors was the formation of spinel at the interface which promotes bonding. It may be mentioned that the authors[71] found such positive feature when the melt was vigorously stirred. However, the tendency of such bond formation cannot be entirely ruled out presently. A conclusive experimental evidence is, however, called for.

Improved densification with addition of alumina in the present case is contrary to the previous work[24] on the role of alumina addition on the sinterability of 2014 aluminium alloy premix, where densification parameter decreased with increase in the alumina content.

In the case of TiC dispersed composites, liquid aluminium does not wet TiC even up to 700°C (contact angle 118 degrees). Panasuk et al.[106] have shown that aluminium does not wet TiC even up to 1150°C for 20 minutes holding period, while at 1250°C wetting is effective such that, at 20 minutes the contact angle falls even to 20 degrees. Naidich[60] has reported 20° contact angle on the same system

in vacuum at 1150°C. McBrigge et al.[58] have indicated the possible use of aluminium as binder for TiC.

Although TiC is not wettable by liquid aluminium in present experimental condition but the composites containing TiC particles showed best sintering characteristics among the four types of composites, viz. those containing graphite, talc, alumina and TiC respectively. TiC, being the hardest dispersoid among the selected ones, would induce stress field around the 6061 alloy matrix during compaction. Such a stress field may enhance diffusivity during sintering along the matrix thus increasing the densification response.[107] However, when the volume fraction of TiC is more than 4 volume percent, the interaction of TiC-TiC particles will be prevailing and thus decreasing its impact on densification. This is reflected in the present investigation (Figure 3.57), as there is practically no effect of TiC addition on densification, when its content was greater than 4 volume percent.

The present system presents a striking case where similar or dissimilar surfaces are in contact, with the consequence that the migration of atoms and defects along and across the dissimilar contact is greatly modified. As the particle size of matrix is much greater than that of the dispersoid phase, it is apparent that second phase particles can easily enter the octahedral and tetrahedral sites in the packing of 6061 alloy particles.[108] However, the assumption is that all the particles are spherical, a situation which is very much different from the real one. Among the presently

selected dispersoids, the average particle size of the dispersoid decreases in the following sequence: graphite (6.2 μm), talc (5.7 μm), TiC (3.5 μm) and alumina (0.3 μm). Apart from this, the shape of these dispersoid particles are also not similar; graphite and talc being lamellar structure, while TiC and alumina being rounded and equiaxed. The sintered porosity variation of 6061 base composite (Figure 4.1) amply illustrates the above fact such that graphite/talc addition increases the porosity value, whereas, TiC and alumina exhibit the reverse trend. Apart from the physical picture for densification, the role of chemical bonds within the dispersoid and at matrix/dispersoid interfaces are also important. Both graphite and talc have weak Vander Waal type forces between the layered structures, whereas, alumina and TiC are covalent or covalent/ionic bonded. The role of capillary force during liquid phase sintering of 6061 alloy is likely to be effective in the transport of small size dispersoid particles viz. alumina and TiC. However, an additional surface treatment of inert particles like graphite by copper has been effective in the better realization of the capillary force and hence better drawing together of the particles. Such a treatment, nevertheless, does not make the situation as effective after TiC/alumina addition, the reason being the same as highlighted earlier i.e. based on physical accommodation aspect. It is interesting that after 4 volume percent addition of alumina/TiC dispersoids the porosity value again picks up. This appears to be

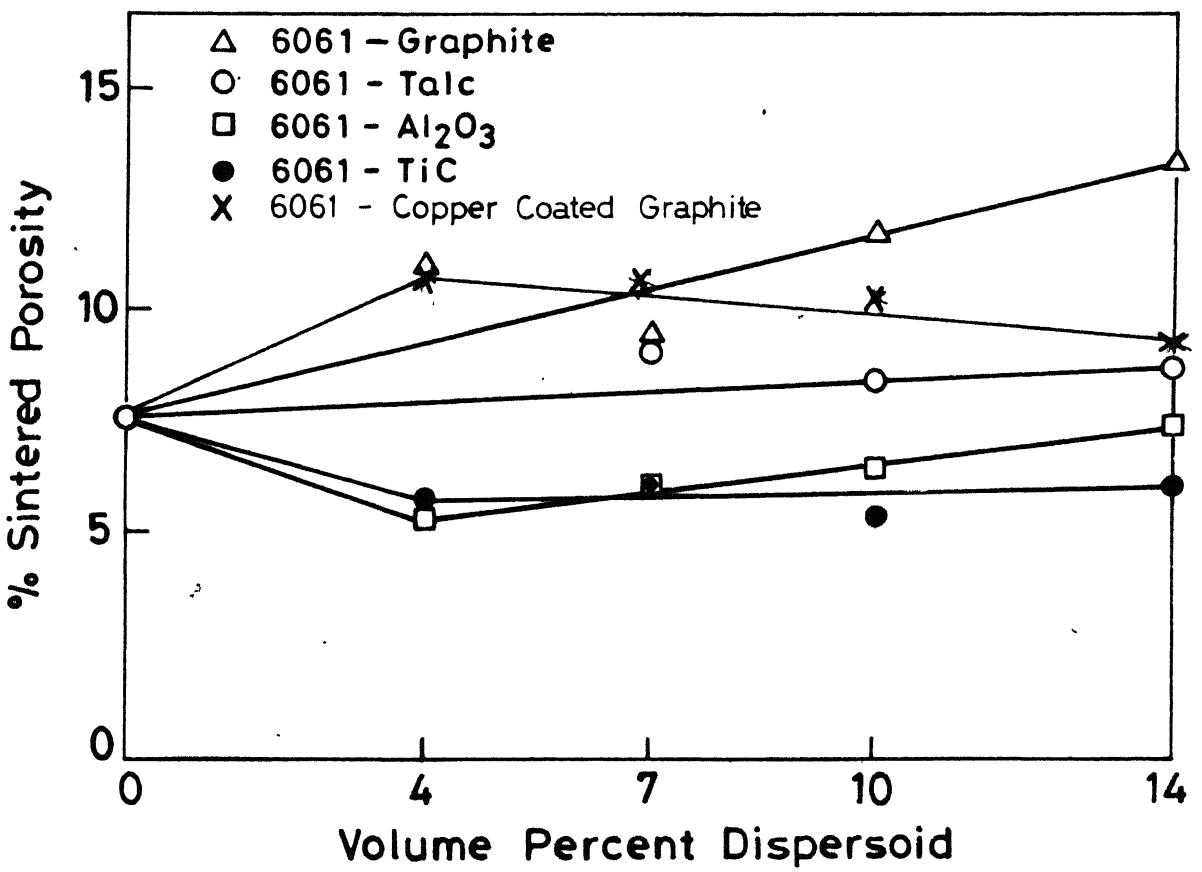

Fig 4.1 Variation in Porosity of argon sintered 6061 alloy base composites as a function of dispersoid content.

related to the higher probability of the presence of dispersoid-dispersoid clusters in those composites, where the dispersoid amount is greater than an optimum.

IV.3. Mechanical Behaviour of Composites:

IV.3.1. Sintered and Heat-Treated Composites:

Overall mechanical properties of any particulate sintered composites would depend on factors, such as:

- porosity
- dispersoid (type, size and volume fraction)
- precipitation hardening, and
- residual stresses, etc.

In the presently investigated composite systems most of the above contributions may be visualized. 6061 aluminium alloy is one which shows dual response of work hardening, as well as precipitation hardening. It is, therefore, an interesting system as far as variables complexity is concerned.

Porosity Effect:

Porosity, which is invariably associated with sintered aluminium alloy affects the tensile properties of the composites in different ways. Indirect weakening of the matrix is caused by poor sintering of composites in presence of porosity. Further, porosity also decreases the effective cross sectional area for normal stress.[109] In a specimen, yielding sets in when the applied normal stress exceeds the yield limit. Effective reduction in cross

section area due to the presence of porosity results in lower applied nominal stress at which yielding starts. Substantial decrease in yield strength of composites containing graphite (Figures 4.3 and 4.4) may be attributed to high porosity level of such composites (Figure 4.1) in addition to other factors.

Dispersoids Effect:

In general, strengthening or weakening of composites depends on the type of dispersoid and in metal matrix-particulate composites it has been explained in terms of micromechanisms such as: (a) direct strengthening[110-111] where direct particle dislocation interactions account for strengthening, (b) indirect strengthening[112] where particles stabilise small grain size and/or dislocation substructure,[113] or macromechanisms such as: (a) constrained plastic flow,[114] and load sharing by dispersoid.[114] Volume fractions of dispersoids used in the present composites are quite low (<0.14) so as to effectively constrain the plastic flow of the matrix. Secondly, since the aspect ratios of dispersoids are near unity, dispersoids may not contribute to load sharing. Therefore, macromechanisms of strengthening can be ruled out in the present cases and strengthening, if at all, is primarily due to the micromechanisms. In direct strengthening model, it has been[110-112] suggested that dislocations during their motion on glide plane would be obstructed by dispersoid particles. Dislocations thus obstructed can continue their motion by bending around the particles by

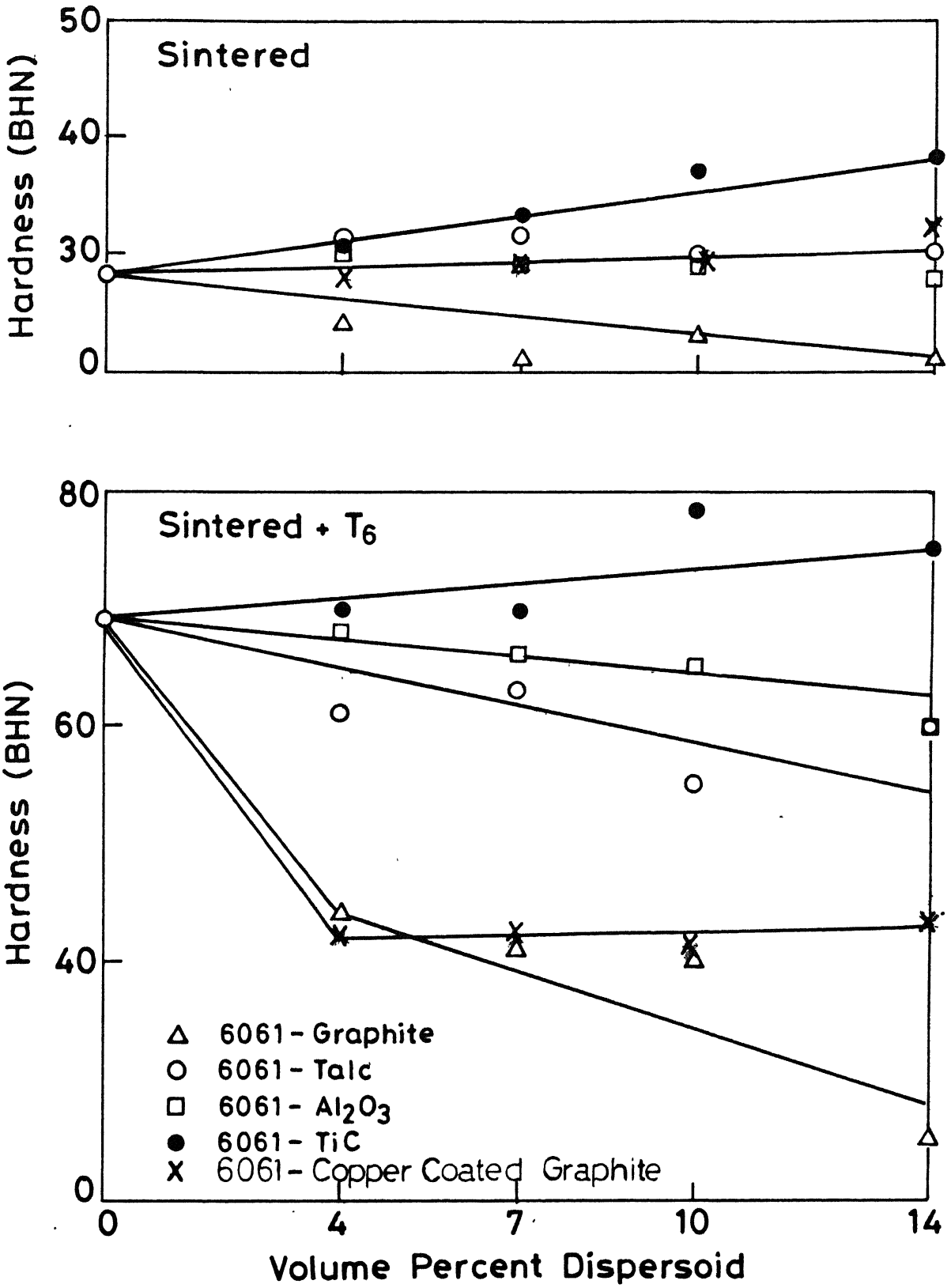

Fig.4.2 Hardness variation of 6061 alloy base composite as a function of dispersoid content

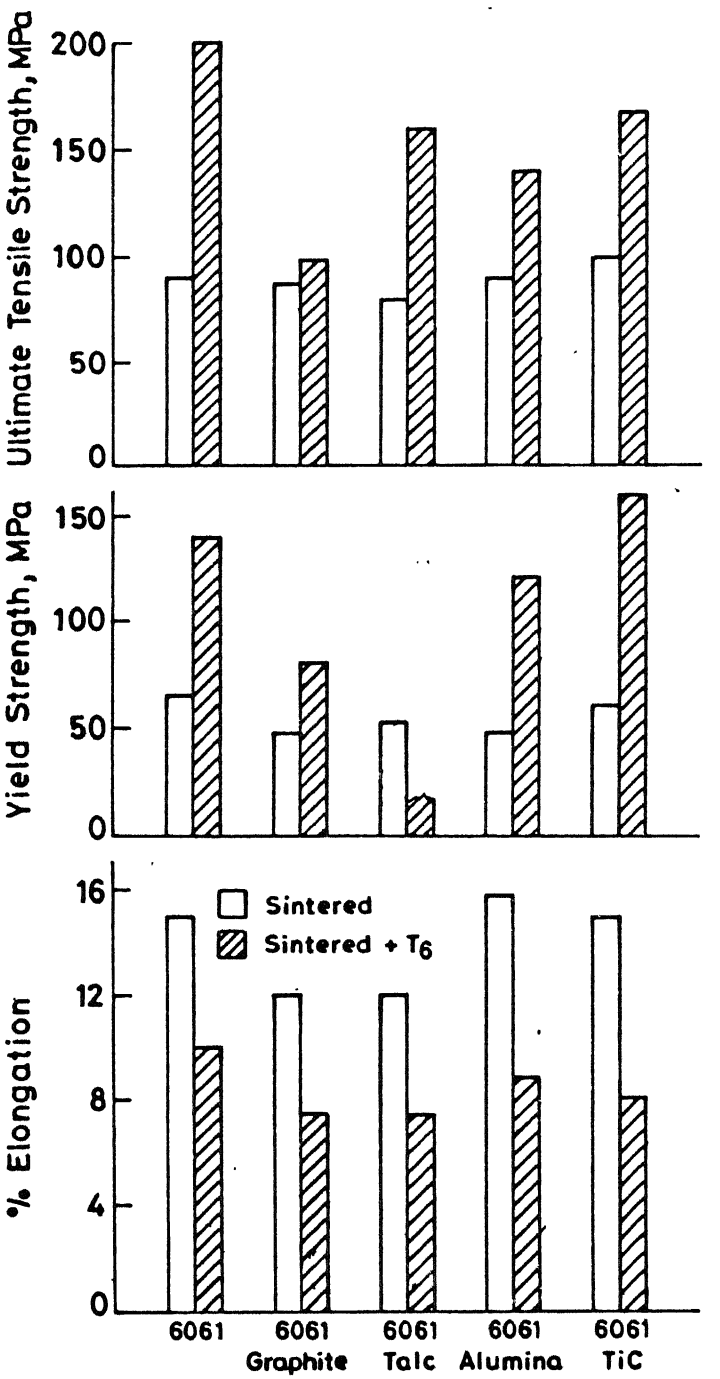

Fig 4.3 TENSILE PROPERTIES OF 6061 ALLOY-7 VOL.% DISPERSOID COMPOSITES.

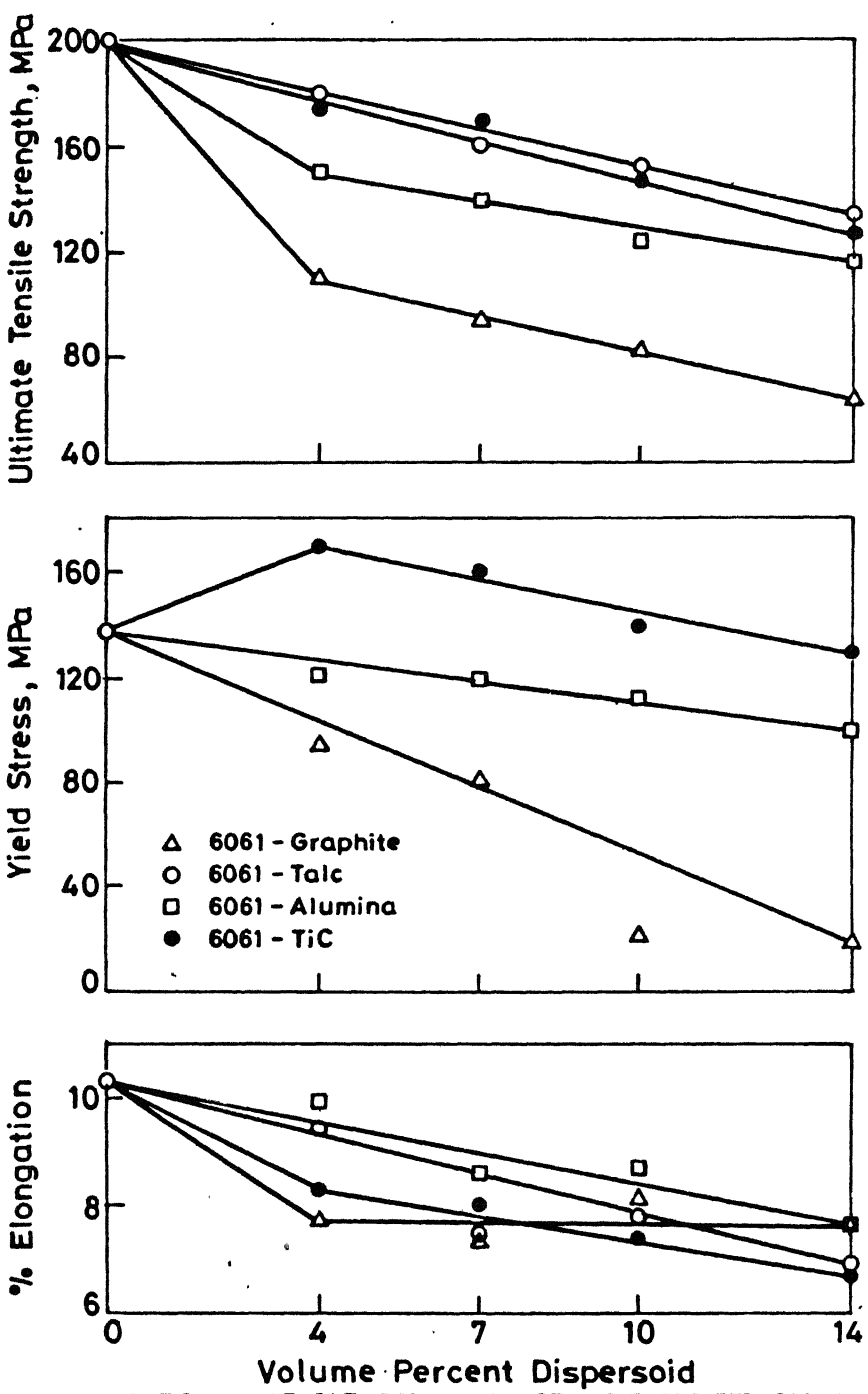

Fig 4.4 VARIATION IN TENSILE PROPERTIES OF HEAT TREATED 6061 ALLOY BASED COMPOSITES AS A FUNCTION OF DISPERSOID CONTENT

Orowan mechanism[110] or modified Orowan mechanism.[111] For such mechanisms to operate the size of the dispersoid should be less than 0.01 μm, whereas, the sizes of all four types of dispersoid in present study are much larger and therefore, strengthening arising due to obstruction to motion of dislocation can be rated out. Indirect strengthening of matrix by dispersoid may also, in principle, influence overall strengthening, but such effect can be classified as more characteristics of the work hardening mechanism thus playing a central role upon the yielding behaviour. However, as the present composites were not fully dense the indirect dislocation-particles interaction through Hall-Petch type relationship is also insignificant. However, the presence of substructure in composites with hard particles is not altogether ruled out.

The crystal structure, particle morphology and intrinsic hardness of dispersoids in the sintered composites do reflect above correlation adequately, such that the TiC and alumina additions which have relatively high hardness values of the order of 3170 and 2370 Kg/mm^2 respectively, when introduced in 6061 matrix increase its hardness (Figure 4.2). On the other hand, soft graphite particle additions show a reverse effect. The exception noticed after talc particles addition may be associated with its high compatability with the matrix, a fact confirmed after the fractured surface examination (Figure 3.33).

Coming to the effect of dispersoid on the tensile properties, the relations more or less follow a parallelism

with hardness variation (Figure 4.3), with the exception of talc which shows the lowest UTS value. However the tensile properties of composites were inferior to that of straight 6061 alloy. As mentioned earlier any positive role played by dispersoid in the composite is mitigated due to presence of porosity in it. The percent elongation follows more or less similar pattern to that of UTS variation such that a higher sintered strength imparts greater ductility. Such a feature is universal in sintered parts where pores invariably act as stress concentration. Ultimate tensile strength of 6061 alloy (90 MPa) is low as compared to the value (124 MPa) reported by Dudas and Dean[1] for alloy 601 AB, composition of which is similar to presently studied alloy. A comparatively low sintering temperature (by 6^{o}C) and high dew point in present case would lead to reduction in UTS of composites. However ductility value is higher in present case.

In exploiting the particulate strengthening the interfacial bonding between dispersoid and matrix has to be perfect. In other words, its strength must be greater than the matrix itself. The other extreme is the totally debonded case, where the interface can support neither tensile nor shear stresses. The intermediate case of limited strength does exist where regions of good bonding are mixed with unbonded ones. A chemical aspect of interfacial bonding based on the electronic configuration model has been attempted by Upadhyaya and Misra.[115] As already mentioned earlier the substructure in such composites, if any, would increase the flow stress, as

a result of work hardening. This postulate is no doubt different than that postulated by Grant and Preston,[116] where the substructure was required in order to achieve dispersion strengthening.

Work Hardening Effect

The work hardening which also contributes to overall strengthening could be assessed by the slope of stress-strain plot in the plastic zone, for which the information of both yield stress and ultimate tensile strength are necessary. The results reveal (Figure 4.3) that all the dispersoid additions lower the yield stress of the base 6061 matrix, with the exception of TiC addition which has practically similar yield stress value. In other words, the presence of hard particles will cause in situ work hardening effect in the matrix. Goodrich and Ansell,[117] while studying the tensile deformation of Al-Al_2O_3 composites at room temperature, observed a high density arrangement of nearing jogged and tangled dislocation with increasing deformation. Further, many small loops not associated with dispersoid particle were resolved near the edge of the dense tangles, which were thought of as 'mushrooming' effect described by Kuhlmann-Wilsdorf et al.[118] for work hardening of single phase face centred cubic material. In the present composites, particularly those containing hard particles, a similar structural change is probable.

Precipitation Hardening Effect

As already mentioned earlier 6061 alloy undergoes precipitation hardening because of fine Mg_2Si coherent precipitate. As expected Brinell hardness value of any heat-treated composite is higher than that for straight sintered 6061 alloy (Figure 4.2). A similar effect is also noticed on the ultimate tensile strength variation of the heat-treated composites (Figure 4.4). Similar to tensile properties of sintered composites UTS value of T6 treated composites in present study is inferior to that of that reported for corresponding alloy by Dudas and Dean.[1] Poor sintered properties of composite would lead to low tensile properties after treatment also. However, when one looks at the yield stress variation of heat-treated composites, the relation is not as simplistic as that for simple sintered ones. One thing is obvious i.e. if graphite and alumina addition lower the yield stress of heat treated 6061, TiC addition increases the value by about 30 MPa. This clearly indicates the additional hardening effect of TiC particles. Another fact emerges that the work hardening response of heat treated 6061 alloy is better than any of the composites processed similarly, although the preponderent contribution of precipitation hardening in all the composites is obvious.

Residual Stresses Effect

The residual stress may be either of thermal or mechanical origin. The first arising out of different thermal

coefficient of expansion of the matrix alloy and dispersoid. Since composites are invariably used at different temperatures than those at which they are fabricated, the difference in thermal expansion or contraction of the dispersoid and matrix set up residual stresses on cooling down from the fabrication temperature. The importance of such residual stresses diminishes if the composite operating temperature is one at which a significant amount of creep can occur. The other type of residual stresses i.e. mechanical, come from the difference in flow stress between the components. This is important when the composite is subjected to mechanical deformation at a level where one or more of the constituent phases begin to flow plastically. In the present composite-processing route such type of residual stresses are absent. Another possible source of residual stresses in composites is the occurrence of phase transformation in the interfacial regions with their accompanying change in volume. Again, such type of stress is not present in the investigated composites.

In the presently selected sintered particulate composites thermal residual stress must be existing as there are widely differing coefficient of thermal expansion of matrix and dispersoids. During cooling of such composites thermal stresses are developed. The extent and sign of these stresses depend on the nature of dispersoid with respect to matrix. Thermal stress may be either compressive or tensile in nature. When $\alpha_m > \alpha_p$, where α_m is matrix thermal coefficient of expansion and α_p is dispersoid thermal coefficient expansion,

a radial compressive stress field is developed around the dispersoids on cooling to room temperature from higher temperature. When such a material is tested in tension, it will require higher tensile stress to start the deformation or yielding. In case, where the above relation is opposite the reverse will be true. In the event of interface rupture bond strength between dispersoid and the matrix is considered weak and the bond ruptures due to the stress concentration at the interface during tensile loading.

In the present case, if one looks at the α values of dispersoids in comparison to that for 6061 matrix ($23 \times 10^{-6}/^{o}C$) it would be clear that talc, alumina and TiC have lower α values than that for the matrix (approximately one third). Graphite which is highly anisotropic in structure has widely different values, for example, along the basal plane α value ($27 \times 10^{-6}/^{o}C$) is much higher than the value corresponding to direction perpendicular to the basal plane ($\alpha = 0.7 \times 10^{-6}/^{o}C$).

From the framework of such model all such dispersoids would introduce compressive type thermal residual stresses. As such an effect is not discernible from the over all UTS variation of the composites with different types of dispersoid (Figure 4.3), it is all likelihood that for sintered alloys, the overall predominating effect of strength loss would be much more than the strengthening effect imparted by the thermal residual stresses.

IV.3.2. Thermomechanical Treated Composites:

Mechanical properties of 6061 aluminium alloy may be enhanced by the use of properly controlled thermomechanical treatments (TMT). Optimal TMT procedures require selection of quench temperature, degree of deformation and ageing temperature and time to be controlled in such a way that uniform tangled dislocation substructure is promoted in the matrix. Influence of thermomechanical treatment on mechanical properties of wrought 6061 aluminium alloy is reported by a number of investigators.[119-122] A 30-40 percent increase in yield strength without any reduction in either notch toughness or stress corrosion resistance utilizing multicycle TMT is reported by Rack and Edstron.[122] Improved properties were attributed to needle shape transition phase as primary strengthening phase in 6061 alloy.

In the present investigation the sintered composites were subjected to the following TMT cycle:

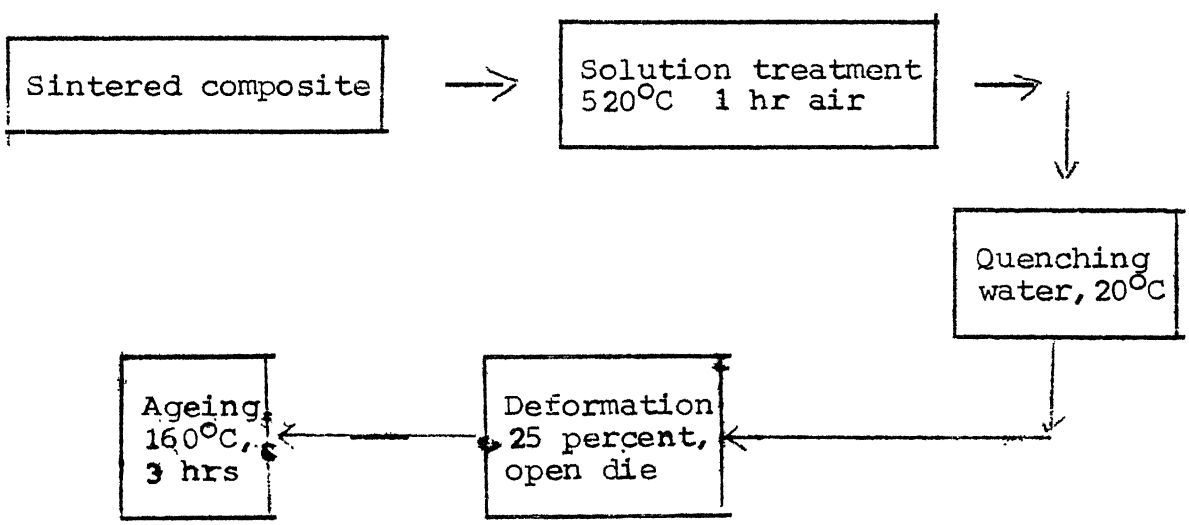

Microhardness value of the sintered composite increased after TMT. Composites containing soft dispersoid (graphite and talc) showed variation in hardness values with increasing volume fraction of dispersoid, whereas hard particles (TiC and Al_2O_3) containing composites had identical values for all dispersoid contents. As evident from Figure 4.4a microhardness values of the TMT composite containing soft particle is more than those containing other types. Increase in hardness value after TMT is a natural consequence of effective age hardening due to the presence of tangled dislocation substructure imparted by deformation during such a treatment. However, degree of deformation is a primary factor in controlling the end properties. As the deformation of various composites was carried out at a constant pressure, comparatively more deformation was noticed for composite containing soft particles. This was also confirmed by increased densification of such composites. Higher degree of deformation for such composites would result in higher hardness after TMT.

Combined effect of particle and enhanced precipitation hardening should, in principle, increase the hardness value of the composites containing hard particles. However, the premature over-ageing of the composites cannot be ruled out. Ceresara and Fiorini[125] reported such overageing in Al-Al_2O_3 composites, which was attributed to the presence of equilibrium stable precipitate at grain boundaries in the matrix. Rack and Krenzer[119] have reported the formation of non-uniform cellular substructure in overaged composite,

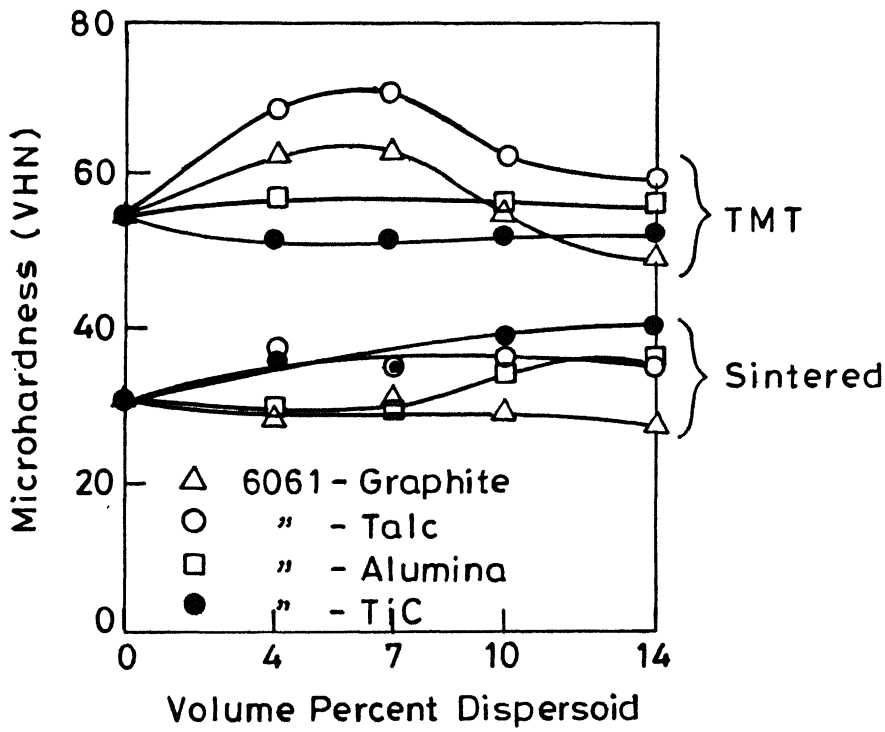

Fig. 4.4a Vickers microhardness variation of sintered and thermomechanically treated (TMT) 6061 composits as a function of dispersoid content.

which was found to be detrimental to tensile properties of TMT 6061 alloy. A detailed fine microstructural study is essential before confirming the above facts.

IV.4. Electrical Resistivity:

A sintered composite may also be characterised by the evaluation of its electrical resistivity value. As aluminium alloys are very sensitive to sintering atmosphere, electrical resistivity can be used as a tool to examine the sintering efficiency. In addition to sintering atmosphere three factors namely: porosity, dispersoid and precipitate influence the electrical resistivity of the composites.

Electrical resistivity value for the 6061 alloy after argon sintering is 43.9 nΩm, which is very near to the value for wrought 6061 alloy (40.28 nΩm).[123] Increased resistivity value in the present case may be attributed to porosity, which is associated with sintered 6061 alloys. Amongst the atmospheres used for sintering, nitrogen gives rise to maximum resistivity (70 nΩm) for the 6061 alloy. This may be due to the fact that nitrogen had a comparatively high dew point and oxygen content in it. Introduction of dispersoid to 6061 alloy resulted in increased resistivity due to higher resistivity values of each dispersoid used. Composites containing graphite had maximum resistivity value whereas, in case of composite containing alumina value was minimum. Although electrical resistivity value of graphite (13750 nΩm) is very low as compared to that of alumina(10^{20} nΩm)[124] a rather

steep increase in resistivity with increasing amount of graphite may be attributed to the accompanying increase in the porosity. Comparatively small increase in the resistivity of the composites containing copper coated graphite as compared to 6061 alloy is due to the improved densification, when copper was present.

Increasing amount of dispersoid increased the resistivity value of the composites with an exception of alumina. Lowest resistivity value of composites containing alumina may be attributed to comparatively lower porosity level in such composites and smallest size of the particles (0.3 μm).

Effect of porosity on electrical resistivity is obvious from the values for repressed-resintered composites. As the porosity of the composites decreased considerably after repressing-resintering electrical resistivity values also fell down. In the present case, T6 heat treatment gave rise to increased electrical resistivity, although marginally, in all the cases, i.e. irrespective of dispersoid and sintering atmospheres. Ceresara and Fiorini[125] reported increase in electrical resistivity in SAP aluminium-alumina composites after age hardening. Increased value was attributed to GP zone formation in the matrix. 6061 alloy in the present study, is also expected to respond in similar way as described above. But a detailed study is necessary for any definite conclusion in this regard.

IV.5. Surface Roughness of Composites:

Surface roughness of sintered compacts is becoming an important specification for many applications. As the sintered component is made to net shape or near net shape, surface is not further subjected to machining or grinding operations. Roughness attained by the surface of sintered compact during P/M processing is final roughness for use in machine parts. Thus specified roughness of the component may be imparted by proper selection of material ingradient and by using suitable processing parameters.

The most commonly used parameter R_a, the arithmatical mean of the departure of the roughness profile from the mean line, is used to specify the surface roughness of the material. However, porous nature of sintered metal creates the discrepancies between surface roughness value obtained on the solid and sintered surface. Surface porosity is also taken into account while measuring the R_a parameter of any sintered surface. In general, surface porosity is different from the volume/bulk porosity. The reason for this is the fact that during compaction particle movement near the die wall surface is of different magnitude than the particle away from the die wall. During ejection, under unfavourable circumstance some grains may be removed from the green compact surface, thus resulting into high value of total surface porosity. Factors such as high density of compacts, die wall lubrication and choice of a tool material without chemical affinity for the compact reduce the true surface porosity.

A parameter skewness S_k, which is a measure of asymmetry of a profile about its centre line was proposed by Barrow and Bampton,[126] and is more relevant to a valid description of a porous rubbing surface than the conventional parameter R_a. Although some results on the surface roughness of sintered compacts are reported,[127] no such work is yet published in the field of sintered aluminium alloys.

In the present investigation R_a parameter of sintered surface is reported. Surface roughness of composites would depend mainly on two factors. Firstly, increase in porosity would lead to increase in surface roughness of material. Secondly, the hardness value of second phase plays important role and harder the second phase higher would be the roughness of composites. The R_a value for composites containing 14 volume percent graphite (R_a: 1.9 μm) is marginally higher than the value for 6061 alloy compact (R_a: 1.8 μm). Although the soft nature of graphite particle should impart low roughness to the composite but high porosity level for such composites (13 percent) as compared 6061 alloy (7 percent) compact (Figure 4.1) can lead to an increase in R_a value of the composites containing graphite. In the case of talc containing composites, low hardness of talc (1 in Mohs scale) as well as its compatability with the matrix, roughness of the composites decreased (R_a: 1.4 μm) substantially as compared to 6061 alloy compacts.

Surface roughness of the composites containing alumina/TiC was identical to that of 6061 alloy compact. It is worth

noting that the sintered porosity of composite containing 14 volume percent hard dispersoid decreased considerably (Figure 4.1) but R_a parameter was comparable to 6061 alloy. Roughness value of composite should decrease due to reduction in porosity but the presence of hard dispersoid would also have its negative effect on roughness. As a result overall roughness of composites remains practically unaffected due to such dispersoid addition.

IV.6. Wear:

Wear is regarded as the unwanted removal of material as a result of rubbing surfaces. According to Burwell[128] since no quantitative relation can be arrived upon (e.g., Coulomb's law of friction, Newton's law of viscous flow or Hooke's law for elastic bodies), there is no wear coefficient. Thus dimensional analysis of laboratory work to the prediction of wear in actual machinary is not applicable. This situation is primarily due to the fact that material removal during wear is a culmination of vastly diverse phenomena, and the basic approach towards the understanding of wear is to recognize that the single term "wear" includes certain distinct and independent phenomena, including adhesive or galling, abrasive and cutting, corrosive, surface fatigue and minor types.

One of the most commonly encountered forms of wear, adhesive or sliding wear, arises whenever two solid surfaces are in relative motion with or without the presence of a lubricant. At microscopic level, the sliding surfaces - flat as they may be - actually touch at a relatively few points.

Since the true areas of contact are considerably smaller than the overall surface, the local pressure is high, frequently exceeding the yield point of the softer of the sliding materials in contact. Consequently, miniature welds may form and then shear, thus resulting in material removal. Schematics of material removal are shown in Figure 4.5. Although in the present study adhesive or sliding wear is predominant, another type, viz. abrasive wear, wherein material removal is accomplished by the ploughing or cutting action of hard grit particles on a relatively softer surface, cannot be completely ruled out.

The present wear system consists of the pin (6061 alloy and its composites) and EN25 steel disc, which have a wide difference in hardness (EN25: 301 BHN, 6061 alloy: 30 BHN). As aluminium alloy is fairly soft, its seizing effect on disc surface is inevitable. As a matter of fact during wear test a thin coating of aluminium alloy forms on the wear path. In the initial stage of test, the asperities on the pin surface shall be in contact with the asperities on the disc.[130,131] In other words, as the contact area in the beginning of the test is far less than the total pin area, the effective local pressure on the pin would be much higher than the nominal applied pressure. Such an effective pressure would first break the tenacious alumina films from 6061 alloy pin. Eventually, normal and tangential loads are transmitted through the contact points by adhesive and ploughing action. The asperities of the softer surface i.e. 6061 alloy will be

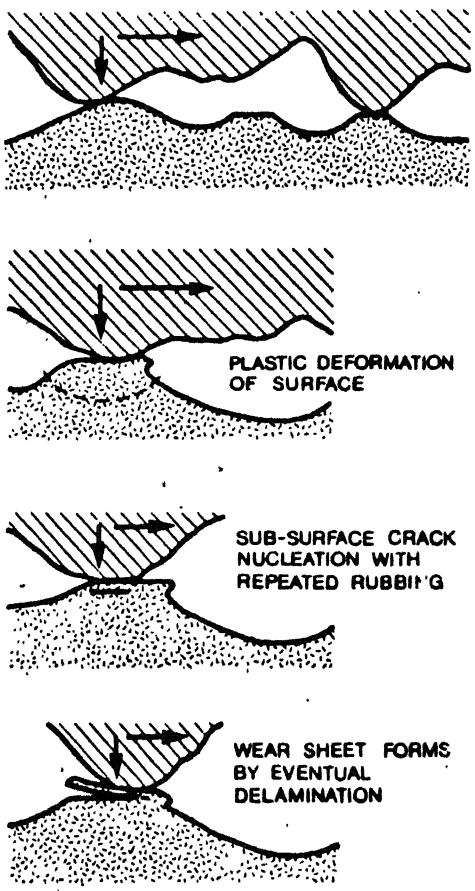

Fig.4.5 Schematic representation of the various stages involved in the formation of delamination wear sheets.

easily deformed and some would be fractured due to the repeated loading action. Relatively smooth surface is generated either when these asperities are deformed or they are removed. Once the surface becomes smooth the contact is not just asperity to asperity, but rather, asperity to plane contact. However, in the present system since there is a coating of aluminium alloy on the wear disc such a prospect seems to be remote. With continued sliding the asperities of the disc would induce plastic shear deformation on the softer pin surface which would accumulate with repeated loading. Subsequently, the subsurface deformation continues causing crack nucleation below the surface. Once cracks are present, owing, either to the crack nucleation process or pre-existing cracks, further loading and deformation cause cracks to extend and thus to join neighbouring ones. When such cracks finally join the surface, at certain weak positions, long and thin wear sheets "delaminate".[132] The thickness of wear sheets is controlled by the normal and tangential loading on the surface. In order to understand the wear mechanisms in the present study worn out surfaces as well as debris were examined in the SEM.

SEM micrographs of worn out surfaces reveal two main features: long and continuous grooves; and patches of severely damaged regions (Figure 3.19). Since no long machining chip type aluminium debris was observed, the abrasion type of wear was ruled out. These grooves may probably be caused by the plastic deformation alone.

The second feature i.e. patches of highly damaged regions, is a result of delamination of the sliding surface of the 6061 alloy and its composites as mentioned above.

The analysis of the debris obtained during wear test of 6061 alloy showed the presence of following four types of particles (Figures 3.22 and 3.23):

i) Long needle shapes (500 μm length)

ii) Flaky (100 to 200 μm size)

iii) Rounded agglomerates (100 μm size) and

iv) Fine particles (2 to 10 μm).

The respective debris particle sizes are of rough order and depend on the testing parameters, such as, applied pressure, speed and sliding distance etc. As the debris contains more than one type of particles, it is obvious that the wear mechanism is not controlled by only adhesion (delamination) mechanism.

Any vibration of even smaller amplitude during the disc movement would generate a cyclic loading and a fretting (oscillating sliding) mechanism may be thought of, thus giving rise to the fine particles in the debris (Figure 3.23c). As the sintered alloys invariably contain pores, it is obvious that once the pores are exposed to the mating surface the accompanying stress concentration would also accelerate fine particle generation in the debris.

The presence of elongated needles (Figure 3.22a) in the debris emerges during the very early stage of the test, when the sharp asperities break rapidly. Such particles will

get contaminated with iron oxide present on the ferrous disc. The rounded agglomerates (Figure 3.23a) are the result of balling of fine particles on the wear path during the test. It is interesting to note that in the fine debris particles, there is no iron contamination as such, since the particles do not dwell on the disc surface under load for any sufficient period of time.

The size of flaky aluminium alloy debris roughly corresponds to the size of the patches of highly deformed regions found on the worn out surface. For example, the size and shape of debris shown in Figure 3.22c match with the deformation region shown in the worn out surface (Figure 3.19c). Debris collected from the wear test of 6061 based composites also showed similar type of debris with an exception that long elongated and rounded agglomerates were absent in these cases.

Wear rates of composites and base alloys depend on the material variables viz. type and amount of dispersoid as well as test parameters such as sliding distance, speed and applied pressure. Effect of different variables on the rate of 6061 alloy based composites is discussed in following sections.

IV.6.1. Effect of Dispersoids:

Contrary to initial expectations none of the four types of composites showed any improvement in wear rate. Among the composites those containing TiC/talc were found to be superior to alumina containing composites followed by the composites containing graphite (Figure 4.5a). It appears that

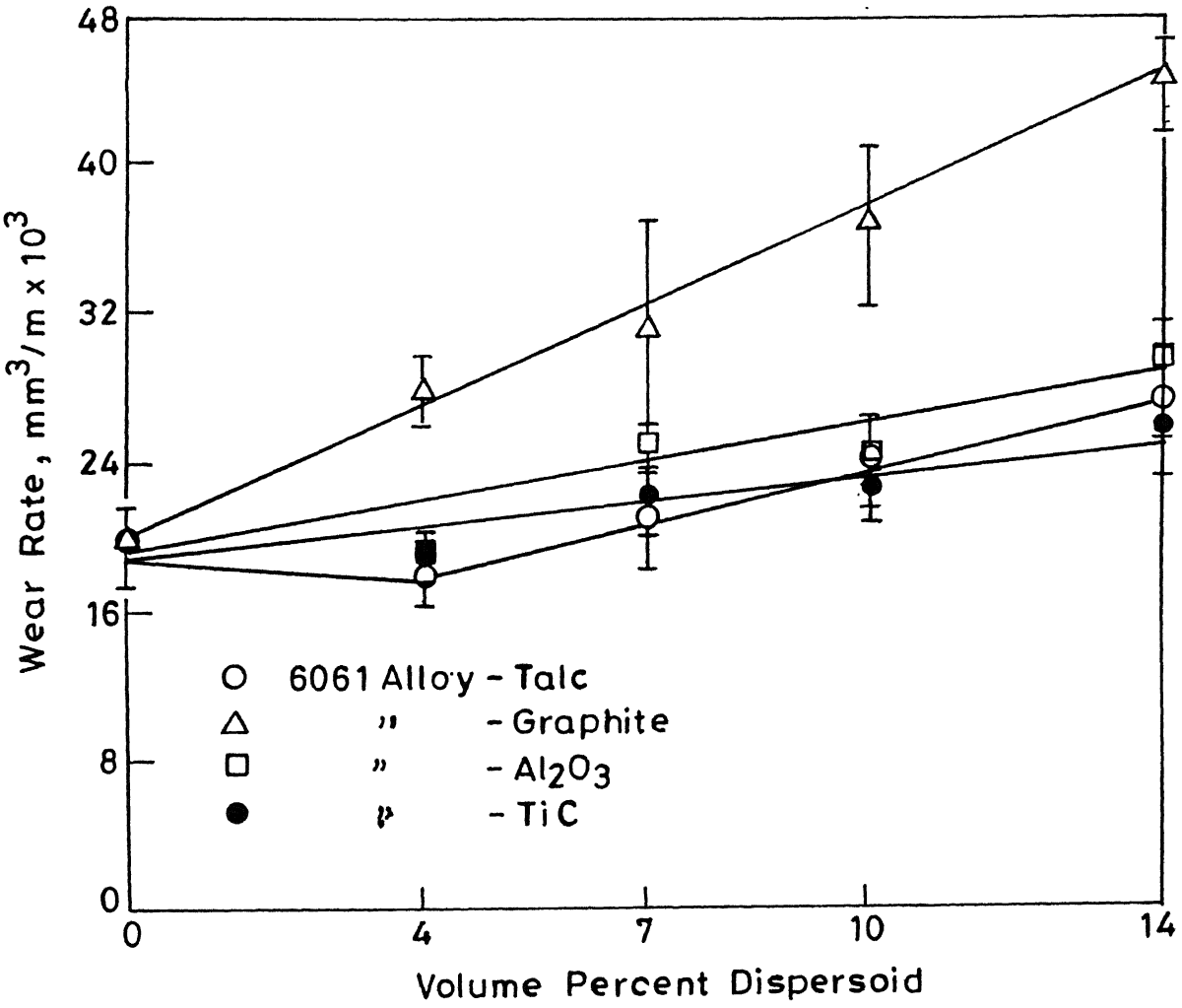

Fig. 4.5a Effect of volume percent of dispersoid on the wear rates of sintered 6061 alloy composites (Sliding speed : 0.5 m/s ; Applied pressure : 12×10^{-2} MPa ; Sliding distance : 250 meters)

wear properties are influenced more by the sintering characteristics rather than by the presence of individual type and volume fraction of dispersoids. Porosity and particle-matrix interface are the decisive factors in governing the wear behaviour of the particular type of composite. For instance, the lowest wear rate was observed for the base alloy (Figure 4.5a). Although the porosity level of the 6061 alloy compacts is more and hardness is lower than those of composites containing TiC. Wear resistance appeared to be superior for such compacts. Absence of interfaces, which would act as pre-existing crack in the matrix may be the probable cause of improved wear resistance for straight 6061 alloy compact.

Increased wear rate for composites containing graphite (Figure 3.5a) may be due to the combined effect of high porosity and poor particle-matrix interfaces. Porosity of composites containing 14 volume percent graphite is nearly twice as compared to the 6061 alloy compact (Figure 4.1). In addition such composites possess interfacial porosity around the graphite particles (Figure 3.9a), which would lead to fast crack propagation during the process of delamination of surface layer. Area fraction of severely damaged regions on the worn out surface of 6061 alloy-7 volume percent graphite was significantly higher as compared to those of 6061 alloy and other composites (Figures 3.19 and 3.20).

As mentioned in the earlier section composites containing talc showed improved densification at relatively low content (4 volume percent) of talc (Figure 3.27). As a result,

wear rate of this composite was not higher than that of 6061 alloy (Figure 4.5a). Comparatively better compatibility of talc particles with matrix and identical porosity value of composite to that of 6061 alloy compact would give rise to similar wear characteristics of these compacts i.e. composites containing 4 volume percent talc and 6061 alloy compact. However, increase in wear rate at high talc content in composites is the direct manifestation of densification fall in such composites.

Although the porosity of composites containing TiC/alumina is low as compared to 6061 alloy compact, wear rate is higher in these cases. It appears that the positive effect due to low porosity is mitigated in the presence of weakly bonded interfaces in such composites. Two factors would contribute to the wear loss of composites containing hard particles. Due to weakly bonded interfaces the pulled out dispersoid particles would lead to additional wear loss. Further, hard dispersoids dislodged from the matrix and trapped between the mating surfaces, could cause plowing and cutting action of the softer matrix[133,134] resulting in the abrasion of the matrix.

A rather insignificant increase in wear rate with higher TiC content in the matrix (Figure 4.5a) may be attributed to the high intrinsic hardness of this particular dispersoid, which has a positive effect on the wear resistance of the composites. This influence is also confirmed after alumina addition which has relatively lower hardness than TiC,

thus not having as much positive effect on the wear resistance. Despite the marginal difference in the porosity level of 6061 alloy-alumina composites and 6061 alloy compacts (Figure 4.1) increased wear rate of former (Figure 4.5a) may be attributed to the small particles size (0.3 μm) of alumina, which provides large number of interfaces with the matrix. This enhances delamination of such composites.

IV.6.2. Effect of Wear Test Parameters:

(i) Sliding Distance:

Wear loss was found to be directly proportional to the sliding distance for all types of composites (Fig. 4.5b). As the measurements were taken after the initial run-in-period a linear increase in the wear loss with increasing sliding distance was quite obvious. Present results are in agreement with the quantitative law of adhesive wear, which predicts that the amount of wear is directly proportional to the sliding distance.[135]

(ii) Applied Pressure:

Another law of adhesive wear states that the amount of wear is proportional to the applied pressure.[135] Results of present study also show the similar effect of applied pressure on the wear rate of composites. However, the slopes of the plots are different for different composites (Figure 3.5c). For example, slope for TiC containing composites is minimum, whereas, the slope of graphite containing composites is maximum. It can be noted that the composites containing

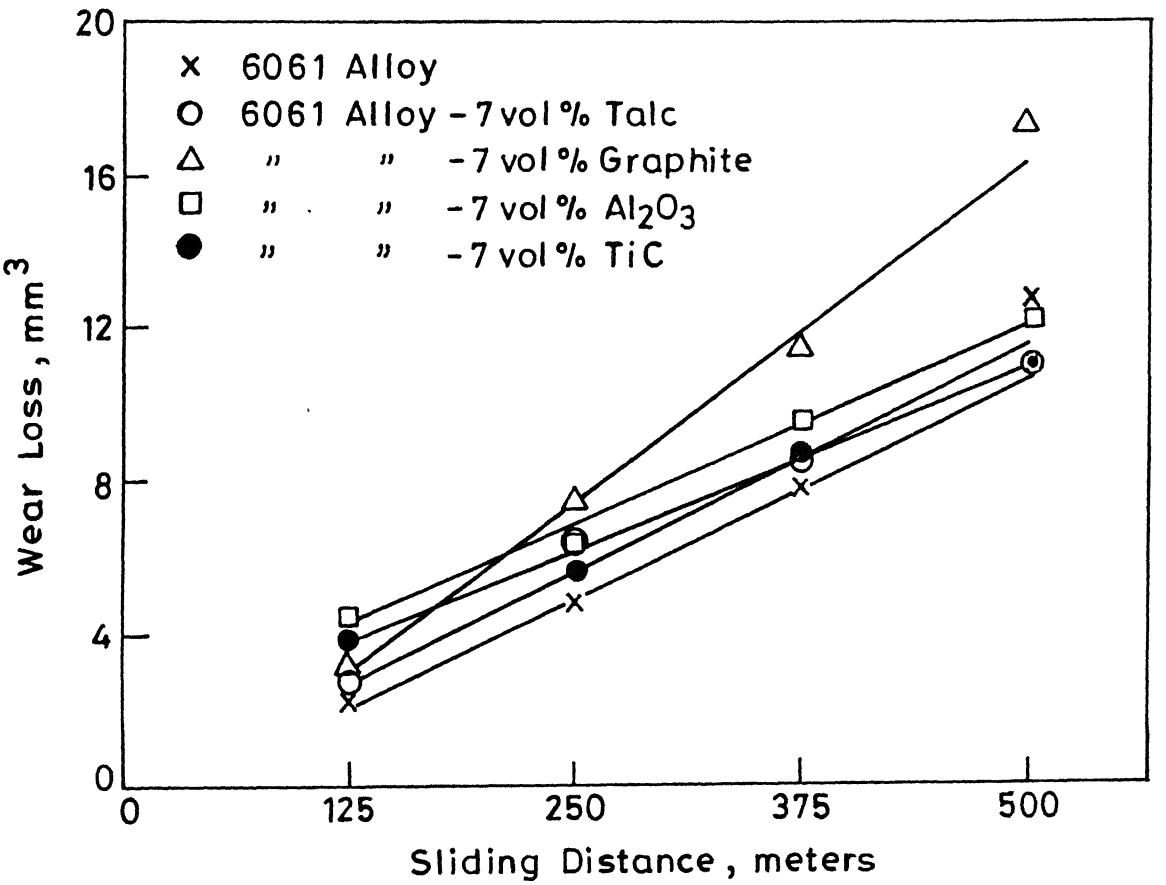

Fig. 4.5 b Effect of sliding distance on wear loss of sintered 6061 alloy and its composites containing 7 vol % of dispersoid (Sliding speed 0.5 m/s ; applied pressure: 12×10^{-2} MPa)

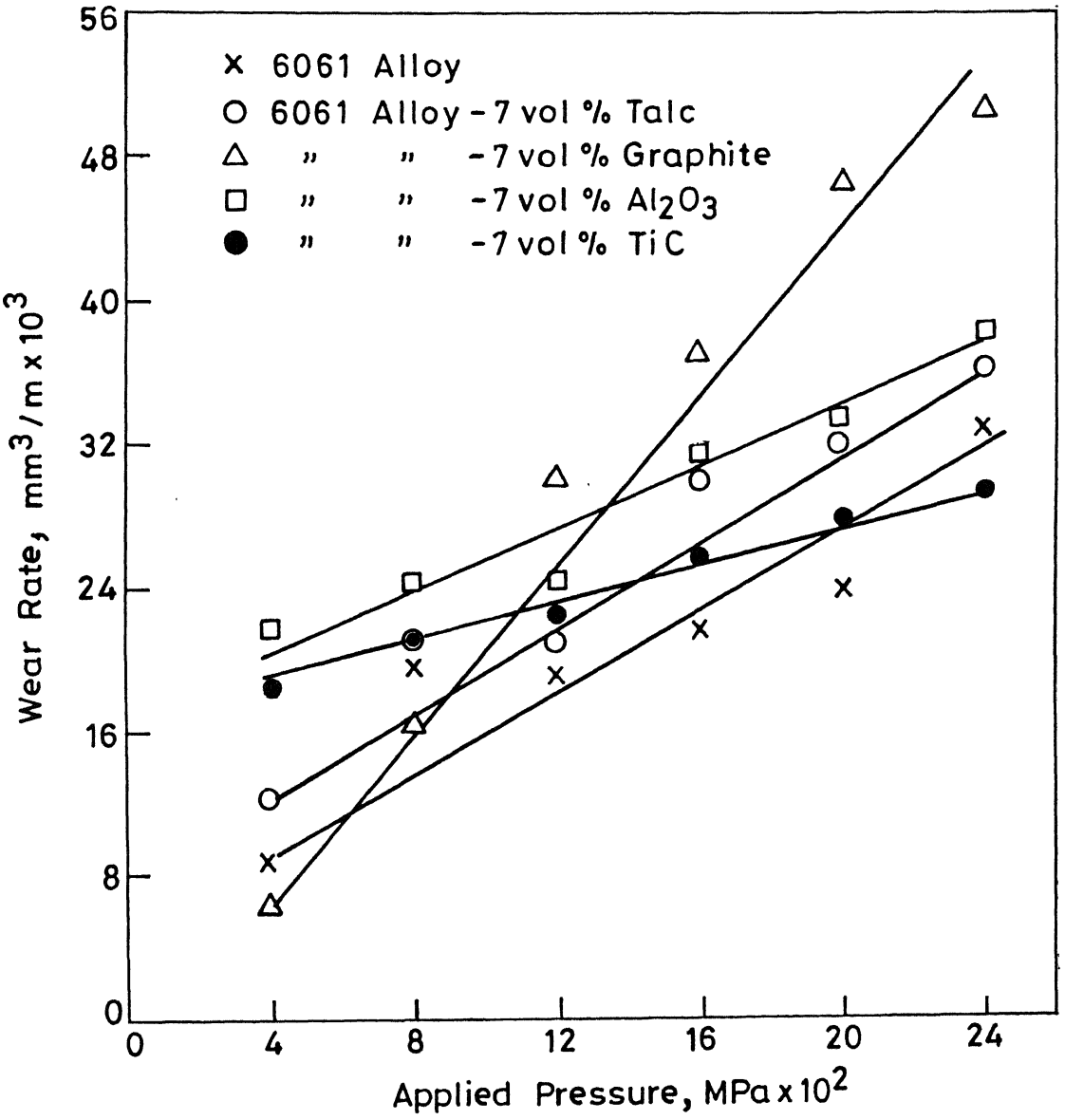

Fig. 4.5c Effect of applied pressure on the wear rates of 6061 alloy and its composites containing 7 vol % dispersoid (Sliding speed: 0.5 m/s ; Sliding distance: 250 meters)

graphite have superior wear properties as compared to the base alloy at lower loads. At the lowest pressure (4×10^{-2} MPa), low wear rate of composites containing graphite may be due to the possible presence of graphite on the mating surface. At low pressure such particles may be effective in preventing metal to metal contact. However, at high pressure, graphite may not be firmly attached to the surface of composites and secondly the higher porosity levels in the graphite containing composites may be responsible for increased wear rate at higher pressure as compared to the base alloy.

Composites containing TiC performed well at higher applied pressure. For example, the wear rate of composites containing 7 volume percent TiC is 15 percent less as compared to that of 6061 alloy compact at maximum pressure i.e. 24×10^{-2} MPa (Figure 3.5c). Variation in wear rate is also minimum for composites containing hard particles (TiC/alumina) (Figure 3.5c). Least effect of applied pressure on wear rate of such composites is a direct manifestation of superior mechanical properties and less porosity of such composites (Figures 4.1 and 4.2) as compared to those containing soft dispersoids.

(iii) Sliding Speed:

Wear rate of composites increased with increasing sliding speed (Figure 3.5d). Several factors effect the wear behaviour of material due to change in the sliding speed. Increased sliding speed results in a decrease in friction,

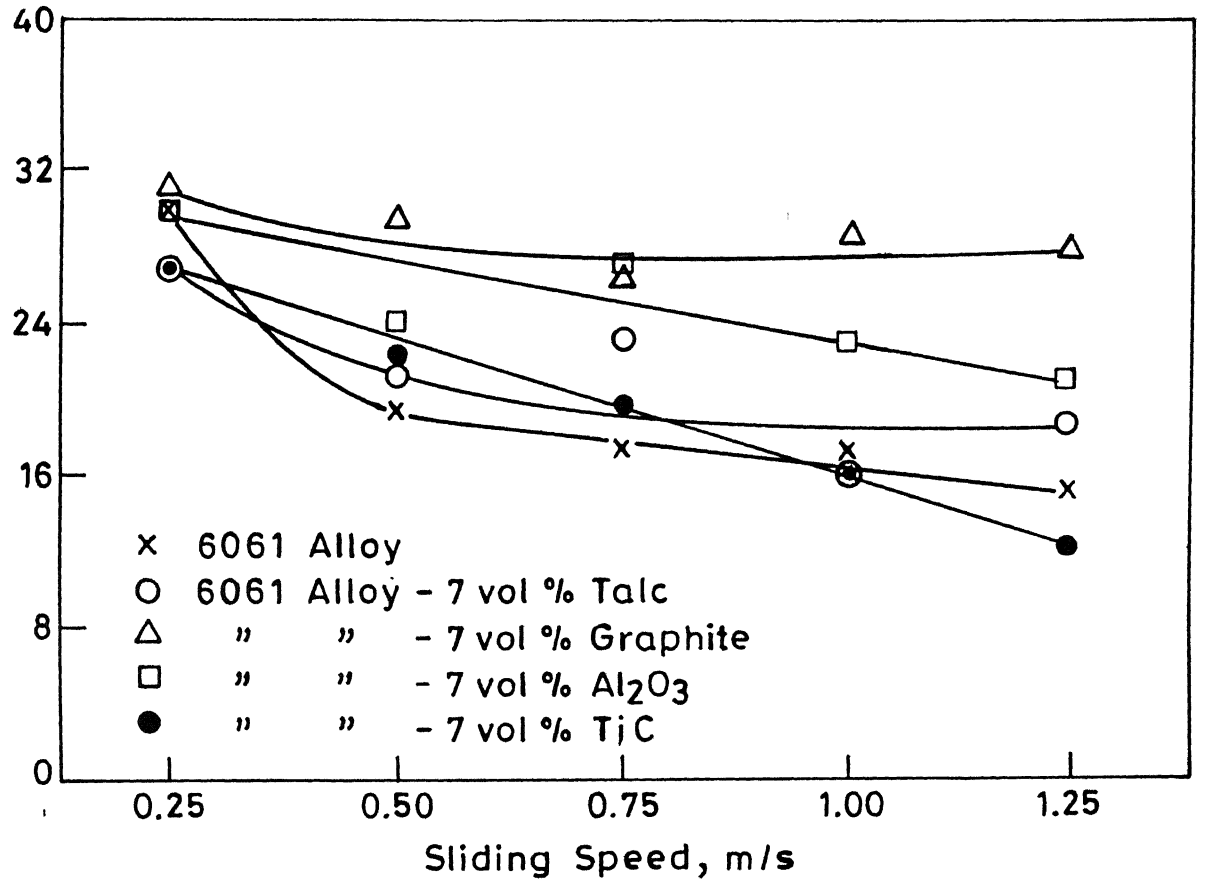

Fig. 4.5d Effect of sliding speed on wear rate of sintered 6061 alloy and its composites containing 7 vol % dispersoid (Applied pressure: 12×10^{-2} MPa; Sliding distance = 250 meters)

increase in temperature and more oxidation on mating surface. As a result wear rate of a material increases or decreases depending on individual test conditions and material properties. For example, 50 percent increase in wear rate of 6061 alloy compact was observed when the sliding speed was decreased from 0.25 to 1.25 m/s, whereas, the increase in wear rate of graphite containing composites due to decrease in sliding speed was marginal.

SEM micrographs of worn out surface of 6061 alloy compact (Figure 3.25) also revealed more severely damaged surface at low sliding speed as compared to the surface tested at high speed. In case of graphite containing composites micrographs of worn out surface did not show any marked difference when tested at different sliding speeds (Figure 3.26). However detailed study is required for more conclusive remarks.

IV.6.3. Mechanism of Lubrication in Composites:

(i) Solid Lubricants:

The lubrication properties of lamellar solids like graphite or talc are due to the interplanar mechanical weakness or slip action.[137] The basal planes of graphite lattice consist of open hexagons with the interatomic distance 1.45 A^{o} and these planes are stacked in an alternative sequence with a spacing of 3.353 A^{o}.[136] Atoms within the basal plane are held together by strong covalent bond, whereas, between the basal planes weak Vander Waal-type of force

exists giving rise to interplanar mechanical weakness. Further presence of water vapour[138] and crystal defects[139] such as dislocation also imparts ease in interlamellar shearing of graphite layers required for providing solid lubrication.

Similarly the structure of pure talc consists of a layer or sheet of brucite (magnesium hydroxide, $MgO.H_2O$) sandwiched between two sheets of silica (SiO_2).[94] These layers are superimposed upon each other and they are held together by weak Vander Waal type forces. These layers slide over each other with considerable ease when a shearing force is applied to it.

If a solid lubricant has to be effective in reducing the metal to metal contact a layer of it must shear and get adhered on the metal surface with major axis parallel to the sliding direction. The overall effectiveness of lubricant would depend on the ability of the sheared layers to adhere on the sliding surfaces. Force of adhesion of sheared layer to metal surface should be higher than the force of cohesion between the lubricant layers.[140] If this criterion is not fulfilled, sheared lubricant layers will not be effective in adhering on the mating surface and they will not prevent the metal to metal contact.

In the present case, wear rate measurements clearly indicate that wear increases linearly with the volume fraction of dispersoid. Since the major wear seems to be due to the formation of junction between steel and aluminium alloy it is

obvious that solid lubricant present in the composites was uneffective in preventing metal to metal contact. This anamoly could be due to the presence of insufficient quantity of dispersoid (graphite or talc) particles on the sliding surface. Smearing of the aluminium as well as pull-out of dispersoid due to week interface may reduce the area fraction of dispersoid present on the sliding surface. It is also logical to deduce that big flake (100 μm) formed due to delamination may envelope small graphite or talc particles (6 μm). As a result solid lubricant particles (graphite or talc) will not have a chance to form a triboinduced layer. This is schematically illustrated in Figure 4.6. Thus, with the volume fraction of the dispersoid added in the present study any improvement in the wear properties could not be achieved.

Some model experiments were carried out to provide the exposure of solid lubricant (graphite and talc) particles to the mating surface in the very beginning of the pin-on-disc wear test and to study its effect on the wear behaviour of sintered 6061 alloy. In the first set of experiments, after the initial run-in period, graphite or talc particles were spread on the wear path and wear tests were continued to a total sliding distance of 125 meters. Table IV.1 lists the wear loss of 6061 alloy compacts with graphite or talc particles on the mating surface. Wear loss of 6061 alloy compact reduced by a factor of seven due to spreading of graphite particles between the mating surfaces, whereas, in case of talc the decrease was not significant.

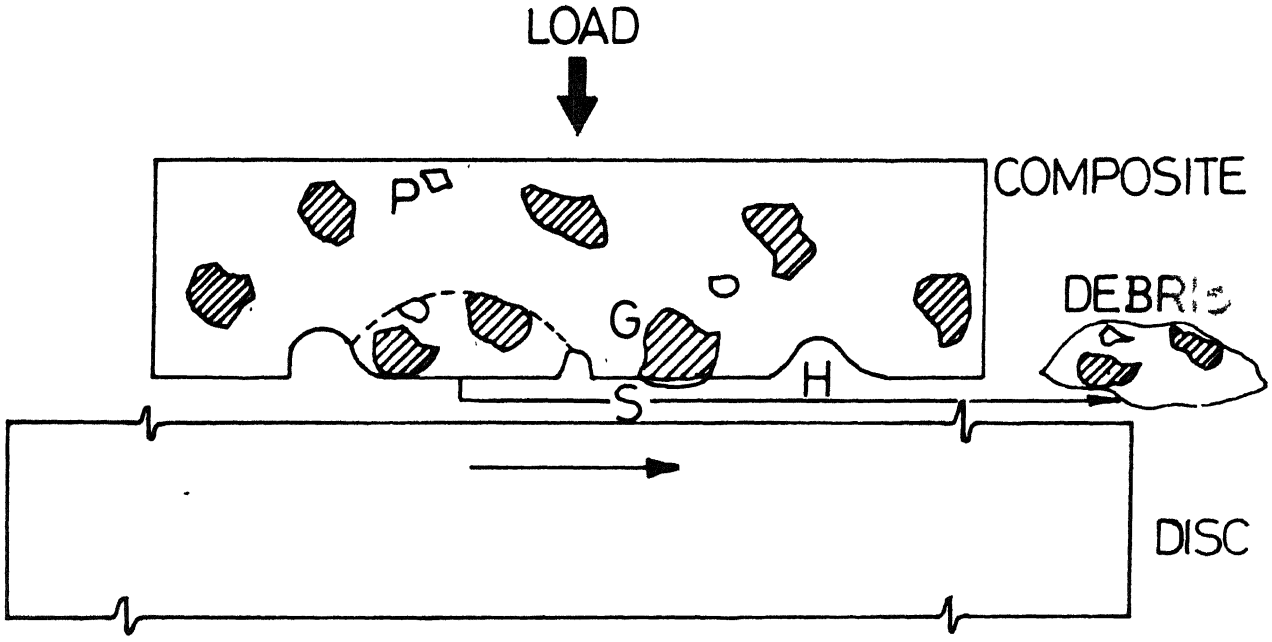

G: GRAPHITE, H: HOLE CREATED BY GRAPHITE PULL OUT, P: PORE, S: SMEARED ALUMINIUM ON GRAPHITE

Fig. 4.6 Schematic Of Sliding Wear Of Composite Against Moving Disc.

Table IV.1. Wear loss of 6061 alloy compact with graphite/talc on mating surface

Wear loss of 6061 alloy compact, mm^3		
Without lubricant	Lubricant on mating surface	
	Graphite	Talc
2.2	0.3	2.1

Since the spreading of loose graphite particles on wear path was found to reduce the wear loss of 6061 alloy significantly, a second set of experiments was performed on deeply etched surface of 6061 alloy containing 14 volume percent of graphite with particle protrusions. In this series of experiments composites were first subjected to initial run-in period till the surface of the specimen was in complete contact with disc surface. The test was stopped at this stage and specimen was immersed in 5 percent HF solution for an optimized period of 15 minutes. Experiments were repeated on the sample surfaces etched for 10 and 20 minutes also. Similar experiments were carried out on talc containing composites. Table IV.2 lists wear loss of composites in etched condition. Wear loss of 6061 alloy composite containing 14 volume percent graphite in optimally etched condition was found to be significantly less than those of unetched composites and base alloy. Etching time also appeared to be effective in controlling the wear rate. For instance, surface etched for 10 and 20 minutes did not show any improvement in

Table IV.2. Wear loss(mm^3) of 6061 alloy based composites in different conditions

Volume percent dispersoid	Unetched	Etched	Under etched	Over etched
14 volume percent graphite	5.19	0.96	5.27	3.79
14 volume percent talc	2.63	1.46	3.31	3.86

the wear rate. Figures 4.7 and 4.8 show the wear loss of 6061 alloy. 14 volume percent dispersoid (graphite or talc) in unetched and etched condition as a function of sliding distance. Wear loss for unetched surface increased linearly with sliding distance. In the case of composite containing graphite it can be seen (Figure 4.7) that wear loss of composites in etched condition was significantly less than that of unetched composite at all sliding distances. It can also be seen that the slope of the curve for the etched composites increased after a sliding distance of approximately 400 meters. It is worth noting that even maximum slope of the wear loss versus sliding distance curve for etched surface is less than that for unetched surface. Marked change in the slope of the curve suggests that in the beginning of this test, relatively large portion of the surface was covered by triboinduced lubricant layers, which with progress of time would be removed due to the sliding action. The absence of flaky type of wear debris (100-200 μm size) in case of the etched composites (Figure 4.9) confirms that the delamination

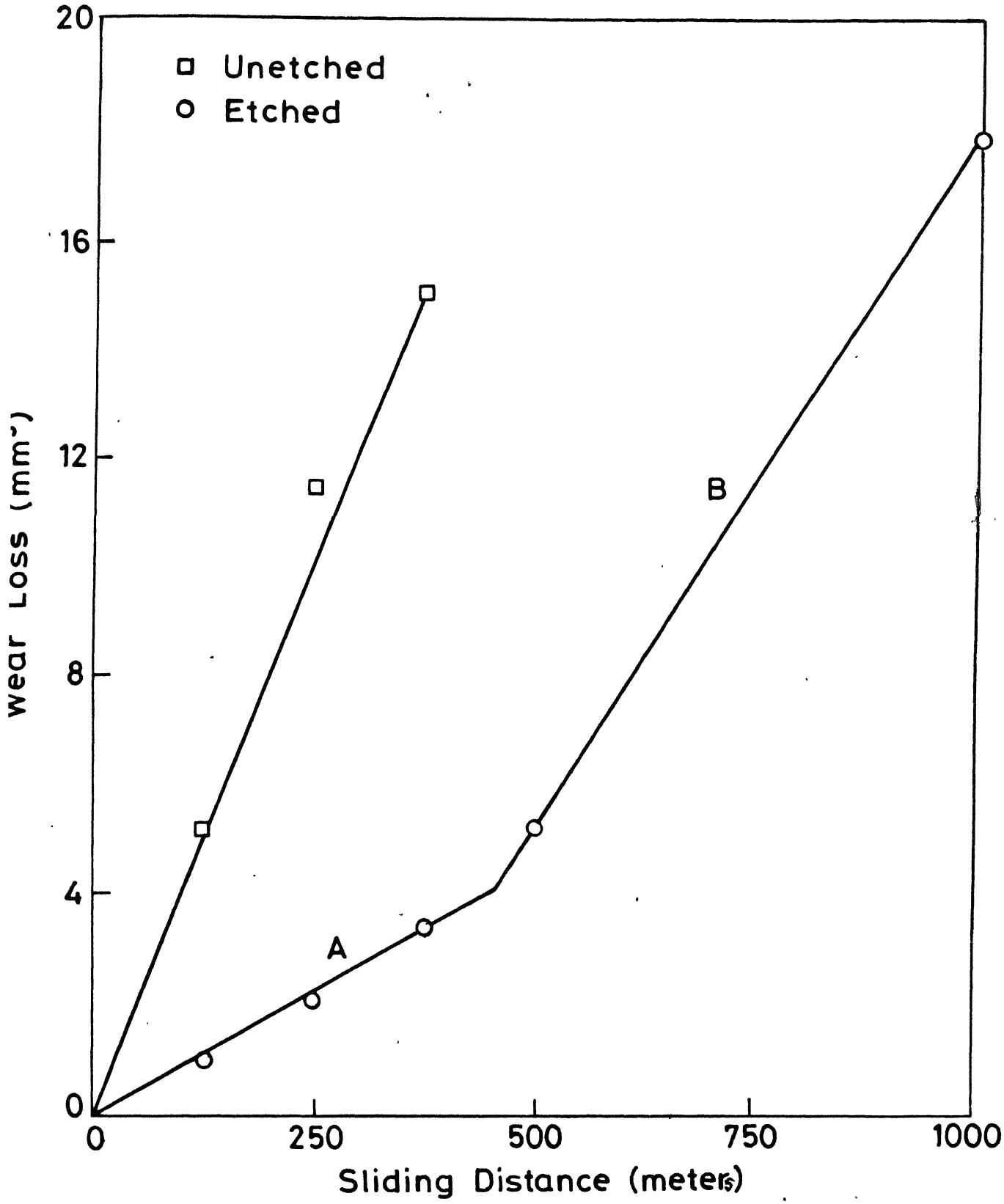

g.4.7 Sliding Distance Vs Wear Loss Of 6061 Alloy-14 Vol % Graphite Composite.

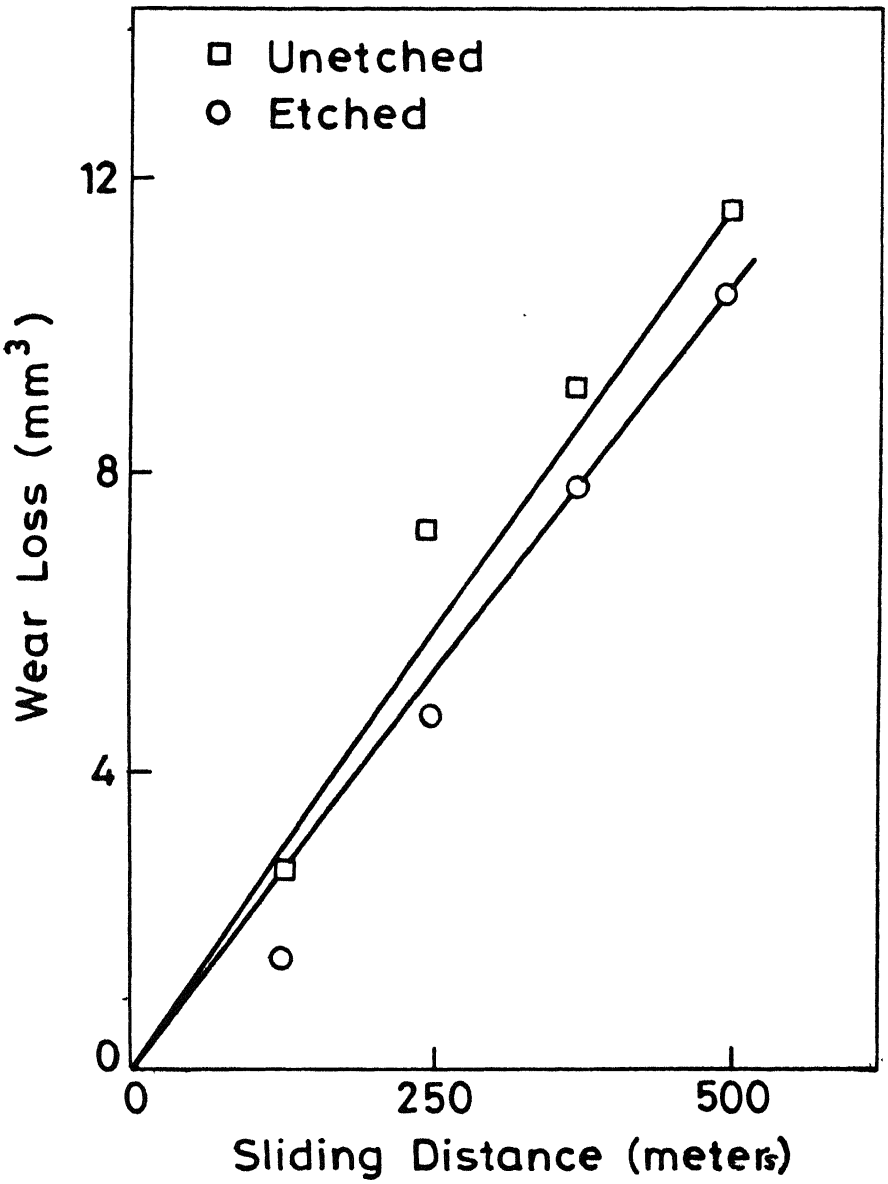

Fig. 4.8 Sliding Distance Vs Wear Loss of 6061 Alloy-14 Vol% Talc Composite.

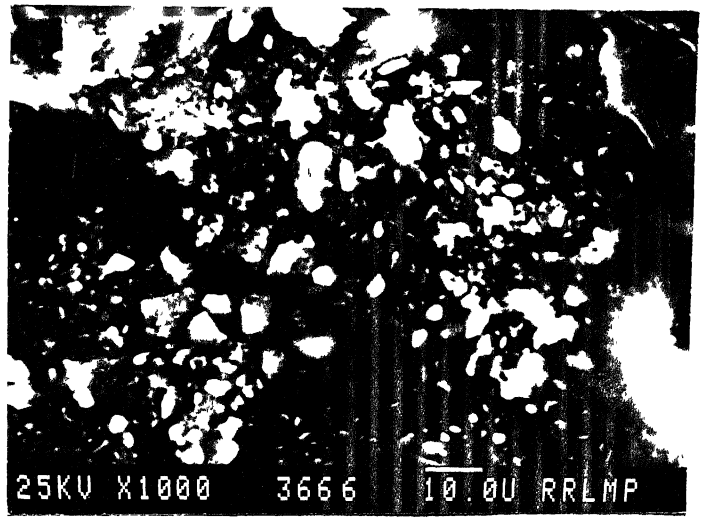

Fig. 4.9. SEM micrograph of fine equiaxed debris particles of composite with protruded graphite on surface after the sliding distance of 125 meters.

mechanism was not predominent when graphite particles were left protruded in the starting surface. This is schematically illustrated in Figure 4.10. In case of composites containing talc (Figure 4.8) difference in wear loss between unetched and etched surface is marginal. It may also be noted that improvement in wear loss was marginal when talc particles were spread on the disc surface (Table IV.1). However, unetched composites show more loss at any sliding distance (Figure 4.8).

From the experimental result it is evident that wear resistance of composites containing talc is superior to those of containing graphite when tests were carried out with unetched specimen, whereas, reverse was found to be true for etched composites. Under conditions favourable to delamination type of wear, sintering characteristics predominantly govern the overall wear behaviour of composites. Micrographs of worn out surface in this case (Figures 3.20 and 3.41) did not show film formation on the surface. However, such film formation was observed on the worn out surface of either 6061 alloy compacts wherein free graphite/talc particles were spread on the disc, or composites in optimally etched condition. Figure 4.11 shows the worn out surface of 6061 alloy with free graphite particles introduced on the wear path. Patches of graphite sticking to the worn out surface can be clearly seen. Micrographs of etched surface of composites are shown in Figure 4.12. Protruded particles can be seen in the micrographs. SEM micrographs of the worn out surface

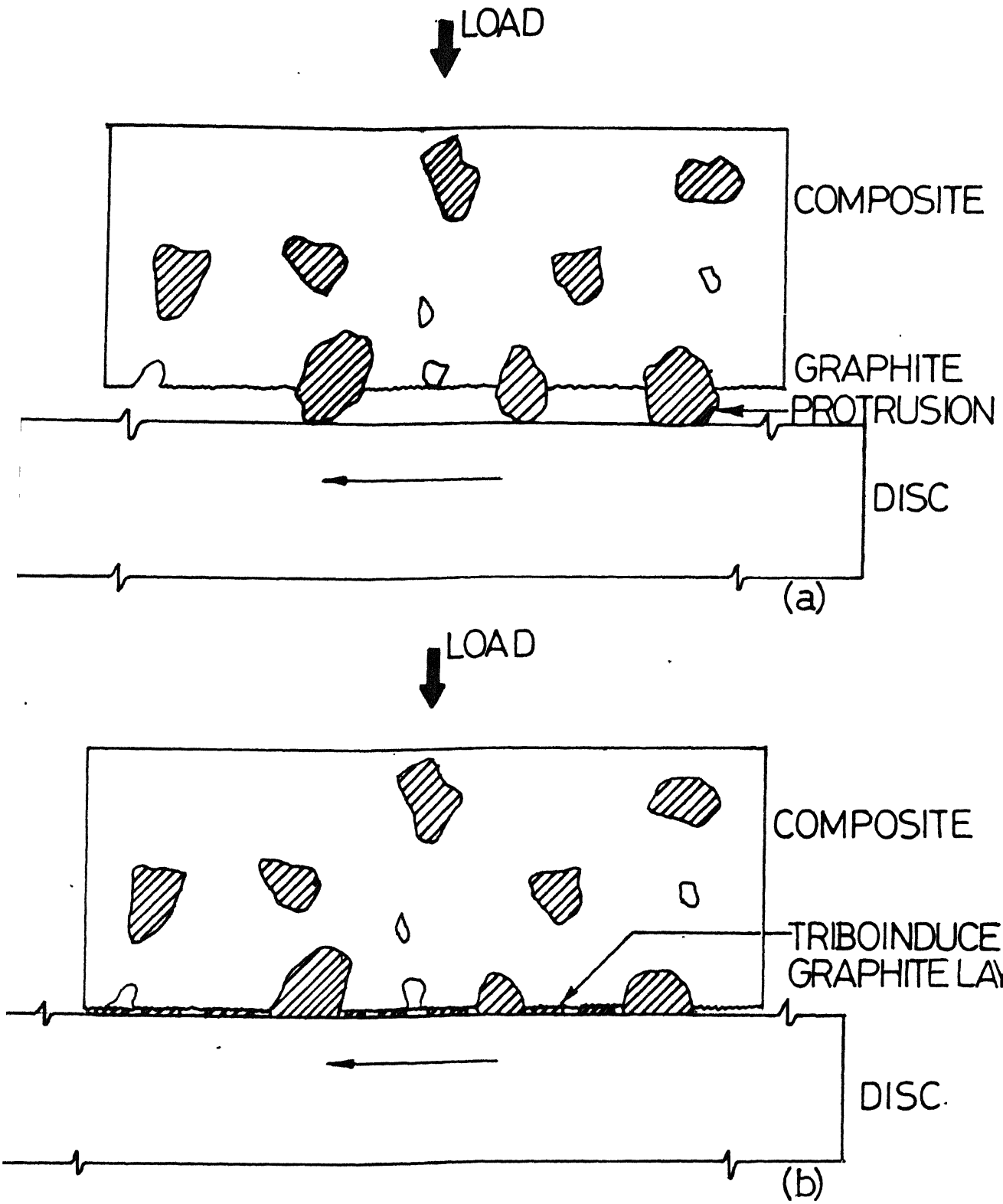

Fig 4.10 Schematic Of (a) Graphite Protrusions On Composite Surface (b) Tribinduced Graphite Layer On Mating Surface.

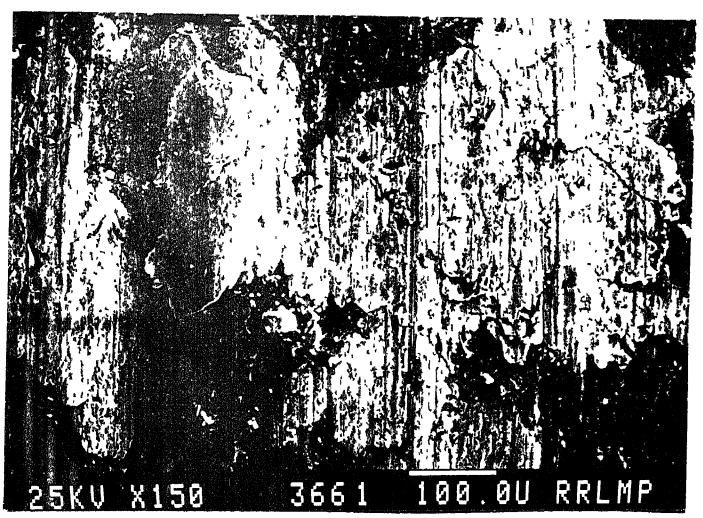

Fig. 4.11. SEM micrograph of worn out surface of 6061 alloy compact with graphite particles on mating surface (after a sliding distance of 125 meters).

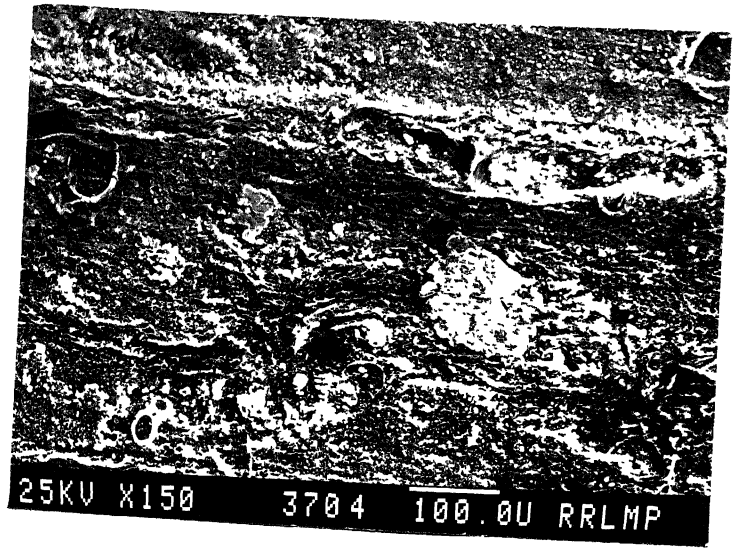

(a)

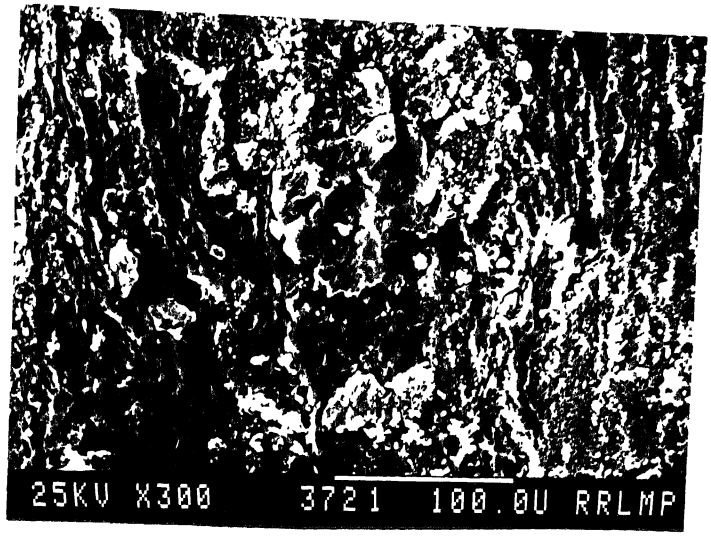

(b)

Fig. 4.12. SEM micrographs of etched surface of 6061 alloy composites containing (a) 14 volume percent graphite (b) 14 volume percent talc.

of 6061 alloy in etched condition are shown in Figures 4.13 to 4.15. There is a marked resemblence between these micrographs in Figure 4.11 and Figure 4.13a where graphite layers can be seen sticking to the surface of the 6061 alloy. At few isolated places graphite particles were seen slightly below the level of matrix (Figure 4.14a). Figure 4.12b represents the corresponding X-ray mapping for carbon. Although it is difficult to distinguish between an embedded and adhered graphite on the metal surface,[141] the similarity between the worn out surface of 6061 alloy-14 volume percent graphite composite in etched condition and the 6061 alloy surface wherein free graphite particles were introduced in the wear path suggests that the graphite particles shown in Figure 4.13 were indeed adhered layers on the surface and not the embedded ones. Similar is the case with talc containing composites (Figure 4.15). This situation is completely different from the previous one, where there were chances of metal to metal contact resulting in delamination type of wear. Considerable iron pick up by triboinduced lubricant layer (Figures 4.13c and 4.15b) indicates that these layers prevented the contact between the 6061 matrix alloy and steel disc. Very close to the present observation a marked transfer of copper to the graphite is reported in literature.[142]

In the model experiments talc particles were found to be inferior to the graphite as far as solid librication property is concerned. The decrease in wear rate of talc containing composites in etched condition (Figure 4.8) was

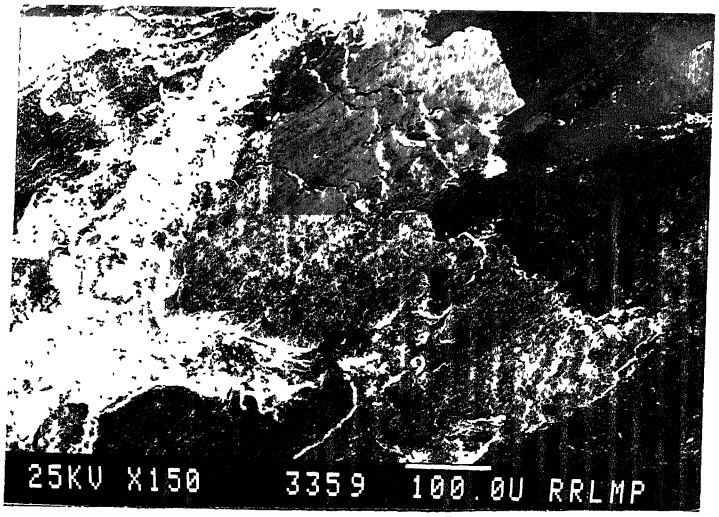

(a)

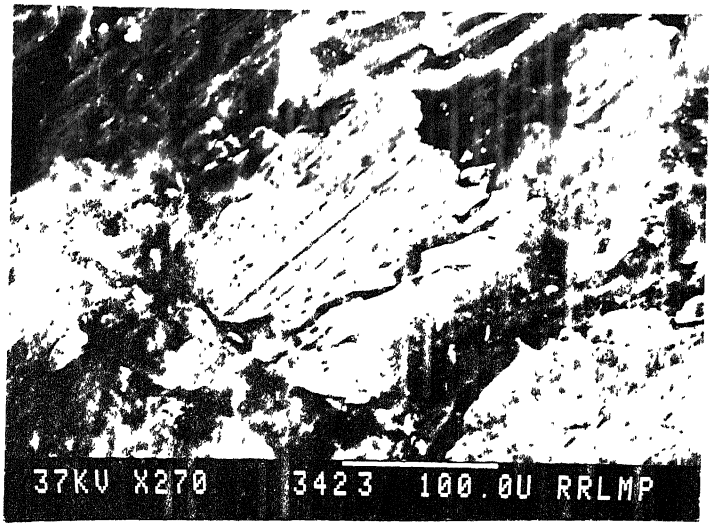

(b)

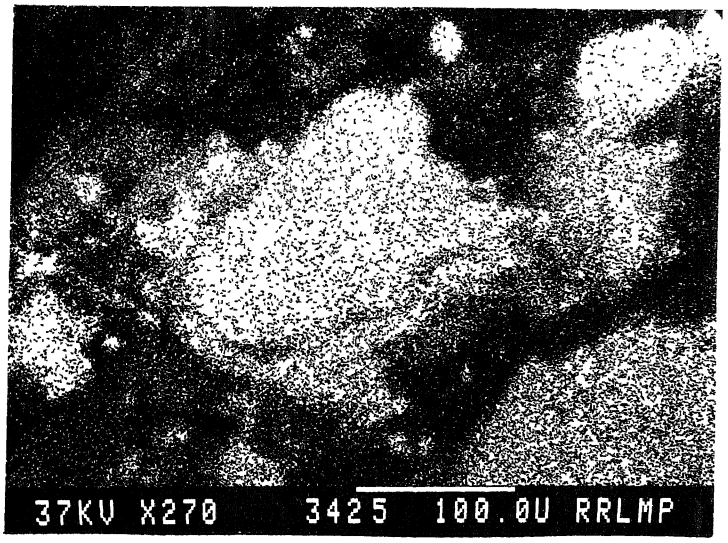

(c)

Fig. 4.13. (a-b) SEM micrographs of worn out surface of optimally etched 6061-14 volume percent graphite composite after sliding distance of 125 meters, (c) corresponding X-ray mapping for FeK_{α} peak of (b).

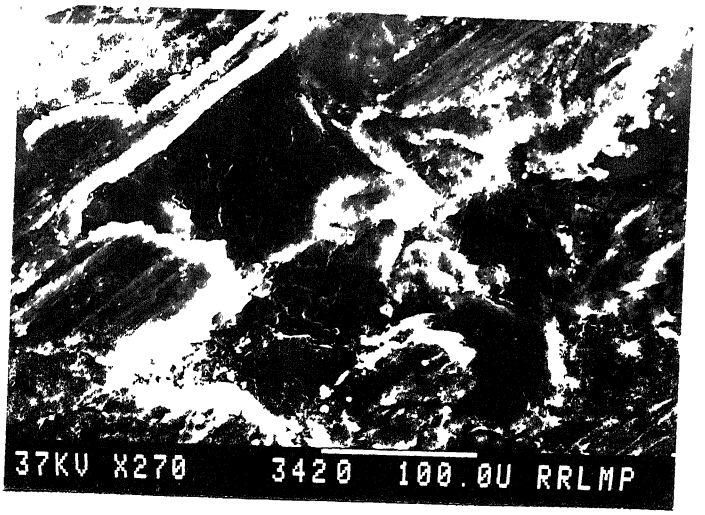

(a)

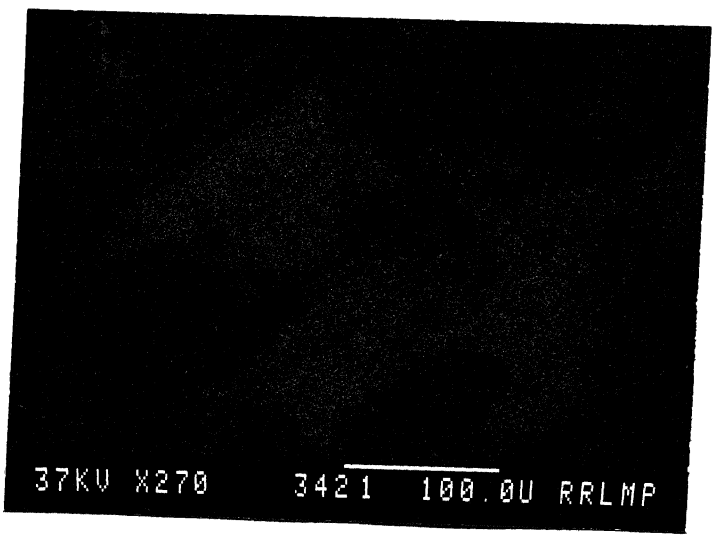

(b)

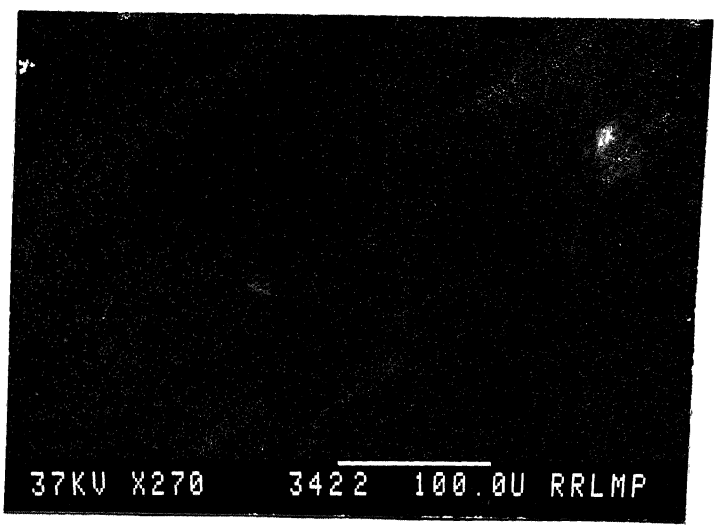

(c)

Fig. 4.14. (a) SEM micrographs of worn out surface of 6061-14 volume percent graphite composites; X-ray mapping for (b) carbon K_α peak (c) FeK_α peak of (a).

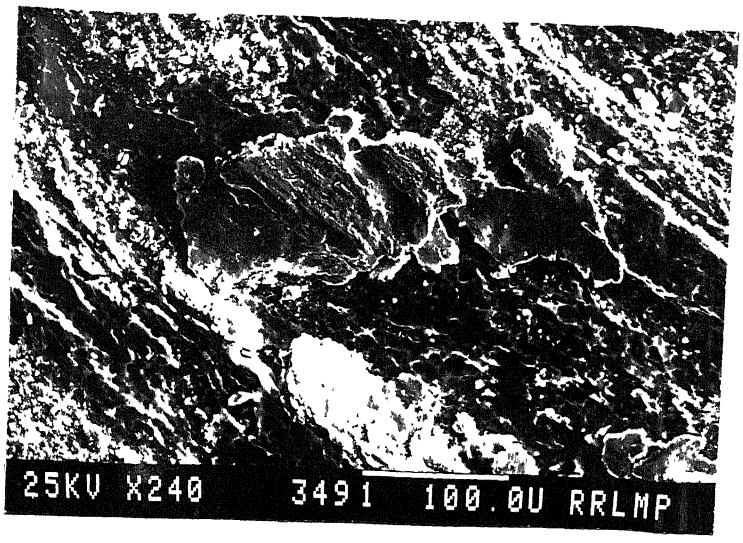

(a)

(b)

Fig. 4.15. (a) SEM micrographs of worn out surface of optimally etched 6061-14 volume percent talc composite, after sliding distance of 125 meters
(b) corresponding X-ray mapping for FeK_{α} peak.

not as pronounced as in the case of graphite containing composites tested under similar conditions. Similar was the case when graphite and talc particles were spread on the disc surface(Table IV.1). The relative hardness of the metal and the solid lubricant crystallites play important role in sliding process as well as in the formation of the layer. When two asperities move together the particles between them will become trapped, and if a particle is soft enough it will not become firmly attached to the surface and will allow metal to metal contact.[141] Talc, being softer than graphite is expected to be less effective in reducing metal to metal contact and will not be effective in reducing wear. Further the force required to shear the layers may be less in the case of graphite. These model experiments clearly demonstrated that graphite is a far better solid lubricant than talc. Under optimum conditions when the area fraction of graphite particles in the beginning of the test is high enough or when the graphite particles were left protruded, triboinduced graphite film formation can be expected. When such film formation occurs there will be several fold decrease in the wear rate of composites. When the area fraction of the solid lubricant particle in composite is low or when the softer matrix smears over the solid lubricant particles there will not be any film formation leading to the delamination type of wear. Under such conditions, type and amount of defects present in composite will predominently govern the wear behaviour. Since talc containing composite has

better sintering characteristics than the graphite containing composites, wear properties of the former is superior to the latter, in unetched condition, when delamination is an operative mechanism.

(ii) Hard Particles:

Even composites containing hard particles did not show improvement in wear behaviour over 6061 alloy compact (Figures 3.50 and 3.65). Formation of flake shape debris (Figures 3.55a and 3.70a) similar to those found in case of wear test of straight 6061 alloy compact (Figure 3.22c) or in case of 6061 alloy-7 volume percent graphite suggests the delamination type wear to be operative in this case also. Since the size of TiC and alumina particles (3.45 and 0.3 μm respectively) is much smaller than the size of flake (100 μm) it is probable that particles would be occluded in the flakes. Therefore, a situation envisaged in Figure 4.6 is also applicable to the present case. Perhaps this is the cause that there is no improvement in the wear behaviour of such composites. Interfaces play important role in governing the wear of hard particle containing composites. If the interfacial bond is poor there is likelihood that the dispersoid will be pulled out from the matrix during the test. This will result in additional material removal, and create voids in the composites increasing the chances of delamination. Also, when the hard particles such as alumina or TiC get pulled out from matrix they are likely to cause

ploughing and cutting action of soft matrix resulting in abrasive type of wear. All these factors might have offset any positive contribution due to the presence of alumina or TiC particles in the matrix. It is conceivable if the area fraction of hard particles in composite is considerably high and interfaces are good, the softer aluminium alloy matrix will get preferentially worn out leaving hard dispersoid particles protruding out of the matrix. If the interparticle distance is small compared to the size of asperities on the steel disc, a situation may arise wherein the hard particles will completely protect the softer matrix from touching the matrix surface. Under such conditions wear of the composites can be governed by the fracture of brittle second phase particles. In the present case, dispersoid content was significantly low and particle matrix interfaces were also not very strong and, therefore, the positive effect arising due to the presence of hard particles in soft matrix was not observed.

Study of present system was undertaken for the development of material for tribological use such as bearing, where sliding wear resistance is an important characteristic for material selection. Use of aluminium alloy as the matrix would result in considerable weight saving of the component and reduction in consumption of scarce metal like, lead and tin which are used in babbits. This study has demonstrated that the sliding wear behaviour of composites can be improved only when certain conditions like, area fraction of

second phase particle and particle-matrix interfacial bonding are fulfilled. Mere dispersions of solid lubricant or hard particles would not invariably lead to reduction in sliding wear rate. Materials for a tribo-component should fulfill, in addition to tribological properties, certain mechanical and physical properties. For achieving these, overlay of composites may be thought of. Reinforcement of aluminium alloy with short fibre or whiskers such as, SiC, may also be considered.

CHAPTER V

CONCLUSIONS

From the investigations carried out in the present study, following conclusions can be drawn:

(1) Dispersoids other than graphite to 6061 alloy substantially improved densification of the composites, when added in low volume fraction (<7 volume percent). This is explained on the basis of better compatibility of dispersoid like talc with 6061 matrix. In case of the composites containing hard dispersoids, the associated stress field appears to contribute in enhanced sintering.

(2) Tensile properties of composites decreased with addition of dispersoids. Among all the dispersoids, graphite addition resulted in poorest properties. This was attributed to the poor interface bond between 6061 alloy and dispersoid and the presence of porosity in the matrix.

(3) Nitrogen sintering imparted poorest densification and mechanical properties to the composites due to comparatively high dew point and the presence of impurities in it.

(4) Repressing and resintering reduced the porosity level and improved the hardness of sintered composites.

(5) Mechanical properties of heat treated composites improved in relation to the as sintered ones. Like sintered ones, heat treated composites too showed deterioration in mechanical properties with increasing dispersoid content.

(6) Thermomechanical treatment of 6061 alloy and its based composites showed hardening particularly for those containing soft particles. It is explained on the fact that deformation of composites containing soft particles is much easier than those containing hard dispersoids. Premature over-ageing of the composites containing hard particle is also one of the causes for inferior mechanical properties.

(7) Surface roughness of sintered 6061 alloy decreased with addition of talc whereas in case of composites with other dispersoids, insignificant variation was noticed. Porosity level in composites and hardness of the dispersoids affect the roughness of the composite surface.

(8) Electrical resistivity of sintered composites increased with increasing amount of dispersoid which is attributed to higher electrical resistivity values for all the dispersoids as compared to 6061 alloy. Heat treatment of the composites resulted in further increase in the resistivity value.

(9) Wear loss of composites as well as base alloy increased with applied pressure and sliding distance.

Wear loss increased with decreasing sliding speed and the increase was minimum for graphite containing composites.

(10) Wear rates of composites increased with increasing amount of dispersoid except for graphite containing composites at low applied pressure. There appears to be direct correlation between wear behaviour and sintering characteristics of composites.

(11) Debris examination revealed four major types of debris, i.e. long needle shape, flake shape, rounded agglomerate and fine equiaxed particles. Flaky debris outnumbered the other types indicating that delamination as the important wear mechanism.

(12) Model experiments carried out on etched surface of composites containing protruded graphite particles showed substantial decrease in wear (by a factor of seven). Such substantial improvement in wear resistance was not observed for the etched composites with talc protrusions on the surface, indicating that graphite is a superior lubricant than talc. Under normal conditions when delamination is the predominant mechanism, talc containing composites were found to be superior to graphite containing composites due to the better densification achieved during sintering.

REFERENCES

1. J.N. Dudas and W.A. Dean, Int. J. of Powder Metall., 5 (1969) 113.

2. J.N. Dudas and C.B. Thompson, in 'Modern Development in Powder Metallurgy', Ed. H.H. Hausner, Vol. 5, Metal Powder Industries Federation (1971) 19.

3. J.P. Lyle, Jr., W.S. Cebulak and K.E. Buchovecky, in 'Progress in Powder Metallurgy', Ed. A.S. Buffered, Vol. 28, Metal Powder Industries Federation, Princeton (1972) 93.

4. J.N. Dudas and K.J. Brondyke, ARL Report No. 7-70-AP167, Alcoa Research Laboratories, Jan. 1970.

5. M.P. Swain and E.L. Buters, Paper presented at Metal Powder Industries Federation, International Conference, Toronto, Canada, July 19 (1973) p. 3.

6. J.P. Lyle and W.S. Cebulak in 'Proc. of 18th Sagamore Army Materials Research Conference on PM High Performance', Ed. J.J. Burke and V. Weiss, Syracuse University Press, Syracuse (1972) p. 231.

7. R. Irmann, Aluminium, 27 (1951) 29.

8. F.V. Lenel, A.B. Backensto, Jr. and M.V. Rose, J. of Metals, Jan. (1957) 124.

9. F.J. Esper and G. Leuze in 'Modern Development in Powder Metallurgy', Ed. H.H. Hausner, Vol. 8 (1973) p. 209.

10. V. Arnhold and J. Baumgarten, Powder Metall. Int., 17 (1985) 168.

11. S. Strochheim, in'Progress in Powder Metall.', Vol. 18 (1962) p. 124.

12. W. Kehl, M. Bugajska and H.F. Fischmeister, Powder Metall., 26 (1983) 221.

13. H.C. Neubing, Powder Metall. Int., 13 (1981) 74.

14. G.G. Goetzel in 'Treatise on Powder Metallurgy', Vol. 2, Interscience Publication Inc., N.Y. (1950) p. 489.

15. G.S. Upadhyaya and P.S. Misra, Powder Metall. Int., 8 (1976) 165.

16. P.F. Mathews, Int. J. of Powder Metall., 4 (1968) 39.

17. F.J. Esper and G. Leuze, Powder Metall. Int., 3 (1971) 123.

18. G.S. Upadhyaya and P. Thareja, Trans., Powder Metall. Association of India, 2 (1975) 22.

19. F.F. Nia and B.L. Davies, Powder Metall., 25 (1982) 209.

20. C.L. Kobria, Iron Age, 30 (1964) 135.

21. A. Bharati, R. Narayan and M.L. Vaidya in 'Recent Trend in Development of Composite Materials', Indian Society for Composite Material, Pune (1983) p. 67.

22. I. Amato, S. Corso and E. Sgambetterra, Paper presented at Powder Metallurgy Group Meeting at Stratford, U.K., 1975.

23. E.M. Daver and D.P. Ferriss, In 'Modern Development in Powder Metallurgy', Ed. H.H. Hausner and P.W. Taubenblat, Vol. 10, Metal Powder Industries Federation, Princeton (1976) p. 357.

24. A.K. Jha, M.Tech. Thesis, I.I.T. Kanpur, Jan. 1983.

25. L.W. Kempf in 'Powder Metallurgy', ASM, Cleveland (1942) p. 314.

26. A.P. Savitsky et al., Poroshkovaya Metallurgia, 10 (1982) 11.

27. F.V. Lenel, 'Powder Metallurgy', Metal Powder Industries Federation, Princeton, 1980.

28. E. Exner and H. Fischmeister, Metall., 19 (1965) 941.

29. W.J. Huppmann, N.A. Keysser, D.N. Yoon and G. Petzow, Powder Metall. Int., 11 (1979) 50.

30. W.A. Kaysser and G. Petzow, Powder Metall., 28 (1985) 145.

31. W. Kehl and H.F. Fischmeister, Powder Metall., 3 (1980) 113.

32. T. Watanabe and K. Yamada, Report of the Casting Research Laboratory, Waseda University, No. 19 (1968) 22.

33. J.R. Pickens, J. Mater. Sci., 16 (1981) 1437.

34. J.R. Pickens and R.D. Schelleng, Air Force Materials Laboratory WPAFB, Ohio, Contract Interim Report F33615-76-65227, 1979.

35. L.A. Arbuzova, V.A. Danllkin and L.L. Kunin in 'Theory Production, Technology and Properties of Powder and Fibres' translation IIDC, Plenum Press, N.Y. (1976).

36. S.G. Robert, AMMRC CTR73-63, October 1975.

37. H.M. Skelly and C.F. Dixon, Int. J. of Powder Metall., 7 (1971) 47.

38. J. Duszczyk and P. Jongenburger, Reviews on Powder Metallurgy and Physical Ceramics, 2 (1985) 268.

39. G.H. Tan, M.A. Zaidi and T. Sheppard, Powder Metall., 27 (1984) 3.

40. N. Kuroishi, Y. Odani and Y. Takeda, Metal Powder Report, Nov. (1985) 642.

41. R.D. Parkinson and T. Sheppard, Powder Metall., 28 (1985) 189.

42. J.P. Lyle and W.S. Cebulak, Metals Engineering Quarterly, Feb. (1974).

43. H.B. McShane and T. Sheppard, Powder Metall., 27 (1984) 101.

44. R. Irmann, Aluminium, 33 (1957) 250.

45. R. Irmann, Metallurgia, 46 (1952) 125.

46. J. Grosch and G.J. Brockmann, Powder Met. Int., 13 (1981) 146.

47. N. Hansen, Powder Metall., 12 (1969) 23.

48. T. Sheppard and P.J.M. Chare, Powder Metall., 15 (1972) 17.

49. N.C. Kothari in 'Sintered Metal Ceramic Composites', Ed. G.S. Upadhyaya, Elsevier Science Publishers, Amsterdam (1984) p. 74.

50. N.C. Kothari, Science of Sintering, 11 (1979) 151.

51. C. Jangg, F. Kutner and G. Korb, Powder Metall. Int., 9 (1977) 24.

52. K.U. Kainer, H.W. Bergmann and B.L. Mordike, Powder Metall., 27 (1984) 30.

53. G. Jangg and W.J. Huppmann, Industrial Heating, January 1981, 20.

54. D. Raybould, Powder Metall., 25 (1982) 35.

55. T. Young, Trans. Roy. Soc., 95 (1805) 65.

56. P.K. Rohatgi, R. Asthana and S. Das, Int. Metals. Rev., 31 (1986) 115.

57. L. Ramqvist, Int. J. Powder Metall., 1 (1965) 2.

58. C.C. McBrigge et al., J. Amer. Ceram. Soc., 35 (1952) 28.

59. A.D. Panasuk et al., In 'Fizicheskay Khimia Pover Khnostnikh Yavlenii pri Visokikh Temperarurakh', Naukova, Dumka, Kiev, 1971.

60. Ya. V. Naidich, Kontaktnie Yavlenia V. Metallicheskikh Rasplavakh', Naukova Dumka, Kiev (1972) 166.

61. G.V. Samsonov, Ukr. Khim. Zh., 31 (1965) 1233.

62. G.V. Samsonov, A.D. Panasyuk and G.K. Kozina, Sov. Powder Metall. Mat. Ceram. (1968) 874.

63. A.P. Divecha, S.G. Fishmen and S.D. Karmarkar, J. Metals, 33 (1981) 12.

64. A. Skinner, M.J. Koczak and A. Lawley, Powder Metall. Int., 14, 3 (1982) 144.

65. Ibid, Met. Trans., 13A (1982) 289.

66. R.J. Arsenault, Mater. Sci. and Engg., 64 (1984) 925.

67. D.L. McDanels, Met. Trans., 16A (1985) 1105.

68. S.R. Nutt, In 'Interfaces in Metal-Matrix Composites', Ed. A.K. Dhingra and S.G. Fishman, AIME, Warrendale (1986) p. 157.

69. K. Robinson, Phil. Mag., 43 (1952) 775.

70. S.R. Nutt and R.W. Carpenter, Mater. Sci. and Engg., 76 (1985).

71. C.G. Levi, G.J. Abbascian and R. Mehrabian, Met. Trans., 9A (1978) 697.

72. B.C. Pai, S. Ray, K.V. Prabhakar and P.K. Rohatgi, Mater. Sci. and Engg., 24 (1976) 31.

73. R.L. Maher, R. Jakes and C.A. Bruch, Tech. Rep. AFML-TR-68, May 1968.

74. R.L. Maher and E. Feingold, J. Mater., 2 (1967) 239.

75. J.J. Brennan and J.A. Pask, J. Amer. Ceram. Soc., 51 (1968) 569.

76. P.K. Rohatgi, B.C. Pai, S.C. Panda, J. Mater. Sci., 14 (1979) 2277.

77. A. Banerji and P.K. Rohatgi, J. Mater. Sci., 17 (1982) 325.

78. P.G. Riewald, W.H. Kruegar and A.K. Dhingra, U.S. Patent 4,012,204 March 15, 1977.

79. F.A. Badia and P.K. Rohatgi, Trans. AFS, 76 (1969) 402.

80. B.C. Pai and P.K. Rohatgi, J. Mater. Sci., 13 (1978) 329.

81. N. Eustathopoulos, J.C. Joud, P. Desre and J.M. Hictor, J. Mater. Sci., 9 (1974) 1233.

82. P.K. Rohatgi, In 'Interfaces in Metal-Matrix Composites', Ed. A.K. Dhingra and S.G. Fishman, AIME, Warrendale (1986) p. 185.

83. I.H. Khan, Met. Trans., 7A (1976) 1281.

84. B. Maruyana and L. Rabenberg, In 'Interfaces in Metal-Matrix Composites', Ed. A.K. Dhingra and S.G. Fishman, AIME, Warrendale (1986) p. 233.

85. T. Erturk, J.A. Cornie and R.G. Dixon, ibid, p. 239.

86. M. Vedula and R.A. Queenley, ibid, p. 227.

87. B.N. Keshavaram, A. Banerji, M.K. Surrappa and P.K. Rohatgi, J. Mater. Sci. Lett., 1 (1982) 29.

88. R.B. Bhagat and P. Ramakrishna, In 'Progress in Science and Engineering of Composites', Ed. T. Hayashi, K. Kawata and S. Umekawa, Vol. 2, Japan Society for Composite Materials (1982) 1.

89. A. Ostermann, W. Reimann and M. Rohrle, 'Sintered Al-Alloys for Piston of I.C. Engine', Mahle Gmbh, Stuttgart, 1978.

90. E. Mosca, G. Pino, Mechanical and Tribological Properties of Aluminium Alloy', Olivetti and Co., Italy (1979) p. 6.

91. K. Anand and Kishore, Wear, 85 (1983) 163.

92. D. Raybould in 'Modern Development in Powder Metallurgy', Vol. 13, Metal Powder Industries Federation, Princeton (1980) p. 443.

93. William Goldie, In 'Metallic Coating of Plastics', Vol. 1, Electrochemical Publication Limited, England (1974).

94. J.A. Rodesta and N.C. Trivedi, In 'Handbook of Fillers and Reinforcements to Plastics', Ed. H.S. Katz and J.V. Milewski (Van Nostrand Reinhold) N.Y. (1978) p. 16.

95. G. Arthur, J. Inst. Metals, 83 (1954) 1329.

96. ASM Metal Reference Book, ASM, Metals Park, , Ohio, (1983) p. 293.

97. R.H. Brown and L.A. Willey, In 'Aluminium: Properties, Physical Metallurgy and Phase Diagram', Ed. K.R.V. Horn, ASM, Ohio (1967) p. 53.

98. A.P. Savitskii and L.S. Martsunova, Poroshkovaya Metallurgia, No. 5 (1977) 14.

99. G. Jangg and H.C. Neubing, In 'Problems with Sintering of Al Parts', Paper presented at seminar on the Development and Use of Powder Metallurgy in Engineering Industries, 25-29 March 1985, Minsk (USSR)

100. R.M. German, Int. J. Powder Metall. and Powder Tech., 4 (1983) 277.

101. N.B. Phadke, Ph.D. Thesis, Brunel Univ. (1978).

102. W. Kehl and H. Fischmeister, In 'Sintering Theory and Practice', Ed. D. Kolar, S. Pejovnik and M.M. Ristic, Elsevier Scientific Publishing Company, Amsterdam (1982) p. 269.

103. H.H. Hausner, In 'Progress in Powder Metallurgy', Vol. 19, Metal Powder Industries Federation, Princeton (1963) p. 67.

104. H. Schreiner and R. Tushe, Powder Metall. Int., 11 (1979) 52.

105. F.V. Lenel, Physics of Sintering, 4 (1972) 1.

106. A.D. Panasuk et al., Proc. Fizicheskaya Khimia Poverkhnostnikh Yovlenii pri Visokikh Temperaturakh, Naukova Dumka, Kiev (1971) p. 185.

107. P.S. Misra and G.S. Upadhyaya, In 'Metal-Ceramic Composites', Ed. G.S. Upadhyaya, Elsevier Science Publisher, B.V. Amsterdam (1984) p. 255.

108. B.N. Singh, Powder Metall., 15 (1972) 216.

109. O. Ishai and L.J. Cohen, J. of Composite Materials, 2 (1968) 302.

110. E. Orowan, 'Symposium on Internal Stresses in Metals', London (Inst. of Metals) (1960) 451.

111. M.F. Ashby, Acta Met., 14 (1960) 679.

112. G.S. Ansell and F.V. Lenel, Acta Met., 8 (1960) 612.

113. V.A. Tracy and D.K. Worn, Powder Met., 10 (1962) 34.

114. C. Nishimatsu and J. Gurland, Trans. ASM, 52 (1960) 469.

115. G.S. Upadhyaya and P.S. Misra, Science of Sintering, 10, Special Issue (1978) 157.

116. N.J. Grant and O. Preston, Trans. AIME, 209 (1957) 349.

117. R.S. Goodrich and G.S. Ansell, Acta Met., 12 (1964) 1097.

118. D. Kuhlmann and H. Wilsdorf, In 'Electron Microscopy and Strength of Crystals', Ed. G. Thomas and J. Washburn, Interscience, N.Y. (1963).

119. H.J. Rack and R.W. Krenzer, Met. Trans., 8A (1977) 335.

120. H.J. Rack, Mater. Sci. Eng., 29 (1977) 179.

121. A.A. Tavassoli, Metall. Sci., 8 (1974) 424.

122. H.J. Rack and C. Edstron, In 'Thermomechanical Processing of Aluminium Alloys', Ed. J.G. Morris, The Met. Soc. of AIME (1979) p. 86.

123. 'ASM Metal Reference Book' (ASM, Metals Park, Ohio) (1983).

124. G.V. Samsonov, In 'Oxide Hand Book', Plenum Press, N.Y. (1973).

125. S. Cerasara and P. Fiorini, Powder Metall., 22 (1979) 1.

126. D.A. Barrow and M.L. Bampton, In Proc. Conf. 'Fourth European Symposium for Powder Metallurgy', Grenoble, 13-15 May 1975, Societe Francaise De Metallurgie, Paris, Vol. 1, p. 131.

127. A. Gallo and G.F. Bocchini, P/M 78, SEMP, Vol. 11, Stockholm, 4-8 June (1978) p. 155.

128. J.T. Burwell, Wear, 1 (1968) 119.

129. N.P. Suh, Wear, 25 (1973) 111.

130. A.D. Sarkar, In 'Friction and Wear', Academic Press, London (1980) p. 133.

131. E. Rabinowicz, In 'Friction and Wear of Materials', John Wiley and Sons, N.Y. (1965) p. 125.

132. N.P. Suh, Wear, 44 (1977) 1.

133. H.C. Sin, N. Saka and N.P. Suh, Wear, 95 (1984) 193.

134. N.P. Suh and H.C. Sin, Wear, 69 (1981) 91.

135. E. Rabinowicz, In 'Friction and Wear of Materials', John Wiley and Sons, N.Y. (1965) p. 136.

136. W.N. Reynolds, In 'Physical Properties of Graphite', Elsevier Publishing Co. Ltd., Amsterdam (1968) p. 1.

137. W.L. Bragg, In 'Introduction to Crystal Analysis' Bell and Sons, London (1948) p. 64.

138. R.H. Savage, J. Appl. Phys., 19 (1948) 1.

139. F.C. Frank, Disc. Faraday Soc., 5 (1948) 48.

140. E.R. Braithwaite, In 'Solid Lubricants and Surfaces', McMillan Company, N.Y. (1964) p. 143.

141. R.F. Deacon and J.F. Goodman, Proc. Roy. Soc., A243 (1948) 464.

142. D.M. Kenyan, cited in 'The Friction and Lubrication of Solid' by F.P. Bowden and D. Tabor, Clarendon Press, Oxford (1986) p. 340.